Ministry of Higher Education & Scientific Research

University Hassiba Benbouali-Chlef

Faculty of Science and Technology

Department of Electrical Engineering

THESIS

Submitted for the fulfillment of the degree of

DOCTORATE

In Electrical Engineering

Option: Electrical Power and Renewable Energy

By

Kamel TOUNSI

Theme:

Decoupled Control of AC Machines Connected in Parallel

Thesis defense on:17/01/2019, in front of the jury composed of:

Djilali BENYOUCEF	MCA	University of Chlef	President
Abdelkader DJAHBAR	Professor	University of Chlef	Supervisor
Said BARKAT	Professor	University of M'sila	Co-Supervisor
Mohammed BOUNADJA	MCA	University of Chlef	Examiner
Benyssaad YSSAAD	MCA	University of Ghilizane	Examiner
Driss RAOUTI	MCA	University of Saida	Invited

Ministère de l'Enseignement Supérieur et de la Recherche Scientifique
Université Hassiba Benbouali de Chlef
Faculté des Sciences et de la technologie
Département de Génie Electrique

THÈSE

Présentée pour l'obtention du diplôme de

DOCTORAT

Filière : Electrotechnique

Spécialité : Electrotechnique des Energies Renouvelables

Par

Kamel TOUNSI

Thème:

Commande Découplée de Machines AC Connectées en Parallèle

Soutenue le 17/01/2019, devant le jury composé de :

Djilali BENYOUCEF	MCA	Université de Chlef	Président
Abdelkader DJAHBAR	Professeur	Université de Chlef	Rapporteur
Said BARKAT	Professeur	Université de M'sila	Co-rapporteur
Mohammed BOUNADJA	MCA	Université de Chlef	Examinateur
Benyssaad YSSAAD	MCA	Université de Ghilizane	Examinateur
Driss RAOUTI	MCA	Université de Saida	Invité

Dedication

This thesis is dedicated to my wonderful parents my father and my mother who have raised me to be the person I am today. Thank you for your unconditional and never-ending love, and for your support that you have always given to me. Thank you for everything.

To my dear wife, for her help, and support.

To my dear grandmother who has always been my caring and tender second mother.

To the living memory of my dear brother.

To my dear sisters for their love and support.

To the sons of my brother and Sisters.

To my brothers in-law.

To all my family TOUNSI.

To all my family Merrad.

To all my relatives, friends, and colleagues.

To all my teachers throughout my career of study.

To all teachers in the Department of Electrical Engineering of Chlef.

TOUNSI Kamel

Acknowledgments

Praise to “Allah” who gave me the faith, courage and patience to complete this research in better and good conditions.

At the end of this research, I would like to thank my supervisors, **Pr. Djahbar Abdlkader** teacher at the Department of Electrical Engineering of Chlef University and **Pr. Barkat Said** teacher at the Department of Electrical Engineering of M'sila University for the advice, encouragement and efforts they gave me during the realization of this work.

I am very grateful to **Pr. Atif Iqbal**, full Professor at Qatar University, director of the Electric Machines and Drives Laboratory, for his invaluable help, guidance and support.

I express my sincere gratitude to the members of my graduate study committee: President of committee member, **Dr. Djilali BENYOUCEF** teacher at the University of Chlef, and the members of the jury: **Dr. Mohammed BOUNADJA** teacher at the University of Chlef, and **Dr. Benyssaad YSSAAD** teacher at University of Ghilizane, and **Dr. Driss RAOUTI** teacher at the University of Saida, for taking the time for revise my thesis and to serving on my committee and for their valuable advice and help. I am thankful that in the midst of all their activities, they accepted to be members of the reading committee.

My thanks go also to the people who helped me to develop and realize this thesis, as well as to all those who helped me near or far to accomplish this work, especially **Mr. Khanfar Mourad**.

Finally, I especially thank my parents, for their unconditional support throughout these long years of study.

List of Publications

Journal Publications

1. **Tounsi Kamel**, Djehbar Abdelkader, Barkat Said, M. Al-Hitmi, and Atif Iqbal," Sliding Mode Control Based DTC of Sensorless Parallel-Connected Two Five-Phase PMSM Drive System", Journal of Electrical Engineering & Technology, vol. 13, no. 3, pp.1185-1201, 2018.

2. **Tounsi Kamel**, Djehbar Abdelkader, Barkat Said, Sanjeevikumar Padmanaban, and Atif Iqbal," Extended Kalman Filter Based Sliding Mode Control of Parallel-Connected Two Five-Phase PMSM Drive System", Electronics, vol. 7, no. 2, pp. 1-19, 2018.

Conference Proceedings

1. **Tounsi Kamel**, Djehbar Abdelkader, and Barkat Said, "Vector Control of Five-Phase Permanent Magnet Synchronous Motor Drive", International Conference on Electrical Engineering (ICEE2015), Boumerdes, pp. 1-4, December 13–15, 2015.

2. **Tounsi Kamel**, Djehbar Abdelkader, and Barkat Said, "DTC-SVM of Five-Phase Permanent Magnet Synchronous Motor Drive", The 8th International Conference on Modelling, Identification and Control (ICMIC 2016), Medea, pp. 1-6, November 15-17 2016.

3. N Bounasla, S Barkat, E Benyoussef, and **K Tounsi**," Sensorless Sliding Mode Control of A Five-Phase PMSM Using Extended Kalman Filter", The 8th International Conference on Modelling, Identification and Control (ICMIC 2016), Medea, pp. 1-6, November 15-17, 2016.

4. **Tounsi Kamel**, Abdelkader Djahbar, Abdallah Zegaoui, M Boutoubat, A Aissa Bokhtache, H Allouache, and M Aillerie, " A Novel Concept of Electrical Drives Based on Two Five-Phases PMSM Connected in Parallel and Supplied by a Single Inverter", The 8th International Conference on Modelling, Identification and Control (ICMIC 2016), Medea, pp. 1-6, November 15-17 2016.

5. **Tounsi Kamel**, Djehbar Abdelkader, Barkat Said, and Atif Iqbal," Direct Torque Control Based on Artificial Neural Network of a Five-Phase PMSM Drive", International Conference on Artificial Intelligence in Renewable Energetic Systems, Tipaza, Algeria, pp. 1-7, 22-24 October 2017.

Abstract

The work presented in this thesis develops a new concept for independent control of two five-phase permanent magnet synchronous machines (PMSMs) connected in parallel and fed by a single five-leg inverter. The proposed scheme presented a reduction in the number of inverter legs, when compared to an equivalent two-machine three-phase drive system. It can be seen from the developed model only two stator current components (d-q) are responsible for torque and flux production, while other components (x-y) do not used. Through an appropriate phase transposition of the stator windings, the other components (x-y) it can be used to connect in parallel the other machine in such a way that the torque and flux producing current components of the first machine do not affect the production of torque and flux of the second machine and vice versa.

The purpose decoupled control strategies for the two five-phase PMSM connected in parallel are made by using filed oriented control (FOC), conventional direct torque control (DTC) and DTC-SVM; all are based on sliding mode control (SMC). The SMC law improve the stability and robustness of parallel-connected two five-phase PMSMs with parameter variations, reduce the ripples of the torque and flux as well as improve the dynamic performance. In order to increase the proposed drive robustness and decrease the number of sensors as well as its cost, an Extended Kalman Filter (EKF) and sliding mode observer (SMO) scheme have been adopted. The results show better speed tracking performance at both dynamic and steady state, acceptable estimations errors, robustness in different tests.

Keywords: Multi-machine connected in parallel, Five-phase PMSM, Space vector modulation, Filed oriented control, Direct torque control, Sliding mode control, Observer, Extended Kalman Filter, Sliding mode observer.

Résumé

Le travail présenté dans cette thèse développe un nouveau concept pour deux machines synchrones à aimants permanents à cinq phases (PMSM) connectées en parallèle et alimentées par un seul onduleur à cinq bras. Le schéma proposé représente une réduction du nombre de bras de l'onduleur, par rapport à un système d'entraînement triphasé à deux moteurs équivalent. On peut voir à partir du modèle développé que seuls deux composants du courant statorique (d-q) sont responsables de la production du couple et flux alors que d'autres composants (x-y) ne sont pas utilisés. Grâce à une transposition de phase appropriée des enroulements du stator, les autres composants (x-y) peuvent être utilisés pour connecter en parallèle l'autre machine de telle manière que le couple et flux produisant les composantes du courant la premier machine n'affecte pas la production de couple et flux de la deuxième machine et vice versa.

Le but des stratégies de contrôle découplées pour les deux MSAP à cinq phases connectés en parallèle est réalisée en utilisant la commande par orientation de flux (FOC), commande directe du couple (DTC) et DTC-SVM basés sur le contrôle par mode glissant (MG). La loi MG améliore la stabilité et la robustesse des PMSM à cinq phases connectées en parallèle lors variations paramétriques, réduit les ondulations du couple et flux ainsi que améliorer les performances dynamiques. Afin d'augmenter la robustesse du system et réduire le nombre de capteurs, ainsi que son coût, un filtre de Kalman étendu (EKF) et un observateur par mode glissant (OMG) ont été adoptée. Les résultats montrent une meilleure performance de suivi de la vitesse à la fois en régime dynamique et permanent des erreurs d'estimation acceptables et une robustesse dans les différents tests.

Mots-clés: Multi-machines connectées en parallèle, MSAP à cinq phases, Modulation vectorielle, Commande par orientation de flux, Contrôle direct de couple, Commande par mode glissant, Observateur, Filtre Kalman étendu, Observateur par mode glissant.

ملخص

يهدف العمل المعروض في هذه الرسالة على تطوير مفهوم جديد لآلتين متزامنتين ذات مغناطيس دائم بخمسة اطوار (PMSMs) متصلة على التوازي ويتم تغذيتها بواسطة منوب واحد خماسي الاذرع. من المخطط المقترح يتبين أنه تم تقليل عدد أذرع المنوب، مقارنة بنظام مكافئ بمحركين ذي ثلاثي أطوار. يمكن ملاحظة ذلك من النموذج الرياضي أن المكونين (d-q) هما المسؤولان عن إنتاج عزم الدوران والتدفق المغنطيسي بينما لا يتم استخدام المكونات الأخرى (x-y). يمكن بفضل التحويل المناسب لربط ملفات المحركين باستخدام المكونات (y-x) لتوصيل المحركات الاخرى بشكل متوازن بحيث لا يؤثر على عزم الدوران والتدفق المغنطيسي الذي ينتج عن المكونات (d-q) للمحرك الثاني على عزم الدوران والتدفق المغنطيسي الخاص بالمحرك الثاني والعكس صحيح.

يتم تحقيق التحكم المنفصل لآلتين متزامنتين ذات مغناطيس دائم بخمسة اطوار (PMSMs) المتصلة بالتوازي باستخدام التحكم في التدفق الموجه (FOC) والتحكم المباشر بعزم الدوران (DTC) التقليدي وDTC-SVM استنادًا إلى التحكم ذو النمط الانزلاقي. يعمل قانون التحكم ذو النمط الانزلاقي على تحسين استقرار ومتانة PMSM ذات الخمس اطوار المتصلة بالتوازي مع التغيرات المفاجئة في معاملات المحرك، يقلل من تموجات العزم والتدفق المغنطيسي، وتحسين الأداء الديناميكي. من أجل زيادة متانة النظام وتقليل عدد أجهزة الاستشعار، وكذا تكلفة النظام، يتم اعتمد مرشح كالمان الموسع (EKF) ونظام مراقبة ذو النمط الانزلاقي (SMO). تظهر النتائج أداء تتبع ديناميكي أفضل وأكثر استقرارًا، وأخطاء تقدير مقبولة، وقوة في اختبارات مختلفة.

الكلمات المفتاحية: محركات متعددة متصلة بشكل متواز، PMSM ذات خمس اطوار، تعديل طول النبضة الشعاعي، التحكم في التدفق، التحكم المباشر بالعزم، تحكم ذو النمط الانزلاقي، مراقب، مرشح كالمان، مراقب ذو النمط الانزلاقي.

List of Abbreviations

AC	Alternative Current.
DC	Direct Current.
PMSM	Permanent Magnet Synchronous Machine
SPMSM	Surface Permanent Magnet Synchronous Machine
IPMSM	Interior Permanent Magnet Synchronous Machine
PM	Permanent Magnet
VSI	Voltage Source Inverters
FOC	Field Oriented Control
DTC	Direct Torque Control
SVM	Space Vector Modulation
PWM	Pulse Width Modulation
PI	Proportional-Integral
SMC	Sliding Mode Control
EKF	Extended Kalman Filter
SMO	Sliding Mode Observer

List of Symbols

v_{abcde}	Voltages.
i_{abcde}	Currents.
Φ_{abcde}	Flux linkage.
r_s	Stator resistance.
Φ_f	Amplitude of fundamental of the permanent magnet flux linkages.
L_s	Stator inductance.
L_{ls}	Leakage inductance.
θ	Rotor position.
$L_{ls} + L_{ms}$	Self-inductance of phase.
v_d, v_q, v_x, v_y	Stator voltages in the *d-q-x-y* axes.
i_d, i_q, i_x, i_y	Stator currents in *d-q-x-y* axes.
v_α, v_β, v_x, v_y	Stator voltages in the *α-β-x-y* axes.
i_α, i_β, v_x, v_y	Stator currents in *α-β-x-y* axes.
v_{z1}, v_{z2}, v_{z3}, v_{z4}	Stator voltages in the z1-z2-z3-z4 axes.
i_{z1}, i_{z2}, v_{z3}, v_{z4}	Stator currents in the z1-z2-z3-z4 axes.
L_d, L_q	Inductances in the *d-q* axes.
$\Phi_{ds}, \Phi_{qs}, \Phi_{xs}, \Phi_{ys}$	Flux linkage in the *d-q-x-y* frame.
$\Phi_{\alpha s}, \Phi_{\beta s}, \Phi_{xs}, \Phi_{ys}$	Flux linkage in the *α-β-x-y* frame.
$\Phi_{z1s}, \Phi_{z2s}, \Phi_{z3s}, \Phi_{z4s}$	Flux linkage in the z1-z2-z3-z4 frame.
ω	Electrical speed.

Ω	Mechanical speed.
T_{em}	Electromagnetic Torque.
J	Inertia coefficient.
f_r	Friction coefficient.
p	Number of poles pairs.
T_l	External load torque.
v_{dc}	Voltage of the dc-link.
$V_a \ V_b \ V_c \ V_d \ V_e$	Inverter leg voltages.
$v_a \ v_b \ v_c \ v_d \ v_e$	Phase to neutral voltages.
V_{no}	Voltage between star point of load and negative rail of dc bus.
$S_a \, S_b \, S_c \, S_d \, S_e$	Switching functions.
T_l, T_m , and T_0	Dwell times of large, medium and zero space.
Ts	Switching period
q	Number of phase.
C	Transformation matrix to α-β-x-y
R	Transformation matrix to d-q-x-y
D	Rotational transformation matrix.
j	Number of machine.
$k_{i\Omega} \, k_{p\Omega}$	Regulator gain of the speed.
$\xi_\Omega \ , \xi_{T_{em1}}, \xi_{T_{em2}} \ \ \xi_{\Phi_{s1}}, \xi_{\Phi_{s2}}$	Damping ratios.
$\omega_{0\Omega} \ \ \omega_{0T_{em1}}, \omega_{0T_{em2}} \ \ \omega_{0\Phi_{s1}}, \omega_{0\Phi_{s2}}$	Natural frequency.
δ	Angle between the stator and rotor flux linkages.

S(x).	Sliding surface.
λ	Positive coefficient.
r	Relative degree.
u_{eqc}	Equivalent control
u_{dic}	Discontinuous control.
V	Lyapunov function.
k	Control gain.
u_{eqc}	Equivalent control.
$k_{\Omega 1}$ and $k_{\Omega 2}$	Positive gains of the speed.
$k_{dsj}, k_{qsj}, k_{xsj}$ *and* k_{ysj}	Positive gains of the currents.
k_{Temj}, $k_{\Phi sj}$	Positive gains of the torque and flux.
u_k , y_k	System input vector and output vector.
f and c	Nonlinear functions
w_k v_k	Process and Measurement noise.
$E\{w\ w^T\}$ $E\{v\ v^T\}$	Process noise and measurement noise
P , Q, and R	Covariance matrices.
x_{k+1} and y_k	Actual state and measurement vectors.
$\hat{x}_{k+1}$ and $\hat{y}_k$	Approximate state and measurement vectors.
A_{jk} , B_{jk}	Discrete system matrix and discrete input matrix
$\hat{x}_k$	State estimation at step *k*.

F_k	Jacobian matrix of partial derivatives of *f*.
C_k	Jacobian matrix of partial derivatives of *c*.
K	Filter coefficients.
I	Unity matrix.
T_e	Sample time.
k, k_1	Observer gains of SMO.

List of Figures

List of Table

Table of Contents

General Introduction

General Introduction

Nowadays, the AC machines have replaced the DC machines in industry applications due to their multiple advantages such as the reliability and the lack of commutator and brushes, which make them able to work under unfriendly conditions.

Recently, multi-phase (greater than three-phases) AC machine drives have gained an increasing attention for a wide variety of industrial applications such as electric vehicles, aerospace applications, naval propulsion systems, and paper mills. Major advantages of using a multi-phase machine over three-phase machine are reducing the amplitude of torque and current pulsations, increasing the frequency of torque pulsations, reducing the stator current per phase without increasing the stator voltage per phase, lowering the DC link current harmonics, higher reliability, and fault tolerance capability [1-3]. In addition, there are three or more possible connections for the windings, which is able to enlarge the speed operation range compared with three-phase machines [4].

Multi-phase machines include either induction or synchronous machines. However, compared with induction machine, under the synchronous machines category, the permanent magnet synchronous machine (PMSM) possesses many advantages such as high power density, better torque generating capability, and high conversion efficiency [5]. The rotor excitation of the PMSM is provided by permanent magnets; therefore, the PMSM do not need extra DC power supply or field windings in order to provide rotor excitations. Consequently, the power losses related to the filed windings are eliminated and PMSM efficiency is improved. In addition, the magnets and redundant teeth in stator allow magnetic decoupling from the different groups of windings [6-7].

An overview of existing multi-machine drive systems and proposed one

Multi-machine drive is the one that consists of more than one machine; it is available in two configurations. The first one consists of a common DC-link feeding a number of three-phase voltage source inverters (VSI) connected in parallel, each inverter feeding a three-phase AC machine (Fig. 1(a)). The speed of each machine can be controlled independently using its own VSI and an appropriate control algorithm. The second method consists of one inverter (Fig. 1(b)), which feeds parallel-connected three-phase machines. This system is useful in traction applications such as locomotives, ships and electric vehicles where. However, in this structure, machines have to be

identical, operate under the same load torque, and have exactly the same angular speed, which is the major disadvantage of this system.

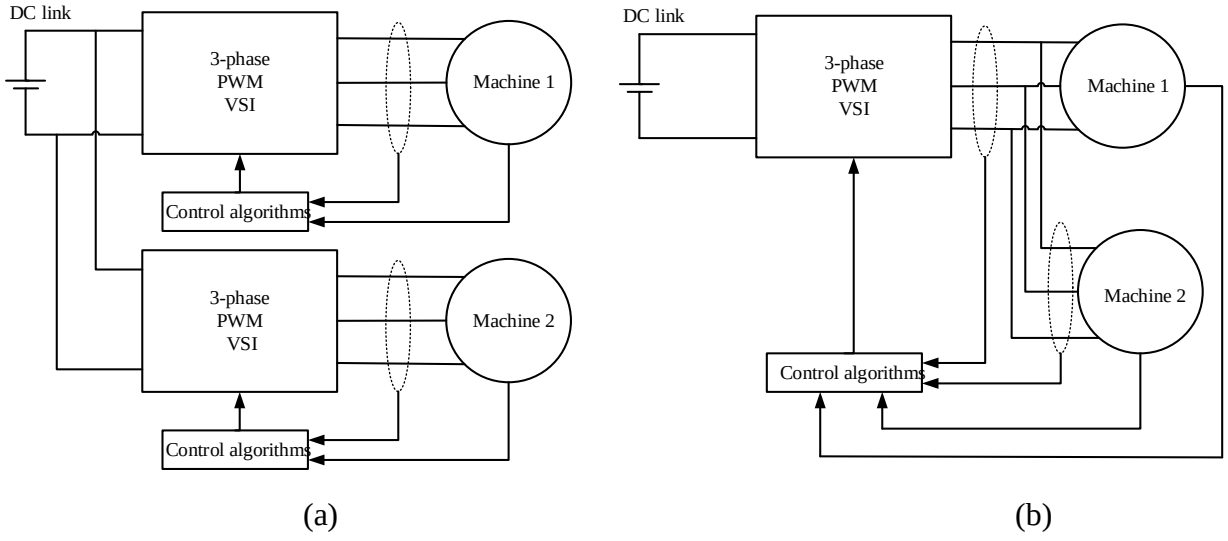

Fig. (1): Standard configurations of a two-machine drive system.

To overcome these drawbacks a new configuration using multi-phase multi-machine fed by one multi-legs VSI have been proposed recently in the literature[8][9]. In multi-phase machine there are more than direct and quadrature current components. Actually, to control the torque and flux of any multi-phase machine only direct and quadrature current components are used; the remaining components can be used to control the others machines, which are fed by a single multi-leg inverter [8]. This allows parallel/series connection of a number of multi-phase machines with an appropriate phase transposition between each phases.

Recently, the parallel/series-connected multi-machine system fed by a single supply becomes strongly suggested due to the following benefits: low cost drive, compactness, and lightness [8-11]. In the series-connected system, both beginning and ending of each phase should be brought out to the terminal box of each multi-phase machine, these results in system complexity and poor efficiency due to higher losses. As a suitable alternative, the parallel connection of multi-phase machines has been suggested in [8][10]. Fig. (2) gives an idea in how multiple multi-phase machines can be connected in parallel and fed by the same inverter.

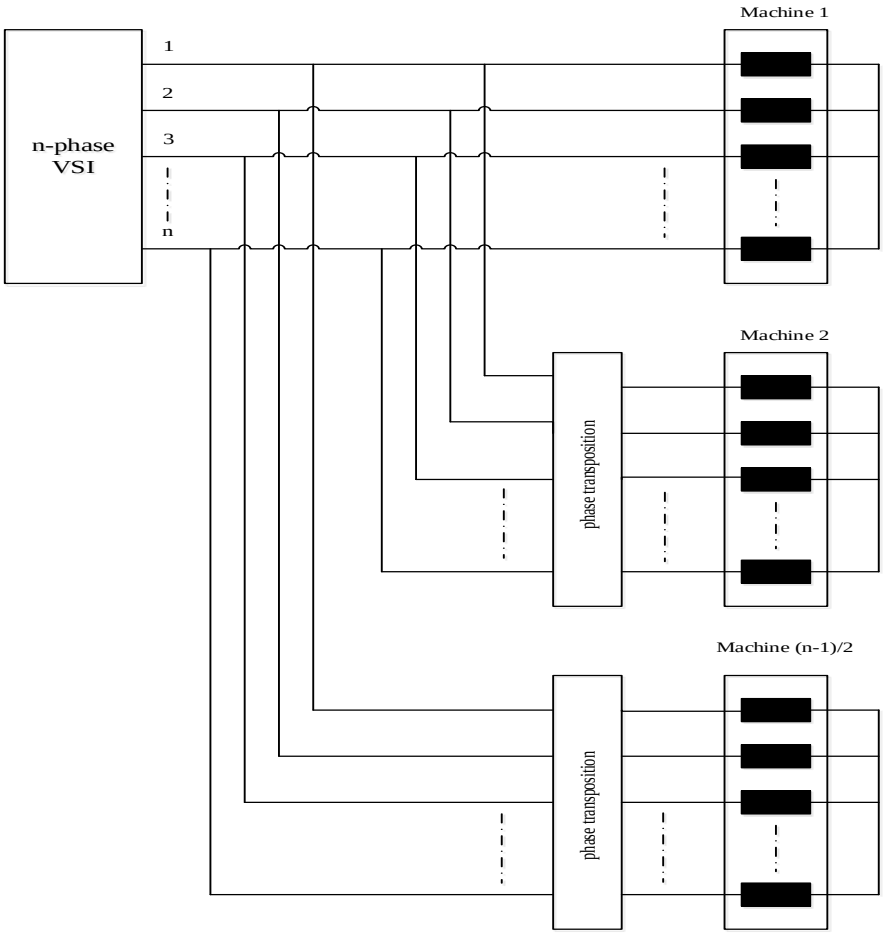

Fig. (2): Supply of (n-1)/2 machine stator windings, connected in parallel, from an n-phase VSI.

Control of multi-phase PMSM connected in parallel

The development of modern semiconductor devices and power electronic converters allow to operate the machines with adjustable frequency by supplying them through a voltage source inverter (VSI). In the recent years, different control methods including direct torque control (DTC), field oriented control (FOC), and scalar control methods have been proposed to control AC drives. Nowadays, FOC and DTC controls are more suggested in the literature.

The purpose of the filed oriented control is to control the five-phase PMSM as a DC machine with independent excitation, which has a natural decoupling between the flux (the excitation current) and the torque (the armature current). The vector representation of the machine quantities makes it valid to work in both steady and dynamic conditions; this achieves a good transient response.

Compared to FOC, DTC eliminates the internal current loops and PWM block, hence eliminating the delay caused by current regulators. It directly selects voltage vectors according to

the error between the reference and the estimated values of the torque and flux, so it is possible to directly control the inverter switching states in order to reduce the torque and flux error within chosen band limits [12]. However, the main problem of this method is the high level of torque ripples, variable switching frequency, and acoustic noises [13]. In order, to overcome these drawbacks, a space vector modulation (SVM) and two regulators (for the torque and flux) are implemented to replace the switching table of the voltage vector selection and provide a constant inverter switching frequency [14-18].

The two control strategies FOC and DTC-SVM are based on PI-controllers. However, some factors such as neglected dynamics, parameter variations, friction forces, and load torques are the main disturbances and uncertainties that can affect the effective functioning of the drive system. [19, 20-23]

To overcome this problems, especially to enhance stability and robustness of the control scheme a sliding mode control (SMC) has been proposed. The SMC is a nonlinear control method known to have robust control characteristics under restricted disturbance conditions or when there are limited internal parameter modeling errors as well as when there are some nonlinear behaviors. [24-28] 26-29]. The robustness of the SMC is guaranteed usually by using a switching control law. Unfortunately, this switching strategy often leads to a chattering phenomenon. In order to mitigate the chattering phenomenon, a common method is to use smooth function instead of the switching function.

On the other hand, those control structures required the installation of a speed sensor on each shaft of the multi-machine drive that poses some technical problems related to their use, since they are fragile and expensive. The replacement of mechanical sensors with software tools makes the control more efficient and less expensive. Indeed, in a five-phase PMSM a solution that consists of replacing these sensors with estimators or observers has become promising and effective. From all observers the extended kalman filter (EKF) and sliding mode observer (SMO) are the most used.

Objectives

The principal objectives of the research work presented in this thesis are:

1- To carry out a comprehensive analytical study suggesting FOC and DTC based independent controls for parallel-connected two five-phase PMSMs supplied by a single voltage source inverter,

2- Design of a five-phase space vector modulation suitable for two PMSM fed by a single inverter,

3- To improve the performance of the parallel-connected two five-phase PMSMs control by using sliding mode control, which is ameliorated the robustness and the stability of control algorithm.
4- Implementation of sensorless FOC and DTC of parallel-connected two five-phase PMSMs by using extended kalman filter and sliding mode observer.

Organization

After the general introduction, which gives an overview about the existing multi-machine drive systems and proposed one, which will be treated in this thesis concerning the control of the two five-phase PMSMs. Therefore, the main body of the thesis is structured as follows:

Chapter 1 presents a literature review in which advantages of multi-phase machines over traditional three-phase machines are highlighted and issues relating to modeling of two five-phase PMSMs connected in parallel are discussed. Modeling of the five-phase PMSM is explained, and the transformation of the model of a five-phase PMSM to an arbitrary reference frame is discussed and the resulting equations are given.

Chapter 2 is dedicated to the decoupled control of the five-phase PMSM connected in parallel by using FOC, conventional DTC and DTC-SVM approaches. It is shown that the control of each machine in the group can be independent and decoupled from the others, even if they are fed by a single VSI.

Chapter 3 presents nonlinear control design using sliding mode control of parallel-connected two five-phase PMSMs, in order to improve the performances of FOC and DTC-SVM methods and get more robust control schemes.

Chapter 4 presents control without mechanical sensors of parallel-connected two five-phase PMSMs. The extended kalman filter and sliding mode observer are adopted to determine the state variables of the system from measuring stators voltages and currents of each machine.

Finally, the thesis will be closed by a general conclusion, which is presenting the different results obtained and the constraints encountered. In addition, we will present the possible perspectives for the continuation of this research.

Chapter 1

Modeling of Parallel-Connected Two Five-Phase PMSMs Drive System

1.1 Introduction

This chapter focuses on modeling of a five-phase permanent magnet synchronous machine and its voltage source inverter (VSI). First, a general description of multi-phase machine in term of (description, types, advantages and disadvantages), will be presented. The five-phase PMSM is represented by a system of five electrical and magnet equations in addition to a mechanical equation. Working with these six equations is not easy even with the digital tool, so using a transformation is essential. The transformations matrix allows the transition from a five-phase system to an equivalent four-phase (d-q-x-y) system, which is simpler and easy for studying. Second, the space vector model of the five-phase inverter is analyzed, and then PWM technique based on SVM strategy is discussed.

At last, the parallel-connected two-machine five-phase PMSM drive system fed by a single five-phase voltage source inverter with appropriate phase transposition, which leads to complete decoupling of the flux/torque of one machine from the flux/torque of other machine.

1.2 Multi-phase Machine

The increase in the number of phases of electrical machines recognized to be suitable for specific applications. Indeed, ship propulsion, more-electric aircraft, hybrid electric vehicles and battery-powered electric vehicles [30]; have been rapidly emerged during the last couple of years as the main potential application areas for multi-phase machine drives [31]. There are usually two types of multi-phase machines, according as the number of stator phases or multiple of three-phase. They can be classified into two groups, which called multi-phase machines type 1 and multi-phase machines type 2 [32].

1.2.1 Multi-phase Machines "Type 1"

Multi-phase machines "Type 1" are the machines with a number of stator phases (q) multiple of three, so that they can be grouped in n (n = 2, 3, 4,...) star three-phase (multi-star three-phase machines). However, for a given number of phases, there are several possible configurations according to the angle α between the two adjacent phases. A dual-star machine (q = 6) whose stars are shifted by α = 30 (asymmetrical) has characteristics different from those of a machine whose stars are shifted by α = 60 (symmetrical). To differentiate the possible configurations, we can introduce the definition by the figures as follows:

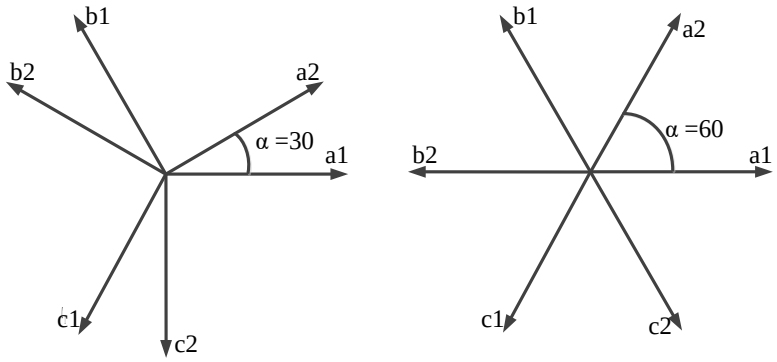

Fig. (1.1): Multi-phase machines "type 1".

1.2.2 Multi-phase Machines "Type 2"

Multi-phase machines "Type 2" are the machines with an odd number of stator phases (q) as indicated in Fig (1.2), with α denotes the angular offset between two adjacent phases; the q phases are then regularly shifted by 2π /q.

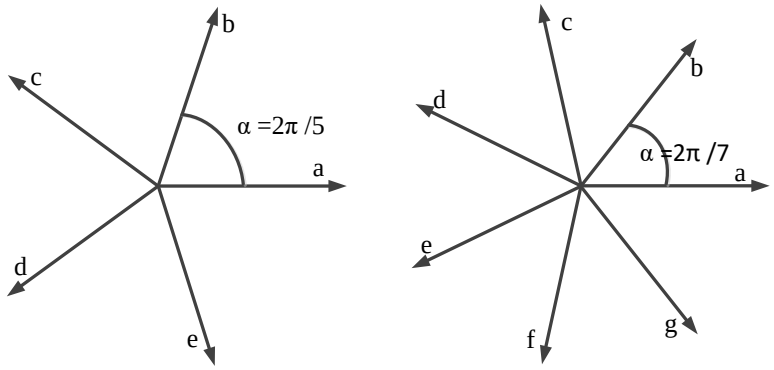

Fig. (1.2): Multi-phase machines "type2".

1.3. Advantages and Disadvantages of Multi-phase Machines

1.3.1 Advantages

Early interest in multi-phase machines was triggered by the need to reduce torque pulsations caused by inverter. Other advantages of multi-phase machines compared to a three-phase machines have been cited in the literature [19-33]:

- **Torque:** multi-phase machines also allow reducing torque ripple (the frequency of torque pulsation increases and its amplitude decreases), which causes improved characteristics noise-vibration [40] due to the elimination of the space and current time harmonics [32].
- **Degrees of freedom:** three-phase machine can utilize only the fundamental component to develop torque, while a five-phase machine can utilize both the fundamental and the third harmonic components. By extension, a seven-phase machine can be controlled to utilize the first, third and fifth harmonics for torque production, while in a nine-phase machine it is possible to use injection

of the third, the fifth and the seventh current harmonics. This feature makes more additional degrees of freedom, which can be utilized to enhance the torque production through injection of higher order current harmonics [32][41].

- **Power segmentation:** an increase in the number of phases supplying the machine results in a reduction of the current per phase without increasing the voltage per phase, which means a reduction in the power per phase compared to an equivalent three-phase machine. This means that there is no need for parallel or series power switches in high power, resulting in a lower component number and a less complex inverter structure. This improved the reliability for high power applications [32] [41-42].
- **Fault tolerance:** It is intuitive and common to low-power applications that a multi-phase design guarantees a higher system reliability and fault tolerance. In fact, in case of a faulty phase, the multi-phase system is capable of continuing operation, even without changes in control system strategies, although with degraded operation and at reduced power. This is an essential requirement for safety-critical applications (such as in vehicle electric propulsion drives), and also in those cases where a drive trip and the consequent driven equipment stop causes important economic losses due to production discontinuity [43].

1.3.2 Disadvantages

Multi-phase machines offer some advantages over conventional three-phase structures. However, their use requires certain special precautions, some constraints that must be taken into account to derive maximum profits as [31], [44]:

-The production of large stator current harmonics, if the machine is fed by multi-legs VSIs. These generate additional losses resulting in an increase in the size and cost of the machine-inverter.

-The high cost of the assembly (machine-converter), due to the increase in the number of components compared to three-phase drive.

1.4 Generality about Five-Phase PMSM

1.4.1 Description

Synchronous machines include all the machines that the rotor speed is equal to the speed of the rotating stator field. In case of PMSM, the rotor excitation is provided by permanent magnets (PM) [45]. The PMSM does not need extra DC power supply or field windings in order to provide rotor excitation. Therefore, the power losses related to the filed windings are eliminated in this kind of machines. In addition, the magnets and redundant teeth in stators allow magnetic decoupling from the different groups of windings [7-8][46].

The stator: is similar to that of induction machine, it consists of a five-phase winding distribution, such that the electromotive forces generated by the rotation of the rotor field are sinusoidal or trapezoidal. This winding is represented by five axes (a, b, c, d, e); two adjacent phases are shifted by 72˚.

The rotor: it consists of permanent magnets. Permanent magnets have the advantage of eliminating: brushless, rotor losses, as well as no need no excitation current (improve the efficiency of the machine). In addition, no need to control the amplitude of the rotor flux. In PM machines, the magnets can be placed in two different ways on the rotor. Depending on the PM placement, they are called either as surface permanent magnet machine or interior permanent magnet machine.

Surface mounted type: the surface mounted magnet rotor (see Fig. 1.3-a) are widely used due to: its simple structure and easy to manufacture [45] [47], which gives a constant air-gap (the permeability of the permanent magnet is almost that of the air, thus the magnetic material becoming an extension of the air-gap $L_d=L_q$) [48]. However, in high speed (higher than 3000 rpm) some dangers related to the fact that the magnets are fixed on the rotor surface (usually with an adhesive); this drawback gives a lower structural integrity and mechanical robustness. In addition, these magnets are not protected against the field created by the stator [47][49].

Inset magnet type: the inserted type magnets are also mounted on the surface of the rotor. However, the spaces between the magnets are filled with iron core (see Fig. 1.3-b). The alternation between the iron and the magnets causes the effect of saliency ($L_q>L_d$). It produces reluctance torque in addition to the mutual torque. Reluctance torque is produced due to the magnet saliency in the quadrature and the direct axis magnetic paths. Burying the magnets inside the rotor of the IPMSM provides a mechanically robust rotor since the magnets are physically contained and protected [45],[50].

Interior magnet type: the magnets are integrated in the rotor iron (Fig. 1.3-c): the machine it has a salient poles, which provide an additional torque (reluctance torque) in addition to the synchronous torque to improve the operating range of the machine. In this case, the magnetic circuit of the rotor is anisotropic; the inductances strongly depend on the position of the rotor. This type of machine is more robust mechanically and allows operation in higher speeds. On the other hand, it is protected mechanically and magnetically, and naturally more expensive to manufacture [45] [47-48].

The cross sections of the interior PM (IPM) type, surface mounted permanent magnet (SPM), and inset type PM synchronous machines are shown in Fig. (1.3).

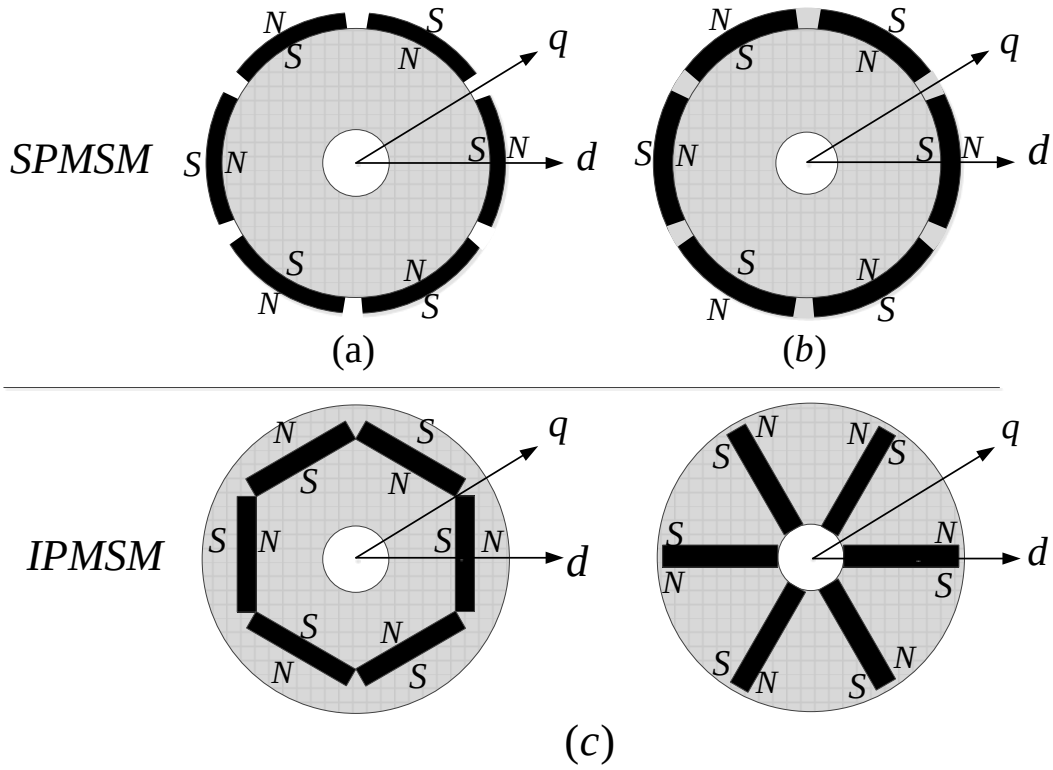

Fig. (1.3): Different placements of permanent magnets on the rotor shaft: (a) Surface Mounted, (b) Inset magnet type, (c) Interior magnet type.

1.5 Modeling of the Five-Phase PMSM

The five-phase PMSM consists of stator with five-phase windings spatially shifted by 72 electrical degrees and rotor with permanent magnets. The stator is star-connected with isolated neutral point, which eliminates the zero sequence voltages. To develop the machine model, the following assumptions are adopted [41][45] [51]:

-The air-gap is uniform;

-The windings resistances and inductances are constant;

-The B-H curve of the iron core is linear and so the main flux saturation can be neglected;

-Iron core losses, magnetic saturation and eddy currents are neglected;

-The currents and voltages are assumed to be sinusoidal;

-Thermal effect on the permanent magnets is omitted.

The studied machine is described in the space by five identical windings for the stator phases whose are distant two by two of an electrical angle equal to $2\pi/5$. In addition, the rotor is a permanent magnet as shown in Fig. (1.4).

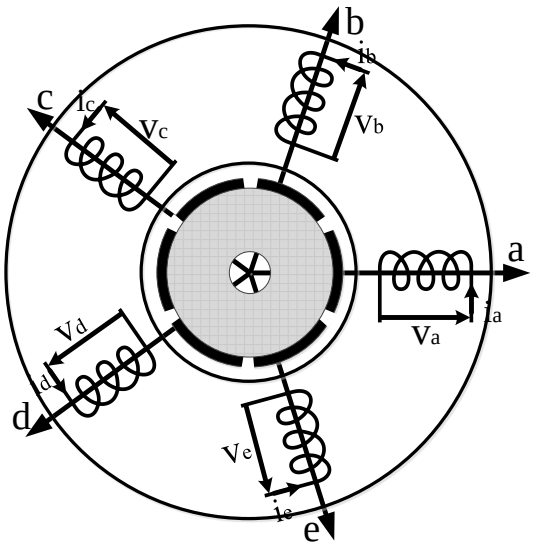

Fig. (1.4): Schematic representation of a five-phase PMSM.

1.5.1 Five-phase Model in Naturel Frame

Five-phase PMSM can then be described with the following voltage and flux linkage equations in matrix form:

$$\begin{aligned}\left[v_{abcde}\right] &= \left[r\right]_s \left[i_{abcde}\right] + \frac{d\left[\Phi_{abcde}\right]}{dt} \\ \left[\Phi_{abcde}\right] &= \left[L_s\right]\left[i_{abcde}\right] + \left[\Phi_{fabcde}\right]\end{aligned} \tag{1.1}$$

with

$$\begin{aligned}\left[v_{abcde}\right] &= \left[v_{as}\ v_{bs}\ v_{cs}\ v_{ds}\ v_{es}\right]^t \\ \left[i_{abcde}\right] &= \left[i_{as}\ i_{bs}\ i_{cs}\ i_{ds}\ i_{es}\right]^t \\ \left[\Phi_{abcde}\right] &= \left[\Phi_{as}\ \Phi_{bs}\ \Phi_{cs}\ \Phi_{ds}\ \Phi_{es}\right]^t \\ \left[r\right]_s &= diag\left[r_s\ r_s\ r_s\ r_s\ r_s\right]^t\end{aligned}$$

The rotor flux is given by:

$$\left[\Phi_{fabcde}\right] = \Phi_f \begin{bmatrix} \cos(\theta) \\ \cos(\theta - 2\pi/5) \\ \cos(\theta - 4\pi/5) \\ \cos(\theta + 4\pi/5) \\ \cos(\theta + 2\pi/5) \end{bmatrix} \tag{1.2}$$

Φ_f is the amplitude of fundamental of the permanent magnet flux linkages and θ is the rotor position.

The matrix of stator inductances (including stator self and mutual inductances) is given by:

$$\left[L_s\right]=\begin{bmatrix} L_{ls}+L_{ms} & L_{ms}\cos(2\pi/5) & L_{ms}\cos(4\pi/5) & L_{ms}\cos(4\pi/5) & L_{ms}\cos(2\pi/5) \\ L_{ms}\cos(2\pi/5) & L_{ls}+L_{ms} & L_{ms}\cos(2\pi/5) & L_{ms}\cos(4\pi/5) & L_{ms}\cos(4\pi/5) \\ L_{ms}\cos(4\pi/5) & L_{ms}\cos(2\pi/5) & L_{ls}+L_{ms} & L_{ms}\cos(2\pi/5) & L_{ms}\cos(4\pi/5) \\ L_{ms}\cos(4\pi/5) & L_{ms}\cos(4\pi/5) & L_{ms}\cos(2\pi/5) & L_{ls}+L_{ms} & L_{ms}\cos(2\pi/5) \\ L_{ms}\cos(2\pi/5) & L_{ms}\cos(4\pi/5) & L_{ms}\cos(4\pi/5) & L_{ms}\cos(2\pi/5) & L_{ls}+L_{ms} \end{bmatrix} \quad (1.3)$$

L_{ls} is the leakage inductance. $L_{ls}+L_{ms}$ is the self-inductance of a phase, $L_{ms}\cos(2\pi/5)$ and $L_{ms}\cos(4\pi/5)$ are mutual inductance between phases.

1.5.2 Model of the Five-Phase PMSM Model in Stationary Frame

The following transformation matrix is therefore applied to the stator five-phase winding [52]:

$$[C]=\frac{2}{5}\begin{bmatrix} 1 & \cos(\alpha) & \cos(2\alpha) & \cos(3\alpha) & \cos(4\alpha) \\ 0 & \sin(\alpha) & \sin(2\alpha) & \sin(3\alpha) & \sin(4\alpha) \\ 1 & \cos(2\alpha) & \cos(4\alpha) & \cos(6\alpha) & \cos(8\alpha) \\ 0 & \sin(2\alpha) & \sin(4\alpha) & \sin(6\alpha) & \sin(8\alpha) \\ 1/2 & 1/2 & 1/2 & 1/2 & 1/2 \end{bmatrix} \quad (1.4)$$

where $\alpha = {}^{2\pi}\!/_{5}$

The model of the five-phase PMSM in a stationary α-β -x-y frame is given as:

$$\begin{aligned} \frac{di_{\alpha s}}{dt} &= (-r_s i_{\alpha s}+\omega\Phi_f\sin(\theta)+v_{\alpha s})/L_s \\ \frac{di_{\beta s}}{dt} &= (-r_s i_{\beta s}-\omega\ \Phi_f\cos(\theta)+v_{\beta s})/L_s \\ \frac{di_{xs}}{dt} &= (-r_{sj} i_{xs}+v_{xs})/L_{ls} \\ \frac{di_{ys}}{dt} &= (-r_s i_{ys}+v_{ys})/L_{ls} \end{aligned} \quad (1.5)$$

The flux components can be obtained from:

$$\begin{aligned} \Phi_{\alpha s} &= L_s i_{\alpha s}+\Phi_f\cos(\theta\ ) \\ \Phi_{\beta s} &= L_s i_{\beta s}+\Phi_f\sin(\theta\ ) \\ \Phi_{xs} &= L_{ls} i_{xs} \\ \Phi_{ys} &= L_{ls} i_{ys} \end{aligned} \quad (1.6)$$

The electromagnetic torque equation is given by:

$$T_{em}=\frac{5p}{2}(\Phi_{\alpha s} i_{\beta s}-\Phi_{\beta s} i_{\alpha s}) \quad (1.7)$$

1.5.3 Five-phase PMSM Model in Synchronous Frame

In order to simplify the model, it is necessary to apply a coordinate transformation that will remove the time varying inductances. The coordinate transformation is utilized to transfers the variables of the five-phase machine into a reference frame (d-q-x-y). The following transformation matrix is therefore applied to the stator five-phase winding [52]:

$$[R]=\frac{2}{5}\begin{bmatrix} \cos(\theta) & \cos(\theta-2\pi/5) & \cos(\theta-4\pi/5) & \cos(\theta+4\pi/5) & \cos(\theta+2\pi/5) \\ \sin(\theta) & \sin(\theta-2\pi/5) & \sin(\theta-4\pi/5) & \sin(\theta+4\pi/5) & \sin(\theta+2\pi/5) \\ \cos(\theta) & \cos(\theta+4\pi/5) & \cos(\theta-2\pi/5) & \cos(\theta+2\pi/5) & \cos(\theta-4\pi/5) \\ \sin(\theta) & \sin(\theta+4\pi/5) & \sin(\theta-2\pi/5) & \sin(\theta+2\pi/5) & \sin(\theta-4\pi/5) \\ 1/2 & 1/2 & 1/2 & 1/2 & 1/2 \end{bmatrix} \tag{1.8}$$

By applying the above transformation to the stator voltages and stator flux linkages equations, The model of the five-phase PMSM in a rotating *d-q-x-y* frame can be expressed as:

$$\begin{aligned} \frac{di_{ds}}{dt} &= (-r_s i_{ds} + \omega L_q i_{qs} + v_{ds}) / L_d \\ \frac{di_{qs}}{dt} &= (-r_s i_{qs} - \omega L_d i_{ds} - \omega \Phi_f + v_{qs}) / L_q \\ \frac{di_{xs}}{dt} &= (-r_s i_{xs} + v_{xs}) / L_{ls} \\ \frac{di_{ys}}{dt} &= (-r_s i_{ys} + v_{ys}) / L_{ls} \end{aligned} \tag{1.9}$$

where *j=1, 2*. v_{ds}, v_{qs}, v_{xs}, v_{ys} are the stator voltages in the *d-q-x-y* axes, respectively. i_{ds}, i_{qs}, i_{xs}, i_{ys} are the stator currents in *d-q-x-y* axes, respectively. L_d, L_q, L_{ls} are inductances in the rotating frames. r_s is the stator resistance.

The flux linkages equation is as follows:

$$\begin{cases} \Phi_{ds} = L_d i_{ds} + \Phi_f \\ \Phi_{qs} = L_q i_{qs} \\ \Phi_{xs} = L_{ls} i_{xs} \\ \Phi_{ys} = L_{ls} i_{xs} \end{cases} \tag{1.10}$$

where $\Phi_{ds}, \Phi_{qs}, \Phi_{xs}, \Phi_{ys}$ are the flux linkage in the *d-q-x-y* frame

The electromagnetic torque In terms of flux and currents are:

$$T_{em} = \frac{5}{2} p(\Phi_{ds} i_{qs} - \Phi_{qs} i_{ds}) \tag{1.11}$$

$$T_{em} = \frac{5p}{2}(\Phi_f i_{qs} + (L_d - L_q) i_{qs} i_{ds}) \tag{1.12}$$

In case the machine has Surface Mounted type ($L_d = L_q$), the term $(L_d - L_q)i_{qs}i_{ds}$) it will be zero (the reluctance torque does not exist).

The torque expression can be written:

$$T_{em} = \frac{5p}{2}(\Phi_f i_{qs}) \tag{1.13}$$

The mechanical equation can be written as:

$$J\frac{d\Omega}{dt} + f_r\Omega = T_{em} - T_l \tag{1.14}$$

with J is the inertia coefficient, f_r is the friction coefficient, p is the number of poles pairs, and T_l is the external load torque.

1.6 Space Vector Model of Two-Level Five-Phase VSI Modeling

The power circuit topology of the two-level five-phase drive is shown in Fig. (1.5). The inverter consists of five legs with IGBT transistors connecter with anti-parallel diodes, The inverter is supplied by a DC voltage source, which can be generated by a diode rectifier with a C filter. The voltage source inverter gives the possibility to connect each of the five machine phase coils to a positive or negative voltage of the DC-link.

The stator windings of the machine are star connected with a single neutral point *n*. The upper and lower switches for each leg work complementarily. The symbol (*a, b, c, d, e, f*) denotes the inverter legs.

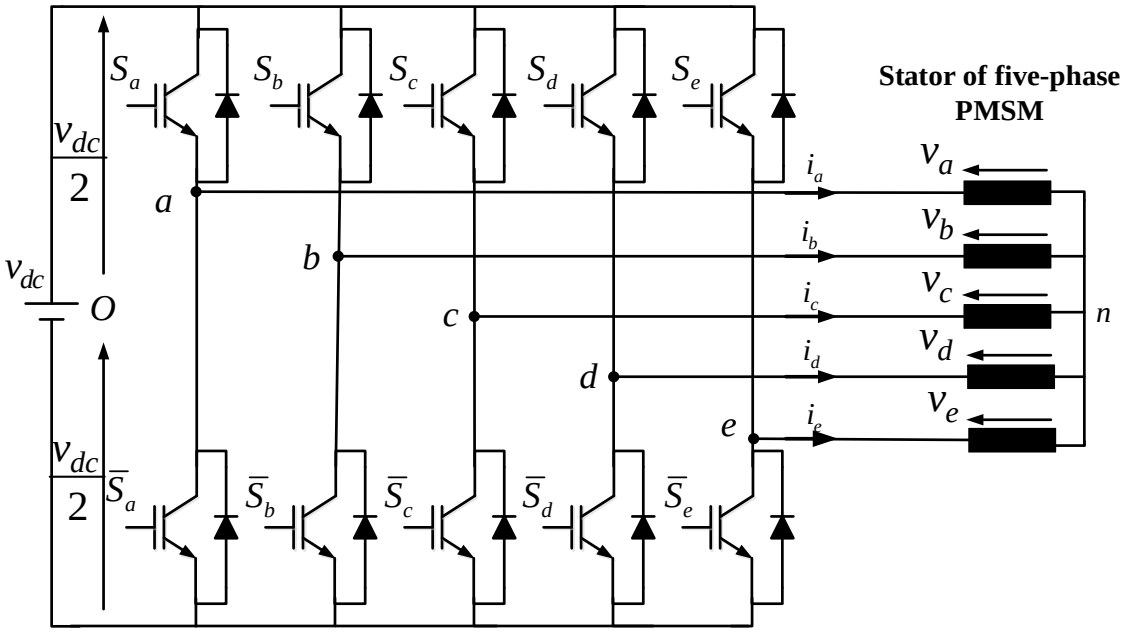

Fig. (1.5): Power circuit topology of two-level five-phase VSI.

The expression of line-to-line voltage are given by:

$$\begin{aligned} v_{ab} &= v_a - v_b \\ v_{bc} &= v_b - v_c \\ v_{cd} &= v_c - v_d \\ v_{de} &= v_d - v_e \\ v_{ea} &= v_e - v_a \end{aligned} \tag{1.15}$$

The correlations between the phase voltages and leg voltages can be again given as follows:

$$\begin{aligned} v_a &= v_{ao} - v_{no} \\ v_b &= v_{bo} - v_{no} \\ v_c &= v_{co} - v_{no} \\ v_d &= v_{do} - v_{no} \\ v_e &= v_{eo} - v_{no} \end{aligned} \tag{1.16}$$

Since the phases are star-connected with a single neutral point, which manes:

$$v_a + v_b + v_c + v_d + v_e = 0 \tag{1.17}$$

Using (1.16), summation of phase voltages given by (1.17) yields:

$$V_{no} = \frac{1}{5}(\mathrm{v}_{ao} + v_{bo} + v_{co} + v_{do} + v_{eo}) \tag{1.18}$$

The relationships between the phase voltages and the leg voltages are obtained by substituting (1.18) into (1.16). The relationship is in essence the same as:

$$\begin{aligned} v_a &= \frac{1}{5}(4v_{ao} - v_{bo} - v_{co} - v_{do} - v_{eo}) \\ v_b &= \frac{1}{5}(-v_{ao} + 4v_{bo} - v_{co} - v_{do} - v_{eo}) \\ v_c &= \frac{1}{5}(-v_{ao} - v_{bo} + 4v_{co} - v_{do} - v_{eo}) \\ v_d &= \frac{1}{5}(-v_{ao} - v_{bo} - v_{co} + 4v_{do} - v_{eo}) \\ v_e &= \frac{1}{5}(-v_{ao} - v_{bo} - v_{co} - v_{do} + 4v_{eo}) \end{aligned} \tag{1.19}$$

with: $v_{Jo} = S_j v_{dc}$, j=a, b, c, d, e

where v_{dc} denotes the DC-link voltage and S_j, $j = a,b,c,d,e$ refer to switching functions.

1.6.1 Five-Phase Space Vectors

The five-phase inverter has totally thirty-two space voltage vectors, thirty non-zero voltage vectors and two zero voltage vectors. Each voltage vector can be mapped by (1.20) onto the *α-β* subspace and *x-y* subspace as shown in Fig. (1.6) [11]:

$$\begin{aligned} v_{\alpha\beta} &= \frac{2}{5}(v_a + v_b e^{j\alpha} + v_c e^{j2\alpha} + v_d e^{j3\alpha} + v_e e^{j4\alpha}) \\ v_{xy} &= \frac{2}{5}(v_a + v_b e^{j2\alpha} + v_c e^{j4\alpha} + v_d e^{j6\alpha} + v_e e^{j8\alpha}) \end{aligned} \tag{1.20}$$

where $\alpha = 2\pi/5$

In the (α-β) and (x-y) planes, the 32 space vectors are positioned at thirty-two locations. Based on their magnitude, the space vectors can be categorized into four different groups, which are large, medium, small and zero space vectors. It can be observed from Fig. (1.6) that medium length space vectors of the *α-β* plane are mapped into medium length vectors in the *x-y* plane, and large vectors of the *α-β* plane are mapped into small vectors in the *x-y* plane, and vice-versa.

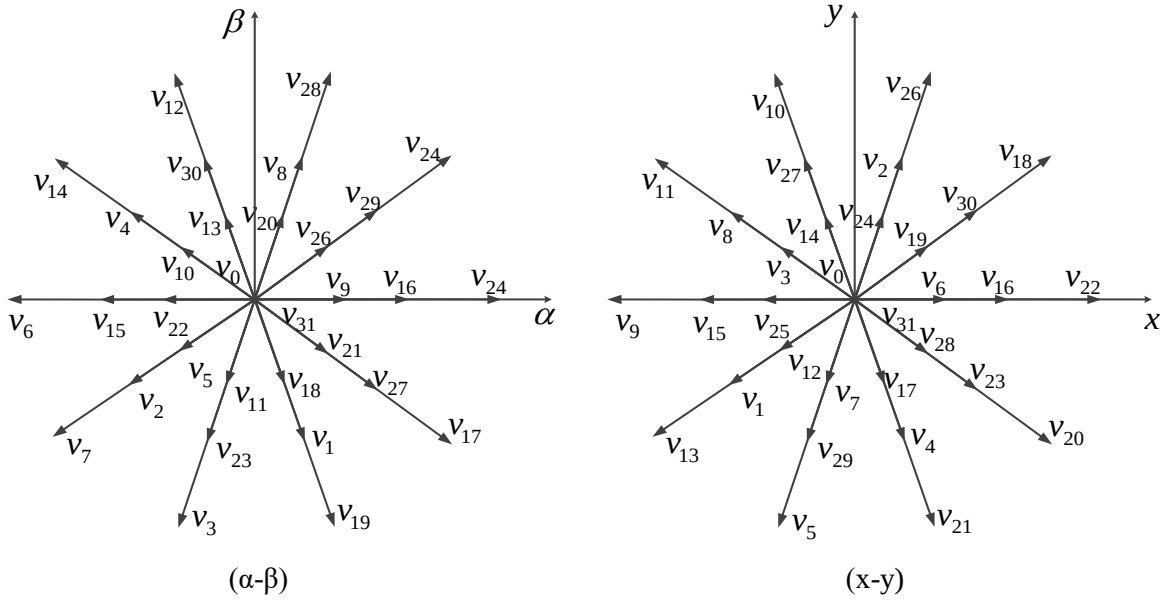

Fig. (1.6): Space vectors of a five-phase inverter in two 2-D subspaces.

The groupings of the space vectors can be expressed using equations presented in Table (1.1).

Table (1.1): Magnitudes of the space vectors

Space vectors	values of space vectors
small (s)	$\lvert V_s\rvert = 4/5\cos(2\pi/5)v_{dc}$
medium (m)	$\lvert V_m\rvert = 2/5 v_{dc}$
large space (l)	$\lvert V_l\rvert = 4/5\cos(\pi/5)v_{dc}$

Fig. (1.7) shows the positions of switches produce an output phase voltage equal to ± 1/5, ± 2/5, ±3/5, ± 4/5 of the DC voltage. The last two (V_0, V_{31}) give zero output voltage. From Fig. (1.7) there are six cases connected with the load to gives a sinusoidal output voltage.

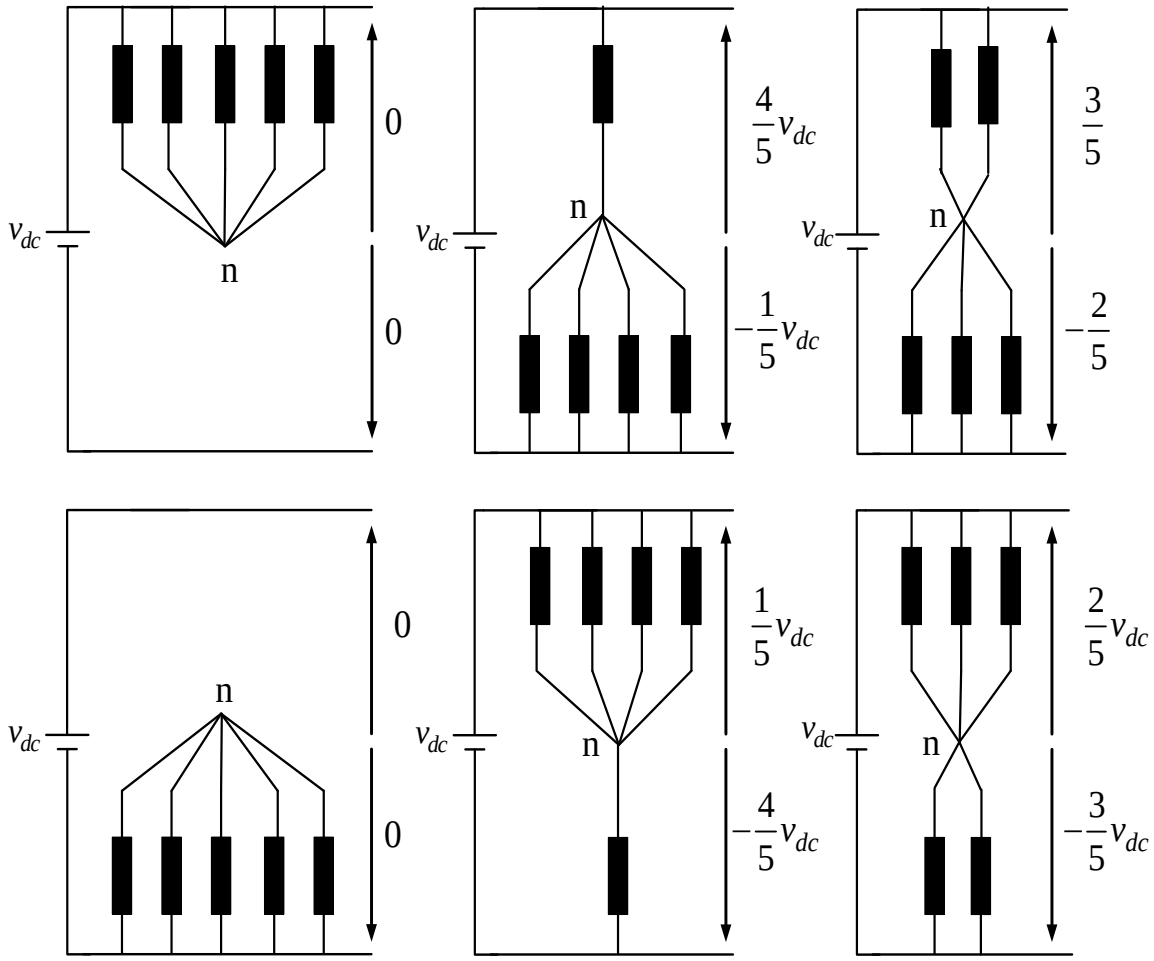

Fig. (1.7): Characteristic configuration of a five-phase load.

1.6.2 SVM Control of Two-Level Five-Phase VSI

The space vector modulation technique is a direct digital method, which is generating the averaging of the reference space vector with pre-selected set of active space vectors over the switching period. Time of application of different vectors is calculated from a set of equations and, by using software (Matlab) unit to generate the switching pulse patterns. In order to establish complete control over the harmonic content of the generated output voltage, the reference vector v_{ref} can be synthesized by combinations of two large and two medium in each sector in one switching period. There are twenty active space vectors and zero vectors involved in the output voltage generation, which appear in Fig. (1.8) [53].

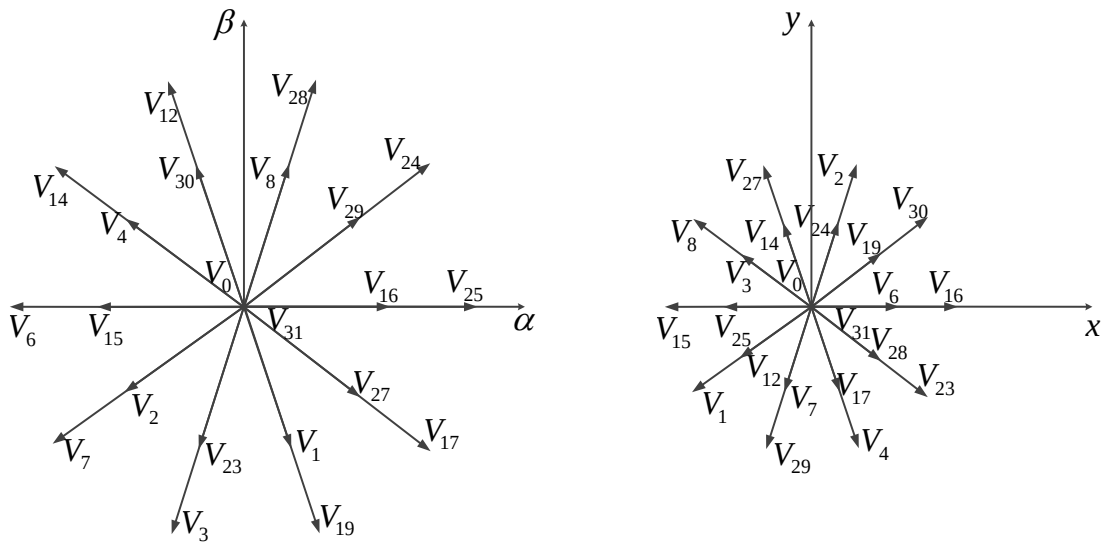

Fig. (1.8): large and medium space vectors of the α-β plane and their mapping in the x-y plane.

The reference space vector is realized in the α-β plane by means of averaging over a switching period, with two medium and two large active space vectors. However, the second plane is now included by setting the reference voltage to zero over the switching period as the requirement. This is illustrated in Fig. (1.9), where it is visible that there is only one reference space vector in the first plane. Suppose that the reference space vector in the first α-β plane, $v_{\alpha\text{-}\beta}= v_{\text{ref}}$, is in sector s=1 (Fig. 1.9 (a)). Two large and two medium neighboring space vectors are selected to reconstruct the desired voltage.

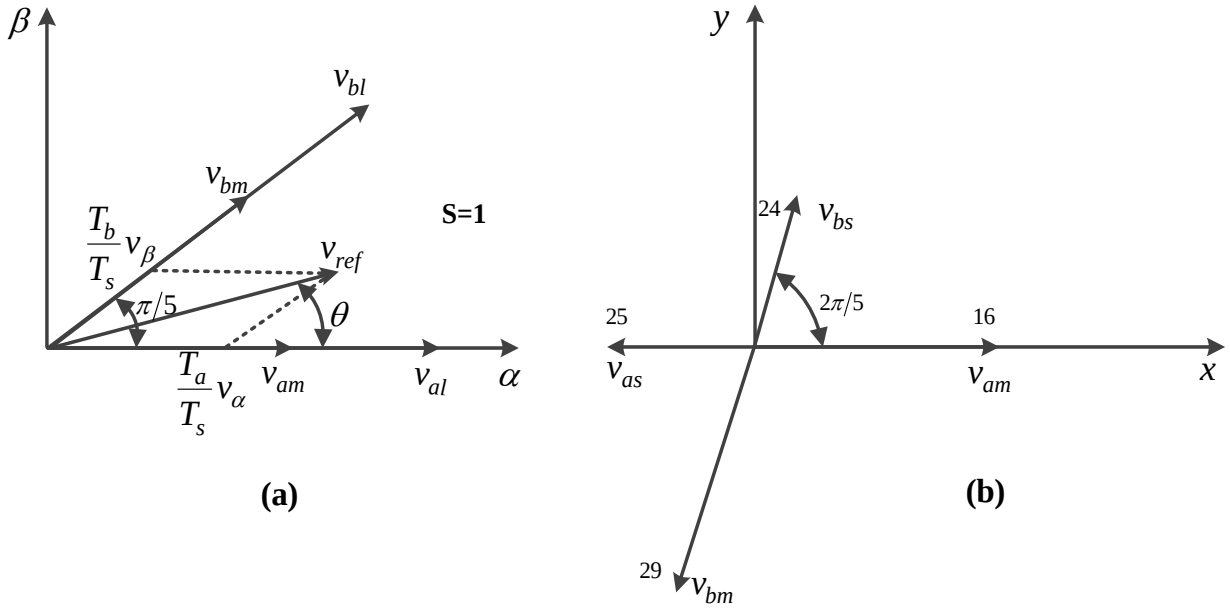

Fig. (1.9): Principle of calculation of times of application of the active space vectors time application.

To calculate the application time the active space vectors have to satisfy the following constraints in order to provide zero average applied voltage in the second x-y plane, $v_{x\text{-}y}= 0$ (Fig. 1.9 (b)):

$$\begin{aligned}
&|v_m|T_{am}+|v_l|T_{al}=\frac{|V^*|\sin(s\pi/5-\theta)}{\sin(\pi/5)}T_s\\
&|v_m|T_{am}-|v_s|T_{al}=0\\
&|v_m|T_{am}+|v_l|T_{al}=\frac{|V^*|\sin(\theta-(s-1)\pi/5)}{\sin(\pi/5)}T_s\\
&|v_m|T_{am}-|v_s|T_{al}=0
\end{aligned} \tag{1.21}$$

where T_l, T_m, and T_0 represent the dwell times of large, medium and zero space vectors. T_s is the switching period θ is the voltage vectors reference position.

By solving (1.21), dwell times for active space vectors T_{1m}, T_{1l}, T_{2m}, T_{2l} are:

$$\begin{aligned}
T_{1l}&=\frac{|v_{ref}|\sin(s\pi/5-\theta)}{(|V_l|+|V_s|)\sin(\pi/5)}T_s\\
T_{2m}&=\frac{|V_s||v_{ref}|\sin(s\pi/5-\theta)}{|V_m|(|V_l|+|V_s|)\sin(\pi/5)}T_s\\
T_{1l}&=\frac{|v_{ref}|\sin(s\pi/5-\varpi)}{(|V_l|+|V_s|)\sin(\pi/5)}T_s\\
T_{2m}&=\frac{|V_s||v_{ref}|\sin(s\pi/5-\theta)}{|V_m|(|V_l|+|V_s|)\sin(\pi/5)}T_s
\end{aligned} \tag{1.22}$$

In addition to the times of application of the active space vectors, total time of application of zero space vectors is now determined with:

$$T_o=T_s-\left(T_{1l}+T_{1m}+T_{2l}+T_{2m}\right) \tag{1.23}$$

This makes it possible to obtain zero average value in the second plane since activated pairs of space vectors in the second plane are acting in opposition. Although with different magnitudes, they will cancel each other due to the mutual relation of the corresponding duty cycles.

Switching pattern is a symmetrical PWM with two commutations for each inverter leg. In order to minimize the total switching losses, the vector sequence for odd sectors is v_0-v_{am}-v_{bl}-v_{al}-v_{bm}-v_{31}-v_{bm}-v_{al}-v_{bl}-v_{am}-v_0, while the sequence v_0-v_{bm}-v_{al}-v_{bl}-v_{am}-v_{31}-v_{am}-v_{bl}-v_{al}-v_{bm}-v_0 is adopted for even sectors.

The switching sequences for one sector is shown in Fig. (1.10). Six switching states are used during a switching half-period, which produce once large, one medium, and twice zero space vector.

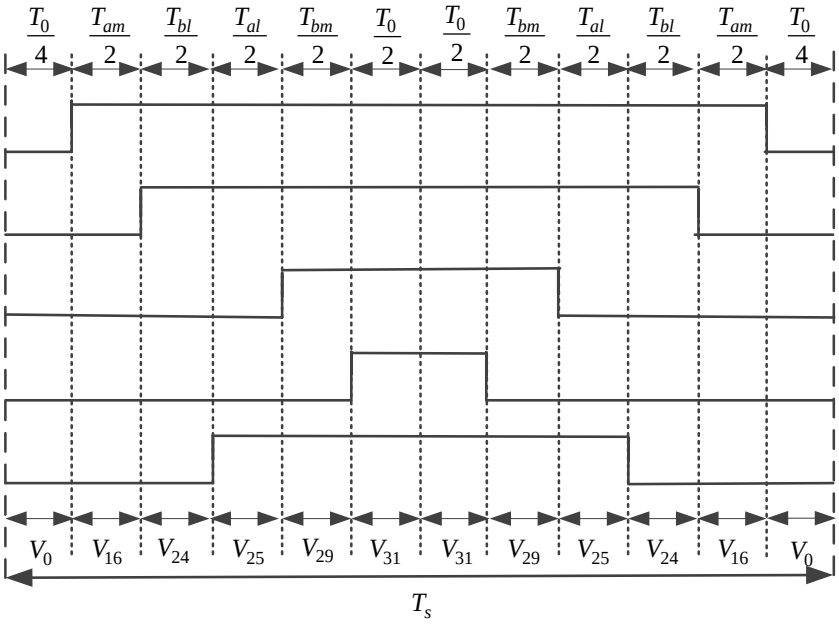

Fig. (1.10): Switching pattern of the SVM in the first sector using large and medium space vectors.

1.7 Modeling of the Two-Machine System Connected in Parallel

1.7.1 Introduction

Some applications require the use of several electrical machines. There are two ways to accomplish such a choice: either using many inverters (the DC-bus are connected in parallel) feeding many machines; this configuration increase the cost and the complexity of the system, or serval machines connected in parallel or series and fed by one inverter.

Parallel-connected multi-phase machines with one inverter are a system consisting of several multi-phase machines connected in Parallel, with an appropriate phase transposition, and fed by a single inverter and controlled independently [8-10]. In this study, the system consists of two five-phase PMSMs connected in parallel. This system is recommended for medium to high power drives.

1.7.2 Parallel Connection of Multi-phase Two-Machine

In this case, the stators are connected in parallel with an appropriate way to give an independent control, it is necessary that the currents producing the torque and flux of one multi-phase machine should not contribute to other multi-phase machines in the group. A phase transposition of the stator phases deduced from the decoupling matrix transformation is a solution for this system [8].

For multi-phase machines with even phase number q, the corresponding decoupling matrix is given by [41] [52]:

$$[C]=\frac{2}{q}\begin{bmatrix} 1 & \cos(\alpha) & \cos(2\alpha) & \cos(3\alpha) & \cos(4\alpha) & ..... & \cos(q-1)\alpha \\ 0 & \sin(\alpha) & \sin(2\alpha) & \sin(3\alpha) & \sin(4\alpha) & ..... & \sin(q-1)\alpha \\ 1 & \cos(2\alpha) & \cos(4\alpha) & \cos(6\alpha) & \cos(8\alpha) & ..... & \cos 2(q-1)\alpha \\ 0 & \sin(2\alpha) & \sin(4\alpha) & \sin(6\alpha) & \sin(8\alpha) & ..... & \sin 2(q-1)\alpha \\ 1 & \cos(3\alpha) & \cos(6\alpha) & \cos(9\alpha) & \cos(12\alpha) & ..... & \cos 3(q-1)\alpha \\ 0 & \sin(3\alpha) & \sin(6\alpha) & \sin(9\alpha) & \sin(12\alpha) & ..... & \sin 3(q-1)\alpha \\ ..... & ..... & ..... & ..... & ..... & ..... & ..... \\ 1 & \cos(\frac{q-2}{2})\alpha & \cos 2(\frac{q-2}{2})\alpha & \cos 3(\frac{q-2}{2})\alpha & \cos 4(\frac{q-2}{2})\alpha & ..... & \cos(q-1)(\frac{q-2}{2})\alpha \\ 0 & \sin(\frac{q-2}{2})\alpha & \sin 2(\frac{q-2}{2})\alpha & \sin 3(\frac{q-2}{2})\alpha & \sin 4(\frac{q-2}{2})\alpha & ..... & \sin(q-1)(\frac{q-2}{2})\alpha \\ 1/2 & 1/2 & 1/2 & 1/2 & 1/2 & 1/2 & 1/2 \\ 1/2 & 1/2 & 1/2 & 1/2 & 1/2 & 1/2 & 1/2 \end{bmatrix} \quad (1.24)$$

For an odd phase number, the decoupling matrix is:

$$[C]=\frac{2}{q}\begin{bmatrix} 1 & \cos(\alpha) & \cos(2\alpha) & \cos(3\alpha) & \cos(4\alpha) & ..... & \cos(q-1)\alpha \\ 0 & \sin(\alpha) & \sin(2\alpha) & \sin(3\alpha) & \sin(4\alpha) & ..... & \sin(q-1)\alpha \\ 1 & \cos(2\alpha) & \cos(4\alpha) & \cos(6\alpha) & \cos(8\alpha) & ..... & \cos 2(q-1)\alpha \\ 0 & \sin(2\alpha) & \sin(4\alpha) & \sin(6\alpha) & \sin(8\alpha) & ..... & \sin 2(q-1)\alpha \\ 1 & \cos(3\alpha) & \cos(6\alpha) & \cos(9\alpha) & \cos(12\alpha) & ..... & \cos 3(q-1)\alpha \\ 0 & \sin(3\alpha) & \sin(6\alpha) & \sin(9\alpha) & \sin(12\alpha) & ..... & \sin 3(q-1)\alpha \\ ..... & ..... & ..... & ..... & ..... & ..... & ..... \\ 1 & \cos(\frac{q-1}{2})\alpha & \cos 2(\frac{q-1}{2})\alpha & \cos 3(\frac{q-1}{2})\alpha & \cos 4(\frac{q-1}{2})\alpha & ..... & \cos(q-1)(\frac{q-1}{2})\alpha \\ 0 & \sin(\frac{q-1}{2})\alpha & \sin 2(\frac{q-1}{2})\alpha & \sin 3(\frac{q-1}{2})\alpha & \sin 4(\frac{q-1}{2})\alpha & ..... & \sin(q-1)(\frac{q-1}{2})\alpha \\ 1/2 & 1/2 & 1/2 & 1/2 & 1/2 & 1/2 & 1/2 \end{bmatrix} \quad (1\text{-}25)$$

where $\alpha = {}^{2\pi}\!/_{q}$

The components $\frac{q-2}{2}$ and $\frac{q-1}{2}$ can be as magnitudes to control the torque /flux of the other machines connected in parallel with the first machine. An appropriate phase transposition in the parallel connection of the two machines leads to complete decoupling of the flux/torque producing currents of one multi-phase machine from the flux/torque producing currents of the other multi-phase machines.

According to this transformation matrix, the first phase of each machine is directly connected in parallel (first column of the transformation matrix), with a zero displacement angle and zero-step. The second phase of the first machine is connected to the third phase of the second machine, which is to be connected to the fourth phase of the third multi-phase machine and so on. The angle displacement for this transposition is equal to α with one-step. This is deducted directly from the second column of the transformation matrix, $\alpha, 2\alpha, 3\alpha, 4\alpha, ..., \left[(q-1)/2\right]\alpha$. In the same way, the third phase of the first multi-phase machine is connected to the fifth phase of the second multi-phase machine with a displacement angle equal to 2α and a two-step, and which is connected to the seventh phase of the third machine and so on as. $2\alpha, 4\alpha, 6\alpha, 8\alpha, ..., \left[(q-1)/2\right]\alpha$

In a general way, the table (1.2) gives the matrix of connection of the multi-phase machines with q phases. In this matrix, the letters (A, B, C, ...) designate the phases of the inverter, the letters (a, b, c, ...) denote the phases of the first multi-phase machine connected to the inverter and (M1, M2, M3, ...) denote the multi-phase machines connected in parallel [41].

Table (1.2): Matrix of connection of the multi-phase machines with q phases.

	A	B	C	D	E	F	G	H	I	J	K
M1	a	b	c	d	e	f	g	h	I	j	k
M2	a	b+1	c+2	d+3	e+4	f+5	g+6	h+7	i+8	j+9	k+10
M3	a	b+2	c+4	d+6	e+8	f+10	g+12	h+14	i+16	j+18	k+20
M4	a	b+3	c+6	d+9	e+12	f+15	g+18	h+21	i+24	j+27	k+30
M5	a	b+4	c+8	d+12	e+16	f+20	g+24	h+28	i+32	j+36	k+40
M6	a	b+5	c+10	d+15	e+20	f+25	g+30	h+35	i+40	j+45	k+50
M7	a	b+6	c+12	d+18	e+24	f+30	g+36	h+42	i+48	j+54	k+60

Multi-phase machines with odd phase number q, which are connected to inverter have certain conditions. Indeed, the number of machines connected in parallel as well as their number of phase depend on three properties of the number q. The number of machines connected in parallel according to the phase transposition is given by:

$$k = \frac{q-1}{2} \tag{1.26}$$

with q=5, 7, …..

1.7.3 Drive System Description and Modeling

The two-machine drive system under consideration is shown in Fig. (1.11). It consists of a five-leg inverter feeding two five-phase PMSMs connected in parallel according to phase transposition. The five-phase PMSM has five-phase windings spatially shifted by 72 electrical degrees. In Fig. (1.11) each stator is star-connected with isolated neutral point, which eliminates the zero sequence voltages.

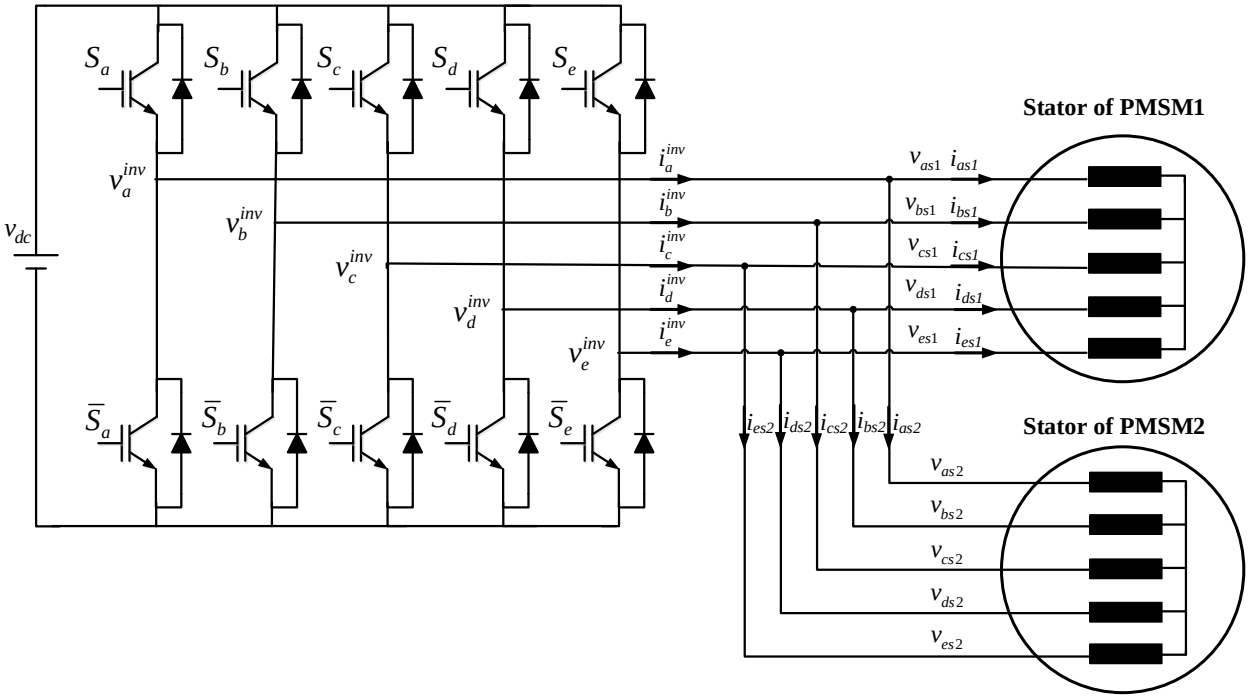

Fig. (1.11): A parallel-connected five-phase two-machine drive.

It can be seen from Fig. (1.11) that the phase transposition rules of parallel-connected two five-phase PMSMs system are as follows [8]: as_1-as_2, bs_1-cs_2, cs_1-es_2, ds_1-bs_2, es_1-ds_2. Where indices 1 and 2 identify the two machines as indicated in Fig. (1.11). Therefore, the relationships between voltages and currents are given as:

$$v_{abcde} = \begin{bmatrix} v_a^{inv} \\ v_b^{inv} \\ v_c^{inv} \\ v_d^{inv} \\ v_e^{inv} \end{bmatrix} = \begin{bmatrix} v_{as1} = v_{as2} \\ v_{bs1} = v_{cs2} \\ v_{cs1} = v_{es2} \\ v_{ds1} = v_{bs2} \\ v_{es1} = v_{ds2} \end{bmatrix} \tag{1.27}$$

$$i_{abcde} = \begin{bmatrix} i_a^{inv} \\ i_b^{inv} \\ i_c^{inv} \\ i_d^{inv} \\ i_e^{inv} \end{bmatrix} = \begin{bmatrix} i_{as1} + i_{as2} \\ i_{bs1} + i_{cs2} \\ i_{cs1} + i_{es2} \\ i_{ds1} + i_{bs2} \\ i_{es1} + i_{ds2} \end{bmatrix} \tag{1.28}$$

The main five dimensional systems can be decomposed into five dimensional uncoupled subsystems (*α-β-x-y-0*). Let the correlation between the original phase variables and the new (*α-β -x- y-*0) variables are given by $f_{\alpha\beta xy} = [C] f_{abcde}$, where C is the following invariant transformation matrix obtained from equation (1.25) (with q=5) as:

$$[C] = \frac{2}{5} \begin{bmatrix} 1 & \cos(\alpha) & \cos(2\alpha) & \cos(3\alpha) & \cos(4\alpha) \\ 0 & \sin(\alpha) & \sin(2\alpha) & \sin(3\alpha) & \sin(4\alpha) \\ 1 & \cos(2\alpha) & \cos(4\alpha) & \cos(6\alpha) & \cos(8\alpha) \\ 0 & \sin(2\alpha) & \sin(4\alpha) & \sin(6\alpha) & \sin(8\alpha) \\ 1/2 & 1/2 & 1/2 & 1/2 & 1/2 \end{bmatrix} \tag{1.29}$$

By applying the transformation matrix (1.26) on equation (1.27) and (1.28), the voltage and current components of the five-phase VSI become:

$$\begin{bmatrix} v_\alpha^{inv} \\ v_\beta^{inv} \\ v_x^{inv} \\ v_y^{inv} \\ v_0^{inv} \end{bmatrix} = [C] v_{abcde} = \begin{bmatrix} v_{\alpha s1} = v_{xs2} \\ v_{\beta s1} = -v_{ys2} \\ v_{xs1} = v_{\alpha s2} \\ v_{ys1} = v_{\beta s2} \\ 0 \end{bmatrix} \tag{1.30}$$

$$\begin{bmatrix} i_\alpha^{inv} \\ i_\beta^{inv} \\ i_x^{inv} \\ i_y^{inv} \\ i_0^{inv} \end{bmatrix} = [C] i_{abcde} = \begin{bmatrix} i_{\alpha s1} + i_{xs2} \\ i_{\beta s1} + i_{ys2} \\ i_{xs1} + i_{\alpha s2} \\ i_{ys1} + i_{\beta s2} \\ 0 \end{bmatrix} \tag{1.31}$$

From (1.30) and (1.31), it is evident that the inverter voltage *α-β* components can control the first machine (PMSM), while the second machine (PMSM) can be controlled separately using the inverter voltage *x-y* components.

In order to transform *α-β -x- y* model into *d-q -x- y* frame, the following rotational transformation matrix [D] is adopted [41]:

$$[D]=\begin{bmatrix} \cos(\theta) & \sin(\theta) & 0 & 0 & 0 \\ -\sin(\theta) & \cos(\theta) & 0 & 0 & 0 \\ 0 & 0 & 1 & 0 & 0 \\ 0 & 0 & 0 & 1 & 0 \\ 0 & 0 & 0 & 0 & 1 \end{bmatrix} \tag{1.32}$$

The correlation between variables obtained upon application of the decoupling transformation and new d-q-x-y variables is defined as:

$$f_{dqxy}=[D]\,f_{\alpha\beta xy} \tag{1.33}$$

The voltage and current components of (1.30) and (1.31) in *d-q-x-y* become:

$$\begin{bmatrix} v_d^{inv} \\ v_q^{inv} \\ v_x^{inv} \\ v_y^{inv} \\ v_0^{inv} \end{bmatrix} = [\mathrm{D}]v_{\alpha\beta xy} = \begin{bmatrix} v_{ds1}=v_{xs2} \\ v_{qs1}=-v_{ys2} \\ v_{xs1}=v_{ds2} \\ v_{ys1}=v_{qs2} \\ 0 \end{bmatrix} \tag{1.34}$$

$$\begin{bmatrix} i_d^{inv} \\ i_q^{inv} \\ i_x^{inv} \\ i_y^{inv} \\ i_0^{inv} \end{bmatrix} = [D]i_{\alpha\beta xy} = \begin{bmatrix} i_{ds1}+i_{xs2} \\ i_{qs1}-i_{ys2} \\ i_{xs1}+i_{ds2} \\ i_{ys1}+i_{qs2} \\ 0 \end{bmatrix} \tag{1.35}$$

The model of each five-phase PMSM is presented in a rotating *d-q-x-y* frame as:

$$\begin{aligned} v_{dsj} &= r_{sj}i_{dsj} + L_{dj}\frac{di_{dsj}}{dt} - \omega_j L_{qj}i_{qsj} \\ v_{qsj} &= r_{sj}i_{qsj} + L_{qj}\frac{di_{qsj}}{dt} + \omega_j L_{dj}i_{dsj} + \omega_j \Phi_{fj} \\ v_{xsj} &= r_{sj}i_{xsj} + L_{lsj}\frac{di_{xsj}}{dt} \\ v_{ysj} &= r_{sj}i_{ysj} + L_{lsj}\frac{di_{ysj}}{dt} \end{aligned} \tag{1.36}$$

where *j=1,2*. v_{dsj}, v_{qsj}, v_{xsj}, v_{ysj} are the stator voltages in the *d-q-x-y* axes, respectively. i_{dsj}, i_{qsj}, i_{xsj}, i_{ysj} are the stator currents in *d-q-x-y* axes, respectively. L_{dj}, L_{qj}, L_{lsj} are inductances in the rotating frames. r_{sj} are the stator resistance.

The electromagnetic torques equations for the first and the second machines are given by:

$$\begin{aligned} T_{em1} &= \frac{5p_1}{2}(\Phi_{f1} i_{qs} + (L_{d1} - L_{q1}) i_{qs} i_{ds}) \\ T_{em2} &= \frac{5p_2}{2}(\Phi_{f2} i_{ys} + (L_{d2} - L_{q2}) i_{ys} i_{xs}) \end{aligned} \tag{1.37}$$

where p_j are pole pairs, Φ_{fj} are the permanent magnet fluxes.

According to the relation (1.37), the torque/flux of the first machine are controlled using the stator currents (d-q), whereas the torque/flux of the second machine are controlled using the stator currents (x-y).

1.7.4 SVM Control for Parallel-Connected Two Five-Phase PMSMs

The aim of this section is to develop an appropriate SVM scheme for five-legs VSI fed two machines connected in parallel. The control strategy adopted herein is based on the approach proposed in [11] [53]. Indeed, in the first switching period, the space vector modulator will apply α-β voltage reference. In the next switching period, the space vector modulator will apply x-y voltage reference as shown in Fig. (1.12).

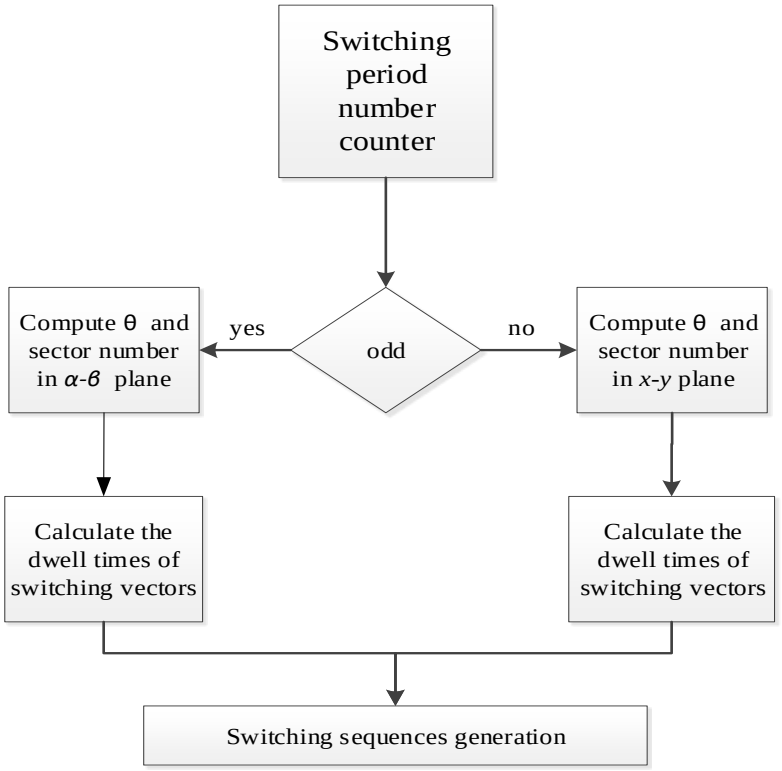

Fig. (1.12): Steps of SVM technique for parallel-connected two-machine drive for five-phase leg inverter feed by two machine connected in parallel.

The selection of switching signals is depicted in Fig. (1.13). So, two independent space vector modulators are further utilized to realize the required two voltage space vector references, with dwell times calculated independently in the two planes using (1.22).

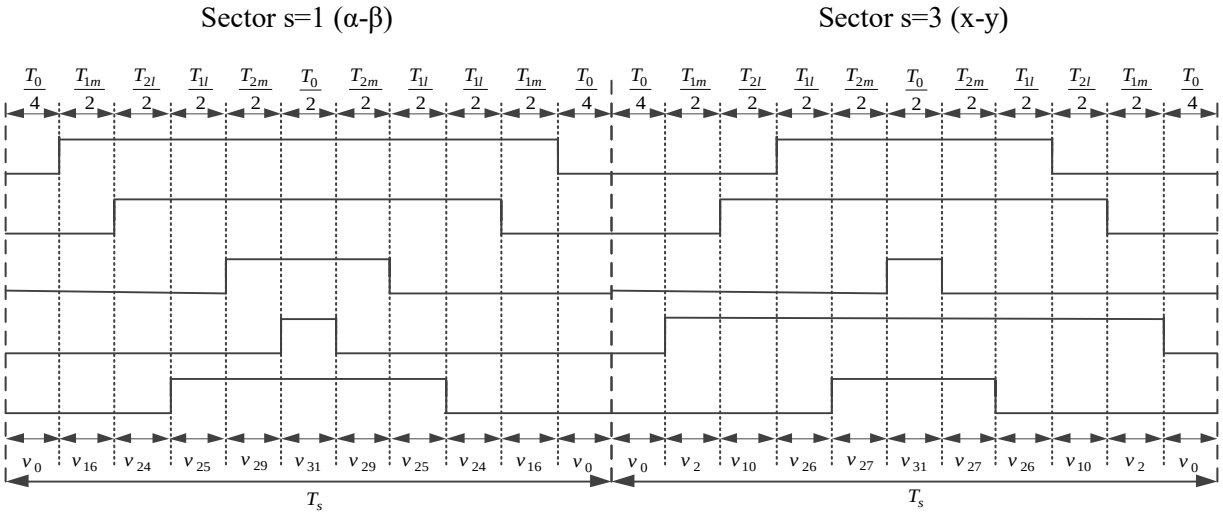

Fig. (1.13): Switching pattern obtained with SVM.

1.8 Conclusion

In this chapter, mathematical modeling of a five-phase PMSM, five-phase VSI, and parallel-connected of two machines have been presented. It has shown that, the application of transformations matrix results in a greatly simplified mathematical model of five-phase PMSM. The space vector modulation techniques for the five-phase voltage source inverters have been presented. The technique is based to use four active space vectors (large and medium) and two zero active space vectors (V0 and V31) to generate a sinusoidal output voltage.

Since only stator *d-q* current components are needed for the flux and torque control for one machine, there is a possibility of using the existing degrees of freedom *x-y* stator current components for controlling the second machine that would be connected in parallel. Consequently, the two machines can be controlled independently in such away the flux/torque producing currents of one machine does not produce flux/ torque in second machine.

The next chapter will deal with the decoupled control of parallel-connected two five-phase PMSMs drive based on filed oriented control and direct torque control.

Chapter 2

Decoupled Controls Based on Linear Regulators PI-type of Two Five-Phase PMSMs Connected in Parallel

2.1 Introduction

The principle control of a five-phase PMSM is to control independently the flux and the torque by using two components of the stator current of axes (α-β) or (d-q), the other currents (x-y) can be used to control the second machine, with appropriate phase transposition to lead a complete decoupling of the two machine.

The purpose of the filed oriented control is to control the five-phase PMSM as a DC machine with independent excitation, which has a natural decoupling between the flux and the torque [48]. In five-phase PMSM the decoupling are assured by the inverter, the reference used to control the inverter, which is feeding the two machine connected in parallel.

The DTC is one of the effective control techniques adopted to control torque and flux linkage. The DTC is considered particularly interesting being less parameters dependency; making the system more robust, fast dynamic response, and a simple control [54]. Furthermore, the DTC avoids the need to the internal current loops, coordinate transformations, and the modulator block; hence the delay caused by current regulator is eliminated. It directly selects voltage vectors according to the error between the reference and the estimated values of the torque and flux [55]. However, the main problem of this method is the high level of torque ripples, variable switching frequency of the inverter, and acoustic noises [54-56]. Recently, numerous studies are proposed to overcome these drawbacks, a space vector modulation is implemented to replace the switching table of the voltage vector selection and provide a constant inverter switching frequency [14-18].

This chapter will deal with a decoupled control of parallel-connected two five-phase PMSMs drive, the complete independent control of the two machines is shown to be possible by feeding them from a single five-phase voltage source inverter based on filed oriented control and direct torque control using proportional integrator regulators as well as conventional DTC (with look up-table).

2.2 FOC of Parallel-Connected Two Five-phase PMSMs Drive

2.2.1 Principle of FOC

The purpose of FOC is to assimilate the behavior of the Five-phase PMSM to that of a DC machine with independent excitation in two aspects [48] [51]:

-The torque and the flux of the machine are controlled independently of each other.

-The optimal conditions of torque production are provided in steady state and transient conditions.

The equations given in section (1.36) are already in the rotor flux oriented reference frame for a PMSM, since d-axis coincides with the direction of the permanent magnet flux [41].

The vector control law is the same principle for both machines and aims to make equivalence between the five-phase PMSM and DC machine. Therefore, Flux and torque of the first machine are controllable by inverter d-q axis current components, while flux and torque of the second machine can be controlled using inverter x-y current components [8]. This objective can be achieved by controlling the *d-x* axes current component to zero, so the torque depends only on the amplitude of *q-y* axes current. Referring to the torques expression given by (1.37), the reference currents can be calculated using the following equations:

$$\begin{cases} i_{dsref} = 0 \\ i_{qsref} = (2/5)(1/p_1\Phi_{f1})T_{em\_ref1} \\ i_{xsref} = 0 \\ i_{ysref} = (2/5)(1/p_2\Phi_{f2})T_{em\_ref2} \end{cases} \quad (2.1)$$

The speed controller output T_{em_ref1} and T_{em_ref2} determines the reference currents i_{qsref} and i_{ysref} of the two machines.

The voltage equations (1.36) can be written by introducing the laplace operator s in the following form:

$$\begin{aligned} v_{dsj} &= (r_{sj} + sL_{dj})i_{dsj} - \omega_j L_{qj} i_{qsj} \\ v_{qsj} &= (r_{sj} + sL_{qj})i_{qsj} + \omega_j L_{dj} i_{dsj} + \omega_j \Phi_{fj} \\ v_{xsj} &= (r_{sj} + sL_{lsj})i_{xsj} \\ v_{ysj} &= (r_{sj} + sL_{lsj})i_{ysj} \end{aligned} \quad (2.2)$$

From (2.2) the voltage command variables $v_{ds\,refj}, v_{qs\,refj}, v_{xs\,refj}, v_{ys\,refj}$ can be expressed as:

$$\begin{aligned} v_{ds\,refj} &= v_{dj} - \omega_j L_{qj} i_{qsj} \\ v_{qs\,refj} &= v_{qj} + \omega_j L_{dj} i_{dsj} + \omega_j \Phi_{fj} \\ v_{xs\,refj} &= v_{xj} \\ v_{ys\,refj} &= v_{yj} \end{aligned} \quad (2.3)$$

where $v_{dj}, v_{qj}, v_{xj}, v_{yj}$ are generated by PI-regulators.

The terms $\omega_j L_{qj} i_{qsj}, \omega_j L_{dj} i_{dsj} + \omega_j \Phi_{fj}$ correspond to the coupling terms between the axes *d-q*. One solution consists of adding identical voltages but of opposite signs to the output of the current regulators to separate the control loops of axes *d-q* as shown in Fig. (2.1).

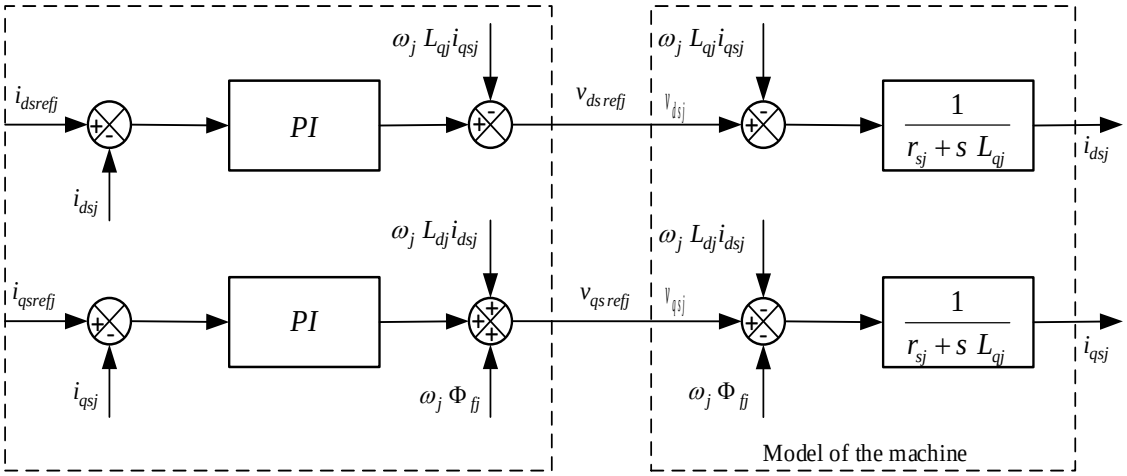

Fig. (2.1): *d-q* axes decoupling by adding of the compensation terms.

The general block diagram of the FOC for parallel-connected two five-phase PMSMs drive system is shown in Fig. (2.2).

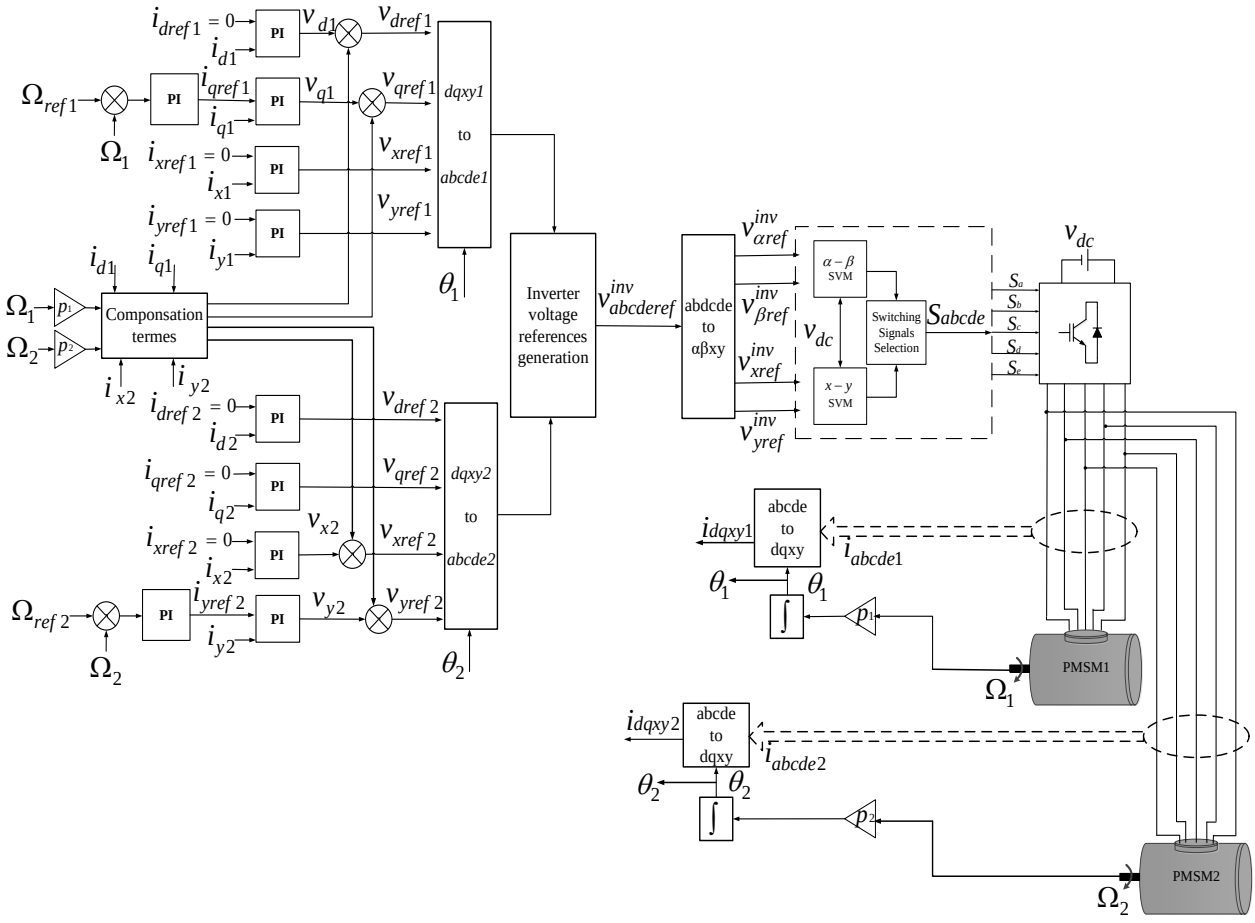

Fig. (2.2): Vector controller of parallel-connected two five-phase PMSMs drive system.

The control voltages given by (2.3) are transformed in *abcde* frame and then the inverter phase voltage references are calculated according to the following expression [8]:

$$\begin{aligned} v_a^{inv} &= v_{as\,ref1} + v_{as\,ref2} \\ v_b^{inv} &= v_{bs\,ref1} + v_{cs\,ref2} \\ v_c^{inv} &= v_{cs\,ref1} + v_{es\,ref2} \\ v_d^{inv} &= v_{ds\,ref1} + v_{bs\,ref2} \\ v_e^{inv} &= v_{es\,ref1} + v_{ds\,ref2} \end{aligned} \tag{2.4}$$

As shown in Fig. (2.2), the reference voltages of the inverter are obtained by the sum of the reference voltages of the two machines phases according to the phase transposition. The speed regulators generate the reference currents (i_q, i_y), which are the inputs of the current regulators.

2.2.2 Synthesis of speeds and currents controllers

2.2.2.1 Speed controller

The block diagram of the closed-loop speeds control is shown in Fig. (2.3).

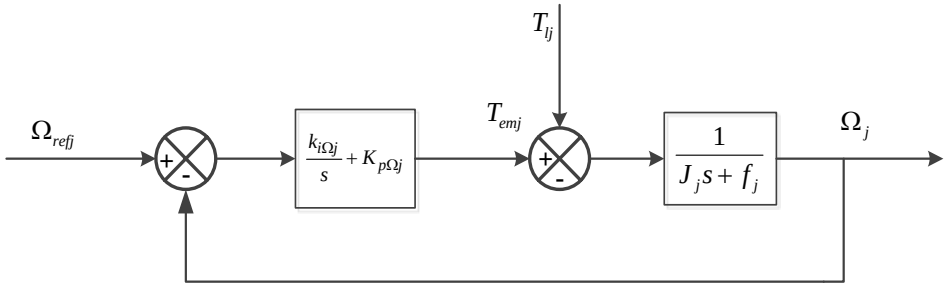

Fig. (2.3): Block diagram of the closed-loop speed control.

The selection of the parameters of the speed controller is done in order to obtain the desired performances for the closed loop system by imposing the damping ratio ζ and the natural frequency ω_0.

The output can be written as:

$$\Omega_j = \frac{1}{J_j s + f_j}\left[\left(\frac{k_{i\Omega_j}}{s} + K_{p\Omega j}\right)(\Omega_{refj} - \Omega_j) - T_{lj}\right] \tag{2.5}$$

Considering the load torque as perturbation (T_{lj}= *0*), the transfer function of the closed loop is given by:

$$G_{\Omega_j}(s) = \frac{k_{p\Omega_j} s + k_{i\Omega_j}}{J_j s^2 + (k_{p\Omega_j} + f_j)s + k_{i\Omega_j}} \tag{2.6}$$

By identifying the denominator of (2.6) with the characteristic equation of the following second order system $\frac{1}{s^2 + 2\xi_{\Omega j}\omega_{0\Omega j}s + \omega_{0\Omega j}^2}$ it yields:

$$\begin{cases} k_{i\Omega_j} = j_j \omega_{0\Omega_j}^2 \\ k_{p\Omega_j} = 2\xi_{\Omega_j} j_j \omega_{0\Omega_j} - f_j \end{cases} \tag{2.7}$$

with $\xi_{\Omega j}$ is the damping ratio and $\omega_{0\Omega j}$ is the natural frequency.

2.2.2.2 Currents controllers

The block diagram of the closed-loop currents controllers are shown in Fig. (2.4) and Fig. (2.5).

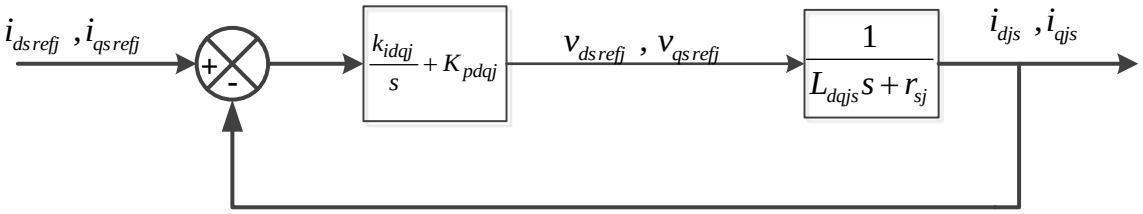

Fig. (2.4): Block diagram of the closed loop i_{dq} currents control.

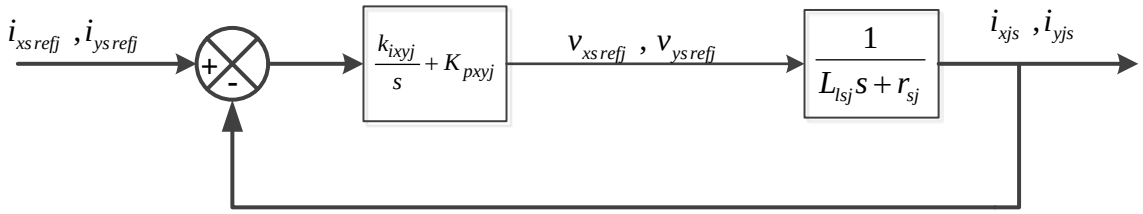

Fig. (2.5): Block diagram of the closed loop i_{xyj} currents control.

The closed-loop transfer functions are given by:

$$G_{dqj}(s) = \frac{(k_{pdqj}s + k_{i\,dqj})(1/L_{dqj})}{s^2 + (\frac{k_{pdqj} + r_{sj}}{L_{dqjs}})s + \frac{k_{i\,dqj}}{L_{dqj}}} \tag{2.8}$$

$$G_{xyj}(s) = \frac{(k_{pxyj}s + k_{i\,xyj})(1/L_{lsj})}{s^2 + (\frac{k_{pxyj} + r_{sj}}{L_{lsj}})s + \frac{k_{i\,xyj}}{L_{lsj}}} \tag{2.9}$$

By identification the denominators of (2.8) and (2.9) with the characteristic equation of a desired second order system, it yields:

$$\begin{cases} k_{i\,dqj} = L_{dqj}\omega_{0dqj}^2 \\ k_{pdqj} = 2\xi_{dqj}L_{dqj}\omega_{0dqj} - r_{sj} \end{cases} \tag{2.10}$$

$$\begin{cases} k_{i\,xyj} = L_{lsj}\omega_{0xyj}^2 \\ k_{p\,xyj} = 2\xi_{xyj}L_{lsj}\omega_{0xyj} - r_{sj} \end{cases} \tag{2.11}$$

with ξ_{dqsj}, ξ_{xysj} are the damping ratio and ω_{0dqj}, ω_{0xyj} are the natural frequency.

2.2.3 Simulation Results

The control scheme for the two-machine drive system of Fig. (2.2) is verified by different simulations, which are performed using two identical 2-pole, 50 Hz five-phase PMSM. The parameters of each machine are listed in table A.1 of appendix A. The tuning parameters for the PI-controllers are also given in table B.I of appendix B. Many simulation tests are performed in order to verify the independent control of the two machines connected in parallel as shown in Figs (2.6) to (2.10).

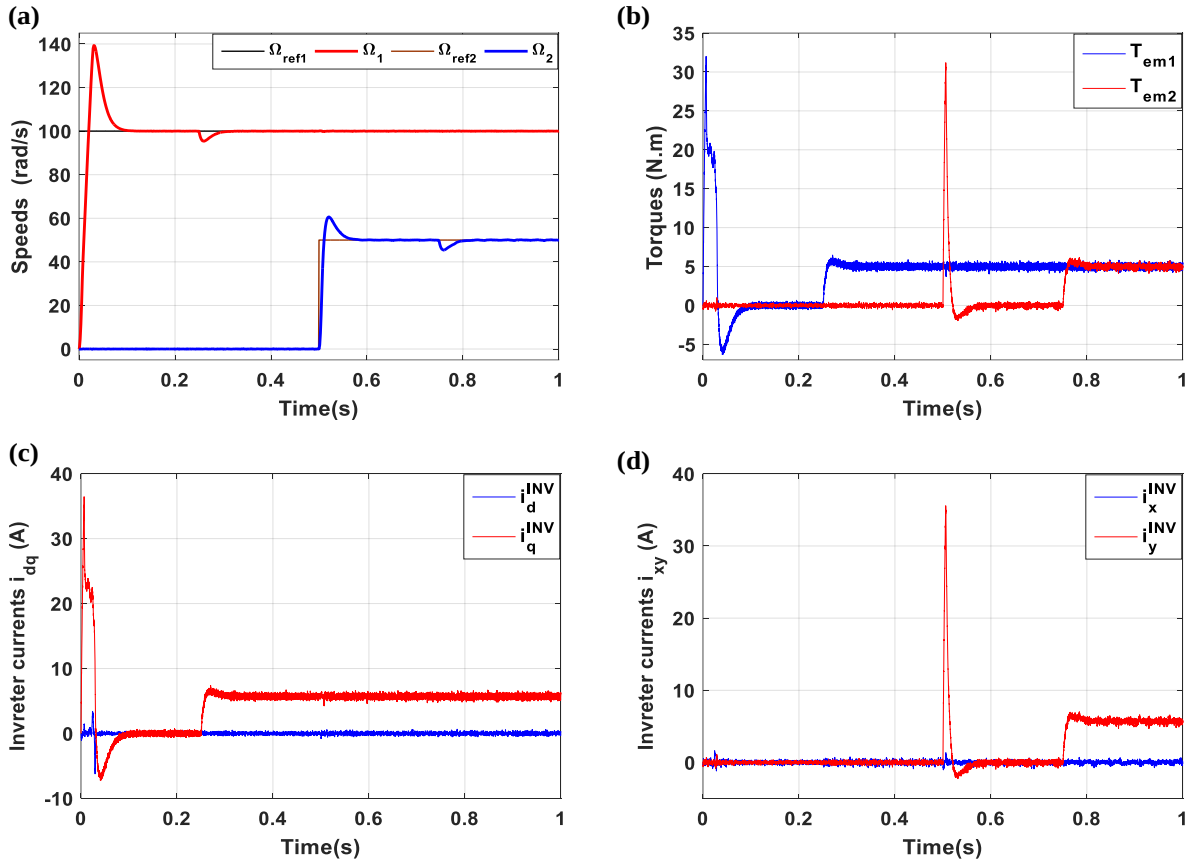

Fig. (2.6): Dynamic responses of parallel-connected two five-phase PMSMs drive controlled by FOC; when the second machine is at standstill and the other is still running: (a) the machine speeds, (b) electromagnetic torques, (c) the d-q axis currents (d) y-x axis currents.

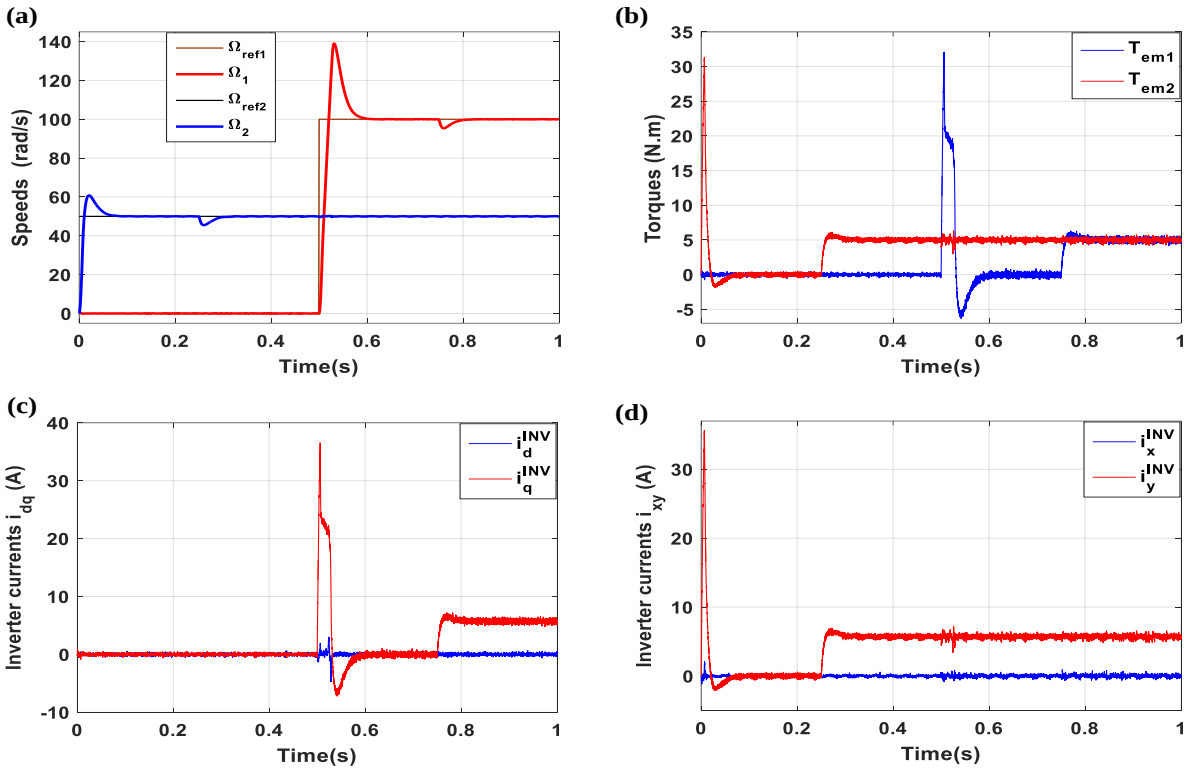

Fig (2.7): Dynamic responses of parallel-connected two five-phase PMSMs system controlled by FOC; when the first machine is at standstill and the other is still running: (a) the machine speeds, (b) electromagnetic torques, (c) the d-q axis currents (d) y-x axis currents.

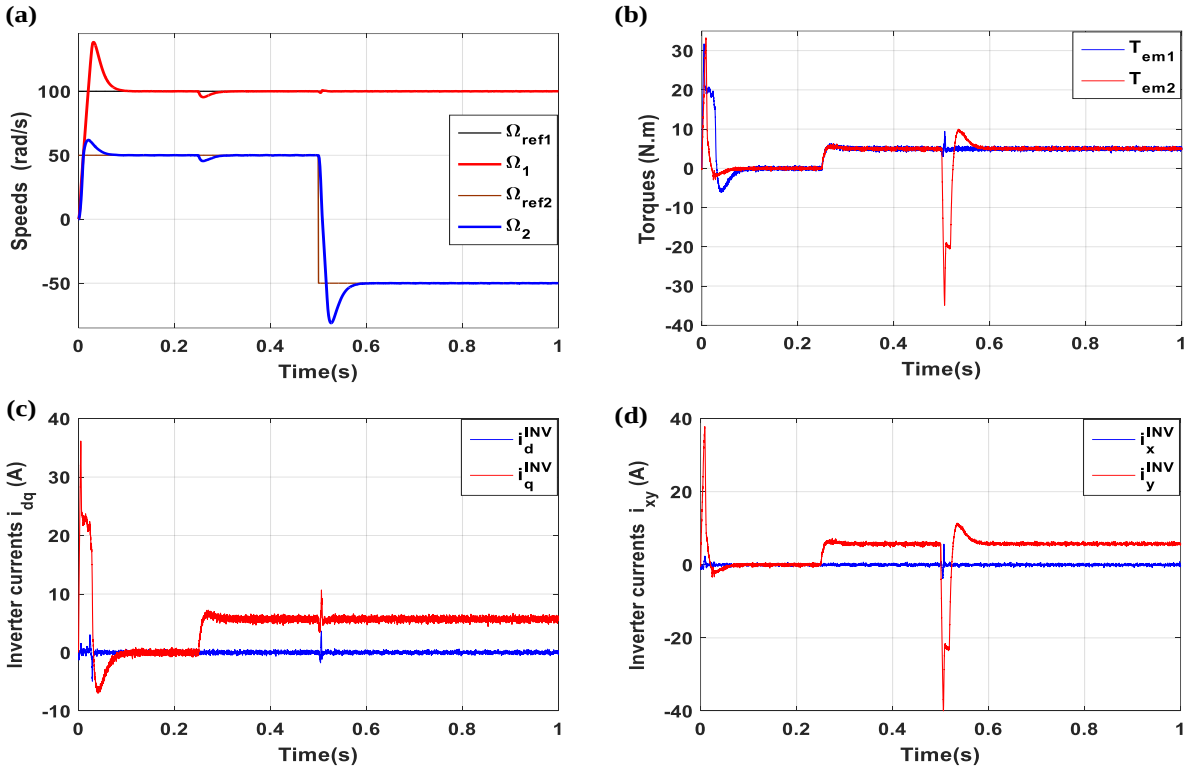

Fig. (2.8): Dynamic responses of parallel-connected two five-phase PMSMs drive controlled by FOC when the first machine is kept constant and the other change the direction: (a) the machine speeds, (b) electromagnetic torques, (c) the d-q axis currents (d) y-x axis currents.

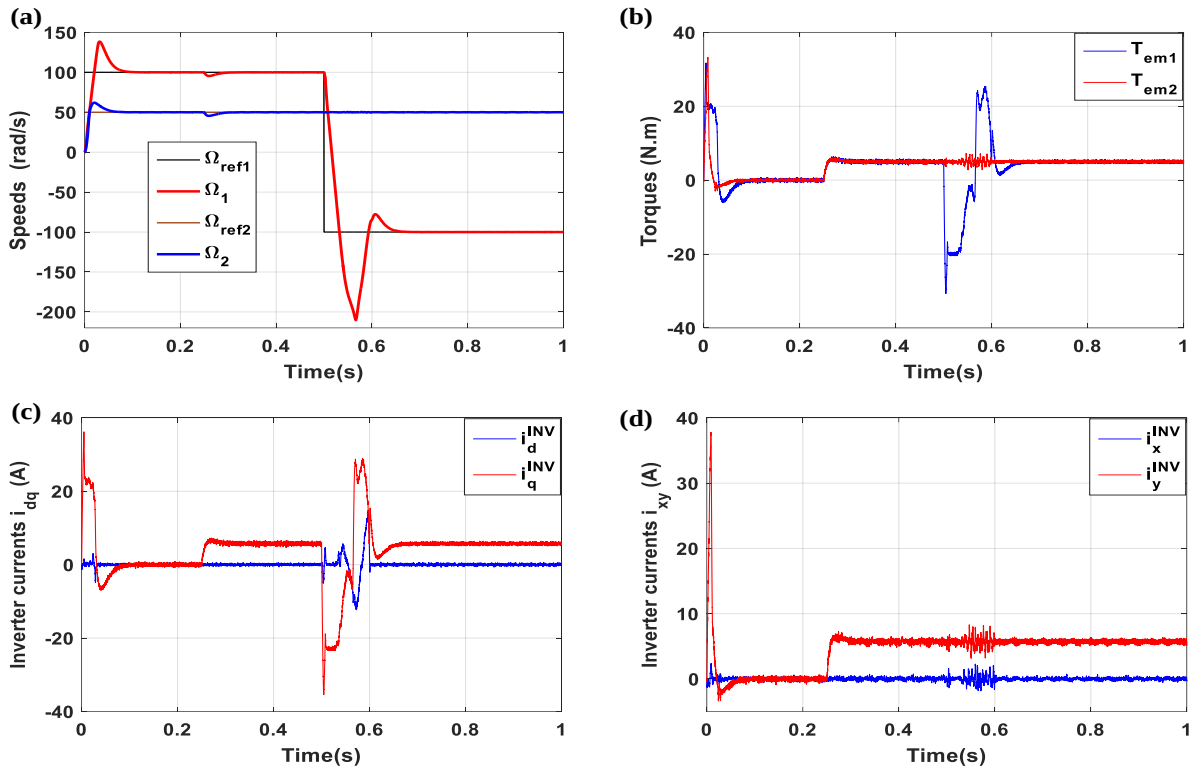

Fig. (2.9): Dynamic responses of parallel-connected two five-phase PMSMs system: when the speed of the second machine is kept constant and the other performance change the direction: (a) the machine speeds, (b) electromagnetic torques, (c) the d-q axis currents (d), y-x axis currents.

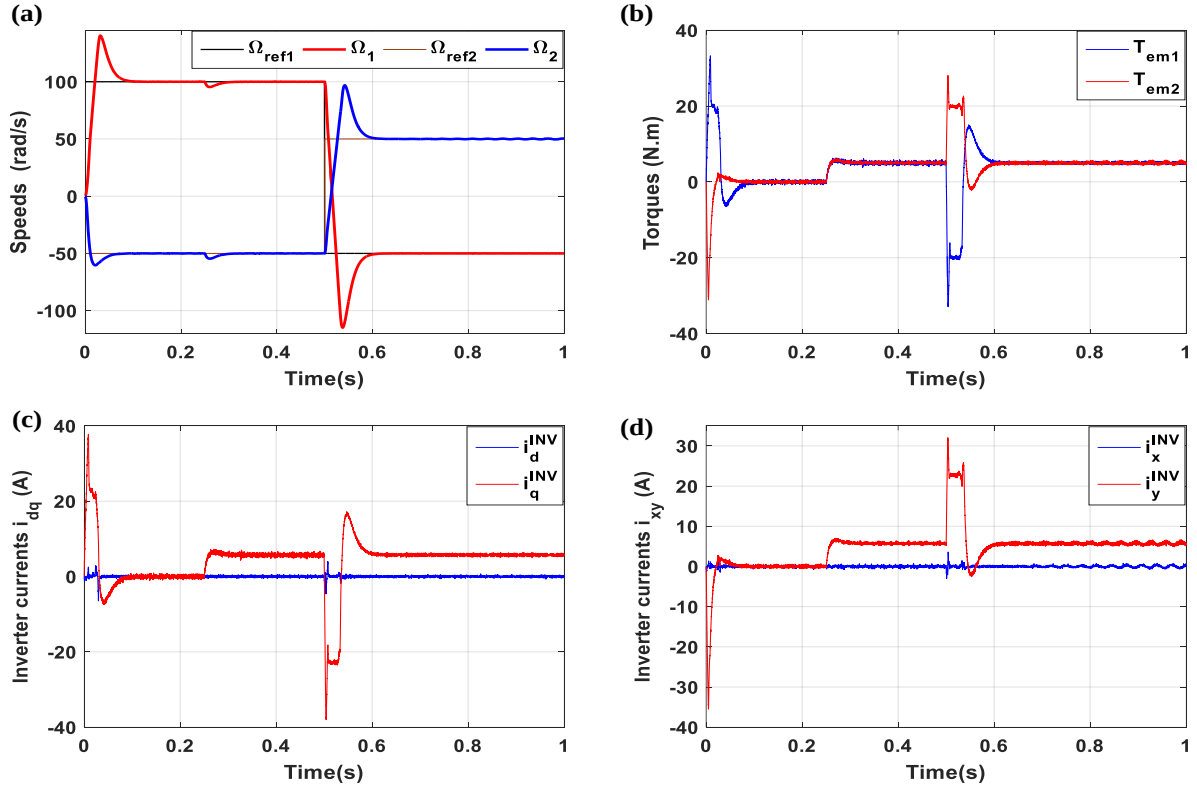

Fig. (2.10): Dynamic responses of parallel-connected two five-phase PMSMs drive controlled by FOC; when the two machines are operating in the opposite directions: (a) the machine speeds, (b) electromagnetic torques, (c) the *d-q* axis currents (d) *y-x* axis currents.

According to Fig. (2.6-a), the second machine is started at t=0.5s to become 50 rad/s, while the speed of the first machine is operating at speed of 100 rad/s. In Fig. (2.7-a) the operations applied in Fig. (2.6) is reversed. As can be seen from Figs. (2.6-b) and (2.7-b) the electromagnetic torque of the first machine is not affected by the starting operation of the second machine.

Effect of the change in rotation direction of one machine on system performance is investigated. Fig. (2.8-a) shows the results when the speed of the second five-phase PMSM is changed from +50 rpm to -50 rad/s at t = 0.5s at the same time the speed of the first machine is kept constant at 100 rad/s. In Fig. (2.9-a) the speed of the first PMSM is changed from +100 rpm to -100 rad/s at t = 0.5s and the speed of the second PMSM is operating at 50 rad/s. Simulation results show that, the independent control of each machine is preserved and the characteristics of both machines are not influenced by these changes or by the acceleration period of the two machine to each other.

It can be observed from Figs (2.6) to (2.10) that, step loading of one machine does not cause any disturbance in the other machine's speed and the inverter d-q-x-y axis currents reference traces. However, the application of the load torque results a noticeable drop of its speed; this drop is very quickly corrected by the speed controller.

2.3 DTC of Parallel-Connected Two Five-phase PMSMs Drive

2.3.1 Conventional DTC

2.3.1.1 Principles of Direct Torque Control

The name direct torque control come from the fact that, on the basis of the errors between the reference and the estimated values of torque and flux, by using a switching table for the selection of an appropriate voltage vector, it is possible to directly control the inverter states without inner current control loop as for FOC [35][57-59]. The basic idea of DTC relies on stator voltage equation of the five-phase PMSM written as:

$$v_s = r_s i_s + \frac{d\Phi_s}{dt} \tag{2.12}$$

In the case where a non-zero voltage vector is applied during a sampling period, and by neglecting the voltage drop on the stator resistor, the stator flux can be written as:

$$\Phi_s = \int (v_s) dt \tag{2.13}$$

From (2.18), it can observed that the stator voltage vector has direct influence on stator flux vector control. The active vectors change the amplitude and position of stator flux vector, while the zero vectors stop the stator flux vector [60] [61].

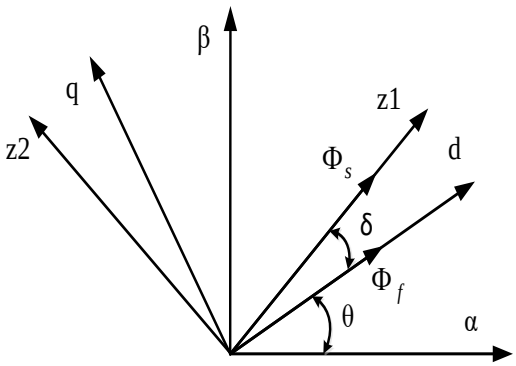

Fig. (2.11): Stator and rotor flux linkages and different reference frames.

Therefore, it is possible to control the torque by controlling the angle (δ) between stator flux vector Φ_s and rotor flux vector Φ_f produced by permanent magnets. From (1.11), the torque of the five-phase PMSM can be expressed in terms of stator and rotor flux as follows [35] [46]:

$$T_{em} = \frac{5p}{2}\left(\frac{\Phi_f |\Phi_s| \sin\delta}{L_{ds}} - \frac{|\Phi_s|^2 (L_{ds} - L_{qs}) \sin 2\delta}{2L_{ds}L_{qs}}\right) \tag{2.14}$$

From (2.14) it is evident that, the torque can be controlled by adjusting the torque angle (δ).

2.3.1.2 DTC of the Two-Machine Drive

DTC of parallel-connected requires two look up-tables for independent flux and torque control. Each up-table has deferent vectors, in order to enable decoupled flux/torque control of one machine from all the other machines in the group. It is necessary that flux/torque producing currents in the first machine do not produce a rotating field in the second machine. This requires introduction of an appropriate phase transposition in the parallel connection of stator windings [8][62].

The DTC has the same principle for both machines as shown in Fig. (2.13), the flux and torque of the first machine are controllable by up-table (1), while flux and torque of the second machine are controlled by using up-table (2).

The principle of controlling the flux in DTC is to keep its magnitude within a predefined hysteresis band [63]. By applying the proper voltage vector, the stator flux can be directly controlled. To select the voltage vectors for controlling the amplitude of the stator flux linkage the voltage plane is divided into ten sectors, as shown in Fig. (2.12); the flux position decides about the sector location. In each sector, the next switching vector is assumed based on the combination between flux and torque errors. For example:

if v_{i+1} is selected then Φ_s is increased and T_{em} is increased.

if v_{i-1} is selected then Φ_s is increased and T_{em} is decreased.

if v_{i+4} is selected then Φ_s is decreased and T_{em} is increased.

if v_{i-4} is selected then Φ_s is decreased and T_{em} is decreased.

If the torque error is within the error limit, $d_{Tem} = 0$, the null voltage vector V_0 or V_{31} is selected.

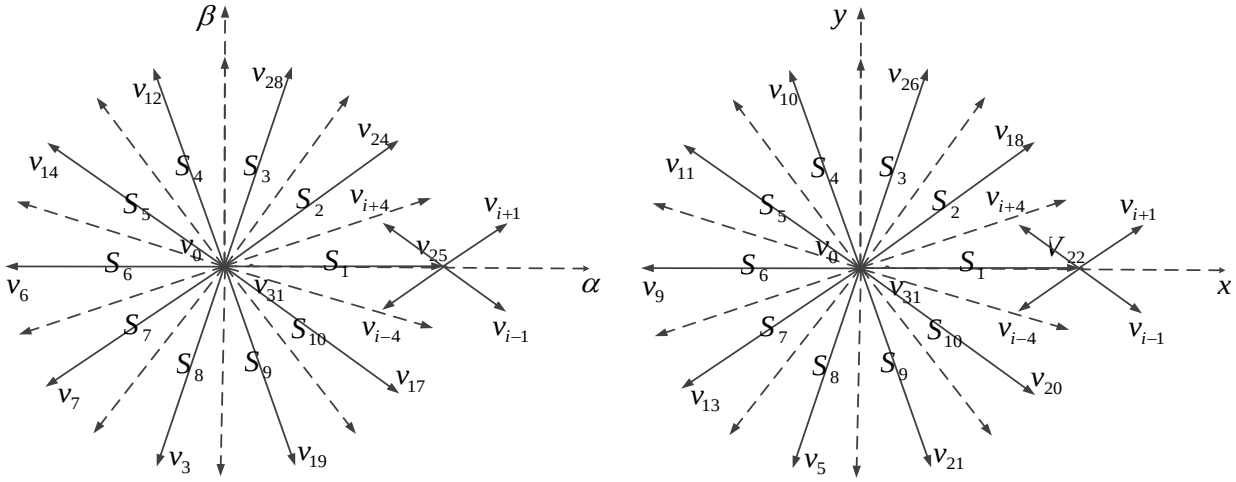

(a) α-β subspace. (b) x-y subspace.

Fig. (2.12): Selection of voltage vectors for controlling stator flux in first sector.

For all the sectors, Tables (2.1) and (2.2) show the optimum switching voltage vector look-up tables.

Table (2.1): Optimum Active Voltage Vector Look-Up Table 1.

$d_{\Phi 1}$	d_{Tem1}	S_1	S_2	S_3	S_4	S_5	S_6	S_7	S_8	S_9	S_{10}
1	1	v_{24}	v_{28}	v_{12}	v_{14}	v_6	v_7	v_3	v_{19}	v_{17}	v_{25}
1	0	v_0	v_{31}	v_0	v_{31}	v_0	v_{31}	v_0	v_{31}	v_0	v_{31}
1	-1	v_{17}	v_{25}	v_{24}	v_{28}	v_{12}	v_{14}	v_6	v_7	v_3	v_{19}
0	1	v_{14}	v_6	v_7	v_3	v_{19}	v_{17}	v_{25}	v_{24}	v_{28}	v_{12}
0	0	v_{31}	v_0	v_{31}	v_0	v_{31}	v_0	v_{31}	v_0	v_{31}	v_0
0	-1	v_7	v_3	v_{19}	v_{17}	v_{25}	v_{24}	v_{28}	v_{12}	v_{14}	v_6

Table (2.2): Optimum Active Voltage Vector Look-Up Table 2.

$d_{\Phi 1}$	d_{Tem1}	S_1	S_2	S_3	S_4	S_5	S_6	S_7	S_8	S_9	S_{10}
1	1	v_{18}	v_{26}	v_{10}	v_{11}	v_9	v_{13}	v_5	v_{21}	v_{20}	v_{22}
1	0	v_0	v_{31}	v_0	v_{31}	v_0	v_{31}	v_0	v_{31}	v_0	v_{31}
1	-1	v_{20}	v_{22}	v_{18}	v_{26}	v_{10}	v_{11}	v_9	v_{13}	v_5	v_{21}
0	1	v_{11}	v_9	v_{13}	v_5	v_{21}	v_{20}	v_{22}	v_{18}	v_{26}	v_{10}
0	0	v_{31}	v_0	v_{31}	v_0	v_{31}	v_0	v_{31}	v_0	v_{31}	v_0
0	-1	v_{13}	v_5	v_{21}	v_{20}	v_{22}	v_{18}	v_{26}	v_{10}	v_{11}	v_9

In each sampling time, the control scheme estimates the electromagnetic torque and stator flux linkage. Two hysteresis controllers compare the torque and flux reference values with their corresponding estimated quantities and generate an optimal switching signal for power switches.

The stator flux linkage components for each machine in the stationary reference frame can be estimated based on the phase currents and voltage measurements as follow:

$$\begin{aligned}
\hat{\Phi}_{\alpha s} &= \int (v_{\alpha s} - r_s i_{\alpha s})dt \\
\hat{\Phi}_{\beta s} &= \int (v_{\beta s} - r_s i_{\beta s})dt \\
\hat{\Phi}_{xs} &= \int (v_{xs} - r_s i_{xs})dt \\
\hat{\Phi}_{ys} &= \int (v_{ys} - r_s i_{ys})dt
\end{aligned} \tag{2.15}$$

The magnitude of the stator flux and its position are calculated as follows:

$$\begin{aligned}
\hat{\Phi}_{s1} &= \sqrt{\hat{\Phi}_{\alpha s}{}^2 + \hat{\Phi}_{\beta s}{}^2} \\
\hat{\theta}_{s2} &= \tan^{-1}\frac{\hat{\Phi}_{\beta s}}{\hat{\Phi}_{\alpha s}} \\
\hat{\Phi}_{s2} &= \sqrt{\hat{\Phi}_{xs}{}^2 + \hat{\Phi}_{ys}{}^2} \\
\hat{\theta}_{s2} &= \tan^{-1}\frac{\hat{\Phi}_{ys}}{\hat{\Phi}_{xs}}
\end{aligned} \tag{2.16}$$

The electromagnetic torques are estimated by:

$$\begin{aligned}
\hat{T}_{em1} &= \frac{5}{2} p_1 (\hat{\Phi}_{\alpha s} i_{\beta s} - \hat{\Phi}_{\beta s} i_{\alpha s}) \\
\hat{T}_{em2} &= \frac{5}{2} p_2 (\hat{\Phi}_{xs} i_{ys} - \hat{\Phi}_{ys} i_{xs})
\end{aligned} \tag{2.17}$$

Fig. (2.13) shows the block diagram of the conventional DTC of the proposed two-machine drive system. In each machine control, there are one speed regulators, two hysteresis comparator, look up-table, stator flux and electromagnetic torque estimator. The block of switching signals selection switches between the two tables through a given frequency to get independent control of two machine connected in parallel. The speed regulators generate the reference electromagnetic torque T_{em1} and T_{em2}, then its compart with their estimated, which are the inputs of look-up tables. The estimators block generate the electromagnetic torque, fluxes, positions, and sectors numbers.

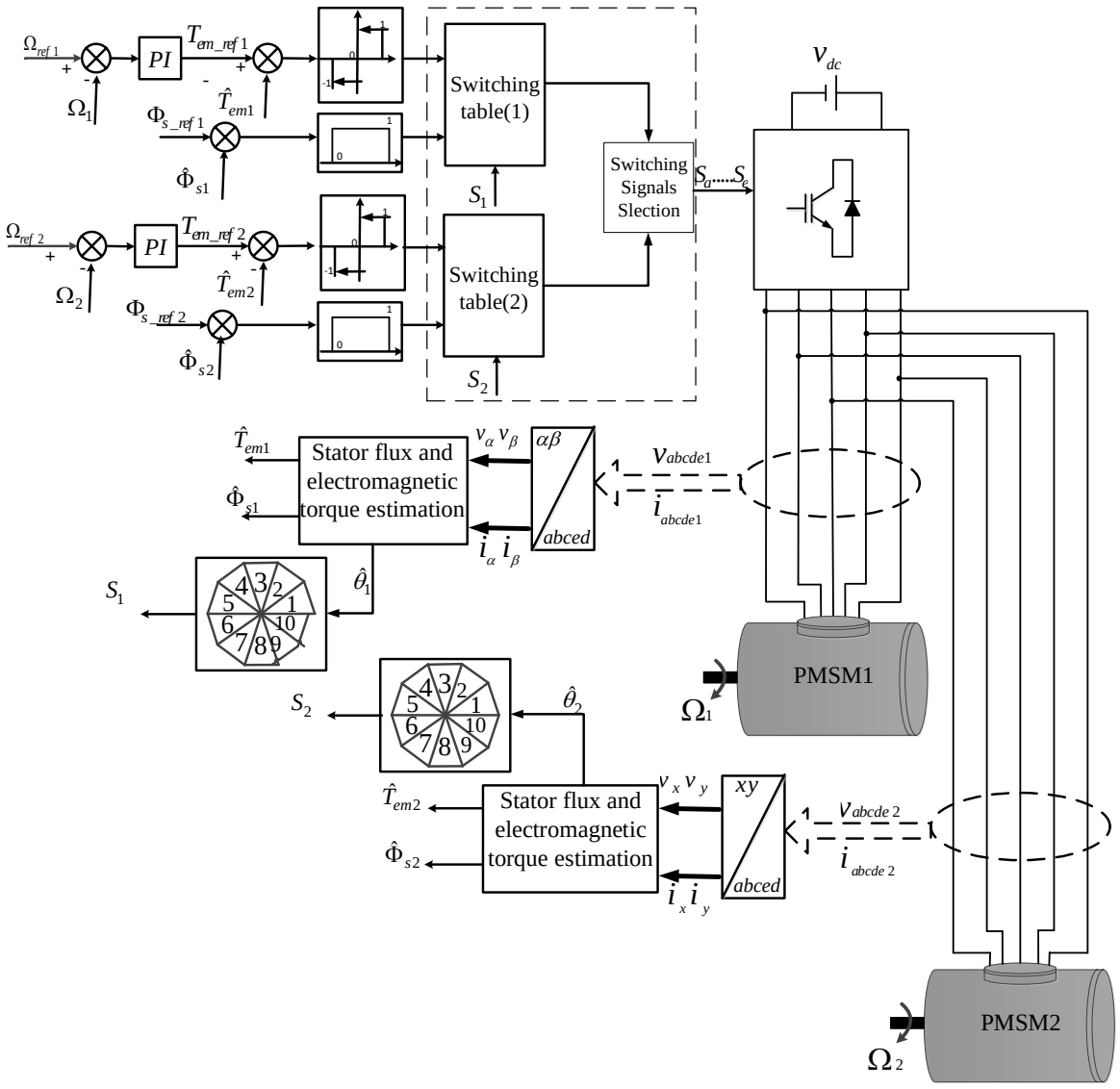

Fig. (2.13): DTC of parallel-connected two five-phase PMSMs drive system.

2.3.1.3 Simulation Results

The conventional DTC control scheme for the two-machine drive system of Fig. (2.13) is verified by using two similar 2-pole, 50 Hz five-phase PMSM. The parameters of the two machines are the same as those adopted in section (2.2.3). The tuning parameters for the PI-controllers are also given in table B.2 of appendix B. The applicability of conventional DTC for the two five-phase PMSMs drive system is verified through different simulation results as shown in Figs (2.14) to (2.16).

In Fig. (2.14), a standstill is included for both machine in different time. The second five-phase PMSM is operated at 0.5s to be equal to 50 rad/s, while the speed of the first five-phase PMSM is maintained constant equal to 100 rad/s then to become standstill at t=1.5s.

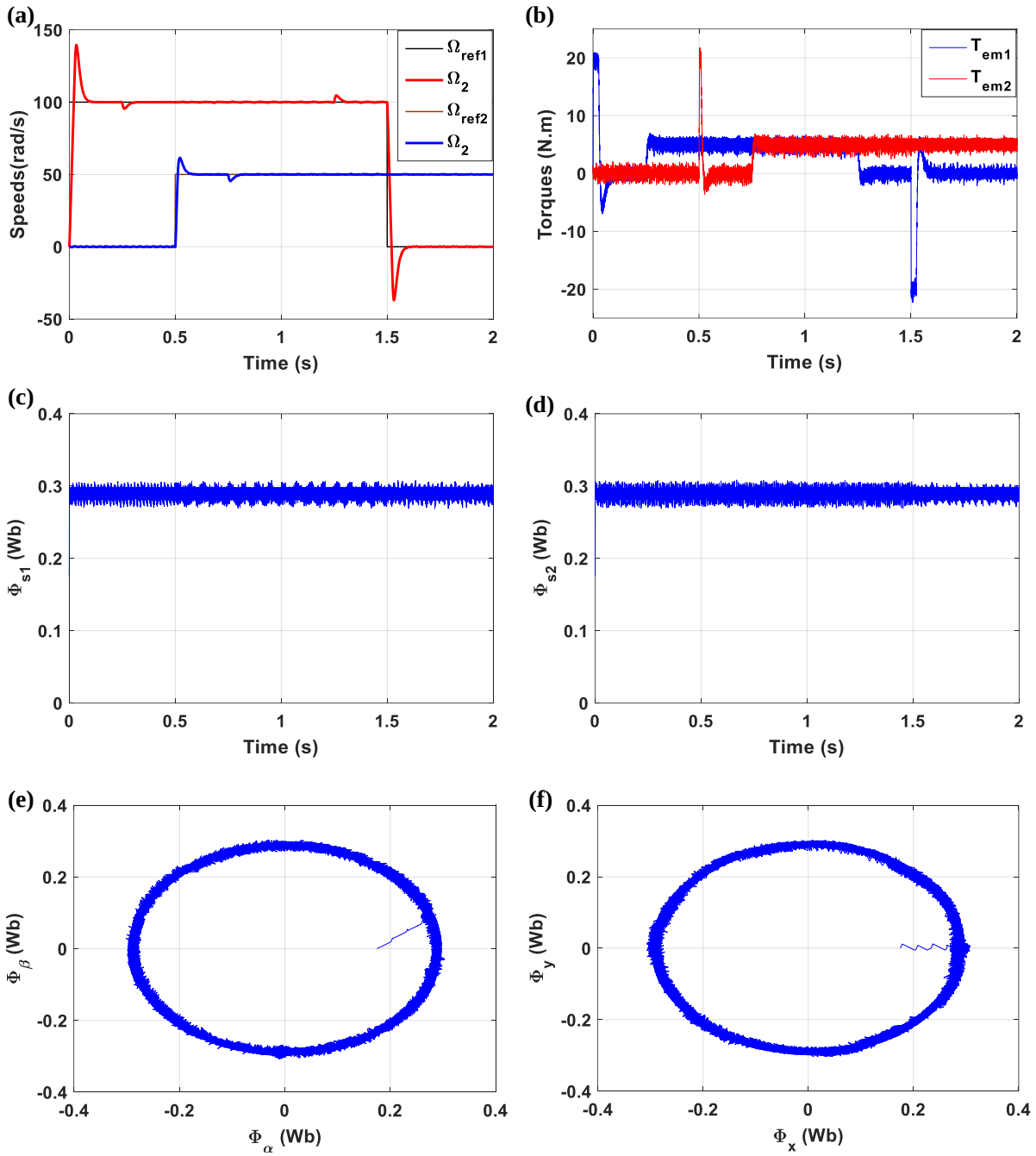

Fig. (2.14): Dynamic responses of parallel-connected two five-phase PMSMs drive controlled by conventional DTC; when one machine is at standstill and the other is still running: (a) the machine speeds, (b) electromagnetic torques, (c-d) Stator fluxes magnitudes, (e-f) Stator fluxes trajectories.

Fig. (2.15) shows the system performances when the speed of one machine is kept constant and the other change the direction. Both machine started at the same time, then the second five-phase PMSM changes the direction at t=0.5s from 50 rad/s to -50 rad/s after it returns to 50 rad/s at t= 1.5s. While the speed of the first five-phase PMSM is maintained constant equal to 100 rad/s then at t=1s is changed to be -100 rad/s. The load torque is applied at t=0.25s on both machines.

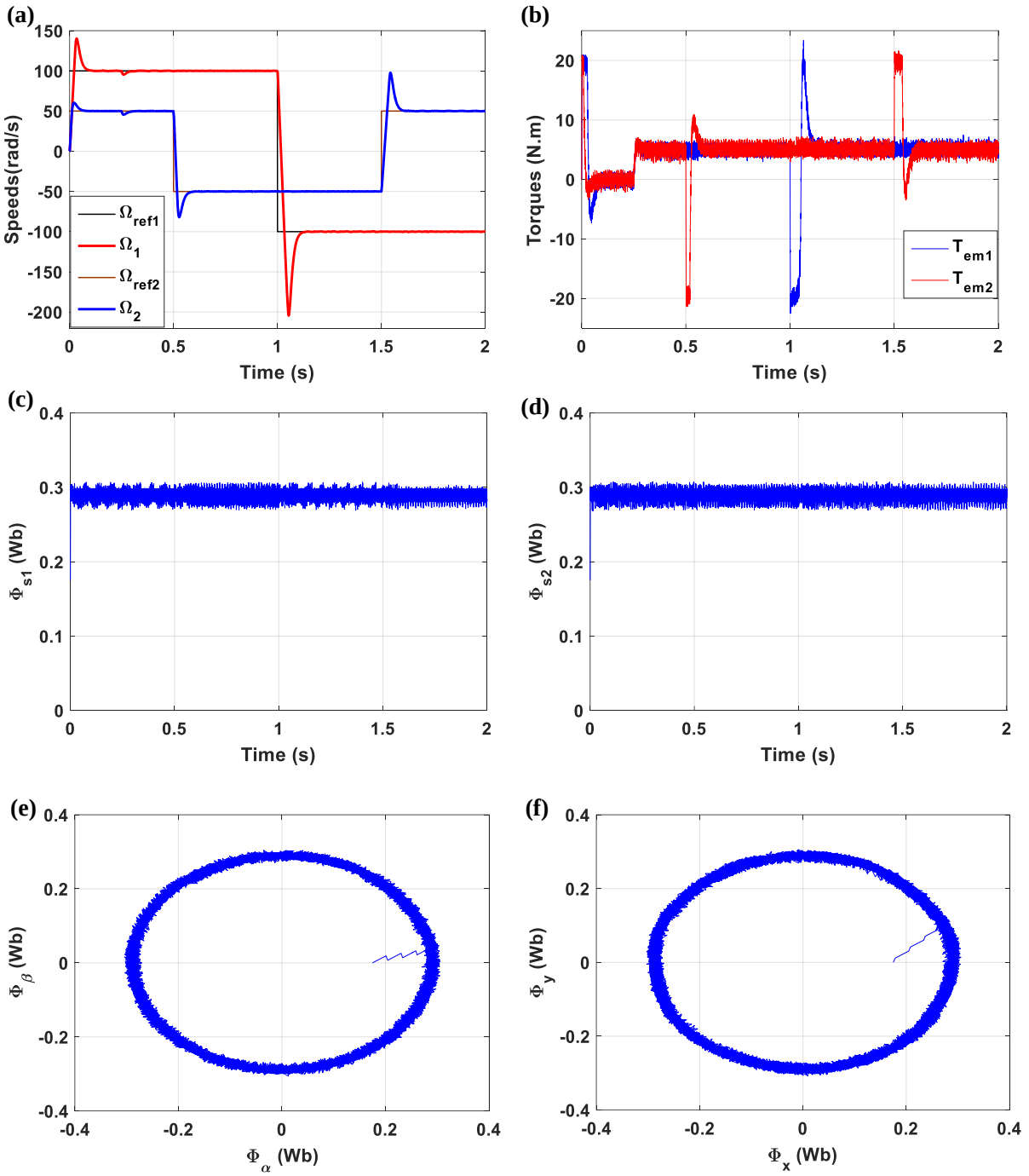

Fig. (2.15): Dynamic responses of parallel-connected two five-phase PMSMs drive controlled by conventional DTC: when the speed of one machine is kept constant and the other change the direction: (a) the machine Speeds, (b) electromagnetic torques, (c-d) Stator fluxes magnitudes, (e-f) Stator fluxes trajectories.

Fig (2.16) shows the performances of the system when the two machines are operating in the opposite directions. In this test, the speed profile of the first five-phase PMSM changes from +100 rad/s to -50 rad/s at t = 1s, while the speed of the second five-phase PMSM changes from - 50 rad to 100 rad/s at t = 1s. As can be noticed from the simulation results, a full-decoupled

control is preserved and the speed and torque of the second five-phase PMSM are not influenced by the acceleration period of the first five-phase PMSM.

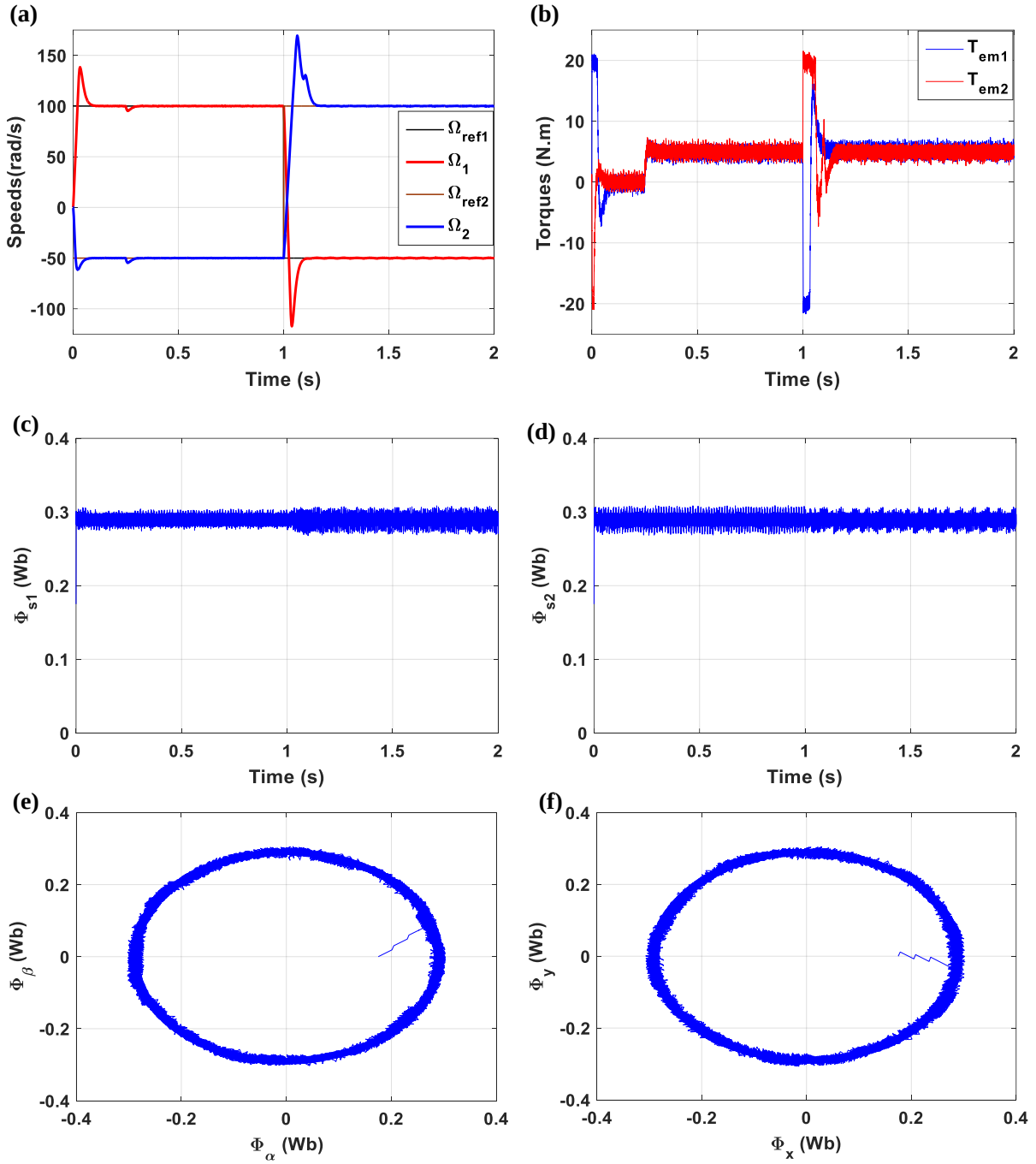

Fig. (2.16): Dynamic responses of parallel-connected two five-phase PMSMs drive controlled by conventional DTC: when the two machine s are operating in the opposite directions: (a) the machine Speeds, (b) electromagnetic torques, (c-d) Stator fluxes magnitudes, (e-f) Stator fluxes trajectories.

From Figs. (2.14) to (2.16), it can be noticed that each machine speed follows closely its reference, but with overshoot in starting-up and in reverse mode. The speed and the electromagnetic torque of one machine are not affected by the starting operation of the second one.

It can be seen that, the stator flux magnitudes and trajectories are without overshoot, and there are no effects even in reverse mode and the stator flux trajectories are almost circular.

From Figs. (2.14) to (2.16) it can be observed that, step loading of one machine does not cause any disturbance in the other machine's speed and torque responses. In addition, these results prove the ability of the speed controllers to reject the effects of the applied load torques keeping the speeds at their reference values with good performance.

It can be noticed that, there are an important ripple in the electromagnetic torque and the stator flux vector, these ripples are caused by the hysteresis comparators. This is the major drawback of conventional DTC, which can increase the noise and vibration of the two machines connected in parallel. To improve the control performance and decrease the torque ripple a DTC based on SVM is recognized to be an effective solution.

2.3.2 Direct Torque Control with Space Vector Modulation

The main problem of conventional DTC is the high level of torque ripples, variable switching frequency of the inverter, and acoustic noises [64]. Recently, among numerous studies, proposed to overcome these drawbacks, the space vector modulation is implemented to replace the switching table of the voltage vector selection and provide a constant inverter switching frequency [14-17].

DTC-SVM of five-phase PMSM machines is a powerful control method, due to achieving fast dynamic response and high performance. The DTC-SVM method is based on space voltage vector theory [60][65]. The decoupled flux and torque control is achieved using appropriate space voltage vectors of the inverter. Several DTC-SVM methods have been proposed according to their structures, such as, the closed loop flux control and the closed loop torque and flux control. In this section, The DTC-SVM is based on closed loop of the torque and flux control, which is used two PI-controller to control the flux and torque of the machine [18].

The machine model equations can be written in stator flux coordinate system z1-z2-z3-z4 by replacing $\Phi_d = \Phi_s$, $\Phi_q = 0$, $L_d = L_q$ in (1.9) which gives:

$$\begin{aligned}
&\frac{d\Phi_{s1}}{dt} = v_{zs1} - r_{s1} i_{zs1} \\
&\Phi_{s1} = (v_{zs2} - r_{s1} i_{zs2})(1/\omega_1) \\
&\frac{d\Phi_{s2}}{dt} = v_{zs3} - r_{s2} i_{zs3} \\
&\Phi_{s2} = (v_{zs4} - r_{s2} i_{zs4})(1/\omega_2)
\end{aligned} \tag{2.18}$$

The torques expression of both machines are:

$$T_{em1} = \frac{5 p_1 \Phi_{s1}}{2 r_{s1}} (v_{zs2} - \omega_1 \Phi_{s1})$$
$$T_{em2} = \frac{5 p_2 \Phi_{s2}}{2 r_{s2}} (v_{zs4} - \omega_2 \Phi_{s2}) \quad (2.19)$$

In this control scheme the reference stator flux magnitude Φ_{s_ref} and reference electromagnetic torque T_{em_ref} are compared with their estimated values, respectively. The flux and torque errors are delivered to PI-controllers. Therefore, the flux and torque quantities can be controlled as shown in Fig. (2.17).

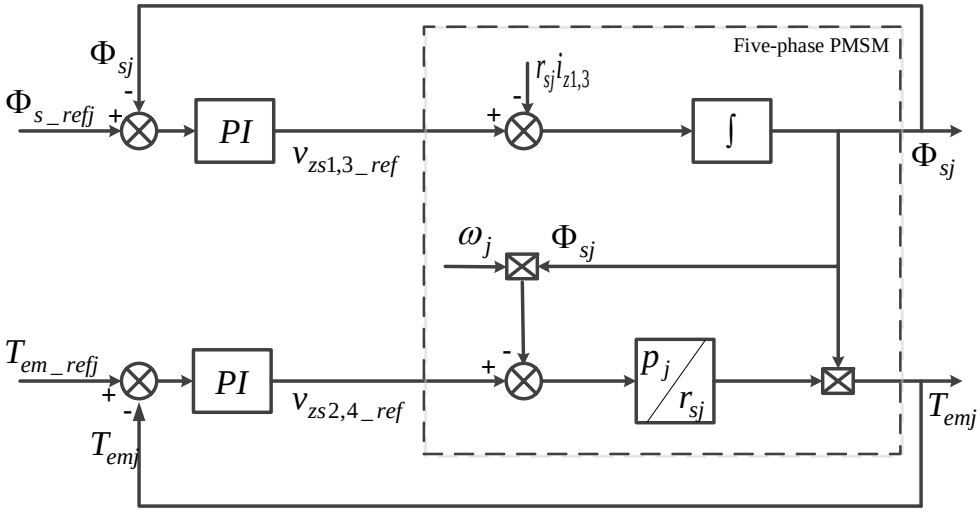

Fig. (2.17): Block diagram of the flux and torque loops.

The block diagram of the control system is presented in Fig. (2.18). In this control scheme, the torques reference are generated by controlling machines speeds. The references stator flux magnitudes and electromagnetic torques are compared with their estimated values. The flux and torque errors of the two machines are delivered to PI-controllers of the fluxes and torques, which generate the stator voltage components in stator flux coordinates v_{zs1}-v_{zs2}, v_{zs3}-v_{zs4}. This voltage signals are transformed to stationary coordinates v_α-v_β, v_x-v_y using the stator flux position. The reference stator voltage vector are delivered to space vector modulator (SVM), which generates the switching signals $S_{a,b,c,d,e}$ of the inverter.

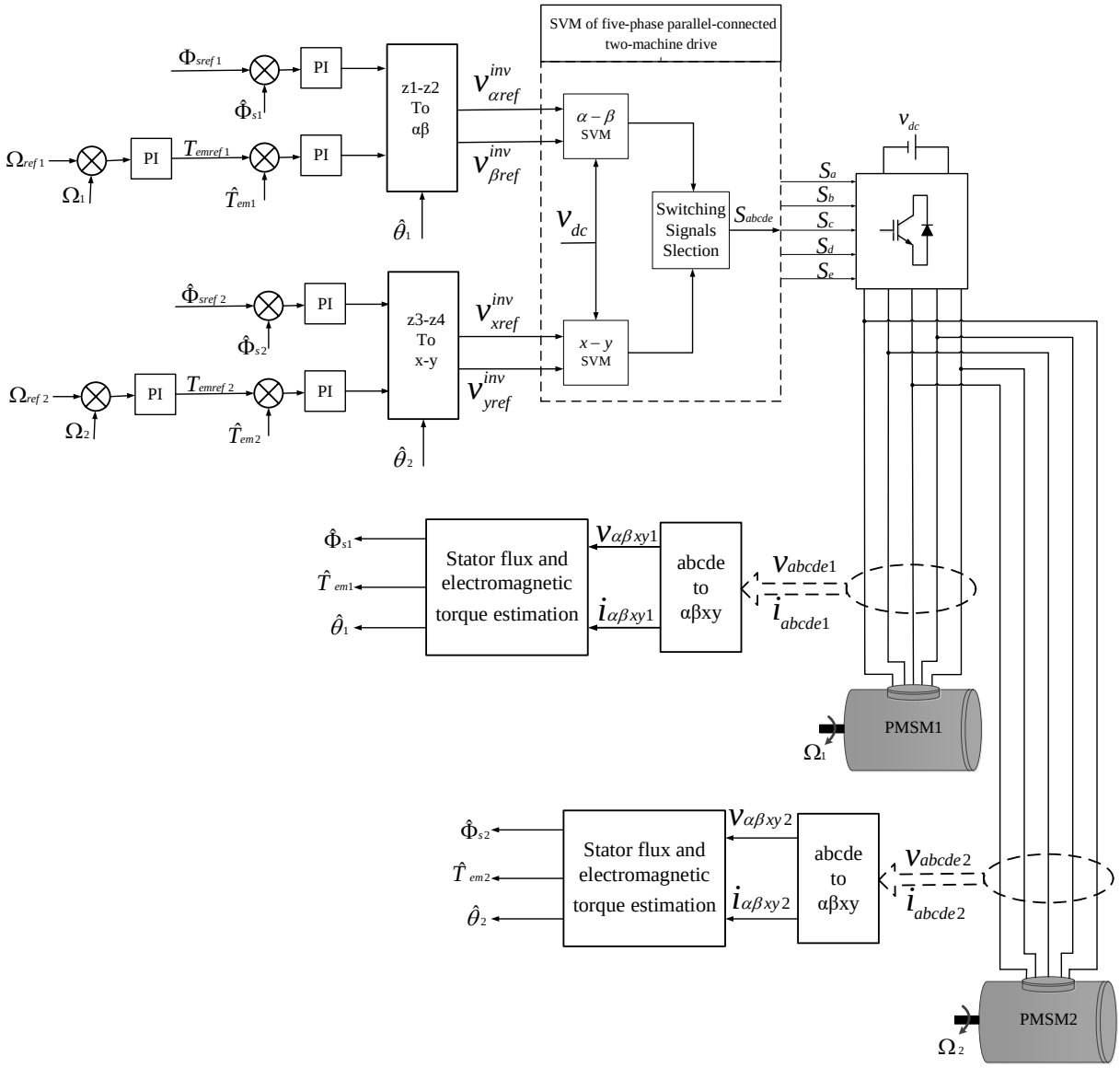

Fig. (2.18): Schematic block diagram of DTC-SVM for parallel-connected two five-phase PMSMs.

2.3.3 Flux and Torque Controllers Synthesis

2.3.3.1 Flux Controllers

The expression from of stator currents in z1-z2-z3-z4 axes are:

$$
\begin{aligned}
i_{zs1} &= \frac{1}{L_{s1}}(\Phi_{s1} - \Phi_{f1}\cos(\delta_1)) \\
i_{zs2} &= \frac{1}{L_{s1}}(\Phi_{f1}\sin(\delta_1)) \\
i_{zs3} &= \frac{1}{L_{s2}}(\Phi_{s2} - \Phi_{f2}\cos(\delta_2)) \\
i_{zs4} &= \frac{1}{L_{s2}}(\Phi_{f2}\sin(\delta_2))
\end{aligned}
\tag{2.20}
$$

By substituting (2.20) into equation (2.18) one it results:

$$\begin{aligned} v_{zs1} &= \frac{r_{s1}}{L_{s1}}\Phi_{s1} - \frac{r_{s1}\Phi_{f1}}{L_{s1}}\cos(\delta_1) + \frac{d\Phi_{s1}}{dt} \\ v_{zs3} &= \frac{r_{s1}}{L_{s12}}\Phi_{s2} - \frac{r_{s2}\Phi_{f2}}{L_{s2}}\cos(\delta_2) + \frac{d\Phi_{s2}}{dt} \end{aligned} \tag{2.21}$$

Using Laplace transform, the equation (2.21) can be written as:

$$\begin{aligned} v_{zs1} &= \Phi_{s1}\left(\frac{r_{s1}}{L_{s1}} + s\right) - \frac{r_{s1}\Phi_{f1}}{L_{s1}}\cos(\delta_1) \\ v_{zs3} &= \Phi_{s2}\left(\frac{r_{s2}}{L_{s12}} + \mathrm{s}\right) - \frac{r_{s2}\Phi_{f2}}{L_{s2}}\cos(\delta_2) \end{aligned} \tag{2.22}$$

Assuming small changes of δ_1 and δ_2, and neglecting the terms $(r_{s1}\Phi_{f1}/L_{s1})\cos(\delta_1)$ and $(r_{s2}\Phi_{f2}/L_{s2})\cos(\delta_2)$, the equations (2.22) reduces to following simplified forms:

$$\begin{aligned} v_{zs1} &= \Phi_{s1}\left(\frac{r_{s1}}{L_{s1}} + s\right) \\ v_{zs3} &= \Phi_{s2}\left(\frac{r_{s1}}{L_{s12}} + \mathrm{s}\right) \end{aligned} \tag{2.23}$$

The transfer functions between stator flux amplitudes and stator voltages are expressed using (2.23) as:

$$\begin{aligned} G_{\Phi_{s1}}(s) &= \frac{\Phi_{s1}}{v_{zs1}} = \frac{1}{s + r_{s1}/L_{s1}} \\ G_{\Phi_{s2}}(s) &= \frac{\Phi_{s2}}{v_{zs3}} = \frac{1}{s + r_{s2}/L_{s2}} \end{aligned} \tag{2.24}$$

The block diagram of the closed-loop flux controllers are shown in Figs. (2.19) and (2.20).

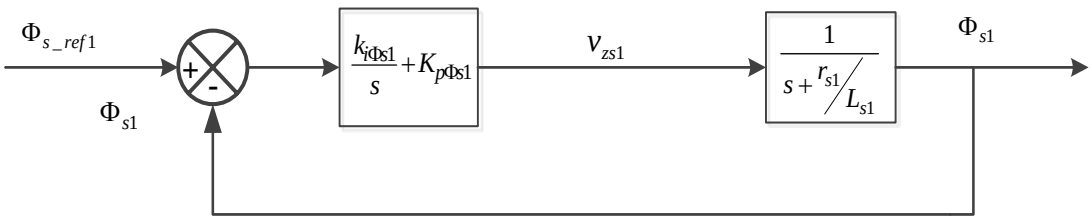

Fig. (2.19: Block diagram of the closed loop flux (Φ_{s1}) control.

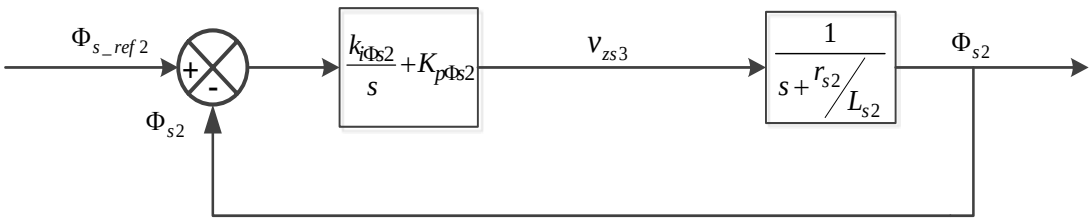

Fig. (2.20): Block diagram of the closed loop flux (Φ_{s2}) control.

The closed-loop transfer functions are given by:

$$G_{\Phi s1}(s)=\frac{(\frac{k_{i\Phi s1}}{s}+sk_{p\Phi s1})}{s^2+(\frac{k_{p\Phi s1}+r_{s1}}{L_{s1}})s+k_{i\Phi s1}/L_{s1}} \tag{2.25}$$

$$G_{\Phi s2}(s)=\frac{(\frac{k_{i\Phi s2}}{s}+sk_{p\Phi s2})}{s^2+(\frac{k_{p\Phi s2}+r_{s2}}{L_{s2}})s+k_{i\Phi s2}/L_{s2}} \tag{2.26}$$

By identification the denominators of (2.25) and (2.26) with the characteristic equation of a desired second order system, it yields:

$$\begin{cases} k_{i\Phi s1}=L_{s1}\omega_{0\Phi s1}^2 \\ k_{p\Phi s1}=2\xi_{\Phi s1}L_{s1}\omega_{0\Phi s1}-r_{s1} \end{cases} \tag{2.27}$$

$$\begin{cases} k_{i\Phi s2}=L_{s2}\omega_{0\Phi s2}^2 \\ k_{p\Phi s2}=2\xi_{\Phi s2}L_{s2}\omega_{0\Phi s2}-r_{s2} \end{cases} \tag{2.28}$$

with $\xi_{\Phi s1},\xi_{\Phi s2}$ are the damping ratio and $\omega_{0\Phi s1}$, $\omega_{0\Phi s2}$ are the natural frequency.

2.3.3.2 Torque Controller

The five-phase PMSM equations in stator flux coordinates under the assumption L_d=L_q can be written as:

$$\begin{aligned} v_{zs2}&=r_{s1}i_{zs2}+\omega_1\Phi_{s1} \\ v_{zs4}&=r_{s2}i_{zs4}+\omega_2\Phi_{s2} \end{aligned} \tag{2.29}$$

$$\begin{aligned} 0&=L_{s1}i_{zs2s}-\Phi_{f1}\sin(\delta_1) \\ 0&=L_{s2}i_{zs4s}-\Phi_{f2}\sin(\delta_2) \end{aligned} \tag{2.30}$$

The torque expression of both machines are:

$$T_{em1} = \frac{5p_1\Phi_{s1}}{2} i_{zs2}$$
$$T_{em2} = \frac{5p_2\Phi_{s2}}{2} i_{zs4} \quad (2.31)$$

From equation (2.30) with assumption that for small angle $\sin(\delta_1) \simeq \delta_1$ and $\sin(\delta_2) \simeq \delta_2$, the torque angle can be expressed as:

$$\delta_1 = \frac{i_{zs2}L_{s1}}{\Phi_{f1}}$$
$$\delta_2 = \frac{i_{zs4}L_{s2}}{\Phi_{f2}} \quad (2.32)$$

The voltage equation (2.29) becomes:

$$v_{zs2} = r_{s1}i_{zs2} + \frac{\Phi_{s1}L_{s1}}{\Phi_{f1}}\frac{di_{zs2}}{dt}$$
$$v_{zs4} = r_{s2}i_{zs4} + \frac{\Phi_{s2}L_{s2}}{\Phi_{f2}}\frac{di_{zs4}}{dt} \quad (2.33)$$

with $\omega_j = \frac{d\delta_j}{dt}$

By replacing $i_{zs2,4}$ calculated from (2.31) into (2.33), it yields:

$$v_{zs2} = \frac{2r_{s1}}{5p_1\Phi_{s1}}T_{em1} + \frac{2L_{s1}}{\Phi_{f1}}\frac{dT_{em1}}{dt}$$
$$v_{zs4} = \frac{2r_{s2}}{5p_2\Phi_{s2}}T_{em2} + \frac{2L_{s2}}{\Phi_{f2}}\frac{dT_{em2}}{dt} \quad (2.34)$$

By applying laplace transform, the equation (2.34) can be written as:

$$v_{zs2} = (\frac{2r_{s1}}{5p_1\Phi_{s1}} + \frac{2L_{s1}}{\Phi_{f1}}s)T_{em1}$$
$$v_{zs4} = (\frac{2r_{s2}}{5p_2\Phi_{s2}} + \frac{2L_{s2}}{\Phi_{f2}}s)T_{em2} \quad (2.35)$$

The transfer functions between torques and voltages (v_{zs2} and v_{zs4}) are:

$$G_{T_{em1}}(s) = \frac{T_{em1}}{v_{zs2}} = \frac{1}{\frac{2r_{s1}}{5p_1\Phi_{s1}} + \frac{2L_{s1}}{5p_1\Phi_{f1}}s}$$
$$G_{T_{em2}}(s) = \frac{T_{em2}}{v_{zs4}} = \frac{1}{\frac{2r_{s2}}{5p_2\Phi_{s2}} + \frac{2L_{s2}}{5p_2\Phi_{f2}}s} \quad (2.36)$$

The block diagram of the closed-loop torques controllers are shown in Figs. (2.21) and (2.22).

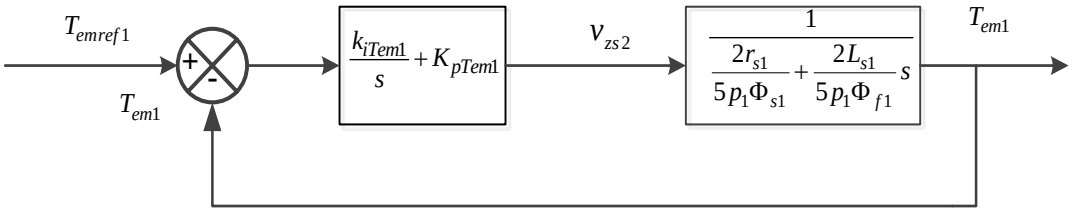

Fig. (2.21): Block diagram of the closed loop torque (T_{em1}) control of the first machine.

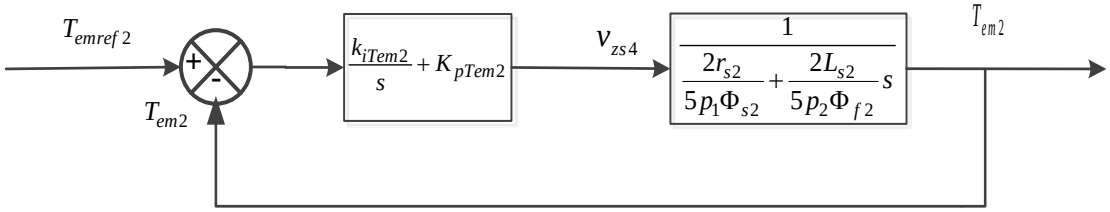

Fig. (2.22): Block diagram of the closed loop torque (T_{em2}) control of the second machine.

The closed-loop transfer functions are given by:

$$G_{T_{em1}}(\mathrm{s}) = \frac{(\frac{k_{iT_{em1}}}{s} + sK_{pT_{em1}})}{s^2 + (\frac{K_{pT_{em1}} + A_{11}}{A_{12}})s + k_{iT1}/A_{12}} \tag{2.37}$$

$$G_{T_{em2}}(\mathrm{s}) = \frac{(\frac{k_{iT_{em2}}}{s} + sK_{pT_{em2}})}{s^2 + (\frac{K_{pT_{em2}} + A_{21}}{A_{22}})s + k_{iT_{em2}}/A_{22}} \tag{2.38}$$

where

$$A_{11} = \frac{2r_{s1}}{5p_1\Phi_{s1}},\ A_{12} = \frac{2L_{s1}}{5p_1\Phi_{f1}}$$

$$A_{21} = \frac{2r_{s2}}{5p_2\Phi_{s2}}\ A_{22} = \frac{2L_{s2}}{5p_2\Phi_{f2}}$$

By identification the denominators of (2.37) and (2.38) with the characteristic equation of a desired second order system, it yields:

$$\begin{cases} k_{iT_{em1}} = A_{12}\omega_{0T_{em1}}^2 \\ k_{pT_{em1}} = 2\xi_{T_{em1}}A_{12}\omega_{0T_{em1}} - A_{11} \end{cases} \tag{2.39}$$

$$\begin{cases} k_{iT_{em2}} = A_{22}\omega_{0T_{em2}}^2 \\ k_{pT_{em2}} = 2\xi_{T_{em2}}A_{22}\omega_{0T_{em2}} - A_{21} \end{cases} \tag{2.40}$$

with $\xi_{T_{em1}}, \xi_{T_{em2}}$ are the damping ratio and $\omega_{0T_{em1}}, \omega_{0T_{em2}}$ are the natural frequency.

2.3.4 Simulation Results

To demonstrate the effectiveness of the DTC-SVM scheme applied for two identical 2-pole, five-phase PMSM connected in parallel, with different simulation results have been presented to demonstrating the decoupling and independent control of the two machines connected in parallel as shown in Figs (2.23) to (2.25). The tuning parameters for the PI-controllers are given in table B.3 of appendix B.

The first five-phase PMSM is changed from 100 rad/s to standstill at t=1.5s, while the second five-phase PMSM is started at t=0.5s and kept constant equal to 50 rad/s until the end of the test. There are no variation in speeds and electromagnetic torques can be seen for any of the machines, during the starting operation, meaning that completely decoupled between the machines have been achieved.

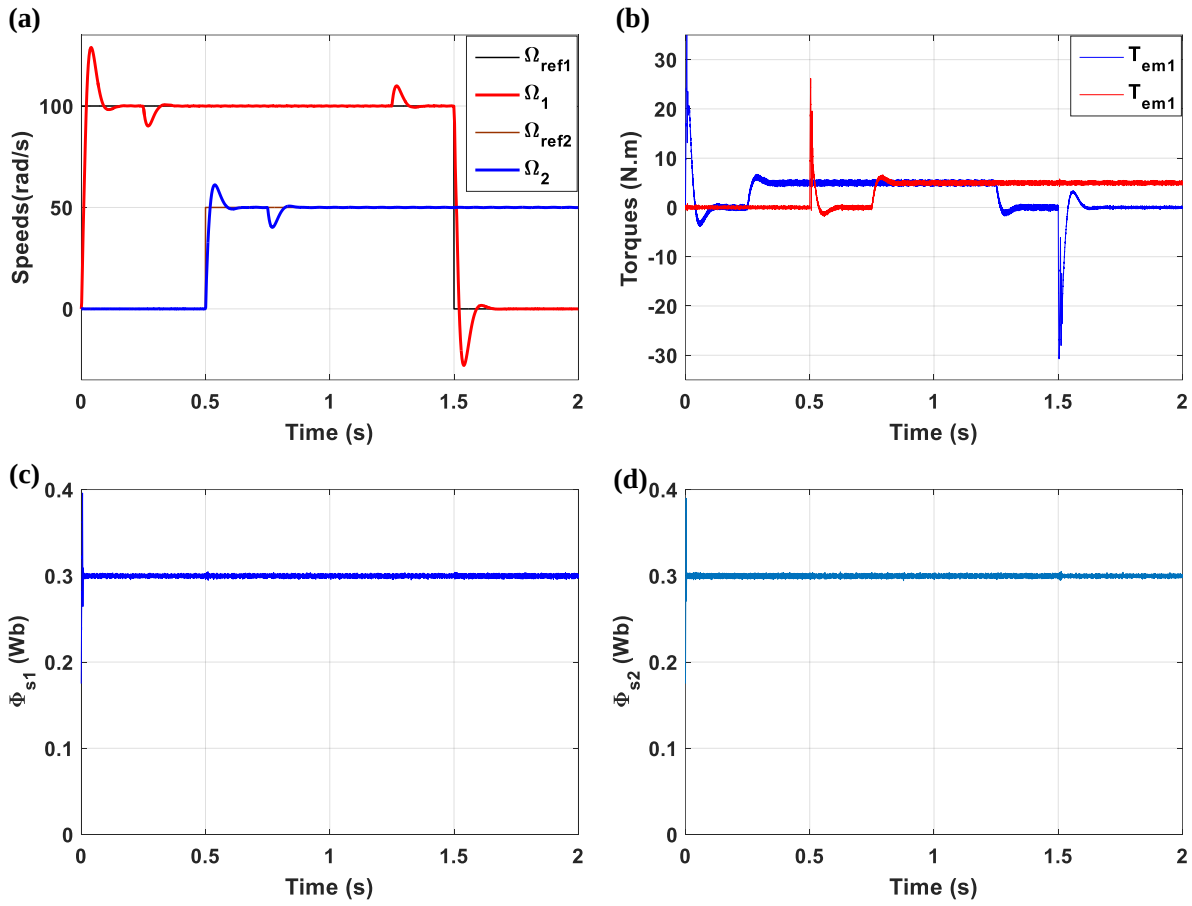

Fig. (2.23): Dynamic responses of parallel-connected two five-phase PMSMs system controlled by DTC-SVM: when one machine is at standstill and the other is still running: (a) the machine Speeds, (b) electromagnetic torques, (c-d) Stator fluxes magnitudes, and (e-f) Stator fluxes trajectories.

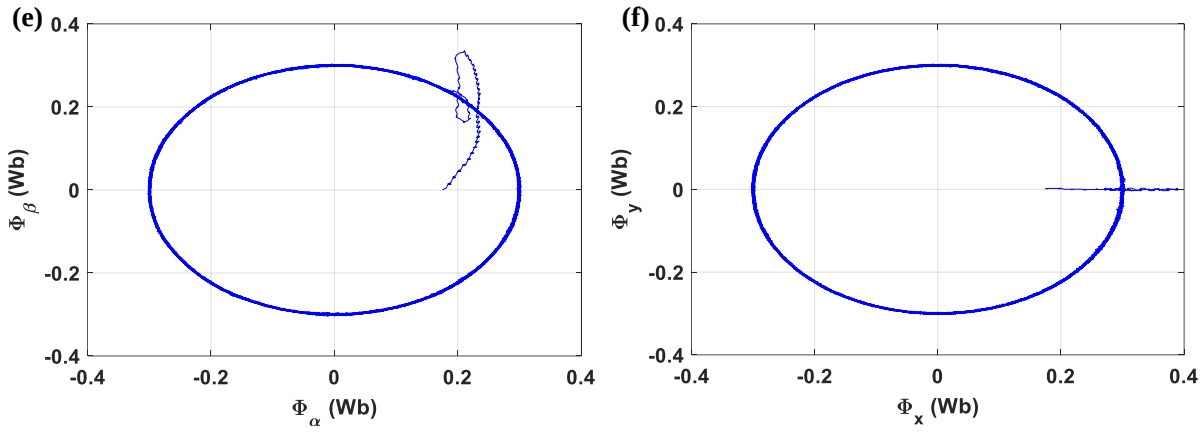

Continued to Fig. (2.23)

Fig (2.24) shows when the machine is kept constant and the other change the direction. Both machine are started at the same time, and then several speeds are applied. The speed of the first five-phase PMSM is changed the direction from 100 rad/s to -100 rad/s at t=1s. The second five-phase PMSM changes the direction from 50 rad/s to -50 rad/s after that return to 50 rad/s at t= 0.5s and 1.5s, respectively. The load torque applies at t=0.25s for both machine.

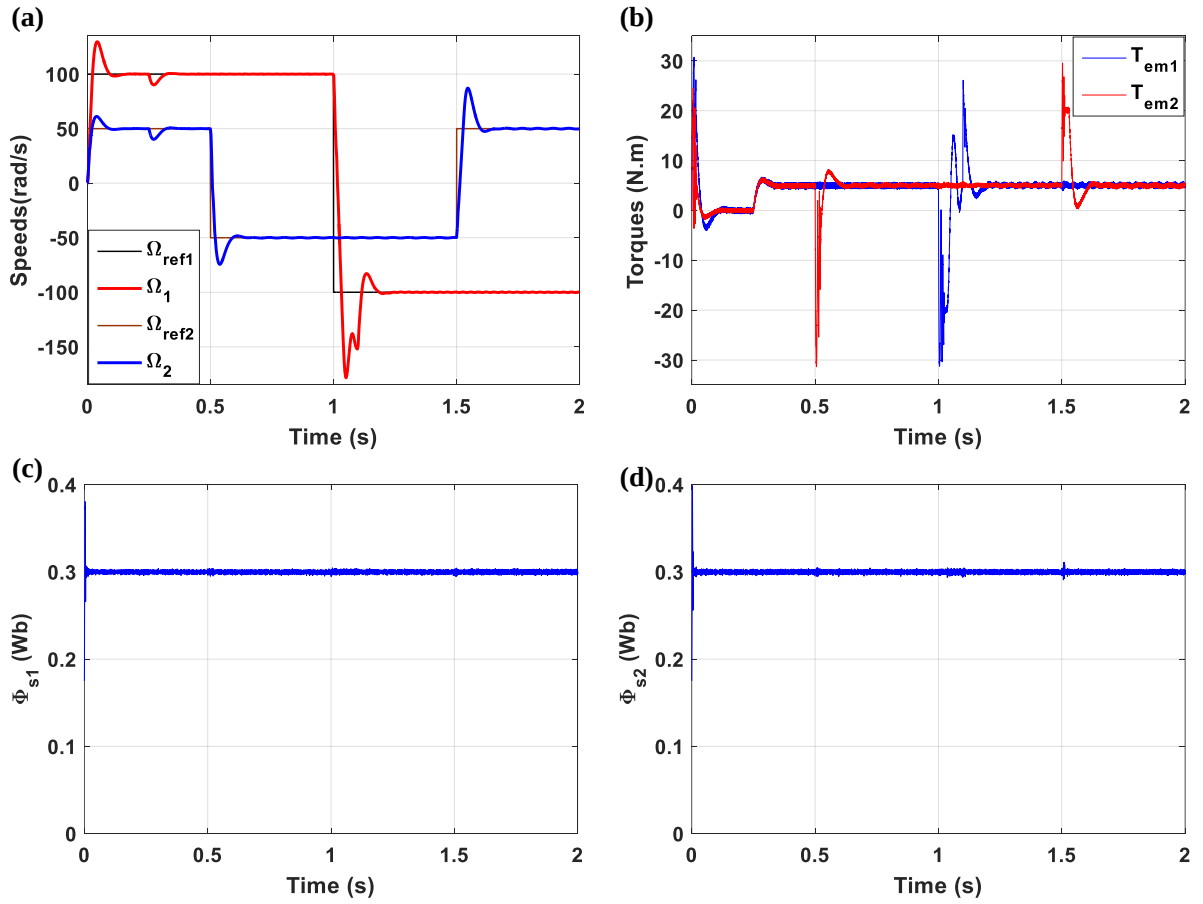

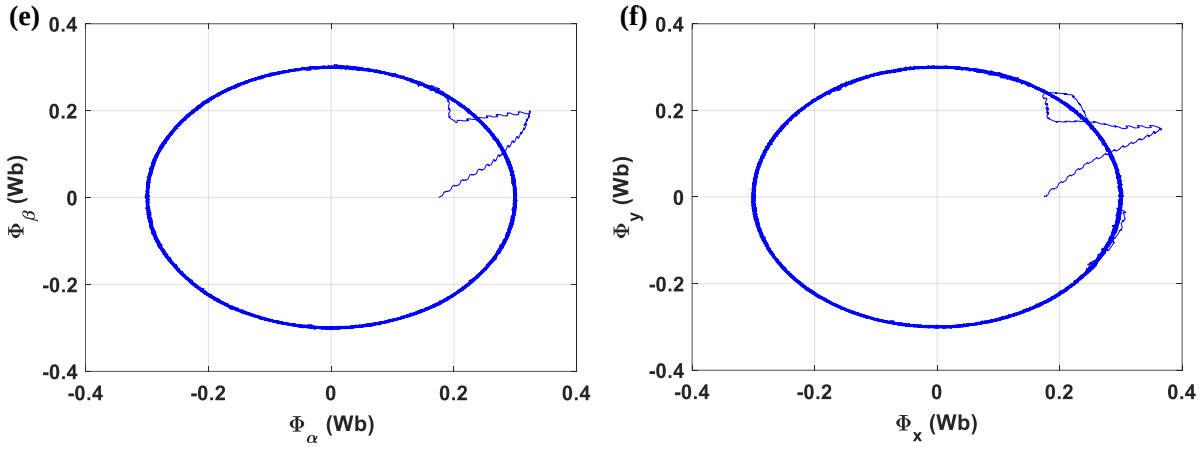

Fig. (2.24): Dynamic responses of parallel-connected two five-phase PMSMs system controlled by DTC-SVM: when one machine is kept constant and the other change the direction: (a) the machine Speeds, (b) electromagnetic torques, (c-d) Stator fluxes magnitudes, and (e-f) Stator fluxes trajectories.

Fig (2.25) shows when the two machines are operating in the opposite directions. Both machine are started in the opposite direction at the same time, then the speed of the first five-phase PMSM changes from +100 rad/s to -50 rad/s at t = 1s, while the speed of the second five-phase PMSM changes from - 50 rad to 100 rad/s at t = 1s.

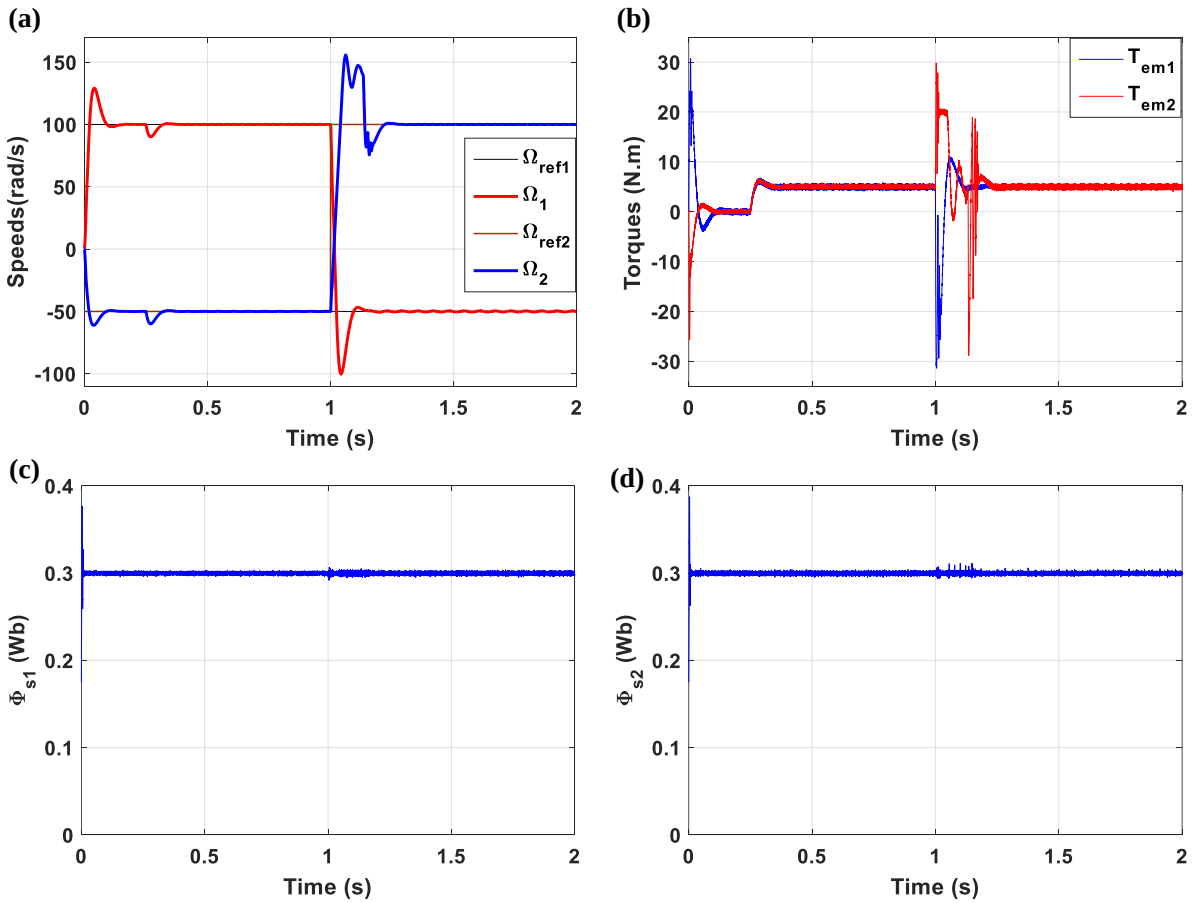

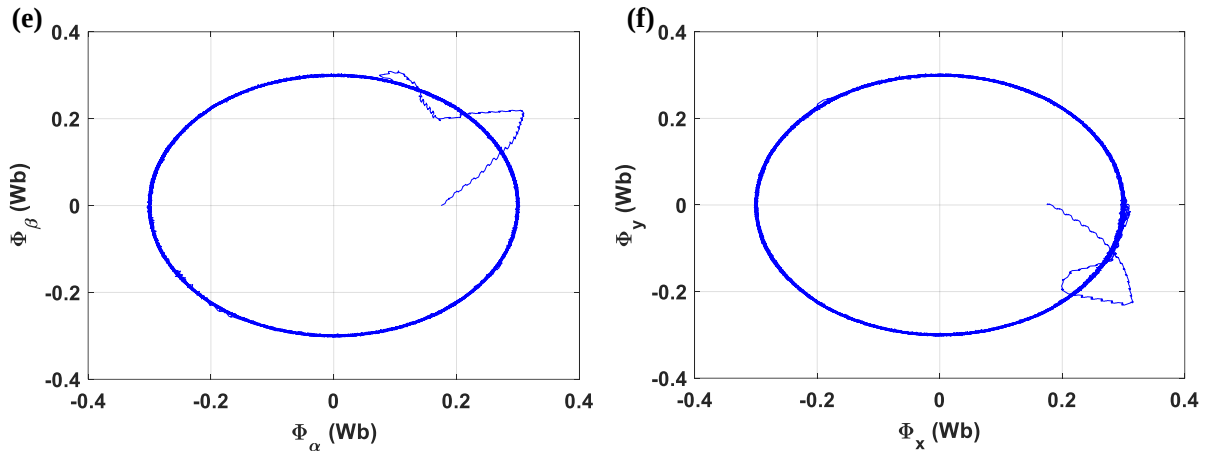

Fig. (2.25): Dynamic responses of parallel-connected two five-phase PMSMs system controlled by DTC-SVM: when the two machine s are operating in the opposite directions: (a) the machine Speeds, (b) electromagnetic torques, (c-d) Stator fluxes magnitudes, and (e-f) Stator fluxes trajectories.

From Figs. (2.22) to (2.24), it can be noticed from the simulation results that the decoupled control is preserved and the characteristics of both machines are unaffected. In addition to that, each machine speed follows closely its reference, and the speed as well as the electromagnetic torque of one machine are not affected by the starting operation of the second one.

It can be seen that, the stator flux magnitudes and trajectories are with overshoot, faster responses, reduce the ripples of the torque and flux as well as there are no effects even in reverse mode and the stator flux trajectories are almost circular. The Stator fluxes magnitudes and trajectories, which are almost circular.

It can be observed from Figs. (2.22) to (2.25) that, step loading of one machine does not cause any disturbance in the other machine's speed and torque responses. In addition, these results prove the ability of the speed controllers to reject the effects of the applied load torques keeping the speeds at their reference values with good performance.

The DTC based on SVM is reduces the ripples of the electromagnetic torque and the stator flux vector, which improves the viability and the performance of parallel-connected two five-phase PMSMs fed by a single five-phase VSI. In addition, the results show a good decoupling between the torque and flux for each machine, which demonstrates the full control capability of DTC-SVM compared with conversional DTC.

2.4 General Comparison between FOC, DTC-SVM and DTC

In this section, we introduce a comparative study between FOC, DTC-SVM and, conventional DTC. To show the viability and the performance of each control of parallel-connected two five-

phase PMSMs fed by five-phase VSI, for different operation modes of the proposed drive have been presented.

2.4.1 Case 1: Two machines operating in the same and opposite directions

Fig. (2.26) shows comparison between dynamic response of the two machines connected in parallel and running sometimes in the same direction and sometimes in the opposite direction for different decoupling controllers. The first PMSM change the direction from 100 rad/s to -100 rad/s at t=1s, while the second PMSM change from 50 rad/s to -50 rad/s than to 50rad/s at t=0.5s and 1.5s, respectively.

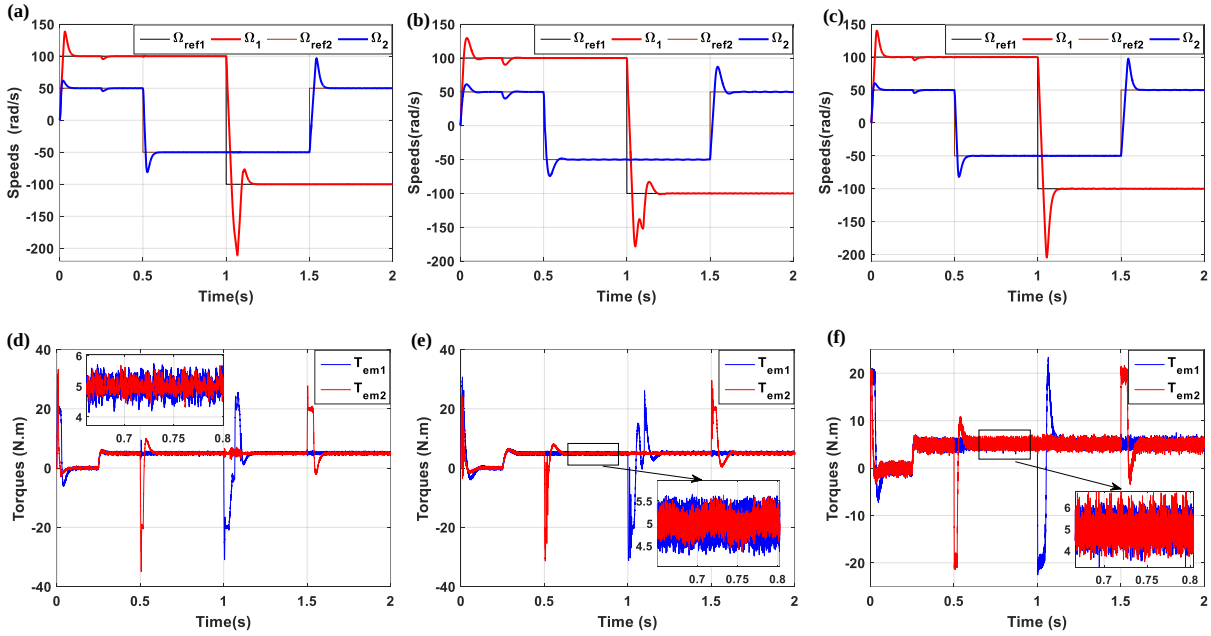

(FOC) (DTS-SVM) (DTC-switching up-table)

Fig. (2.26): Dynamic responses of parallel-connected two five-phase PMSMs system operating at different speed references: (a, d) the machine speeds and electromagnetic torques controlled by FOC: (b, e) the machine speeds and electromagnetic torques controlled by DTC-SVM, (c, f) the machine speeds electromagnetic and torques controlled by conventional DTC.

2.4.2 Case 2: Low speed operation

The two machine are running at two speeds in the opposite directions. In starting phase, the first PMSM is rotating at +20 rad/s; the second PMSM is running at the opposite speed (-10 rad/s). After that at the same time (t=1s) the first PMSM changes the direction from 20 rad/s to -10 rad/s, while the second PMSM change the direction from -10 rad/s to 20 rad/s.

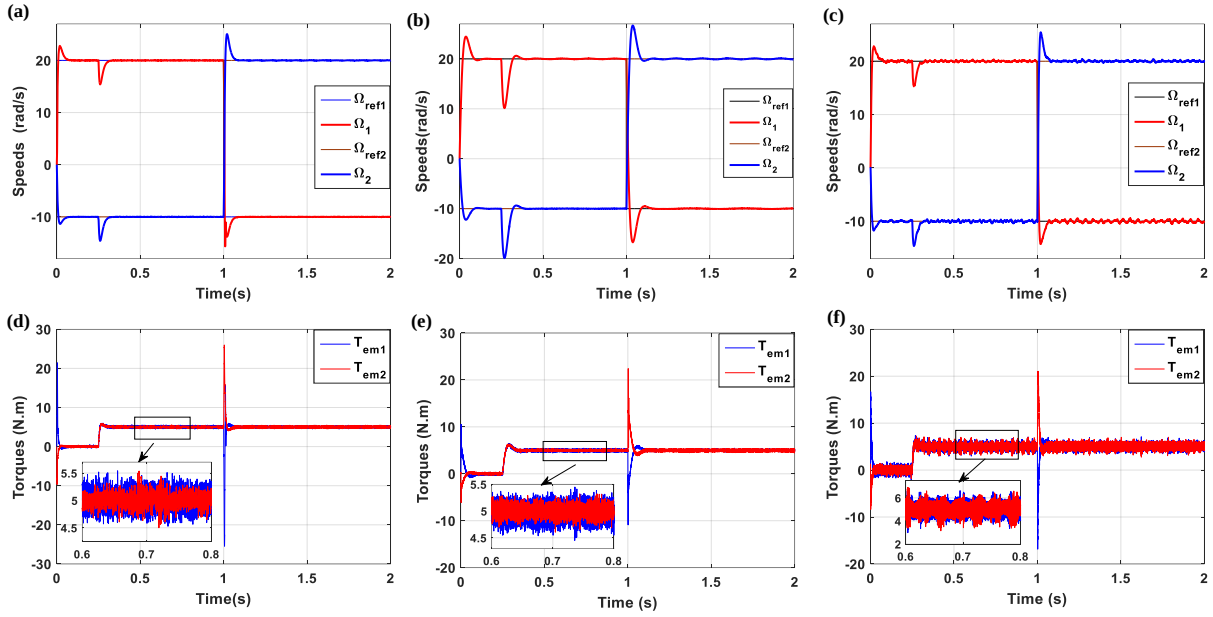

(FOC) (DTS-SVM) (DTC-switching up-table)

Fig. (2.27): Dynamic responses of parallel-connected two five-phase PMSMs system operating at low speed conditions**:** (a, d) the machine speeds and electromagnetic torques controlled by FOC, (b, e) the machine speeds and electromagnetic torques controlled by DTC-SVM, (c, f) the machine speeds electromagnetic and torques controlled by conventional DTC.

2.4.3 Case 3: Parameters variations

Fig. (2.28) shows the profile of the change in stator resistances in which the resistances are increased by 100 % compared to their nominal values.

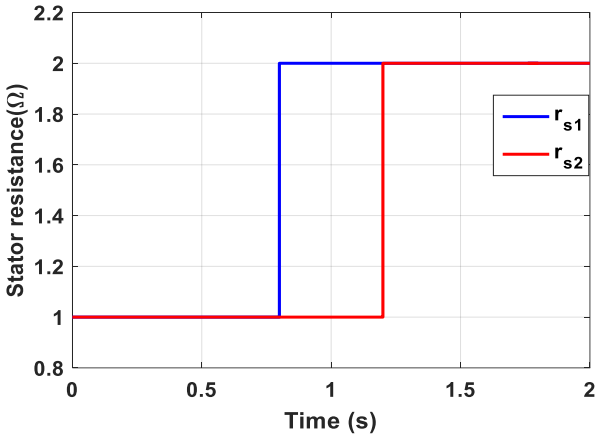

Fig. (2.28): Profile of resistances variations.

The two machines are running in the same directions at +100 rad/s and 50 rad/s, respectively. After the load application at t=0.25s, a stator resistances variations are introduced at t=0.8s and t=1.2s for the first and second machine respectively.

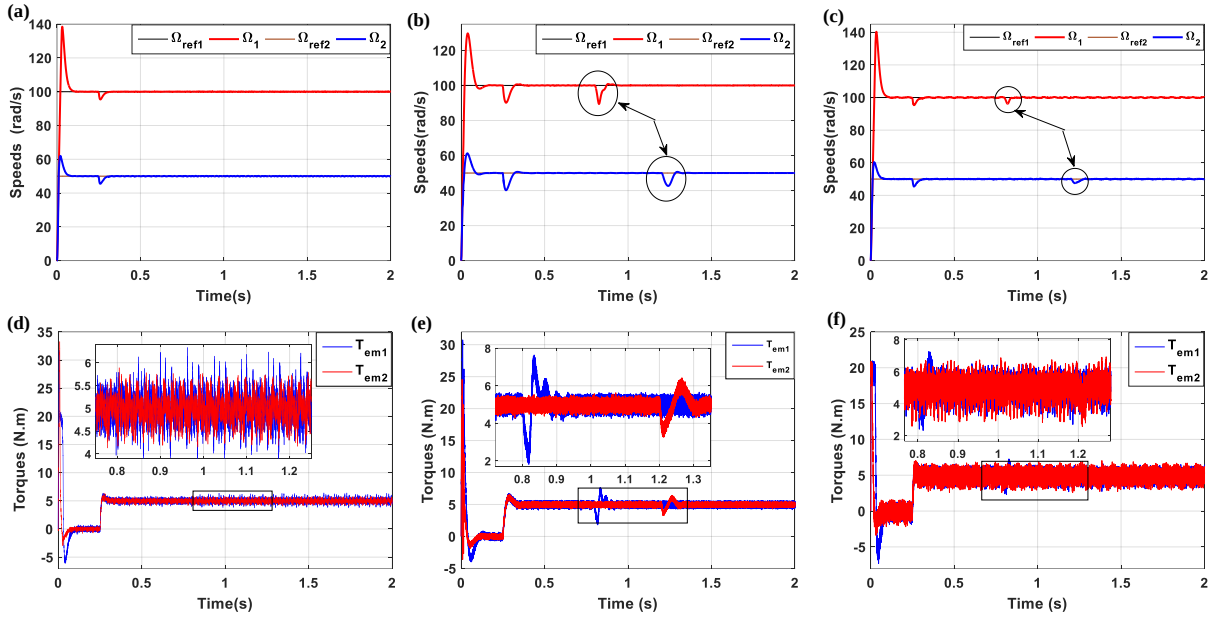

(FOC) (DTS-SVM) (DTC-switching up-table)

Fig. (2.29): Dynamic responses of parallel-connected two five-phase PMSMs system operating at stator resistance variations**:** (a, d) the machine speeds and electromagnetic torques controlled by FOC: (b, e) the machine speeds and electromagnetic torques controlled by DTC-SVM, (c, f) the machine speeds electromagnetic and torques controlled by conventional DTC**.**

From Figs. (2.26) to (2.29), it can be noticed that both the torque and the speed of each machine follows closely their references. It can be seen also that for each control, the speed as well as the electromagnetic torque of one machine are not affected by the starting operation of the second one. The comparison study between FOC, DTC-SVM and shows a better response of both methods in low speed operation and stator resistance variations. The comparison study can be summarized on four aspects:

- **Ripple**: both control FOC and DTC-SVM reduce the electromagnetic torque compared with the conventional DTC,
- **Overshoot**: the overshoot in DTC-SVM is less than FOC and conventional DTC, even in reversal mode,
- **Speeds drops:** the speeds drops in case of FOC and conventional DTC are less than DTC-SVM,
- **Stator resistance variations:** there are a speed drops in case of DTC-SVM and conventional DTC due to the increasing in the stator resistance, on the other hand there is no effect obvious in FOC. The increase stator resistance variations value causes speeds drops for both DTC approaches. However, for the FOC approach there is no obvious effected on speeds responses.

Table (2.3) summarized a general comparison between FOC, DTC-SVM and Conventional DTC in many aspects, in order to show the properties and feature of each control.

Table (2.3): Comparison between FOC, DTC-SVM and Conventional DTC

Controlled variable	Comparison criterion	FOC	DTC-SVM	Conventional DTC
Rotor speed	Settling time (s)	0.1	0.16	0.11
	Overshoot (rad/s)	38	30	40
	Speeds drops (%)	4.6	10	4.7
	Recovery time (at abrupt load) (s)	0.07	0.07	0.07
	Overshoot in reversal mode (%)	110	78	104
Electromagnetic torque	Settling time (s)	0.1	0.1	0.1
	Overshoot (rad/s)	6	4	7
	Ripple (N.m)	1.4	1.2	3.57
Stator flux	Settling time (s)	--	0.005	0.001
	Overshoot (rad/s)	--	0.08	0
	Overshoot in reversal mode (%)	--	0.005	0
	Ripple (N.m)	--	0.0095	0.0335

Finley, a table summarized the advantages and disadvantages of each control method for parallel-connected two five-phase PMSMs drive supplied by a single inverter, as shown in table (2.4).

Table (2.4): Comparison of control methods.

	FOC	DTC-SVM	Conventional DTC
Advantages	- Constant switching frequency - Low switching losses - Low sampling frequency - Current control loops - Simple implementation of sensorless operation - No estimator	- Constant switching frequency - Low switching losses - Low sampling frequency - No current control loops	- Structure independent on rotor parameters - No coordinate transformation - No current control loops - No PWM modulator

Disadvantages	-Need for Coordinates transformation - A lot of control loops (ten-regulators) - Control structure depended on rotor parameters - Compensation term	- Need for Estimator - Need for coordinate transformation - Control structure depended on rotor parameters - Complex implementation of sensorless operation	- Need for estimator - Variable switching frequency - High switching losses - High sampling frequency - Complex implementation of sensorless operation

2.5 Conclusion

This chapter has presented three types of controls for parallel-connected two five-phase PMSMs supplied by a single inverter, which are FOC, conventional DTC and DTC-SVM schemes. The independent control of the two machines has been demonstrated for each control of the system.

The FOC demonstrated that d-q components of the inverter voltages control the flux and torque of the first machine, while the x-y components of inverter voltages control the flux and torque of the second machine. In addition, FOC shows good performance in term of reducing the ripple and speed drops.

The performances of conventional DTC and DTC-SVM of parallel-connected two five-phase PMSMs drive have been highlighted. Simulations results show that superior torque and speed responses are achieved using the proposed five-phase DTC-SVM with remark ability of robustness in different tests such as load application and speed reference reversion. Compered to conventional DTC, DTC-SVM is not only able to reduce the torque and the flux ripples but also to operate with a constant switching frequency.

The previous strategies of control are based on PI-regulators, which are sensitive to parametric variations. To overcome this drawback, sliding mode control combined with FOC and DTC-SVM seems to be a best options.

Chapter 3

Decoupled Controls Based on Sliding Mode Control of Two Five-Phase PMSMs Connected in Parallel

3.1 Introduction

Five-phase PMSM is known by its highly nonlinear and coupled dynamic model, due to the *d-q* axes quantities. Furthermore, the dynamics of the PMSM may not be fully known, since some of parameters appearing in the equations may vary. For instance, the resistance and inductance can be change as function of the temperature or saturation.

Generally, the standard controllers have been widely used to control the multi-phase drive. However, neglected dynamics, parameter variations, friction forces, and load disturbances are the main disturbances and uncertainties that can affect the effective functioning of the drive system. Therefore, it will be very difficult to limit these disturbances effectively if linear control methods like PI-controllers are adopted [19, 20-23]. To overcome the aforementioned problems other advanced methods have been proposed [33, 24-25]. These approaches include among others the sliding mode control (SMC). The SMC is a nonlinear control method known to have robust control characteristics under restricted disturbance conditions or when there are limited internal parameter modeling errors [26-29]. The robustness of the SMC is guaranteed usually by using a switching control law. Unfortunately, this switching strategy often leads to a chattering phenomenon. In order to mitigate the chattering phenomenon, a common method is to use the smooth function instead of the switching function [19] [66-67].

In this chapter, the PI-regulators have been replaced by SM-regulators for the two strategy of control FOC and DTC-SVM. So, first we start by a summary about sliding mode theory, than the sliding mode control is applied on the parallel-connected two five-phase permanent magnet synchronous machines fed by a five-phase VSI, based on FOC and DTC-SVM.

3.2 Basic principle of sliding mode control

Historically, the concept of sliding mode control first has been developed in Russian literature in the 1950s. Since then, much work has been done on this control mode [68-70].

3.2.1 Basic concepts

Sliding Mode Control is a variable structure control that can change structure and switch between two values according to a very specific switching logic. The principle of sliding mode control is to force the system to reach a given surface called the sliding surface and to remain there until it reaches equilibrium. This control is done in two steps: the state trajectory converges to the sliding surface and is restricted to the surface for all subsequent time as shown in Fig. (3.1) [71] [72] [73].

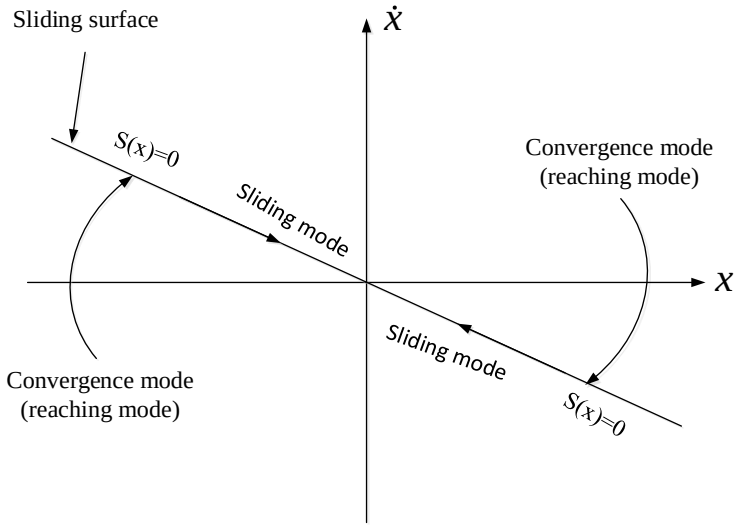

Fig. (3.1): Sliding mode principle in phase plane.

The structure of the controller has two parts. The first one is continuous representing the dynamics of the system during the sliding mode and another discontinuous representing the dynamics of the system during the convergence mode. The second term of SMC is important in the nonlinear control, because its role to eliminate the effects of imprecision and disruption of the model. The synthesis of this controller can be divided into two steps [68] [71] [72][74]:

- Choice of a suitable sliding surface so that the dynamic of the system confined to the sliding manifold produces a desired behavior,
- Design the control law, which forces the system trajectory to the sliding surface and maintains it there.

3.2.1.1 Sliding Surface Choice

If the sliding surface is a linear combination of the error and its corresponding differentiations, it becomes a linear sliding surface S(x). Alternatively, if it is a nonlinear combination of the error and its corresponding differentiation, it becomes a nonlinear sliding surface *S(x,t)*. Slotine [76] proposed a general form, which consists of a scalar function given by:

$$S(x) = (\frac{d}{dt} + \lambda)^{r-1} e(x) \tag{3.1}$$

with:

$e(x) = x_{ref} - x$

λ : is a positive coefficient.

r : is the relative degree, which is the number of times required to differentiate the surface before the input appears explicitly.

3.2.1.2 Conditions of Existence and Convergence of the Sliding mode

The method of Lyaponov provides a dynamic system stable analysis approach. If we can construct a positive definite function V so that its derivative $\dot{V} < 0$, the system is stable. This kind of method is usually used to design sliding mode controller.

The Lyapunov function candidate can be defined as following:

$$V = \frac{1}{2} S^2(x) \tag{3.2}$$

The derivative of (3.2) is:

$$\dot{V} = \dot{S}(x) S(x) \tag{3.3}$$

The control stability is ensured under the following two conditions:

-The Lyapunov function V is positive definite.

- The derivative of the Lyapunov function should be negative $\dot{V} < 0$, it is sufficient to ensure that:

$$\dot{S}(x) S(x) < 0 \ (\forall S) \tag{3.4}$$

This approach is used to estimate the performance of the control and ensures asymptotically the convergence towards the sliding surface.

3.2.1.3 Control Law

In order to drive the state variables to the sliding surface, the following control law expression is given by:

$$u = u_{eqc} + u_{dic} \tag{3.5}$$

The equivalent control u_{eqc} is capable to keep the state variables on the switching surface, once they reach it, and to achieve the desired performance under nominal model. It is derived as the solution of the following equation:

$$S(x) = \dot{S}(x) = 0 \tag{3.6}$$

The discontinuous control u_{dic} is needed to assure the convergence of the system states to sliding surfaces in finite time, and it should be designed to eliminate the effect of any unpredictable perturbation.

By considering the following state system:

$$\dot{x} = A(x) + B(x) u \tag{3.7}$$

The time derivative of the sliding surface is given as:

$$\dot{S} = \frac{\partial S}{\partial t} = \frac{\partial S}{\partial x}\frac{\partial x}{\partial t} \tag{3.8}$$

By substituting (3.8) into (3.7):

$$\dot{S} = \frac{\partial S}{\partial t} A(x) + \frac{\partial S}{\partial t} B(x)(u_{eqc} + u_{dic}) \tag{3.9}$$

During the convergence mode and the steady state, the surface and its derivative are nulls $S = \dot{S} = 0$ as well as $u_{dic} = 0$.

$$u_{eqc} = -\left[\frac{\partial S}{\partial x} B(x)\right]^{-1} \frac{\partial S}{\partial x} A(x) \tag{3.10}$$

with the condition of existence:

$$\frac{\partial S}{\partial x} B(x) \neq 0 \tag{3.11}$$

By substituting (3.10) in (3.9), the new sliding surface expression can be as follow:

$$\dot{S} = \frac{\partial S}{\partial x} B(x) u_{dic} \tag{3.12}$$

The discontinuous control u_{dic} is determined during the convergence state and must guarantee the finite time convergence condition $S\dot{S} < 0$, which is given by:

$$S\dot{S} = S\frac{\partial S}{\partial x} B(x) u_{dic} < 0 \tag{3.13}$$

In order to satisfy this condition, the sign of u_{dic} must be the opposite of the sign of $S\frac{\partial S}{\partial x} B(x)$.

The so-called reaching stability condition $(\dot{V} = S\dot{S} < 0)$ is fulfilled using the following discontinuous control:

$$u_{dic} = k\, sign(S(x)) \tag{3.14}$$

where $sign(S(x)) = \begin{cases} +1 & (S(x) > 0) \\ -1 & (S(x) < 0) \end{cases}$ and k is a control gain.

3.2.2 Drawback of Sliding Mode Control

The sliding mode control is arriving at sliding mode surface S=0 from the initial value after a period time. The sliding mode trajectory is shown in Fig. (3.2). From the Fig. (3.2), the drawback is chattering problem due to the discontinuous control law acting on the sliding mode when system goes into sliding mode state. This is phenomenon can increase the loss and reduce the life of components. Therefore, it should be overcome as possible as we can.

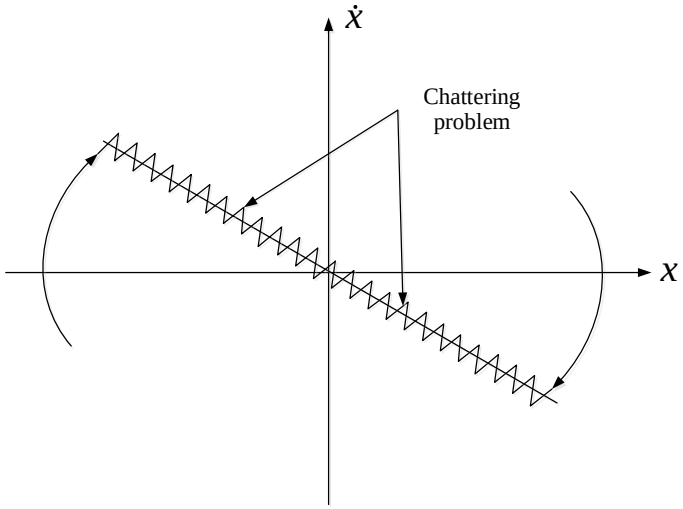

Fig. (3.2): Chattering phenomenon.

3.2.2.1 Solving the Chattering Problem

The chattering phenomenon has become the biggest developing obstacle of sliding mode control technology. The academics have continued to weaken or prevent the chattering without interruption. In order to reduce or eliminate the chattering phenomena, a large number of researches have been using: saturation function, smooth function, filters (by adopt a low-pass filter), observer, neural sliding, fuzzy sliding mode and higher-order sliding mode [68]. The smooth function has been chosen in order to limit the effect of chattering and to give a better response as well as its simplicity.

The smooth function $smooth(S(x))$ is used instead of sign function *sign(S(x))* to realize the sliding mode control.

The smooth function depicted in Fig. (3.3) is expressed as follows:

$$smooth(S(x)) = \frac{e^{x} - e^{-x}}{e^{x} + e^{-x}} = \frac{S(x)}{|S(x)| + \sigma} \tag{3.15}$$

with σ is the boundary layer width.

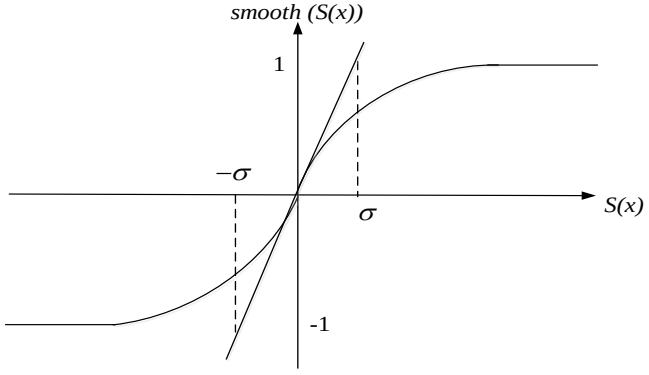

Fig. (3.3): Smooth function.

3.3 Application of Sliding Mode Control on Field Oriented Control

3.3.1 Sliding Mode Control of Parallel-Connected Two Five-Phase PMSMs Drive

The proposed sliding mode control of the parallel-connected two five-phase permanent magnet synchronous machines fed by a five-phase VSI is presented in Fig. (3.4). The reference speed, actual speed and load torque of each machine are the inputs of the speeds SMCs to determine the q_1-y_2 axes reference current components. The other current components are maintained to zero. The measured currents are processed in the current SMCs to obtain as outputs the *d-q-x-y* axes reference voltages components. These reference voltages are transformed into the *abcde* frame and transformed again to *α-β-x-y* frame to become input signals to the SVM blocks. The SVM transmits the signals to the inverter to drive the two five-phase PMSMs connected in parallel.

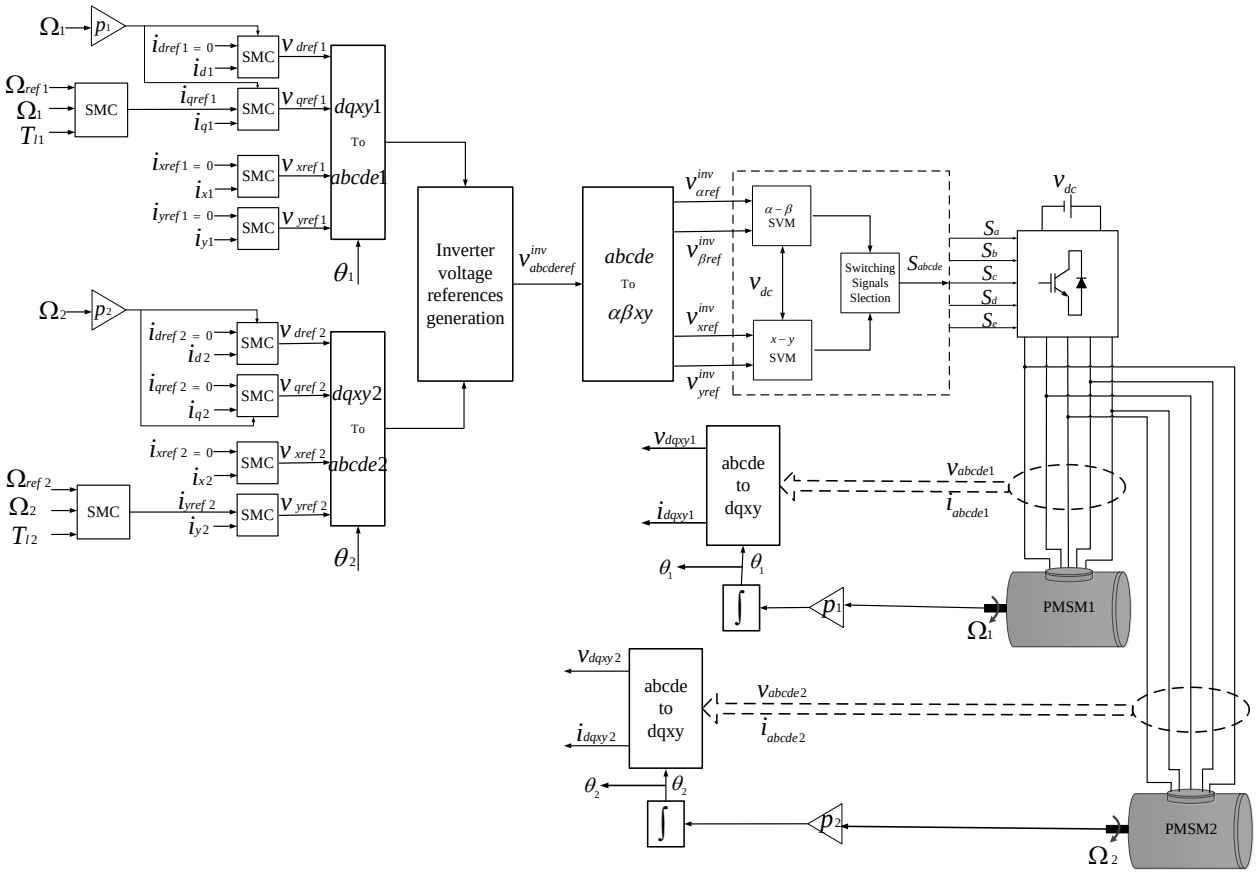

Fig. (3.4): FOC-SMC of parallel-connected two five-phase PMSMs drive system.

3.3.2 Synthesis of Speeds and Currents Controllers

3.3.2.1 Speeds SMC Design

The first task in the speeds SMC design process is to select suitable sliding surfaces $S(\Omega_j)$. Since the relative degree is one, the following sliding surfaces are adopted:

$$S(\Omega_j) = \Omega_{refj} - \Omega_j \tag{3.16}$$

By taking the derivative of sliding surfaces (3.16) with respect to time and using the machines motion equations, it yields:

$$\begin{aligned}\dot{S}(\Omega_1) &= \dot{\Omega}_{ref1} - \frac{5p_1(L_{d1}-L_{q1})i_{ds1} + 5p_1\Phi_{f_1}}{2J_1} i_{qs1} + \frac{T_{l1}}{J_1} + \frac{f_1\Omega_1}{J_1} \\ \dot{S}(\Omega_2) &= \dot{\Omega}_{ref2} - \frac{5p_2(L_{d2}-L_{q2})i_{xs2} + 5p_2\Phi_{f_2}}{2J_2} i_{ys2} + \frac{T_{l2}}{J_2} + \frac{f_2\Omega_2}{J_2}\end{aligned} \tag{3.17}$$

where J_j, f_j and T_{lj} are moment of inertia, damping coefficient, and load torque of each machine. The currents controls i_{qs1} and i_{ys2} are defined by:

$$\begin{aligned} i_{qs1} &= i_{qseqc1} + i_{qsdic1} \\ i_{ys2} &= i_{yseqc2} + i_{ysdic2}\end{aligned} \tag{3.18}$$

where the equivalent current control components are:

$$i_{qseqc1} = -\frac{J_1\dot{\Omega}_{ref1} + T_{l1} + f_1\Omega_1}{\frac{5}{2}p_1(L_{d1}-L_{q1})i_{ds1} + \frac{5}{2}p_1\Phi_{f1}}$$

$$i_{yseqc2} = -\frac{J_2\dot{\Omega}_{ref2} + T_{l2} + f_2\Omega_2}{\frac{5}{2}p_2(L_{d2}-L_{q2})i_{xs2} + \frac{5}{2}p_2\Phi_{f2}}$$

The discontinuous current control components are:

$$i_{qsdic1} = k_{\Omega 1} smooth(S(\Omega_1))$$

$$i_{ysdic2} = k_{\Omega 2} smooth(S(\Omega_2))$$

During the convergence mode, the condition $\dot{V} = \dot{S}(x)S(x) < 0$ must be verified. By replacing (3.18) into (3.17), we get:

$$\begin{aligned}\dot{V}(\Omega_1) &= -S(\Omega_1)\left\{\frac{5p_1(L_{d1}-L_{q1})i_{ds1} + 5p_1\Phi_{f_1}}{2J_1} k_{\Omega 1} smooth(S(\Omega_1))\right\} < 0 \\ \dot{V}(\Omega_2) &= -S(\Omega_2)\left\{\frac{5p_2(L_{d2}-L_{q2})i_{xs2} + 5p_2\Phi_{f_2}}{2J_2} k_{\Omega 2} smooth(S(\Omega_2))\right\} < 0\end{aligned} \tag{3.19}$$

It can be seen that, the terms of (3.19) are negative as long as $k_{\Omega 1}$ and $k_{\Omega 2}$ are positive. Therefore, the stability condition has been guaranteed.

3.3.2.2 Currents SMC Design

The control objectives are to track the desired currents trajectories. So, the sliding surfaces can be calculated as follows:

$$\begin{aligned} S(i_{dsj}) &= i_{dsrefj} - i_{dsj} \\ S(i_{qsj}) &= i_{qsrefj} - i_{qsj} \\ S(i_{xsj}) &= i_{xsrefj} - i_{xsj} \\ S(i_{ysj}) &= i_{ysrefj} - i_{ysj} \end{aligned} \tag{3.20}$$

The time derivative of (3.20) is:

$$\begin{aligned} \dot{S}(i_{dsj}) &= \dot{i}_{ds\,refj} - \dot{i}_{dsj} \\ \dot{S}(i_{qsj}) &= \dot{i}_{qs\,refj} - \dot{i}_{qsj} \\ \dot{S}(i_{xsj}) &= \dot{i}_{xs\,refj} - \dot{i}_{xsj} \\ \dot{S}(i_{ysj}) &= \dot{i}_{ys\,refj} - \dot{i}_{ysj} \end{aligned} \tag{3.21}$$

Using (1.36), the equation (3.21) can be rewritten as:

$$\begin{aligned} \dot{S}(i_{dsj}) &= \dot{i}_{dsrefj} + \frac{r_{sj}}{L_{dj}} i_{dsj} - \frac{L_{qj}}{L_{dj}} \omega_j i_{qsj} - \frac{1}{L_{dj}} v_{dsj} \\ \dot{S}(i_{qsj}) &= \dot{i}_{qsrefj} + \frac{r_{sj}}{L_{qj}} i_{qsj} + \frac{L_{dj}}{L_{qj}} \omega_j i_{dsj} + \frac{\omega j \Phi_{fj}}{L_{qj}} - \frac{1}{L_{qj}} v_{qsj} \\ \dot{S}(i_{xsj}) &= \dot{i}_{xsrefj} + \frac{r_{sj}}{L_{lsj}} i_{xsj} - \frac{1}{L_{lsj}} v_{xsj} \\ \dot{S}(i_{ysj}) &= \dot{i}_{ysrefj} + \frac{r_{sj}}{L_{lsj}} i_{ysj} - \frac{1}{L_{lsj}} v_{ysj} \end{aligned} \tag{3.22}$$

Therefore, it is possible to choose the control laws for stator voltages as follows:

$$\begin{aligned} v_{dsj} &= v_{dseqcj} + v_{dsdicj} \\ v_{qsj} &= v_{qseqcj} + v_{qsdicj} \\ v_{xsj} &= v_{xseqcj} + v_{xsdicj} \\ v_{ysj} &= v_{yseqcj} + v_{ysdicj} \end{aligned} \tag{3.23}$$

where the equivalent voltage control components are:

$$v_{dseqcj} = (\dot{i}_{dsrefj} + \frac{r_{sj}}{L_{dj}} i_{dsj} - \frac{L_{qj}}{L_{dj}} \omega_j i_{qsj}) L_{dj}$$

$$v_{qseqcj} = (\dot{i}_{qsrefj} + \frac{r_{sj}}{L_{qj}} i_{qsj} + \frac{L_{dj}}{L_{qj}} \omega_j i_{dsj} + \frac{\omega_j \Phi_{fj}}{L_{qj}}) L_{qj}$$

$$v_{xseqcj} = (\dot{i}_{xsrefj} + \frac{r_{sj}}{L_{lsj}} i_{xsj}) L_{lsj}$$

$$v_{yseqcj} = (\dot{i}_{ysrefj} + \frac{r_{sj}}{L_{lsj}} i_{ysj}) L_{lsj}$$

The discontinuous voltage control components are:

$$\begin{aligned} v_{dsdicj} &= k_{dsj} smooth(S(i_{dsj})) \\ v_{qsdicj} &= k_{qsj} smooth(S(i_{qsj})) \\ v_{xsdicj} &= k_{xsj} smooth(S(i_{xsj})) \\ v_{ysdicj} &= k_{ysj} smooth(S(i_{ysj})) \end{aligned}$$

During the convergence mode, the condition $\dot{V} = \dot{S}(x)S(x) < 0$ must be verified. By replacing (3.23) into (3.22), we get:

$$\begin{aligned} \dot{V}(i_{dsj}) &= -S(i_{dsj})\left[(1/L_{dj}) k_{dsj} smooth(S(i_{dsj})) \right] < 0 \\ \dot{V}(i_{qsj}) &= -S(i_{qsj})\left[(1/L_{qj}) k_{qsj} smooth(S(i_{qsj})) \right] < 0 \\ \dot{V}(i_{xsj}) &= -S(i_{xsj})\left[(1/L_{lsj}) k_{xsj} smooth(S(i_{xsj})) \right] < 0 \\ \dot{V}(i_{ysj}) &= -S(i_{ysj})\left[(1/L_{lsj}) k_{ysj} smooth(S(i_{ysj})) \right] < 0 \end{aligned} \tag{3.24}$$

It can be seen that, the terms of (3.24) are negative as long as $k_{dsj}, k_{qsj}, k_{xsj}$ and k_{ysj} are positive. Therefore, the stability condition has been guaranteed.

The control voltages given by (3.23) are transformed in *abcde* frame, and then the inverter phase voltage references are calculated according to the following expression:

$$\begin{aligned} v_a^{inv} &= v_{as\,ref\,1} + v_{as\,ref\,2} \\ v_b^{inv} &= v_{bs\,ref\,1} + v_{cs\,ref\,2} \\ v_c^{inv} &= v_{cs\,ref\,1} + v_{es\,ref\,2} \\ v_d^{inv} &= v_{ds\,ref\,1} + v_{bs\,ref\,2} \\ v_e^{inv} &= v_{es\,ref\,1} + v_{ds\,ref\,2} \end{aligned} \tag{3.25}$$

3.3.3 Simulation Results

The behavior of the overall FOC-SMC drive system based on SM-regulators is tested by different test conditions. The tuning parameters for the SM-controllers are given in table B.4 of appendix B. The simulation results demonstrating the decoupling and independent control of the two machines connected in parallel as shown in Figs (3.5) to (3.9).

In Fig. (3.5) the second five-phase PMSM is run at t=0.5s to reach its reference speed equal to 50 rad/s, while the first five-phase PMSM speed is maintained constant equal to 100 rad/s. Fig. (3.6) shows the same results as those presented in Fig. (3.5) but the operating condition of

the two machines are reserved. From those results it as can be noticed that, the speed and electromagnetic torque of the first five-phase PMSM are not affected by the starting operation of the second five-phase PMSM.

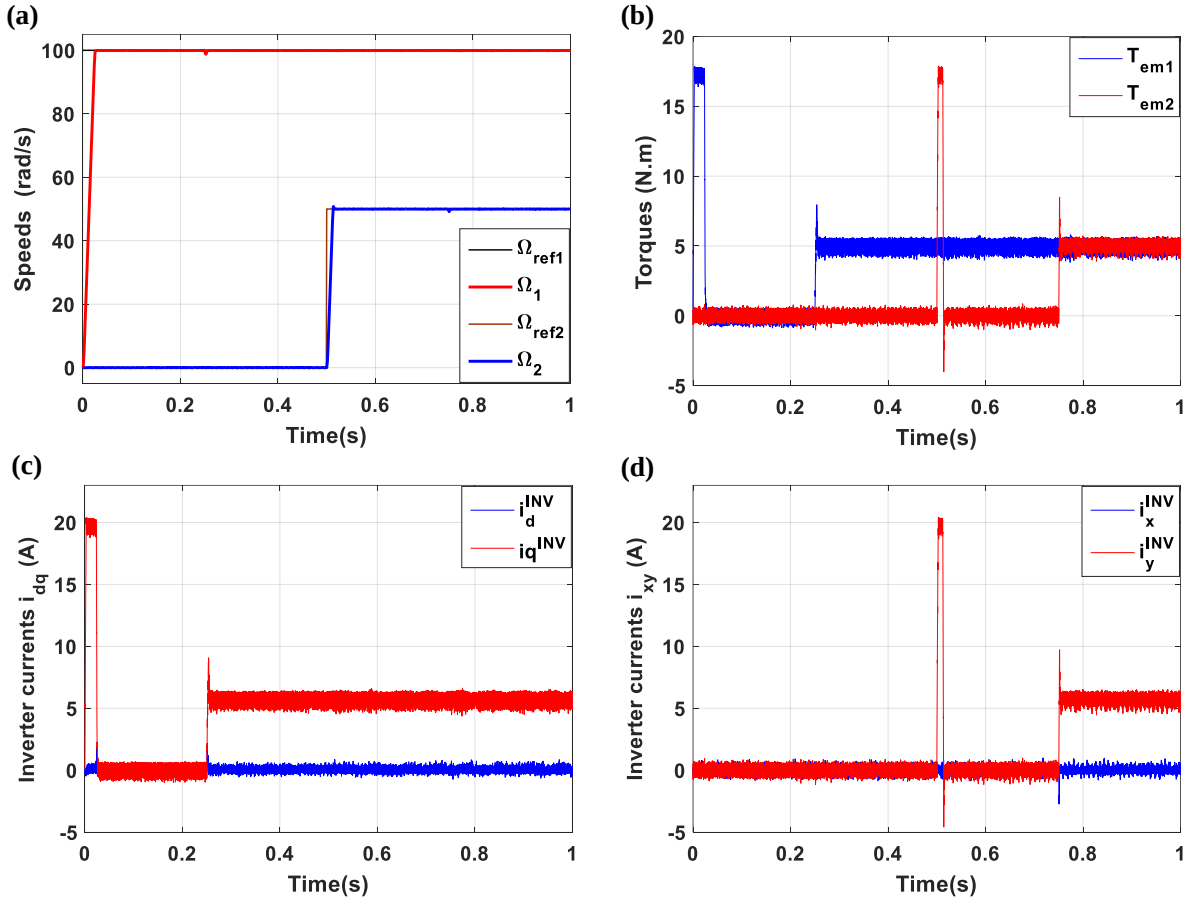

Fig. (3.5): Dynamic responses of parallel-connected two five-phase PMSMs drive controlled by FOC-SMC: when the second machine is at standstill and the other is still running: (a) Machine speeds, (b) Torques, (c) Inverter currents *d-q*, (d) Inverter currents *x-y*.

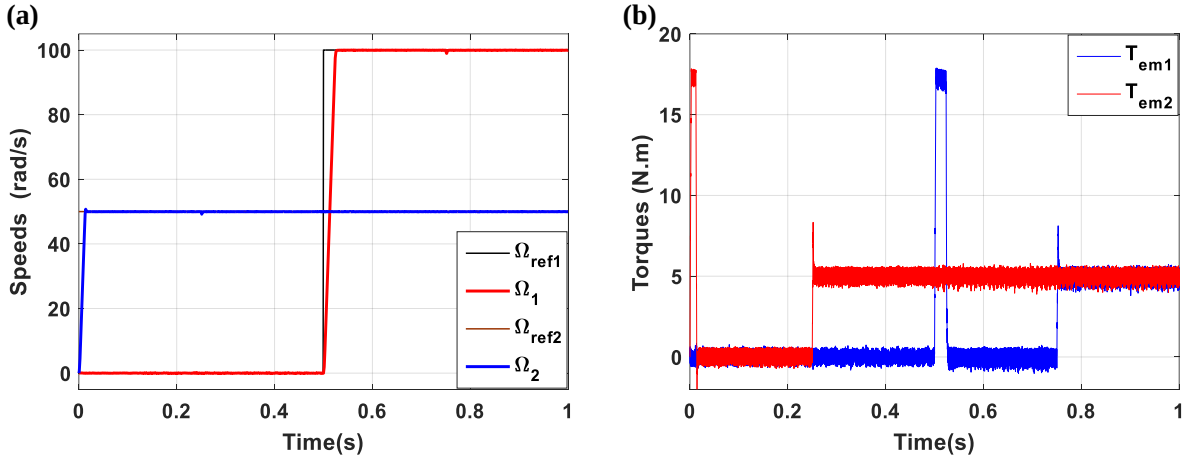

Fig. (3.6): Dynamic responses of parallel-connected two five-phase PMSMs drive controlled by FOC-SMC: when the first machine is at standstill and the other is still running: (a) Machine speeds, (b) Torques, (c) Inverter currents *d-q*, (d) Inverter currents *x-y*.

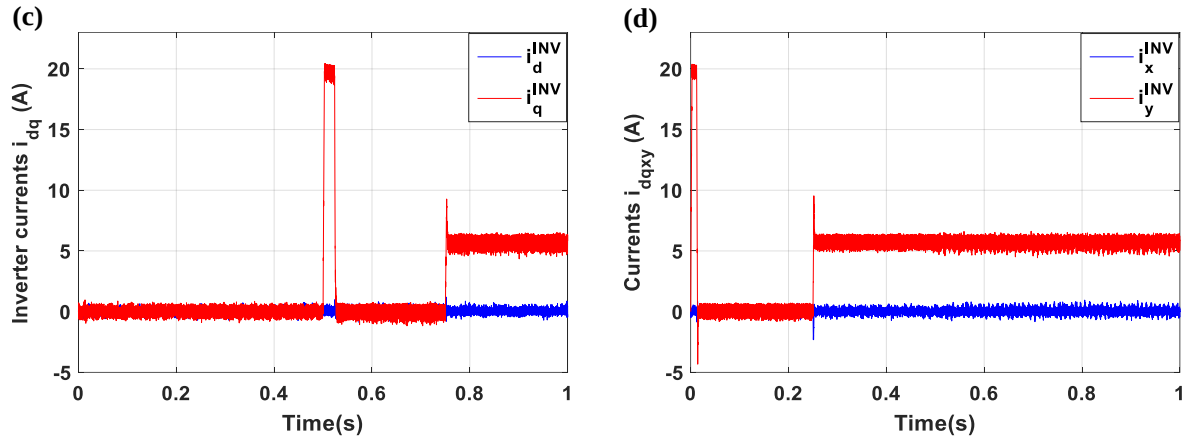

Continued to Fig. (3.6).

Effect of the change rotation in direction of one of the two machines on system performance is investigated in Fig. (3.7) and (3.8). Fig. (3.7) show the results when the speed of the first five-phase PMSM is kept constant (100 rad/s), while the second five-phase PMSM changes from +50 rad/s to -50 rad/s at t = 0.5s. Fig. (3.6) shows same results as those presented in Fig. (3.5) but with reversal operating condition of the two machines.

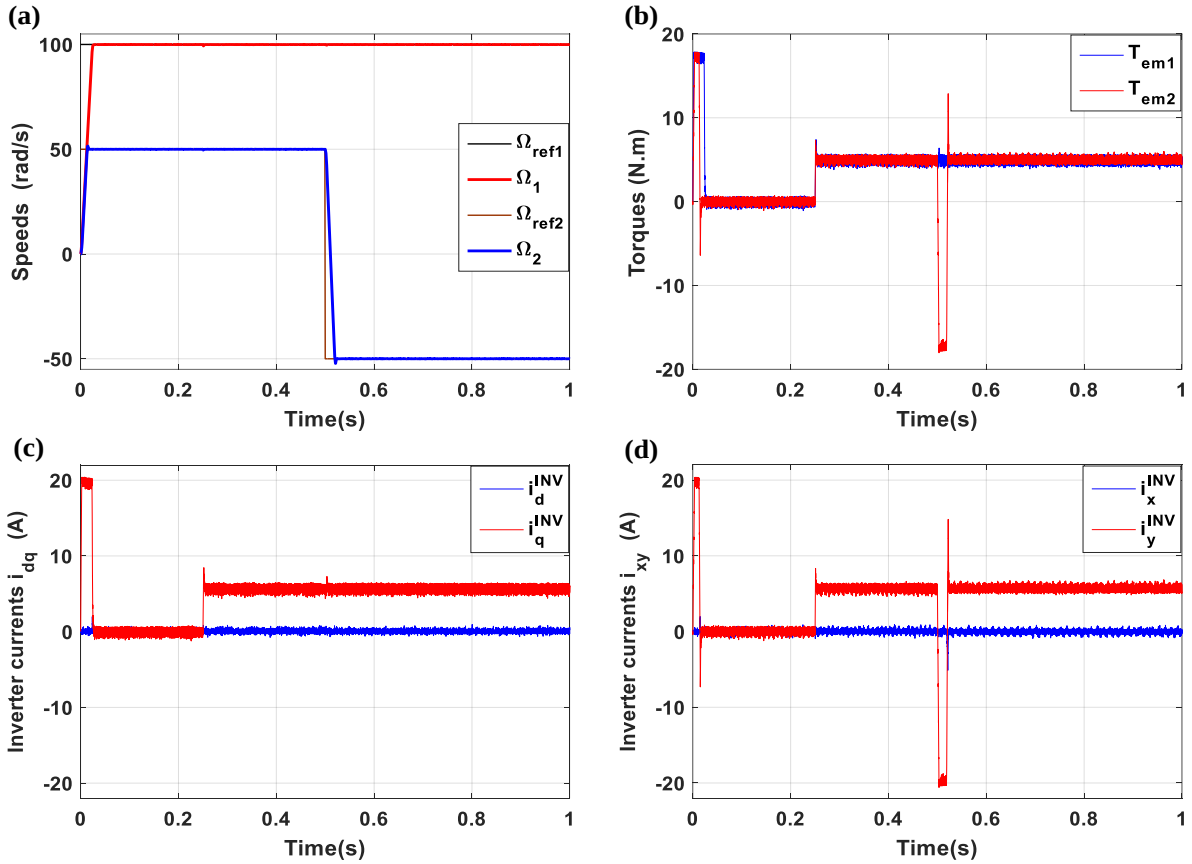

Fig. (3.7): Dynamic responses of parallel-connected two five-phase PMSMs drive controlled by FOC-SMC: when the first machine is kept constant (100 rad/s) and the other change the direction: (a) Machine speeds, (b) Torques, (c) Inverter currents *d-q*, (d) Inverter currents *x-y*.

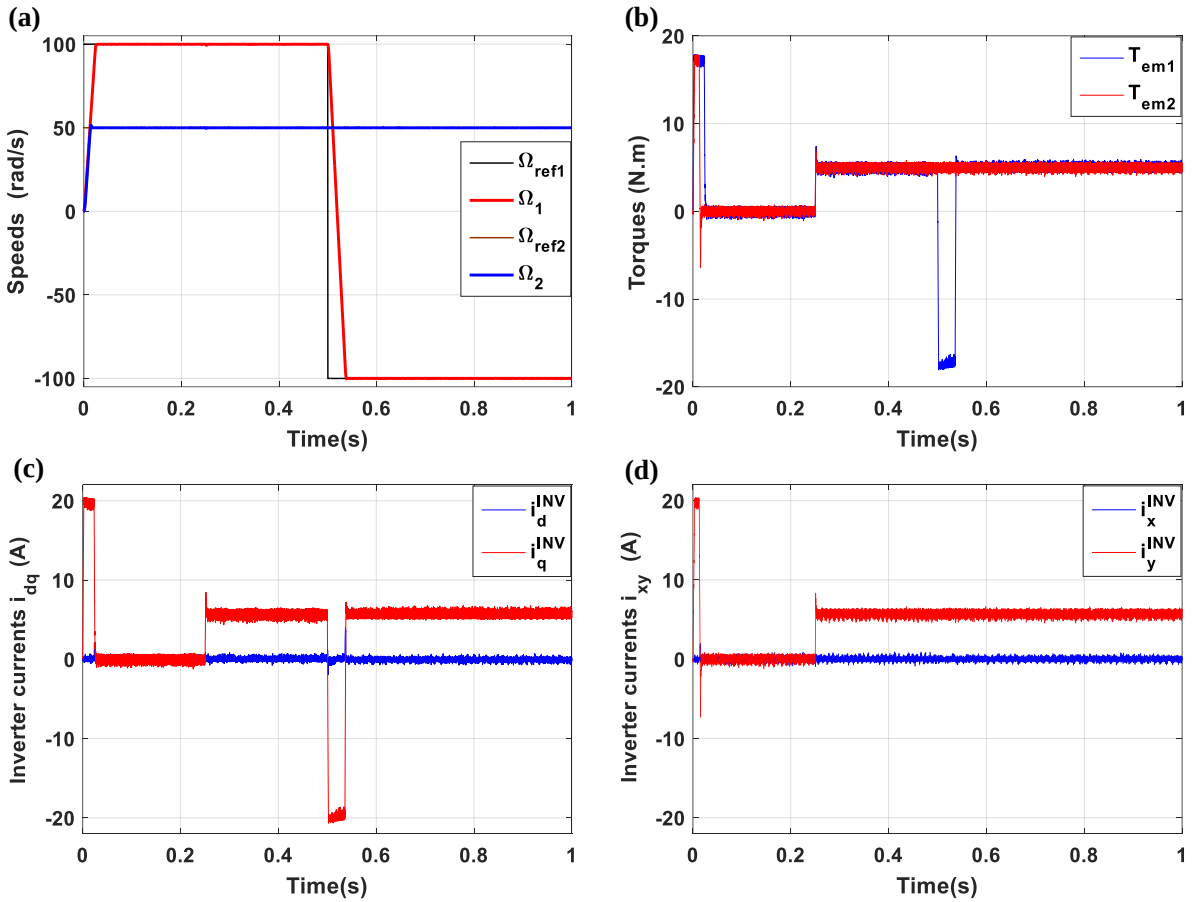

Fig. (3.8): Dynamic responses of parallel-connected two five-phase PMSMs drive controlled by FOC-SMC: when the speed of the second machine is kept constant (50 rad/s) and the other machine speed change the direction: (a) Machine speeds, (b) Torques, (c) Inverter currents *d-q*, (d) Inverter currents *x-y*.

The investigation of effect of the speed rotation reversion of one machines on the other machine performance in Fig. (3.9). In this test, when one machine is rotating in a direction, the other is running at the opposite speed and vise-versa. The two machine started in opposite direction, then change the rotation direction at t=0.5s.

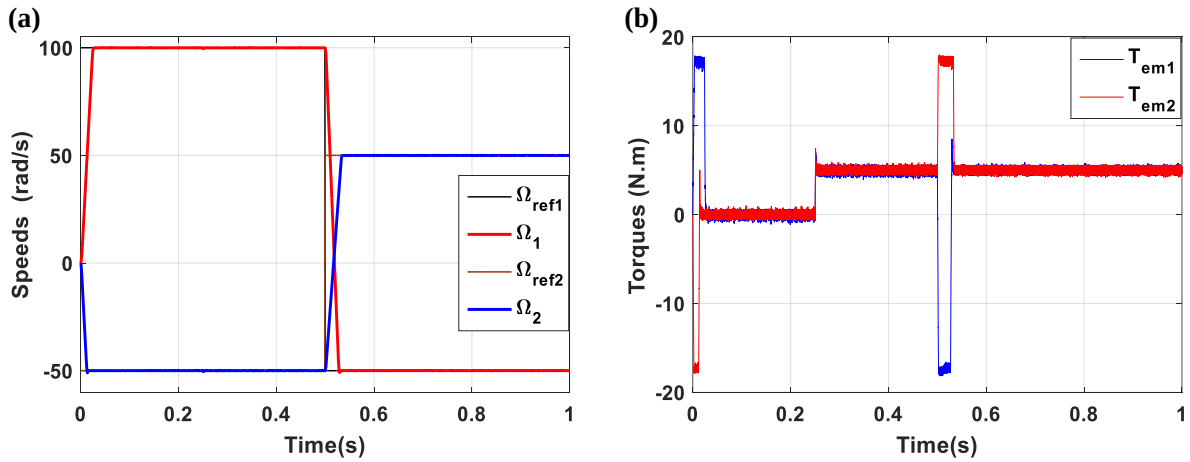

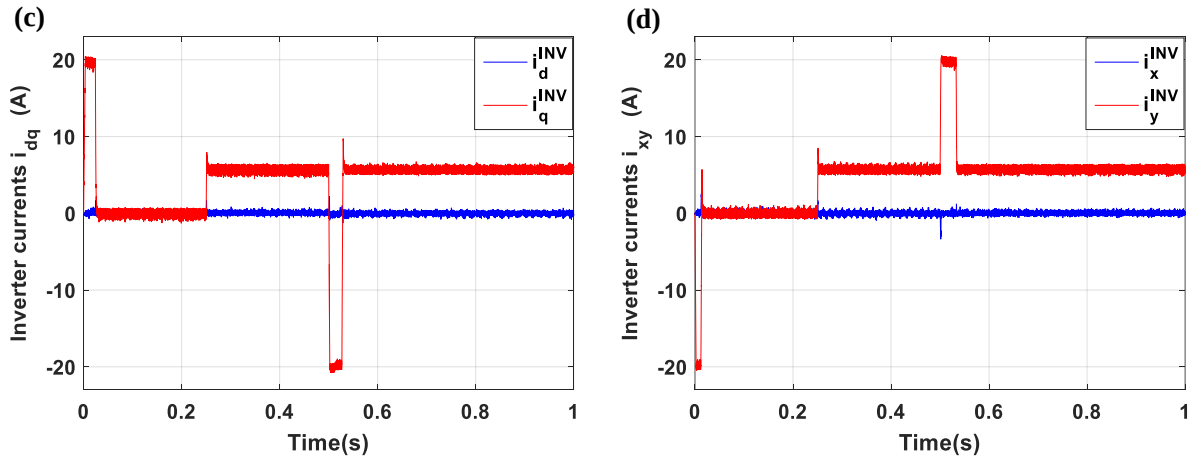

Fig. (3.9): Dynamic responses of parallel-connected two five-phase PMSMs drive controlled by FOC-SMC: when the two machine s are operating in the opposite directions: (a) Machine speeds, (b) Torques, (c) Inverter currents *d-q*, (d) Inverter currents *x-y*.

All Figs. (3.5 to 3.9) show the responses of the two five-phase PMSMs under a sudden change in load torque. From Fig. (3.5 to 3.9) it can be observed that, the step loading of one machine does not cause any disturbance in the other machine's speed and inverter currents d-q-x-y axis.

In the case when the speed of one machine is kept at zero, while the second is reversed, the speed of one machine and its electromagnetic torque remain completely undisturbed during the reversion of the other machine, indicating a complete decoupling in the control of both machines.

The electromagnetic torque generated by each machine during the simulated speed step response are directly proportional to the *q-y* axes currents and fully decoupled from *d-x* axes currents.

Comparison of results in Figs. (3.5 to 3.9) shows once more that the control of the two machines is completely decoupled. There is hardly any evidence of torque disturbance of one machine during the reversal of the other one. Furthermore, the direct axis currents responses remain completely unaffected during these transients.

The starting and reversing transients of one machine do not have any tangible consequence on the operation of the second machine. The decoupled control is preserved and the characteristics of both machines are unaffected as shown in Fig. (3.5) to (3.9).

3.3.3.1 Comparative Study between FOC-SMC and FOC-PI

In this section a comparative study between FOC-SMC and FOC-PI have been presented at the same condition such as inverter frequency, DC-link. In each Figure, is including machine speeds, torques, and inverter currents d-q-x-y.

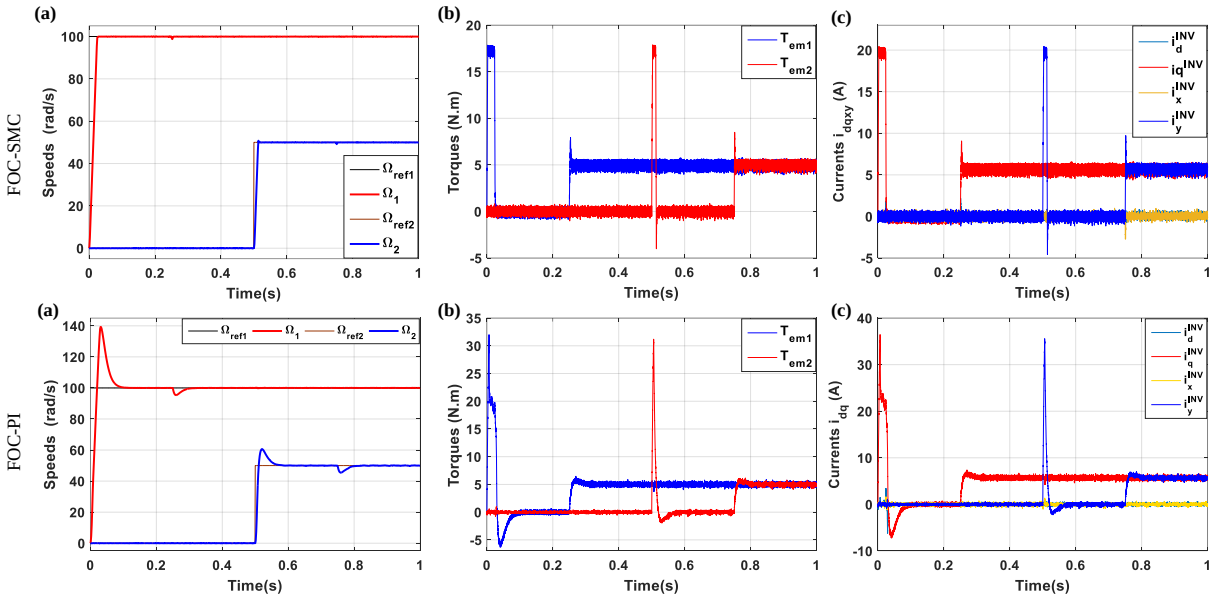

Fig. (3.10): Comparative study between FOC-SMC and FOC-PI of parallel-connected two five-phase PMSMs drive: when the second machine is at standstill and the other is still running: (a) Machine speeds, (b) Torques, (c) Inverter currents *d-q-x-y*.

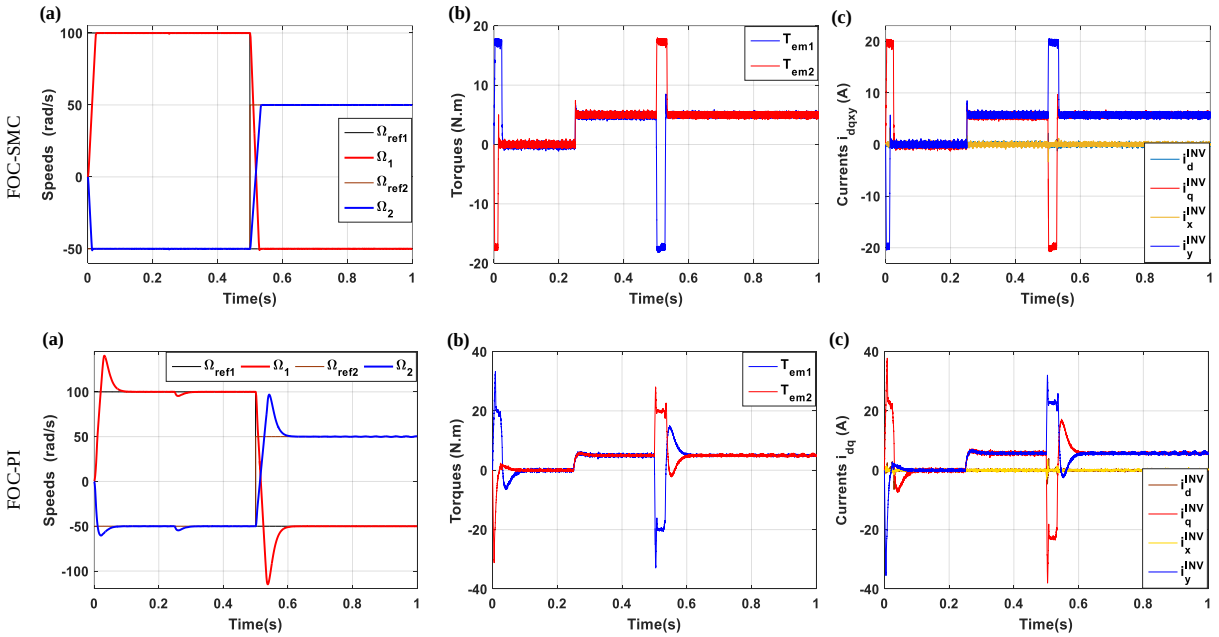

Fig. (3.11): Comparative study between FOC-SMC and FOC-PI of parallel-connected two five-phase PMSMs drive: when the two machines are operating in the opposite directions: (a) Machine speeds, (b) Torques, (c) Inverter currents *d-q-x-y*.

According to the mentioned comparative results, the comparison study between FOC-SMC and FOC-PI can be summarized on three aspects:

Speeds responses: Figs. 3.10-a (SMC) to 3.11-a (SMC), show comparable dynamic behavior using SMC. However, it is clear from these figures that the system reaches steady state at 0.028s without overshoot. In Figs. 3.10-a (PI) to 3.11-a (PI), the system behavior using PI-controller exhibits the expected step response characteristic of a second order system. The response has a short rise time, an overshoot during reverse modes, and short settling times. By analyzing the transient of two-machine drive controlled by PI-controller, it is easy to observe speeds drops taken place at the moments of loads changes. On the other hand, the SMC (Figs. 3.10-a (SM) to 3.11-a (SM)) keep the speeds close to their references without overshoots and without drops. Therefore, the SMC can be considered as more robust under loads variations.

Torques responses: Figs. (3.10-b to 3.11-b), illustrate the behavior of the torque for both controllers. In case of the PI-controller, the torque T_{em1} and T_{em2} peak above 38 *N.m*, then decay exponentially to the steady state. Figs. 3.10-b (SM) to 3.11-b (SM) show torque in case of sliding mode control. In contrast, the torque T_{em1} and T_{em2} peak slightly above 18 N.m, and continue on this value, until the speed reaches its reference value, this leads to a short settling time and without overshoot except in the loading application.

Currents responses: Figs. (3.10-c to 3.11-c), illustrate the behavior of the inverter *dq*-axes and *xy*-axes currents for both controllers. In case of the PI-controller, the stator currents i_q^{inv} and i_y^{inv} peak above 37A, then decay exponentially to the steady state, while the currents i_d^{inv} and i_x^{inv} are maintained at zero. Figs. 3.10-c (SM) to 3.11-c (SM) show inverter currents in case of sliding mode control. In contrast, the i_q^{inv} and i_y^{inv} currents peak slightly above 20A, and continue on this value, until the speed reaches its reference value, this leads to a short settling time.

A general comparison between SMC and PI is given in table (3.1). Compared to PI-controller, SMC shows superiority in terms of settling time and overshoot. However, it needs more energy in starting transient then that needed by the conventional controller.

Table (3.1): Comparison between FOC-SM and FOC-PI.

Controlled variable	Comparison criterion	FOC-S M	FOC-PI	Reduction Ratio (%)
Rotor speed	Settling time (s)	0.03	0.1	70
	Overshoot (rad/s)	0	38	100
	Speeds drops (%)	1.2	4.6	73.91
	Recovery time (at abrupt load) (s)	0.0065	0.07	90.07
	Overshoot in reversal mode (%)	0	110	100
Electromagnetic torque	Settling time (s)	0.03	0.1	70
	Overshoot (rad/s)	0	6	100
	Ripple (N.m)	1.4	1.4	----
Currents	Settling time (s)	0.027	0.09	70
	Overshoot (A)	0	7	100

3.4 Application of Sliding Mode Control on Direct Torque Control

3.4.1. Sliding Mode Control of Parallel-Connected Two Five-Phase PMSMs Drive

This section presents a direct torque control combined with sliding mode approach and space vector modulation to achieve mainly a high performance and reduce torque and flux ripples of the parallel-connected two five-phase PMSMs drive system as presented in Fig. (3.12).

The estimators are designed to estimate the torque and flux of each machine by using voltages and currents measurements. The reference speed, actual speed and load torque are the inputs of the speeds regulator based on sliding mode control (SMCs) to determine the torques references. The estimated flux and torque as well as the actual speed and stator flux angle are processed in DTC-SVM-SMCs to obtain as outputs the α-β-x-y axes reference voltages components. These reference voltages become the input signals to the SVM blocks. The SVM transmits the gating signals (Sa, Sb, Sc, Sd, Se) to the five-leg inverter to drive independently the two five-phase PMSMs connected in parallel.

The stator flux equation in stationary frame of parallel-connected two five-phase PMSMs can be written as follows:

$$\begin{aligned}
\frac{d\Phi_{\alpha sj}}{dt} &= -r_{sj} i_{\alpha sj} + v_{\alpha sj} \\
\frac{d\Phi_{\beta sj}}{dt} &= -r_{sj} i_{\beta sj} + v_{\beta sj} \\
\frac{d\Phi_{xsj}}{dt} &= -r_{sj} i_{xsj} + v_{xsj} \\
\frac{d\Phi_{ysj}}{dt} &= -r_{sj} i_{xsj} + v_{xsj}
\end{aligned} \tag{3.26}$$

The actual flux components can be obtained from:

$$\begin{aligned}
\Phi_{\alpha sj} &= L_{sj} i_{\alpha sj} + \Phi_{fj} \cos(\theta_j) \\
\Phi_{\beta sj} &= L_{sj} i_{\beta sj} + \Phi_{fj} \sin(\theta_j) \\
\Phi_{xsj} &= L_{lsj} i_{xsj} \\
\Phi_{ysj} &= L_{lsj} i_{xsj}
\end{aligned} \tag{3.27}$$

By substituting (3.27) in (3.26), The model of parallel-connected two five-phase PMSMs in a stationary α-β -x-y frame with L_d=L_q=L_s is given as:

$$\begin{aligned}
\frac{di_{\alpha sj}}{dt} &= (-r_{sj} i_{\alpha sj} + \omega_j \Phi_{fj} \sin(\theta_j) + v_{\alpha sj}) / L_{sj} \\
\frac{di_{\beta sj}}{dt} &= (-r_{sj} i_{\beta sj} - \omega_j \Phi_{fj} \cos(\theta_j) + v_{\beta sj}) / L_{sj} \\
\frac{di_{xsj}}{dt} &= (-r_{sj} i_{xsj} + v_{xsj}) / L_{lsj} \\
\frac{di_{ysj}}{dt} &= (-r_{sj} i_{ysj} + v_{ysj}) / L_{lsj}
\end{aligned} \tag{3.28}$$

The torques expression for the first and the second machine are given by:

$$\begin{aligned}
T_{em1} &= \frac{5p_1}{2} (\Phi_{\alpha s} i_{\beta s} - \Phi_{\beta s} i_{\alpha s}) \\
T_{em2} &= \frac{5p_2}{2} (\Phi_{xs} i_{ys} - \Phi_{ys} i_{xs})
\end{aligned} \tag{3.29}$$

where p_1 and p_2 are the pole pairs.

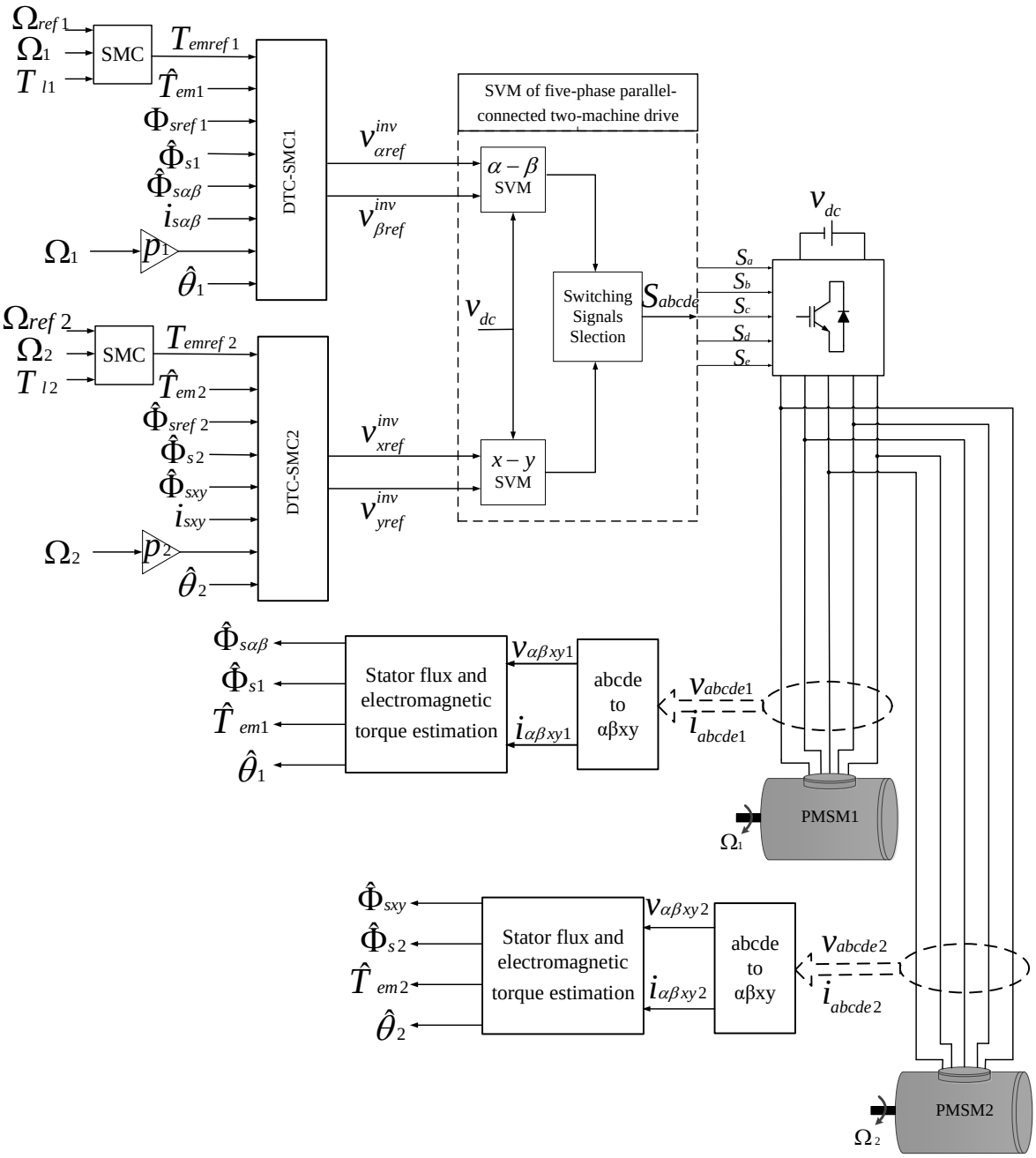

Fig. (3.12): DTC-SMC of a parallel-connected two five-phase PMSMs drive system.

3.4.2 Synthesis of Speeds Torques and Fluxes Controllers

3.4.2.1 Speed SMC Design

The sliding mode speed controller for each five-phase PMSM is designed by selecting the suitable sliding surfaces $S(\Omega_j)$. Since the relative degree is one, the following sliding surfaces are adopted:

$$S(\Omega_j) = \Omega_{refj} - \Omega_j, \quad j = 1,2 \tag{3.30}$$

By taking the derivative of the sliding surfaces given by (3.30) with respect to time and using the machines motion equations, it yields:

$$\begin{aligned}\dot{S}(\Omega_1) &= \dot{\Omega}_{ref1} - \frac{1}{J_1}(T_{em1} - T_{l1} - f_1\Omega_1)\\ \dot{S}(\Omega_2) &= \dot{\Omega}_{ref2} - \frac{1}{J_2}(T_{em2} - T_{l2} - f_2\Omega_2)\end{aligned} \tag{3.31}$$

where J_j, f_j and T_{lj} are the moment of inertia, damping coefficient, and load torque of each machine, respectively.

The torques controls T_{em1} and T_{em2} are defined by:

$$\begin{aligned}T_{em1} &= T_{emeqc1} + T_{emdic1}\\ T_{em2} &= T_{emeqc2} + T_{emdic2}\end{aligned} \tag{3.32}$$

where the equivalent torques control components are:

$$\begin{aligned}T_{emeqc1} &= T_{l1} + f_1\Omega_1\\ T_{emeqc2} &= T_{l2} + f_2\Omega_2\end{aligned}$$

The discontinuous torques control components are:

$$\begin{aligned}T_{emdic1} &= k_{\Omega1}\,smooth(S(\Omega_1))\\ T_{emdic2} &= k_{\Omega2}\,smooth(S(\Omega_2))\end{aligned}$$

$k_{\Omega1}$ and $k_{\Omega2}$ are positive constants.

3.4.2.1.1 Stability Analysis

During the convergence mode, the condition $\dot{V}(x) = S(x)\dot{S}(x) < 0$ must be verified. Indeed, by replacing (3.32) into (3.31), one gets:

$$\begin{aligned}\dot{V}(\Omega_1) &= -S(\Omega_1)\left[(1/J_1) k_{\Omega1}\,smooth(\mathrm{S}(\Omega_1)) \right] < 0\\ \dot{V}(\Omega_2) &= -S(\Omega_2)\left[(1/J_2) k_{\Omega2}\,smooth(\mathrm{S}(\Omega_2)) \right] < 0\end{aligned} \tag{3.33}$$

The (3.33) can be written as follows:

$$\begin{aligned}\dot{V}(\Omega_1) &= -\frac{1}{J_1} k_{\Omega1} |\mathrm{S}(\Omega_1)| < 0\\ \dot{V}(\Omega_2) &= -\frac{1}{J_2} k_{\Omega2} |\mathrm{S}(\Omega_2)| < 0\end{aligned} \tag{3.34}$$

From (3.34) the derivatives are negative, which means that the stability condition is ensured.

3.4.2.2 Torques and Fluxes SMCs Design

The DTC-SMC is designed to generate the stator voltage command from the torque and flux errors to track the electromagnetic torque and flux by controlling the input voltage of the machine. The electromagnetic torque and stator flux linkage squared are given by:

$$\begin{aligned} T_{emj} &= \frac{5p_j}{2}(\Phi_{\alpha sj} i_{\beta sj} - \Phi_{\beta sj} i_{\alpha sj}) \\ \Phi_{sj}^2 &= \Phi_{\alpha sj}^2 + \Phi_{\beta sj}^2 \end{aligned} \tag{3.35}$$

The control objectives are to track the desired torques and fluxes trajectories. Therefore, the sliding surfaces can be calculated as follows:

$$S = \begin{bmatrix} T_{emj}^* - T_{emj} \\ \Phi_{sj}^{*2} + \Phi^2{}_{sj} \end{bmatrix} = \begin{bmatrix} S(T_{emj}) \\ S(\Phi_{sj}) \end{bmatrix} \tag{3.36}$$

Using (3.26) and (3.27), the time derivative of (3.36) can be rewritten as:

$$\begin{aligned} \begin{bmatrix} \dot{S}(T_{emj}) \\ \dot{S}(\Phi_{sj}) \end{bmatrix} = &\begin{bmatrix} \frac{-5p_j}{2}(r_{sj} i_{h1s} - \omega_j \Phi_{fj} \sin(\theta_j))\Phi_{h2s} & \frac{-5p_j}{2}(r_{sj} i_{h2s} + \omega_j \Phi_{fj} \cos(\theta_j))\Phi_{h1s} \\ -2r_{sj} i_{h1s}\Phi_{h1s} - 2r_{sj} i_{h2sj}\Phi_{h2s} & \end{bmatrix} \\ &+ \begin{bmatrix} \frac{-5p_j}{2}(i_{h2s} - \frac{\Phi_{h2sj}}{L_{sj}}) & \frac{-5p_j}{2}(\frac{\Phi_{h1s}}{L_{sj}} - i_{h1s}) \\ -2\Phi_{h1s} & -2\Phi_{h2s} \end{bmatrix} \begin{bmatrix} v_{h1s} \\ v_{h2s} \end{bmatrix} \end{aligned} \tag{3.37}$$

with

h_1=α, x and h_2=β, y.

Therefore, the equation (3.37) can be expressed in the following matrix form:

$$\dot{S} = F + DU \tag{3.38}$$

with:

$$\dot{S} = \begin{bmatrix} \dot{S}(T_{emj}) \\ \dot{S}(\Phi_{sj}) \end{bmatrix}$$

$$F = \begin{bmatrix} \frac{-5p_j}{2}(r_{sj} i_{h1s} - \omega_j \Phi_{fj} \sin(\theta_j))\Phi_{h2s} & \frac{-5p_j}{2}(r_{sj} i_{h2s} + \omega_j \Phi_{fj} \cos(\theta_j))\Phi_{h1s} \\ -2r_{sj} i_{h1s}\Phi_{h1s} - 2r_{sj} i_{h2s}\Phi_{h2s} & \end{bmatrix}$$

$$D = \begin{bmatrix} \frac{-5p_j}{2}(i_{h2s} - \frac{\Phi_{h2s}}{L_{sj}}) & \frac{-5p_j}{2}(\frac{\Phi_{h1s}}{L_{sj}} - i_{h1s}) \\ -2\Phi_{h1s} & -2\Phi_{h2s} \end{bmatrix}$$

$$U = \begin{bmatrix} v_{h1s} \\ v_{h2s} \end{bmatrix}$$

Therefore, it is possible to choose the control laws for stator voltages as follows:

$$\begin{aligned} v_{h1s} &= v_{h1seqc} + v_{h1sdic} \\ v_{h2s} &= v_{h2seqc} + v_{h2sdic} \end{aligned} \tag{3.39}$$

where the equivalent voltages control components are:

$$\begin{bmatrix} v_{h1seqc} \\ v_{h2seqc} \end{bmatrix} = -D^{-1} \begin{bmatrix} \mathrm{F}_1 \\ \mathrm{F}_2 \end{bmatrix}$$

The discontinuous torques control components are:

$$\begin{bmatrix} v_{h1sdic} \\ v_{h2sdic} \end{bmatrix} = -D^{-1} \begin{bmatrix} \mathrm{k}_{Temj}\, smooth(S(T_{emj})) \\ \mathrm{k}_{\Phi j}\, smooth(S(\Phi_{sj})) \end{bmatrix}$$

with k_{Temj} and $\mathrm{k}_{\Phi j}$ are positive gains.

3.4.2.2.1 Stability Analysis

During the convergence mode, the condition $\dot{V}(x) = S(x)\dot{S}(x) < 0$ must be verified. Indeed, by replacing (3.39) into (3.38), one gets:

$$\dot{V}(S) = -S^T \begin{bmatrix} \mathrm{k}_{Tem_j}\, smooth(S(T_{emj})) \\ k_{\Phi_{sj}}\, smooth(S(\Phi_{sj})) \end{bmatrix} < 0 \tag{3.40}$$

The (3.33) can be written as follows:

$$\dot{V}(S) = \begin{bmatrix} \mathrm{k}_{Tem_j} \left| S(T_{emj}) \right| \\ k_{\Phi_{sj}} \left| S(\Phi_{sj}) \right| \end{bmatrix} < 0 \tag{3.41}$$

From (3.41) it is obvious that the system is globally stable, S and will be forced to zero in a definite period, which also means that the torque and flux of each five-phase PMSM will follow their reference values.

3.4.3 Simulation Results

The applicability of DTC-SVM-SMC for the two five-phase PMSMs connected in parallel is verified through different simulation results under the same load torque as shown in figs 3.13 to 3.15. Furthermore, it is showing a full decoupling and independent control for the two machines. The tuning parameters for the SM-controllers can be found in table B.5 of appendix B.

Fig. (3.13) shows the system performance, when one machine is at standstill and the other is still running. A speed reference of value 100 rad/s is applied to the first five-phase PMSM then standstill at t=1.5s , while a speed reference of value 50 rad/s is applied to the second five-phase PMSM at t=0.5s and kept constant until the end of the test. The two five-phase PMSM's speeds and electromagnetic torques are not affected by the starting operation of each other.

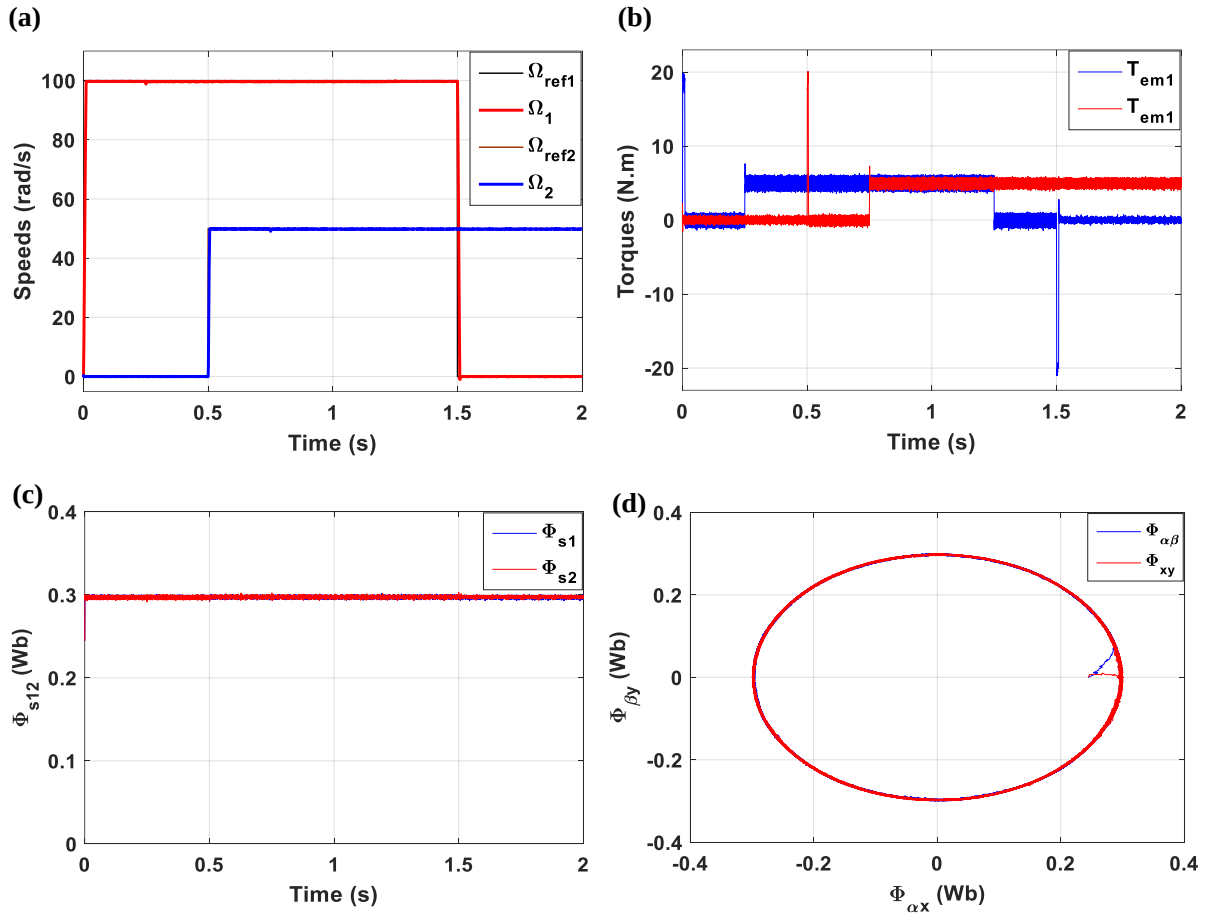

Fig. (3.13): Dynamic responses of parallel-connected two five-phase PMSMs drive controlled by DTC-SVM-SMC: when one machine is at standstill and the other is still running: (a) the machine Speeds, (b) electromagnetic torques, (c) Stator fluxes magnitudes, and (d) Stator fluxes trajectories.

Fig. (3.14) shows the system performance, when one machine is kept constant and the other machine changes the direction. Both machine started at the same time, then the speed of the first five-phase PMSM is maintained constant equal to 100 rad/s then is changed to be -100 rad/s at t=1s. The second five-phase PMSM changes the direction from 50 rad/s to -50 rad/s after that it returns to 50 rad/s at t= 0.5s, 1.5s, respectively. The load torque is applied at t=0.25s for both machines.

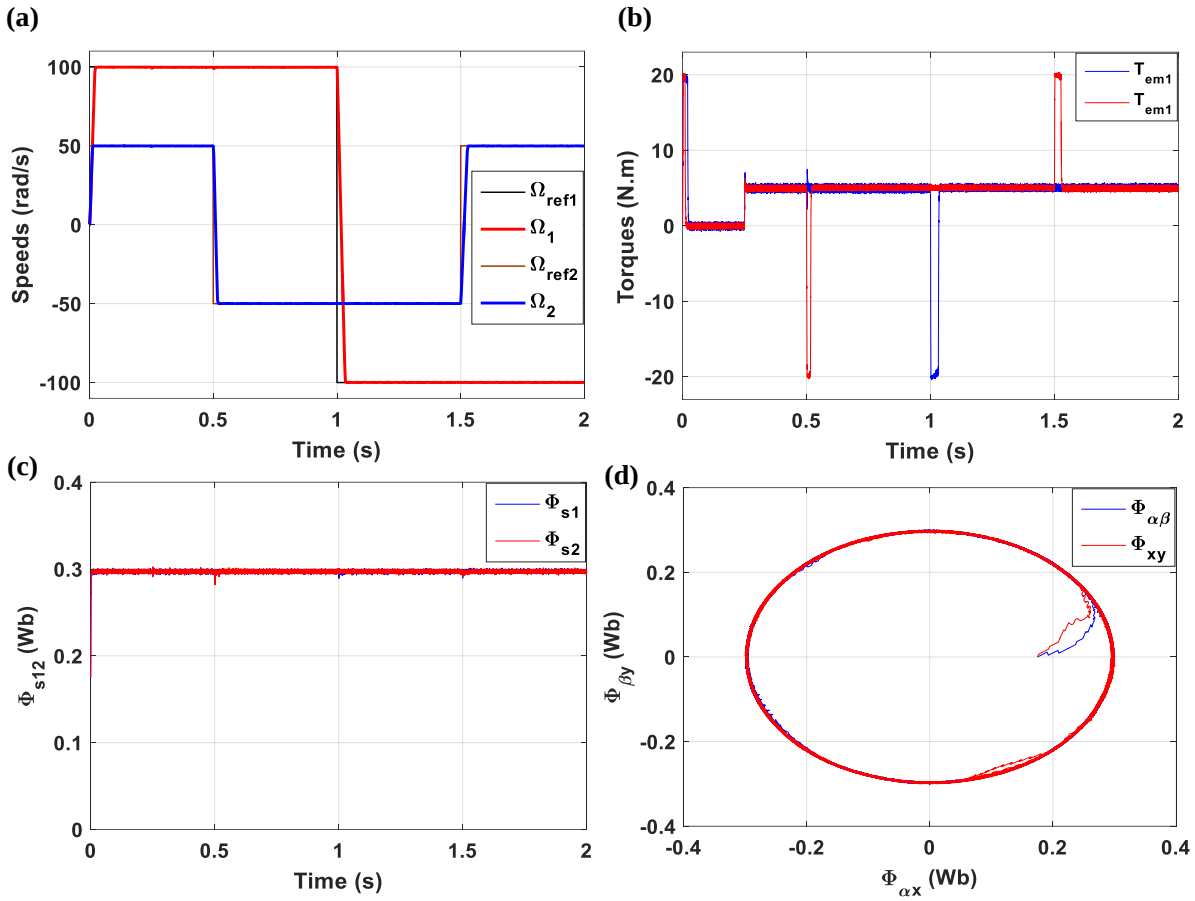

Fig. (3.14): Dynamic responses of parallel-connected two five-phase PMSMs drive controlled by DTC-SVM-SMC: when the speed of one machine is kept constant and the other change the direction: (a) the machine Speeds, (b) electromagnetic torques, (c) Stator fluxes magnitudes, and (d) Stator fluxes trajectories.

Fig. (3.15) shows the system performance when the two machines are operating in the opposite directions. The speed of the first five-phase PMSM changes from +100 rad/s to -50 rad/s at t = 1s, while the speed of the second five-phase PMSM changes from - 50 rad to 100 rad/s at t = 1s. As can be seen a full-decoupled control is assured and the speed and torque of the second five-phase PMSM are not influenced by the acceleration period of the first five-phase PMSM.

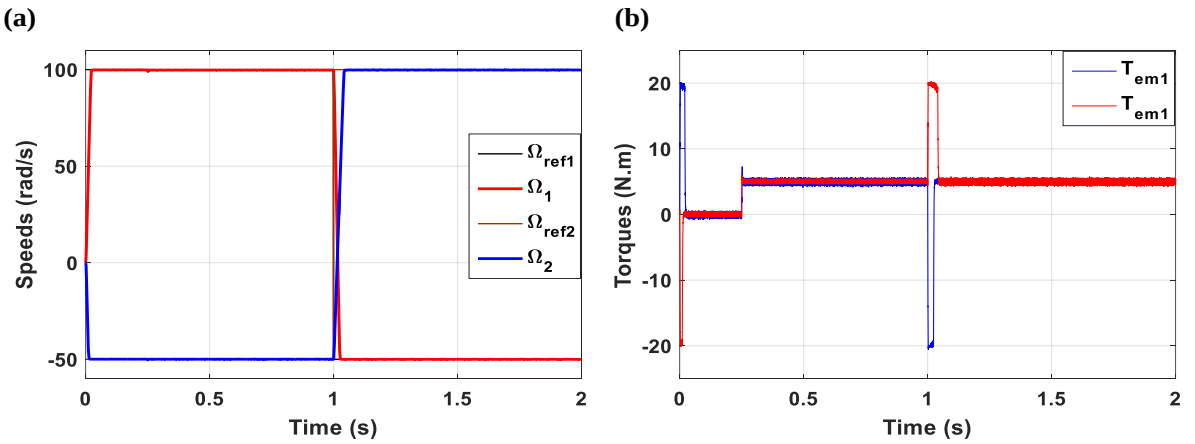

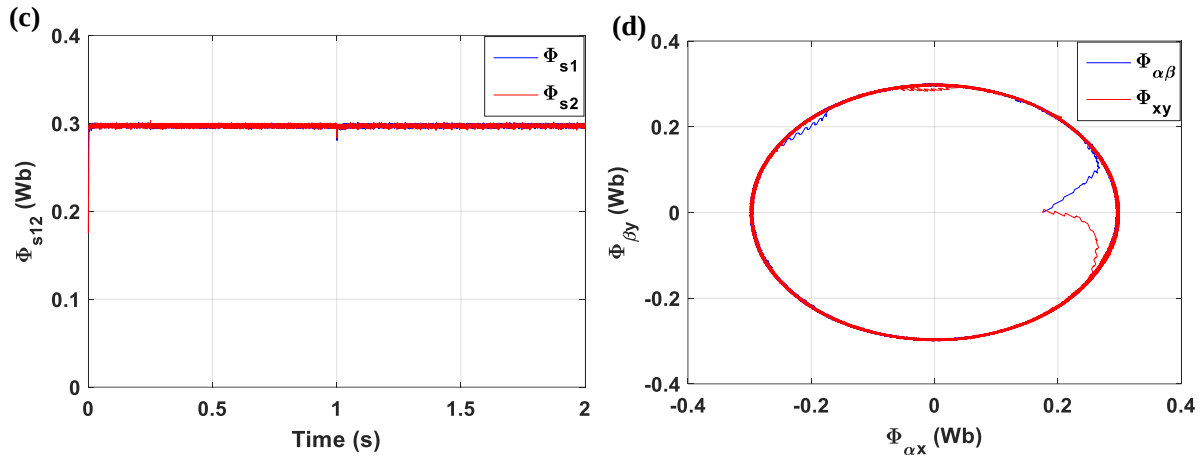

Fig. (3.15): Dynamic responses of parallel-connected two five-phase PMSMs drive controlled by DTC-SVM-SMC: when the two machines are operating in the opposite directions: (a) the machine Speeds, (b) electromagnetic torques, (c) Stator fluxes magnitudes, and (d) Stator fluxes trajectories.

Figs. (3.13) to (3.15) show the responses of both five-phase PMSM under a sudden change in load torque for the two machine. It can be observed from Figs. (3.13) to (3.15) that, step loading of one machine does not cause any disturbance in the other machine's speed, electromagnetic torque, stator flux magnitudes and stator flux trajectory.

All tests demonstrate that, the starting and reversing transients of one machine do not have any tangible consequence on the operation of the second machine. The decoupled control is preserved and the characteristics of both machines are unaffected.

The results shows a good decoupling between the torque and flux for each machine, which means that the stability condition is ensured and demonstrating the full control capability by using sliding mode control.

As can be seen from Figs. (3.13) to (3.15), the DTC-SVM-SMC gives responses without overshoot in term of speeds and fluxes. In addition to that, the ripple is reduced and has a good setting time.

3.4.3.1 Comparative Study Between DTC-SVM-SMC and DTC-SVM-PI

The aims of this comparison is to show the difference between SMC and PI, where the SMC can give a better responses compared to PI-regulators as can be seen in Figs (3.16) to (3.17). Fig. (3.16) shows the dynamic responses of the tow machines at deferent speed references including standstill. In Fig. (3.16) both machines started at the opposite direction and then the operation is reversed at the same time.

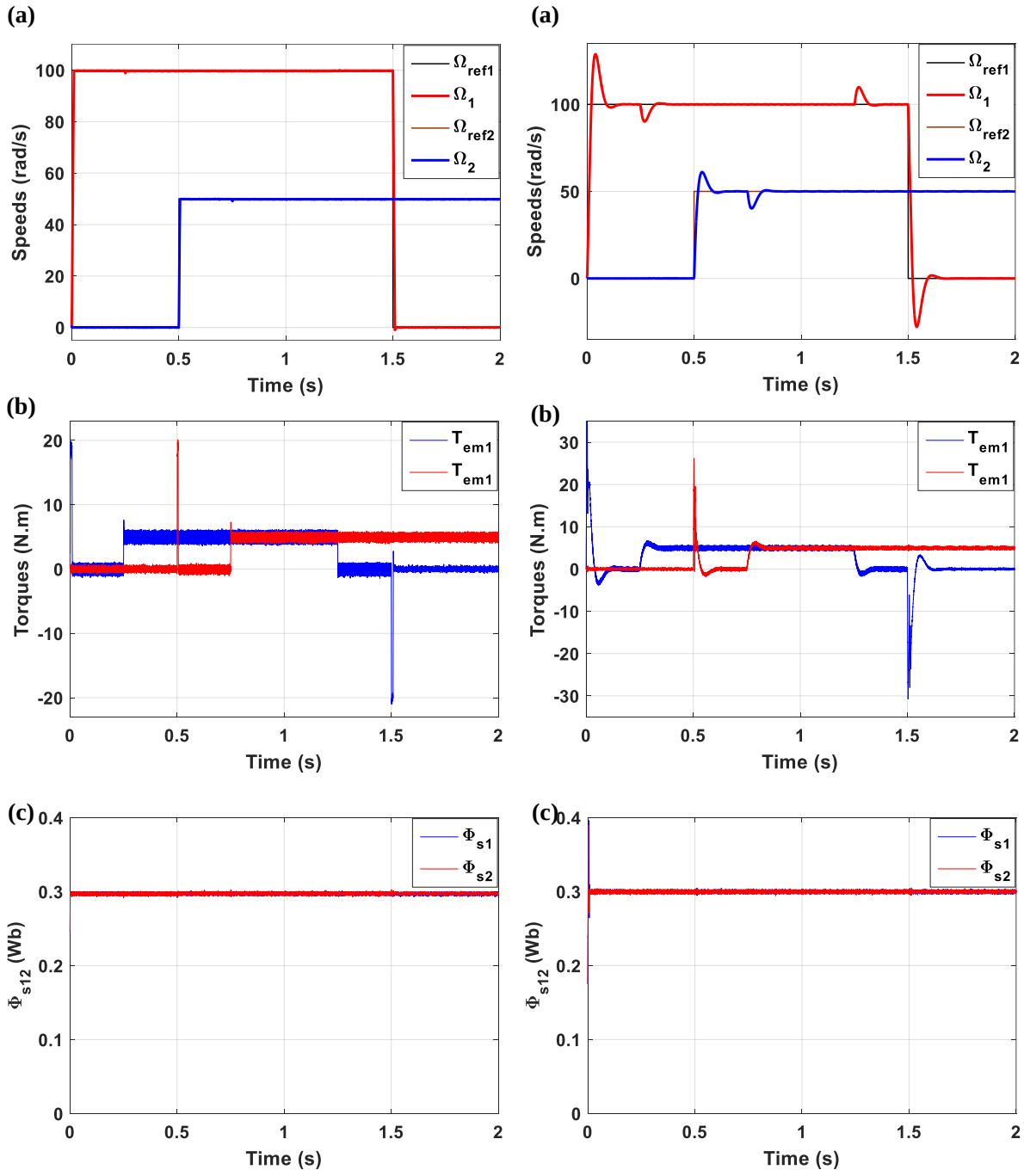

Fig. (3.16): Comparative study between DTC-SVM-SMC and DTC-SVM-PI of parallel-connected two five-phase PMSMs drive: when one machine is at standstill and the other is still running: (a) the machine Speeds, (b) electromagnetic torques, (c) Stator fluxes magnitudes, and (d) Stator fluxes trajectories.

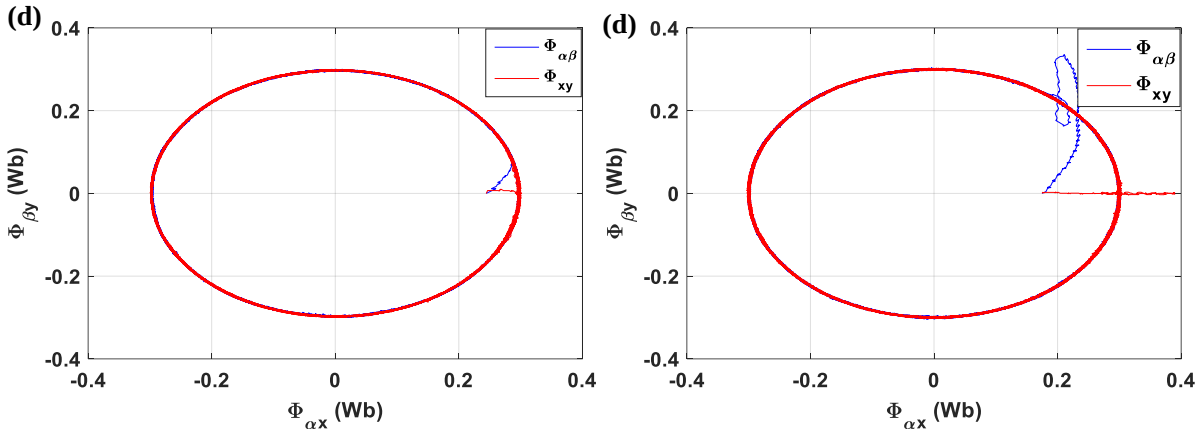

Continued to Fig. (3.16).

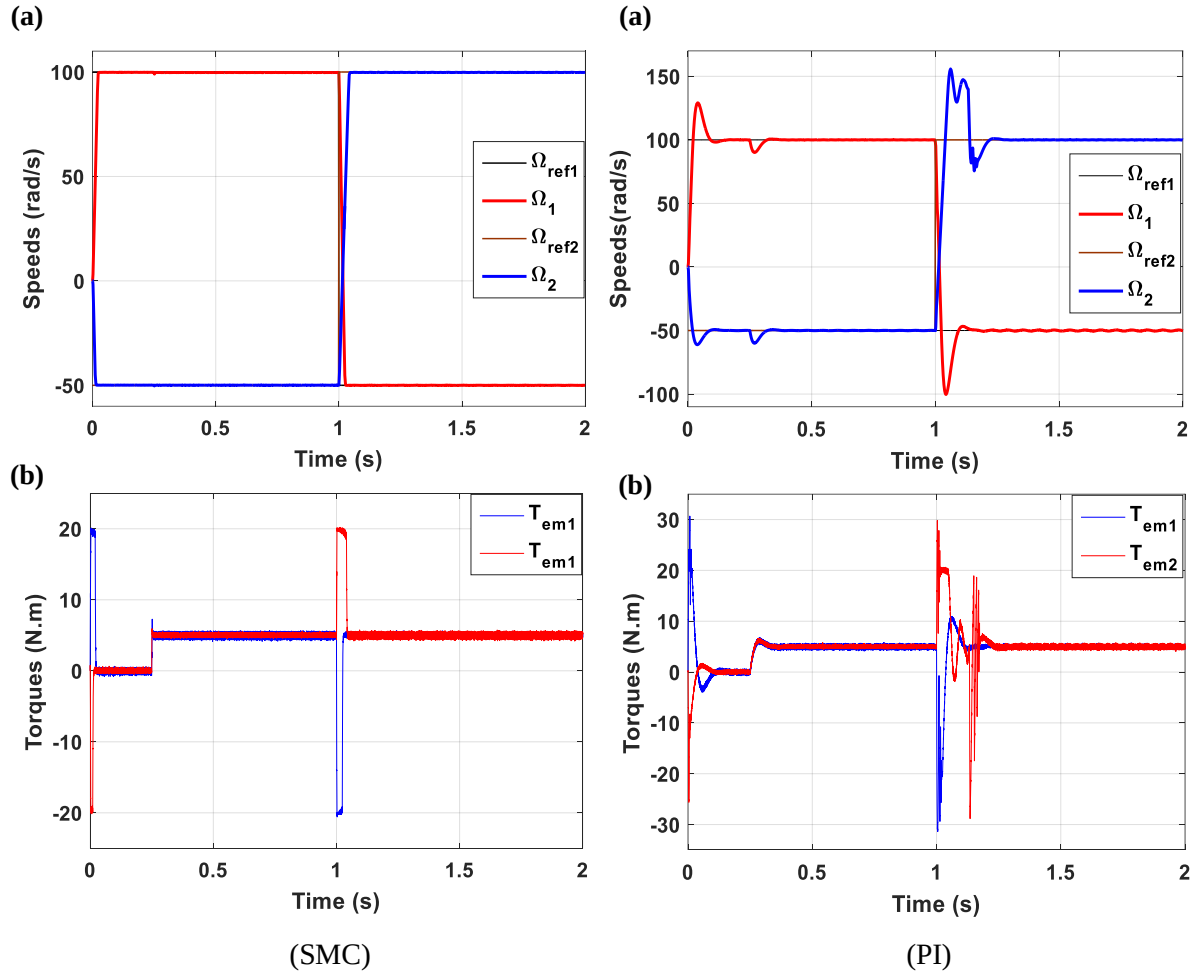

Fig. (3.17): Comparative study between DTC-SVM-SMC and DTC-SVM -PI of parallel-connected two five-phase PMSMs drive: when the two machines are operating in the opposite directions: (a) the machine Speeds, (b) electromagnetic torques, (c) Stator fluxes magnitudes, and (d) Stator fluxes trajectories.

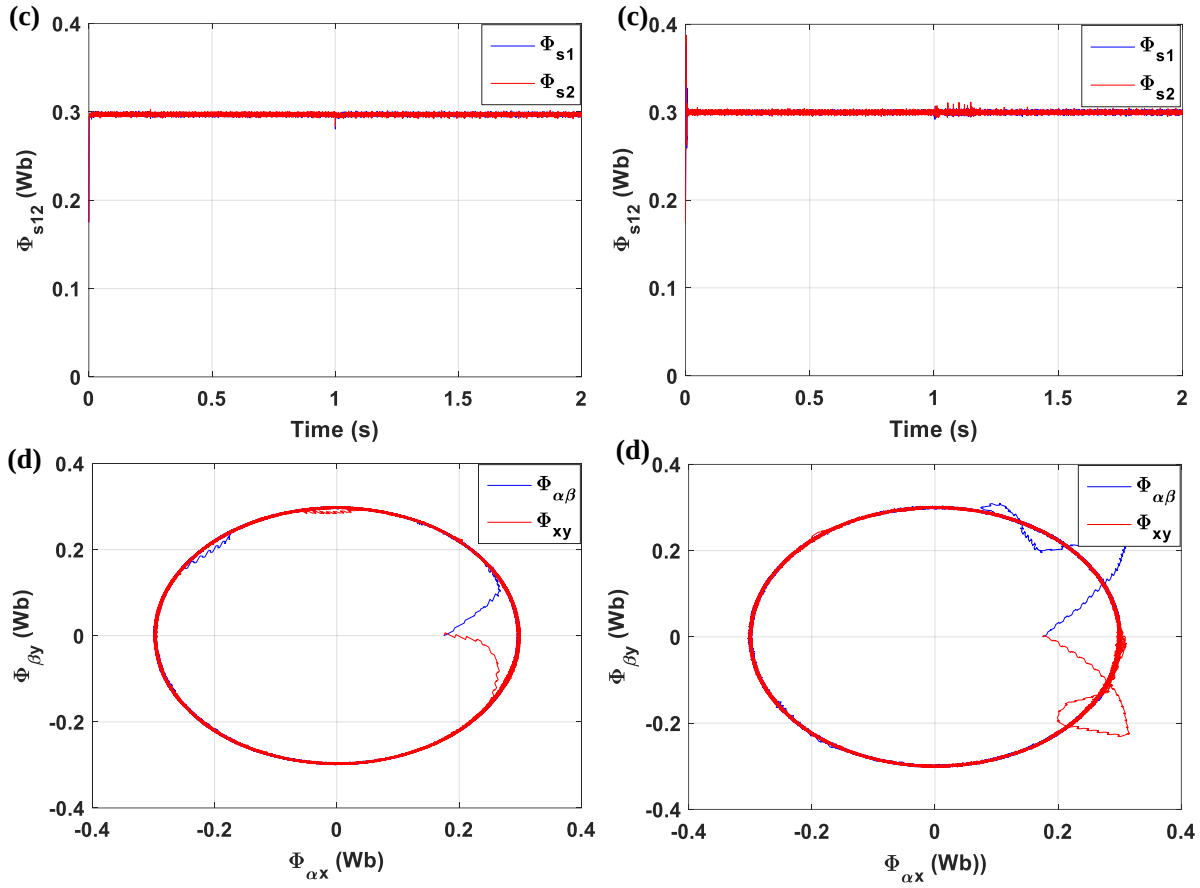

Continued to Fig. (3.17).

From the above simulation results, it can be summarized the comparison through three aspects as follow:

Speed response: Figs. (3.16-a (SM) to 3.17-a (SM)), show comparable dynamic behavior of DTC-SVM using SMC. However, it is clear from these figures that, the system reaches steady state without overshoot and fast settling times.

In Figs. (3.16-a (PI)) to (3.17-a (PI)), show the system behavior using PI-controller, which have response characteristics of a second order system. It can be seen the response has a short rise time, an overshoot even in reverse modes, and slow settling times.

By analyzing the speed responses of two-machine drive controlled by PI-controller, it can be observed easily, a speeds drops taken place at the moments of loads changes. On the other hand, the SMCs Figs. (3.16-a (SM) to 3.17-a (SM)) keep the speeds close to their references without overshoots and without drops. Therefore, the SMC can be considered as more robust under loads variations.

Torque response: Figs. (3.16-b) to (3.17-b), illustrate the behavior of the torque for both controllers. In case of the PI-controller, the torque T_{em1} and T_{em2} peak at maximum, then decrease progressively to the steady state with overshoot even in the load application. In addition, there are perturbation in reverse mode then settling when the system reaches steady state. Figs. (3.16-b (SM)) to (3.17-b (SM)) show torque in case of sliding mode control. In contrast, the torque T_{em1} and T_{em2} is maintained longer at its maximum value (20 N.m), until the speed reaches its reference value. This leads to a short settling time and without overshoot except in the loading application. Furthermore, the perturbation in case of PI-controller is overcame.

Flux response: Figs. (3.16-c, d) to (3.17-c, d), illustrate the behavior of the stator fluxes magnitudes and stator fluxes trajectories for both controllers. In case of PI-controller, the stator magnitudes Φ_{s1} and Φ_{s2} peak above 0.4 Wb, then decrease to the steady state while the fluxes trajectories $\Phi_{\alpha\beta}$ and Φ_{xy} are almost circular with overshoot in starting operation. In case of SMC-controller Figs. (3.16-c (SM)) to (3.17-c (SM)) show fluxes magnitudes peak to its reference rapidly without overshoot. In contrast, the $\Phi_{\alpha\beta}$ and Φ_{xy} peak to steady state with short settling time and without overshoot.

The general comparison between DTC-SVM-SMC and DTC-SVM-PI can be summarized in terms of quantitative as shown in table (3.2).

Table (3.2): Comparison between DTC-SVM-SM and DTC-SVM-PI.

Controlled variable	Comparison criterion	DTC-SMC	DTC-PI	Reduction Ratio (%)
Rotor speed	Settling time (s)	0.028	0.16	0.825
	Overshoot (rad/s)	0	30	100
	Speeds drops (%)	1	10	90
	Recovery time (at abrupt load) (s)	0.006	0.07	91.42
	Overshoot in reversal mode (%)	0	78	100
Electromagnetic torque	Settling time (s)	0.026	0.1	74
	Overshoot (rad/s)	0	4	100
	Ripple (N.m)	1.2	1.2	----
Stator flux	Settling time (s)	0.003	0.005	40
	Overshoot (rad/s)	0.003	0.08	96.25
	Overshoot in reversal mode (%)	0.012	0.005	Increase
	Ripple (N.m)	0.005	0.0095	58.3

3.5 General Comparison the FOC and DTC-SVM Based SMC

In this section, a comparative study between FOC-SMC and DTC-SVM –SMC is investigated. Figs. (3.18) to (3.21) shows the viability and the performance of each control of parallel-connected two five-phase PMSMs fed by five-phase VSI, under the same supply parameters, and the same operating modes.

3.5.1 Case 1: Two Machines Operating in the Same and Opposite Directions

The two machines are running in the same and opposite directions. The first five-phase PMSM changes the direction from 100 rad/s to -100 rad/s at t=1s, while the second five-phase PMSM changes its direction from 50 rad/s to -50 rad/s than to 50rad/s at t=0.5s and 1.5s, respectively.

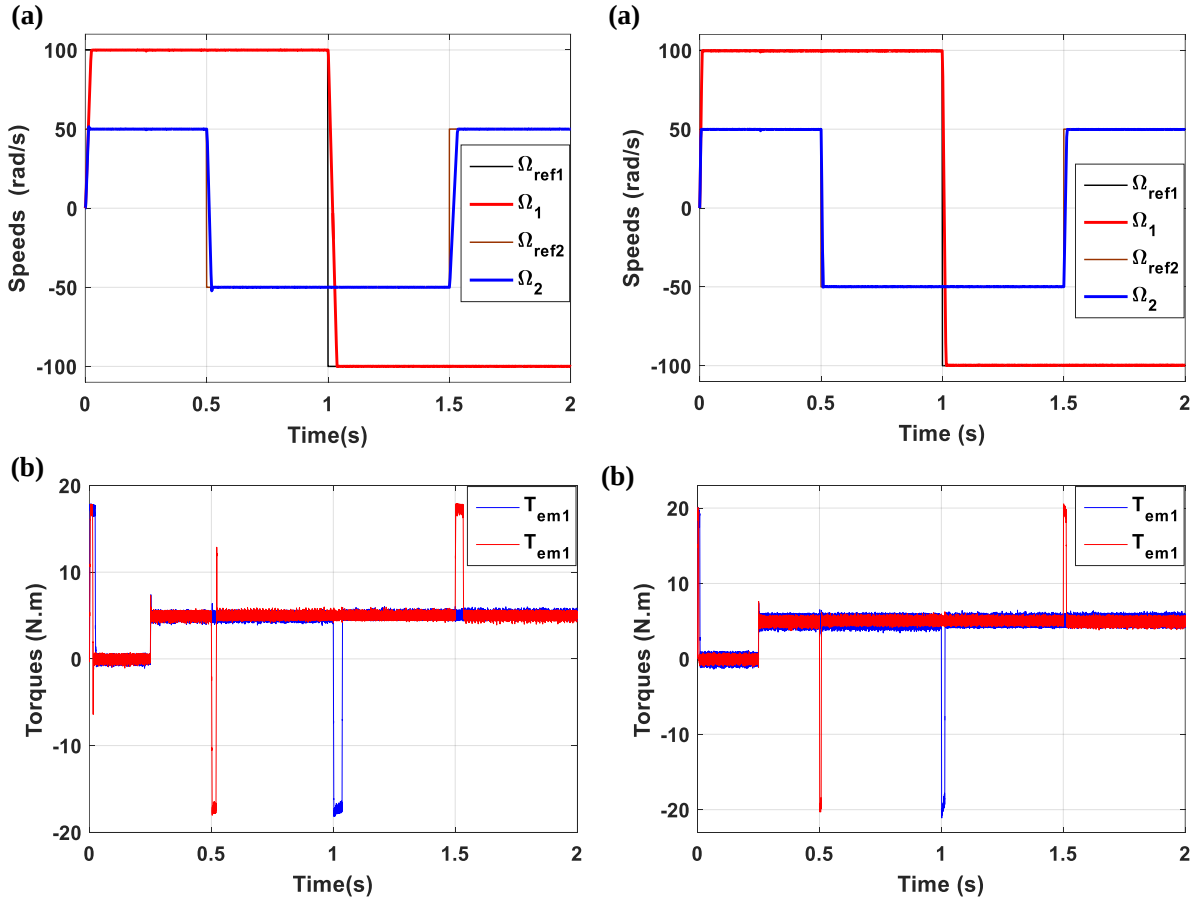

(FOC-SMC) (DTS-SVM-SMC)

Fig (3.18): Comparison between dynamic responses of parallel-connected two five-phase PMSMs drive operating at different references : (a-b) the machine Speeds and electromagnetic torques controlled by FOC-SMC, (a-b) the machine Speeds and electromagnetic torques controlled by DTC-SVM-SMC.

3.5.2 Case 2: Low Speed Operation

The two machine are running in the opposite directions with low speed. In the starting phase, the first five-phase PMSM is rotating at +20 rad/s; the second five-phase PMSM is running at the opposite speed (-10 rad/s). After that at the same time (t=1s) the first five-phase PMSM changes the direction from 20 rad/s to -10rad/s, while the second five-phase PMSM changes from -10 rad/s to 20 rad/s.

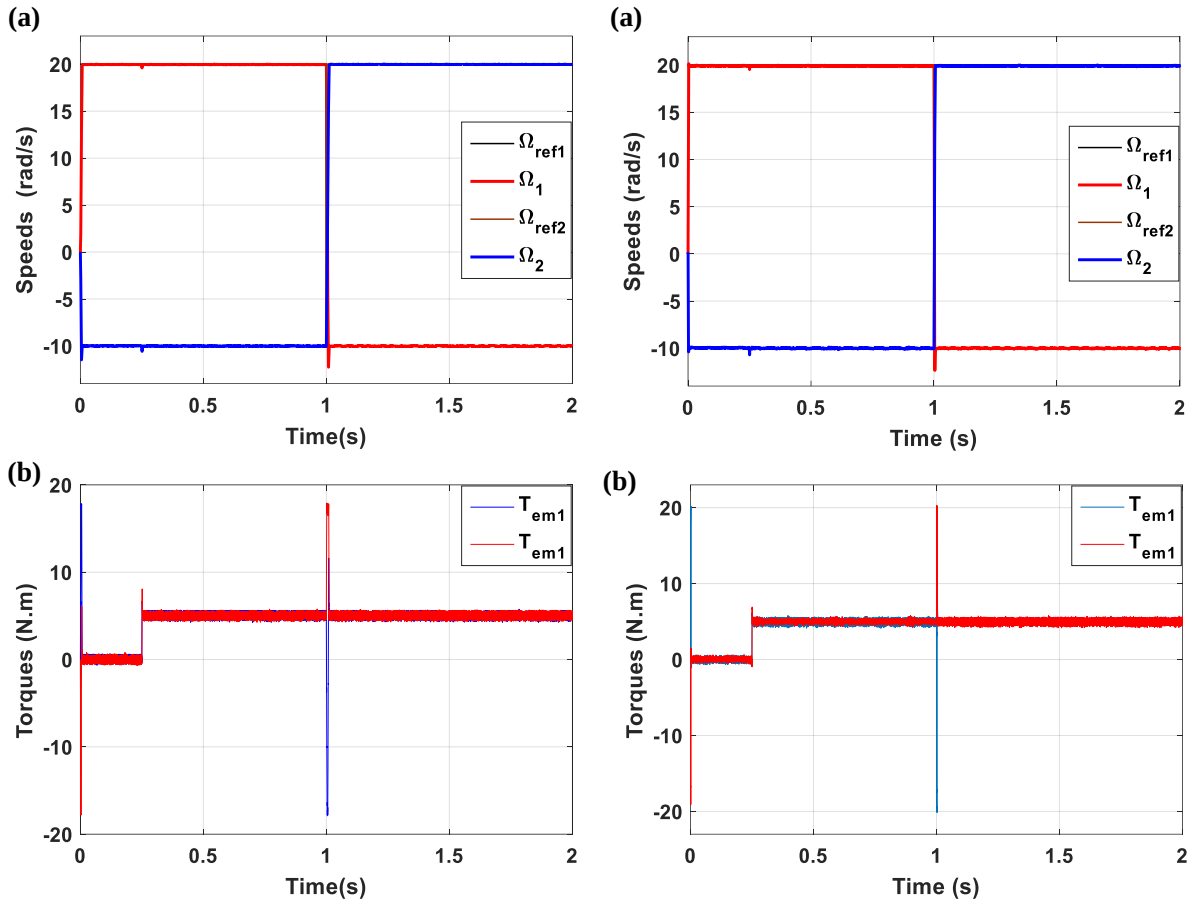

(FOC-SMC) (DTS-SVM-SMC)

Fig. (3.19): Comparison between dynamic responses of parallel-connected two five-phase PMSMs system operating at low speed conditions: (a-b) the machine Speeds and electromagnetic torques controlled by FOC-SMC, (a-b) the machine Speeds and electromagnetic torques controlled by DTC-SVM-SMC.

3.5.3 Case 3: Parameters Variation

Fig. (3.20) shows the profile of the changes in stator resistances. Note that these changes occur with 100% increasing in both stators resistances at 0.8s and 1.2s, respectively.

In this case, the two machines are running in the same directions; in the starting phase, the first five-phase PMSM is rotating at +100 rad/s and the second five-phase PMSM is running at 50 rad/s.

After the load application at t=0.25s, stator resistance variations are introduced at t=0.8s and 1.2s for the first and second machine, respectively.

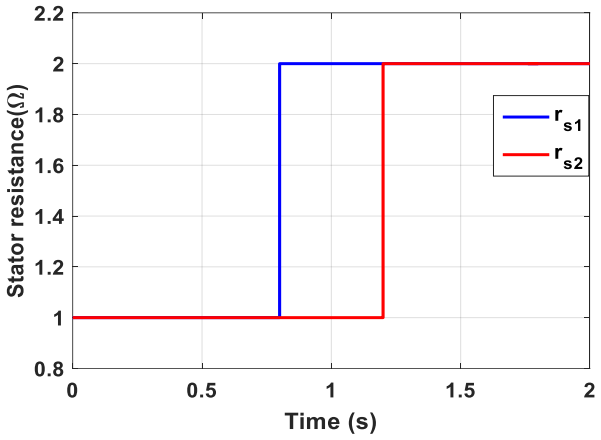

Fig. (3.20): Profile of stators resistances variations.

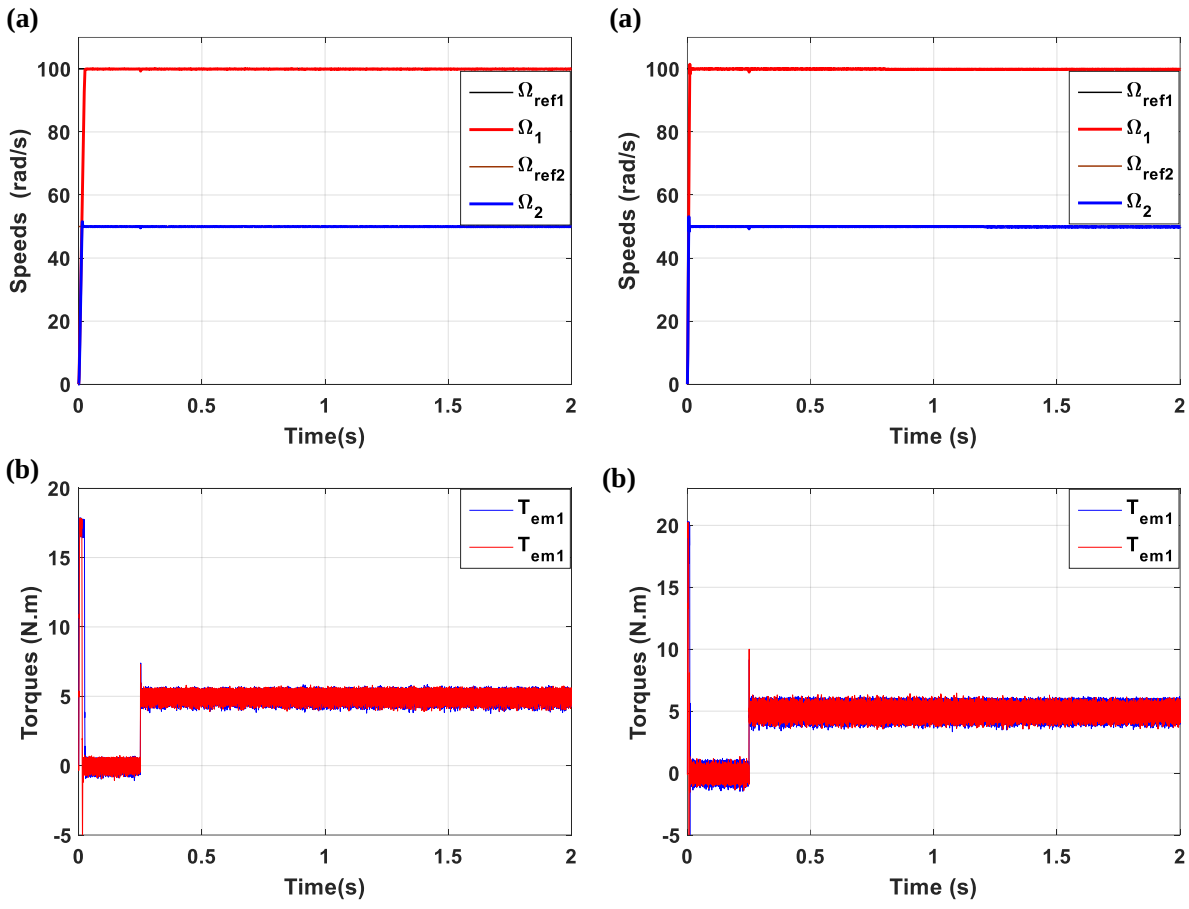

(FOC-SMC) (DTS-SVM-SMC)

Fig. (3.21): Comparison between dynamic responses of parallel-connected two five-phase PMSMs drive operating at stator resistances variations: (a-b) the machine Speeds and electromagnetic torques controlled by FOC-SMC, (a-b) the machine Speeds and electromagnetic torques controlled by DTC-SVM-SMC.

From Figs. (3.18) to (3.21), it can be noticed that both torque and the speed of each machine follow closely their references. In addition, the electromagnetic torque and the speed of one machine are not affected by the starting operation of the second one for each control. The comparison study between FOC-SMC and DTC-SVM-SMC shows a better response in low speed operation and during stator resistance variations. The comparison study can be summarized on following points:

- **Ripple**: both controls FOC-SMC and DTC-SVM-SMC reduce the ripple of electromagnetic torque, but in case of FOC-SMC there is more reduction in ripple than DTC-SVM-SMC.
- **Overshoot**: dynamic responses of system with both controls FOC-SMC and DTC-SVM-SMC are without overshoot, even in reversal mode
- **Speeds drops:** there is no drops in speeds responses for both controls FOC-SMC and DTC-SVM-SMC.
- **Stator resistance variations:** both control methods of control FOC-SMC and DTC-SVM-SMC give a batter response, and there are not affected when stator resistances varied, which demonstrates the robustness of sliding mode control against parameter variations.

Table (3.3) shows summarized quantitative comparison between FOC-SMC and DTC-SVM-SMC. As can be seen the DTC-SVM-SMC is better in term of settling time and recovery time (at abrupt load) as well as the reduction of the ripple.

Table (3.3): Comparison between FOC-SMC and DTC-SVM-SMC.

Controlled variable	Comparison criterion	FOC-SMC	DTC-SVM-SMC	Reduction ratio (%)
Rotor speed	Settling time (s)	0.03	0.011	63
	Overshoot (rad/s)	0	0	0
	Speeds drops (%)	0.9	0.9	0
	Recovery time (at abrupt load) (s)	0.004	0.002	50
	Overshoot in reversal mode (%)	0	0	0
Electromagnetic torque	Settling time (s)	0.0265	0.0106	60
	Overshoot (rad/s)	0	0	0
	Ripple (N.m)	1.4	2	30

3.6 Conclusion

This chapter presents a nonlinear sliding mode control applied on FOC and DTC-SVM of parallel-connected two five-phase PMSMs drive fed by a single inverter has been developed. The sliding mode control has several advantages such as, robustness, high precision, stability and simplicity, very low settling time. The effectiveness of the control approach has also been verified through extensive computer simulations and compared with PI-controller. Simulation results have demonstrated not only truly decoupled operation between the two machines but also many improvements on the dynamic response as well as the steady state performance, in terms of speed response, accuracy, and ripple reduction. The main improvements brought by the proposed FOC-SMC and DTC-SVM-SMC compared to each other are listed below:

- Faster rise time;
- Good speed tracking without overshoots or drops;
- Low torque and flux ripples;
- Good robustness against parameters variation.

Therefore, the FOC-SVM-SMC can be considered as more robust compared with DTC-SVM-SMC in terms of ripple reduction and parameters variations, but DTC-SVM-SMC offers a short settling and recovery times at abrupt load.

In order to increase the proposed drive robustness and decrease its complexity and cost, the well-known sensorless control technology is a possible solution. The next chapter will present a design of serval sensorless based FOC and DTC-SVM techniques to estimate speed, flux and torque.

Chapter 4

Senserlees Control Schemes for Parallel-Connected Two Five-Phase PMSMs Drive System

4.1 Introduction

In the most electric drives, an accurate knowledge on rotor position is crucial for feedback control. It can be achieved from some types of shaft sensors such as an optical encoder or resolver connected to the rotor shaft [77],[78]. However, the use of these sensors will increase the cost and reduce the reliability of the drive, and may suffer from some restrictions such as temperature, humidity, and vibration. These problems can be solved by using the well-known sensorless control technology. Various methods of sensorless control have been proposed by several researchers [79-81]. The main idea of sensorless control of parallel-connected two five-phase machines is to estimate the rotor positions and their corresponding speeds through an appropriate way using measurable quantities such as five-phase currents and voltages. However, few applications deal with the sensorless control of multi-phase machines such as, model reference system[82], Kalman filtering technique [83] and sliding mode observer of five-phase IM and PMSM [84], [85] .

Unlike the other approaches, the extended kalman filter (EKF) is more attractive because it delivers rapid, precise, and accurate estimation. The feedback gain used in EKF achieves quick convergence and provides stability for the observer [86]. For stochastic systems, the extended Kalman filter is the preferable solution capable to provide states estimation or of both the states and parameters estimation. The sliding mode observer (SMO) is more attractive due to its advantages as following: robustness against the system parameters variations (disturbances, and noises), simple and less restrictive design, no need for extensive computations, and achievement of desired dynamic performance [87].

This chapter is to study and designe two sensorless sliding mode control schemes of the parallel-connected two five-phase PMSMs fed by a single five-leg inverter. The first approach consist of using the extended Kalman filter for sensorless operation purposes, and the SMC is implemented for speeds and currents control. The resulting control scheme combines the features of the robust control and the stochastic observer to enhance the performances of the proposed two-machine drive. The second approach consist of a sensorless DTC sliding mode control scheme (DTC-SMC) equipped with a sliding mode observer for parallel-connected machines. To obtain the desired characteristics, the SMC is implemented for speeds, fluxes and electromagnetic torques control and the SMO is used for sensorless operation purposes. The developed control scheme combines the features of the robust control and the robust estimation.

The performances of the two observers and each control scheme are tested under variations of the load torque and velocity reference.

4.2 General Observers

An observer is an estimator in closed-loop with independent dynamic system. The state observer is a mathematical model that is running in parallel to the actual system and provides the estimation of the system state vectors, including the rotor position and speed. Hence, the PMSM rotor position information can be estimated through a state observer [51][88] [89].

The principle of constructing an observer is consisted of correcting the dynamics of the estimate by taking into account the difference between the real output (RO) and the observer output (OO) and multiple by gene *K* to operate the closed loop. This leads to the following observer's equation [51] [74]:

$$X_{k+1} = X_k + K(Y_{OO} - Y_{RO}) \tag{4.1}$$

From the input *U*, the variable *X* can be determined from the equation as:

$$\dot{X} = AX + BU \tag{4.2}$$

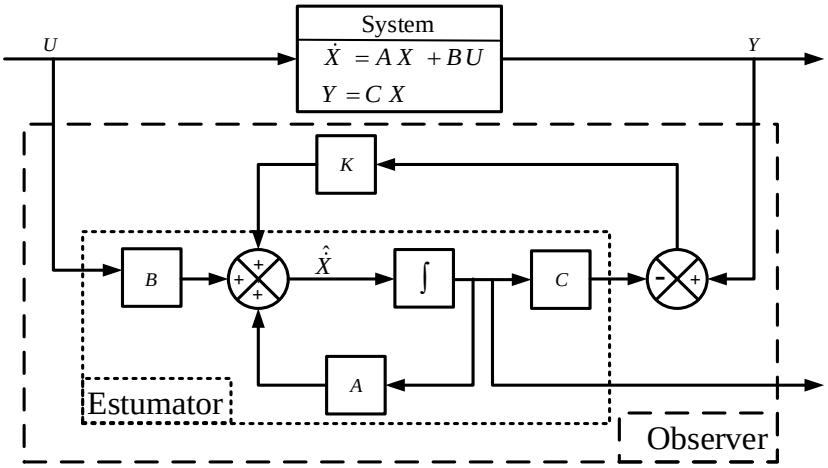

Fig. (4.1): Schéma de principe d'un observateur.

4.3 Extended Kaman Filter Based Speed Estimator for Parallel-Connected Two-Machine Drive

The proposed sensorless control of the parallel-connected two five-phase permanent magnet synchronous machines is presented in Fig. (4.2), where the two main parts EKF and SMC are considered. The EKF is designed to estimate the rotor position, speed and load torque of each machine by using a current observer. The feedback actual speed, estimated speed and load torques are the inputs of the speeds SMCs to determine the q_1-y_2 axes reference current components. The other current components are maintained to zero. The measured currents are processed in

the current SMCs to obtain as outputs the *d-q-x-y* axes reference voltages components. These reference voltages are transformed into the *abcde* frame and transformed again to *α-β-x-y* frame to become input signals to the SVM blocks. The SVM transmits the signals to the inverter to drive the two five-phase PMSMs connected in parallel.

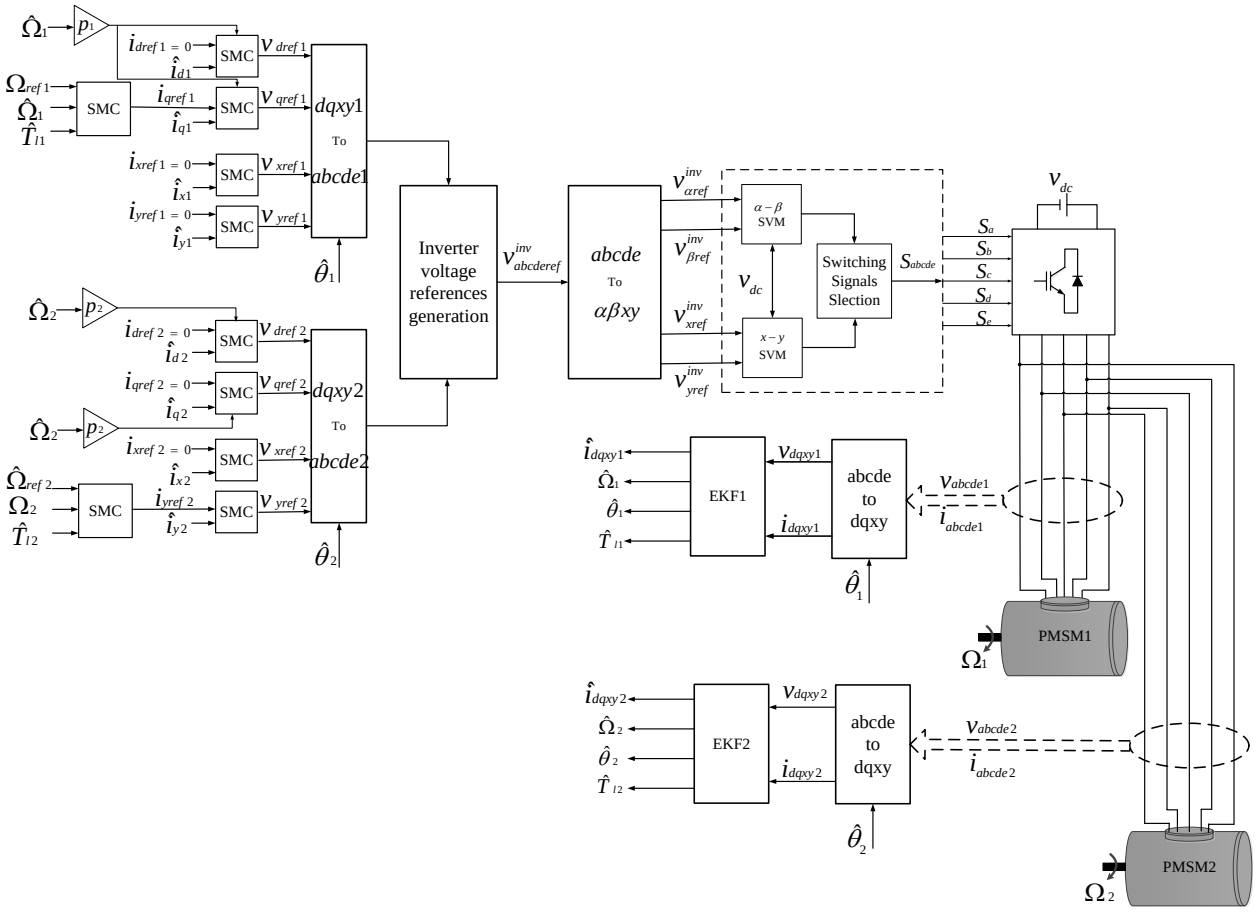

Fig. (4.2): Sensorless SMC of parallel-connected two five-phase PMSMs drive system.

The SMC block diagram based on extended kalman filter of parallel-connected two five-phase machines drive system is shown in Fig. (4.2). The main task of EKF is to find the best estimate of state variables and the unknown load torques since the knowledge of the load torque is necessary for each speed SMC implementation.

4.4 Extended Kalman Filter

The Extended Kalman Filter (EKF) is used to perform state observer based control of the five-phase PMSM that is a nonlinear controlled drive system. The speed and the rotor position are determined by directly measuring the voltages and currents of the five-phase PMSM by using

the mathematical model of the five-phase PMSM machine dynamics. Since the controlled system is time varying and nonlinear, the measured voltages and currents are transformed into time-invariant components and the nonlinear system is linearized around the present operating point. The unknown state variables (rotor speed and position) are estimated through the FKF method [88]. Fig. (4.3) shows the block diagram of the principle of the algorithm FKF estimator,

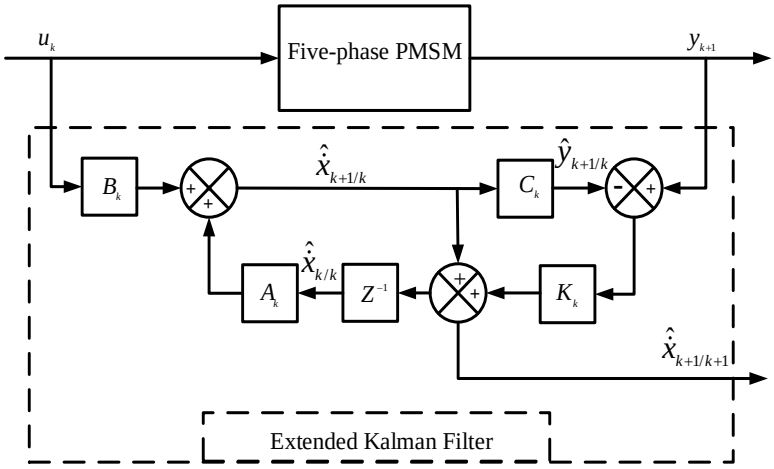

Fig. (4.3): Structure of the kalman filter estimator.

4.4.1 Principles of Extended Kalman Filter

The Kalman filter solves the general problem of estimating the state $x \in \mathrm{R}^n$ of a discrete-time process that is expressed by a linear stochastic difference equation. However, in actual applications, the processes to be estimated are usually non-linear. An extended Kalman filter therefore is derived from the Kalman filter to solve this problem [88][89].

The nonlinear relationships around the current time step can be linearized by using the partial derivatives of the process and measurement functions. To realize linearization of a nonlinear process, some parts in solution equations of the Kalman filter must be modified. Assuming $x \in \mathrm{R}^n$ to be a state vector of a process, it can then be governed by the nonlinear stochastic difference equation [88] [90] [91]:

$$\begin{cases} x_{k+1} = f(x_k, u_k, w_k) \\ y_k = c(x_k, v_k) \end{cases} \tag{4.3}$$

with

$E\{w\, w^T\}$: Process noise

$E\{v\, v^T\}$: Measurement noise

The added white-noise vectors are Gaussian and uncorrelated from each other with zero mean and covariance *Q* and *R*, respectively. The covariance matrices *Q* and *R* of these noises are defined as:

$$Q = E\left\{w_k w_{k'}^T\right\}, \text{ for } k \neq k' \tag{4.4}$$
$$R = E\left\{v_k v_{k'}^T\right\}, \text{ for } k \neq k'$$

From equation (4.3), the nonlinear function f relates the state at the previous time step k to the state at the current time step $k+1$ and includes control function u_k and the zero-mean process noise w_k . In the measurement equation, the nonlinear function c shows a relationship between the state vector x_k and the measurement vector y_k .

The individual values of the noise w_k and v_k at each time step are not known in practice. However, the state and measurement vectors without noise could be approximated as:

$$\begin{cases} x_{k+1} = f(x_k, u_k) \\ y_k = c(x_k) \end{cases} \tag{4.5}$$

where x_k is the posteriori state estimation at the previous time step *k*. Thus, a nonlinear process can be approximately linearized as:

$$\begin{cases} x_{k+1} \approx \hat{x}_{k+1} + F_k(x_k - \hat{x}_k) + w_k \\ y_k \approx \hat{y}_k + C_k(x_k - \hat{x}_k) + v_k \end{cases} \tag{4.6}$$

where

x_{k+1} and y_k are the actual state and measurement vectors,

$\hat{x}_{k+1}$ and $\hat{y}_k$ are the approximate state and measurement vectors,

$\hat{x}_k$ is the posteriori state estimation at step *k*,

w_k and v_k are the random variables representing the process and measurement noise

F_k is the Jacobian matrix of partial derivatives of f with respect to x, given by:

$$F_k = \frac{\partial f}{dx}(\hat{x}_k, u_k) \tag{4.7}$$

C_k is the Jacobian matrix of partial derivatives of *c* with respect to x, expressed by:

$$C_k = \frac{\partial c}{dx}(\hat{x}_k) \tag{4.8}$$

In a first main stage, the state $x_{(k+1)}$ is predicted using discrete matrices and previous state. In the second main stage, the feedback correction weight matrix *K* (filter coefficients) is used to have an accurate prediction of the state $x(k+1/k)$. This is obtained by computing *K* depending not only on the error made, but also with an adjustment using weight *P* (covariance state matrix). This allows estimating accurately *x* with respect to *Q* and *R* covariance matrices corresponding state noise and measurement noise levels, respectively [79]][88] [89] 90] [92]:

The extended Kalman filter algorithm is described as follows:

- Sate prediction:

$$\hat{x}_{k+1/k} = f(\hat{x}_{k/k}, u_k) \tag{4.9}$$

- Estimation of the matrix of the covariance error:

$$\hat{P}_{(k+1/k)} = F_k P_{(k/k)} F_k^T + Q \tag{4.10}$$

- Kalman coefficient update:

$$K_{(k+1)} = \hat{P}_{(k+1/k)} C_k{}^T [C_k \hat{P}_{(k+1/k)} C_k{}^T + R\ ]^{-1} \tag{4.11}$$

- State estimation:

$$\hat{x}_{(k+1/k+1)} = \hat{x}_{(k+1/k)} + K_{(k+1)}(y_{(k+1)} - C_k \hat{x}_{(k+1/k)}) \tag{4.12}$$

- Covariance error matrix update:

$$\hat{P}_{(k+1/k+1)} = \hat{P}_{(k+1/k)} - K_{(k+1)} C_k \hat{P}_{(k+1/k)} \tag{4.13}$$

4.4.2 Application EKF for Parallel-Connected Two-Machine Drive

The extended nonlinear state model of each five-phase PMSM in the rotating frame is:

$$\begin{aligned}
\dot{x}_{1j} &= \left(-r_{sj}/L_{dj}\right) x_{1j} + \left(L_{qj}/L_{dj}\right) p_j x_{5j} x_{2j} + \left(1/L_{dj}\right) v_{sdj} \\
\dot{x}_{2j} &= -\left(L_{dj}/L_{qj}\right) p_j x_{5j} x_{1j} + \left(-r_{sj}/L_{qj}\right) x_{2j} - \left(p_j \Phi_{fj}/L_{qj}\right) x_{5j} + \left(1/L_{qj}\right) v_{sqj} \\
\dot{x}_{3j} &= \left(-r_{sj}/L_{lsj}\right) x_{3j} + \left(1/L_{lsj}\right) v_{sxj} \\
\dot{x}_{4j} &= \left(-r_{sj}/L_{lsj}\right) x_{4j} + \left(1/L_{lsj}\right) v_{syj} \\
\dot{x}_{5j} &= \left(5p_j/2J_j\right)\left(L_{dj} - L_{qj}\right) x_{1j} x_{2j} + \left(5p_j/2J_j\right) \Phi_{fj} x_{2j} - \left(f_j/J_j\right) x_{5j} - \left(1/J_j\right) x_{7j} \\
\dot{x}_{6j} &= p_j x_5 \\
\dot{x}_{7j} &= 0
\end{aligned} \tag{4.14}$$

The model of the five-phase PMSM in (4.14), can be rewritten as matrix representation as follow:

$$\begin{aligned} \dot{x}_j &= A_j x_j + \mathrm{B}_j u_j \\ y_j &= c_j x_j \end{aligned} \tag{4.15}$$

With

$$x_j = \begin{bmatrix} i_{dsj} & i_{qsj} & i_{xsj} & i_{ysj} & \Omega_j & \theta_j & T_{lj} \end{bmatrix}^t,\ u_j = \begin{bmatrix} v_{dsj} \\ v_{qsj} \\ v_{xsj} \\ v_{ysj} \end{bmatrix},\ c_j = \begin{bmatrix} i_{dsj} & 0 & 0 & 0 & 0 & 0 & 0 \\ 0 & i_{qsj} & 0 & 0 & 0 & 0 & 0 \\ 0 & 0 & i_{xsj} & 0 & 0 & 0 & 0 \\ 0 & 0 & 0 & i_{ysj} & 0 & 0 & 0 \end{bmatrix}$$

$$A_j = \begin{bmatrix} -\frac{r_{sj}}{L_{dj}} & p_j\Omega_j\frac{L_{qj}}{L_{dj}} & 0 & 0 & 0 & 0 & 0 \\ -p_j\Omega_j\frac{L_{dj}}{L_{qj}} & -\frac{r_{sj}}{L_{qj}} & 0 & 0 & -\frac{p_j\Phi_{fj}}{L_{qj}} & 0 & 0 \\ 0 & 0 & -\frac{r_{sj}}{L_{lsj}} & 0 & 0 & 0 & 0 \\ 0 & 0 & 0 & -\frac{r_{sj}}{L_{lsj}} & 0 & 0 & 0 \\ \frac{5p_j}{2J_j}\left(L_{dj}-L_{qj}\right)i_{qsj} & \frac{5p_j}{2J_j}\left(L_{dj}-L_{qj}\right)i_{dsj}+\frac{5p_j}{2J_j}\Phi_{fj} & 0 & 0 & -\frac{f_j}{J_j} & 0 & \frac{1}{J_j} \\ 0 & 0 & 0 & 0 & p_j & 0 & 0 \\ 0 & 0 & 0 & 0 & 0 & 0 & 0 \end{bmatrix}, B_j = \begin{bmatrix} \frac{1}{L_{dj}} & 0 & 0 & 0 \\ 0 & \frac{1}{L_{qj}} & 0 & 0 \\ 0 & 0 & \frac{1}{L_{lsj}} & 0 \\ 0 & 0 & 0 & \frac{1}{L_{lsj}} \\ 0 & 0 & 0 & 0 \\ 0 & 0 & 0 & 0 \\ 0 & 0 & 0 & 0 \end{bmatrix}$$

In the five-phase PMSM control case, *d-q-x-y* currents and voltages are measured, and the equation (4.15) is sampled to obtain a discrete state space representation to be used in the observer synthesis. Assuming that the sampling interval T_e is very short compared to the system dynamics, the augmented discrete-time of each five-phase PMSM model is given as follows:

$$\begin{aligned} \dot{x}_{j(k+1)} &= f(x_{jk}, u_{kj}, w_{jk}) = A_{jk} x_{jk} + \mathrm{B}_{jk} u_{jk} + w_{jk} \\ y_{jk} &= c(x_{jk}, v_{jk}) = c_j x_{jk} + v_{jk} \end{aligned} \tag{4.16}$$

with:

$$A_{jk} = (I + T_e A_j)$$

$$\mathrm{B}_{jk} = T_e \mathrm{B}_j$$

$$x_{jk} = [i_{dsjk}\ i_{qsjk}\ i_{xsjk}\ i_{ysjk}\ \Omega_{jk}\ \theta_{jk}\ T_{ljk}]^t$$

$$y_{jk} = [i_{dsjk}\ i_{qsjk}\ i_{xsjk}\ i_{ysjk}\ ]^t$$

where

x_{jk} , u_{jk} and y_{jk} are the augmented state vector, input vector and output vector at the sampling instant *k* of machine *j*, respectively.

A_{jk} and B_{jk} are discrete system matrix and discrete input matrix for each machine, respectively.

w_{jk} and v_{jk} are the system noise and measurement noise, respectively.

I is the unity matrix.

T_e is the sample time.

The matrix F_{jk} is calculated by calculating The Jacobian matrix of partial derivatives of f with respect to x as follows:

$$F_{jk} = \frac{\partial A_{jk}}{dx} \tag{4.17}$$

which yields:

$$F_{jk} = \begin{bmatrix} 1-T_e\frac{r_{sj}}{L_{dj}} & p_j\Omega_j\frac{L_{qj}}{L_{dj}}T_e & 0 & 0 & p_j i_{qsj}\frac{L_{qj}}{L_{dj}}T_e & 0 & 0 \\ -p_j\Omega_j\frac{L_{dj}}{L_{qj}}T_e & 1-T_e\frac{r_{sj}}{L_{qj}}T_e & 0 & 0 & \frac{-T_e p_j}{L_{qj}}(L_{dj}i_{dsj}+\Phi_{fj}) & 0 & 0 \\ 0 & 0 & 1-T_e\frac{r_{sj}}{L_{lsj}} & 0 & 0 & 0 & 0 \\ 0 & 0 & 0 & 1-T_e\frac{r_{sj}}{L_{lsj}} & 0 & 0 & 0 \\ T_e\frac{5p_j}{2J_j}\left(L_{dj}-L_{qj}\right)i_{qsj} & T_e(\frac{5p_j}{2J_j}\left(L_{dj}-L_{qj}\right)i_{dsj}+\frac{5p_j}{2J_j}\Phi_{fj}) & 0 & 0 & 1-T_e\frac{f_j}{J_j} & 0 & \frac{-T_e}{J_j} \\ 0 & 0 & 0 & 0 & T_e p_j & 1 & 0 \\ 0 & 0 & 0 & 0 & 0 & 0 & 1 \end{bmatrix} \tag{4.18}$$

The Jacobian matrix of partial derivatives of *c* with respect to x is calculated by:

$$C_{jk} = \frac{\partial c_j}{dx}(\hat{x}_{jk}) \tag{4.19}$$

$$C_{jk} = \begin{bmatrix} 1 & 0 & 0 & 0 & 0 & 0 & 0 \\ 0 & 1 & 0 & 0 & 0 & 0 & 0 \\ 0 & 0 & 1 & 0 & 0 & 0 & 0 \\ 0 & 0 & 0 & 1 & 0 & 0 & 0 \end{bmatrix} \tag{4.20}$$

4.4.2 Simulation Results

In order to verify the applicability of the proposed control scheme for the two-machine drive system of Fig. (4.2), the following simulations are performed using two identical 2-pole, 50 Hz five-phase PMSM. The parameters of each machine are listed in table A.1 of appendix A. The performance of the SMC controller is compared with that of the conventional controller. The tuning parameters for the PI-controllers, SMC controllers and EKF Parameters are also given in table B.1 and B.4 of appendix B, respectively. Many simulation tests are performed in order to verify the independence of the control of the two machines in sensorless mode.

The behavior of the overall drive system is presented in Figs. (4.4) to (4.8) at different test conditions. Fig. (4.4) shows then estimated speeds, currents and torques of the unloaded two machines for many different speeds references. At the beginning, the first five-phase PMSM is running at 100 rad/s, at t=0.7s then it decelerated to -10 rad/s, after that, it is accelerated again to the speed 60 rad/s at t=1.4s. For the second five-phase PMSM the speed reference is set at 50 rad/s, 25 rad/s, 100 rad/s, -100 rad/s, and 80 rad/s at t=0s, 0.4s, 0.9s, 1.2s, 1.7s, respectively.

Effect of the speed rotation reversion of one machine on the other machine performance is investigated in Fig. (4.5). In this test, most of the time when one machine is rotating at +100 rad/s the other is running at the opposite speed.

Fig. (4.6) displays results for the case when the speed the second five-phase PMSM is kept at standstill, while the first five-phase PMSM is reversed from: +100 to -100 rad/s at t=0.5s, and returns to zero at t= 1s. At the subsequent test, the speed of the first five-phase PMSM is held at zero, while the speed of the second five-phase PMSM is reversed from 100 to -100 rad/s at 1.5s.

Fig. (4.7) shows the speeds, torques and currents of the two-machine drive controlled by both PI and SMC controller in the presence of load torques variations. The reference of the first speed is fixed at 100 rad/s, while the speed reference of the second machine is fixed at 50 rad/s. Load torques are applied on the two machines at t=0.5s and t=0.7s, respectively.

Fig. (4.8) shows the performance of the senseorless feedback control under low speed condition. The speed reference of the first machine is set to 30 rad/s, 0 rad/s, -30 rad/s, -15rad/s and 15 rad/s at t=0s, 0.7s, 1s, 1.4s and 1.7s, respectively. For the second machine, the speed reference is set to -30 rad/s, 0 rad/s, 30 rad/s 15rad/s and -15 rad/s at t=0s, 0.4s, 0.7s, 1.4s and 1.7s, respectively. A torque of 5 Nm was applied on the shafts of the first machines at the instants t = 0.2 s 1.2s and 1.8s, respectively. While, the second machine is loaded at the instants t = 0.2 s 1.8s and 1.8s, respectively.

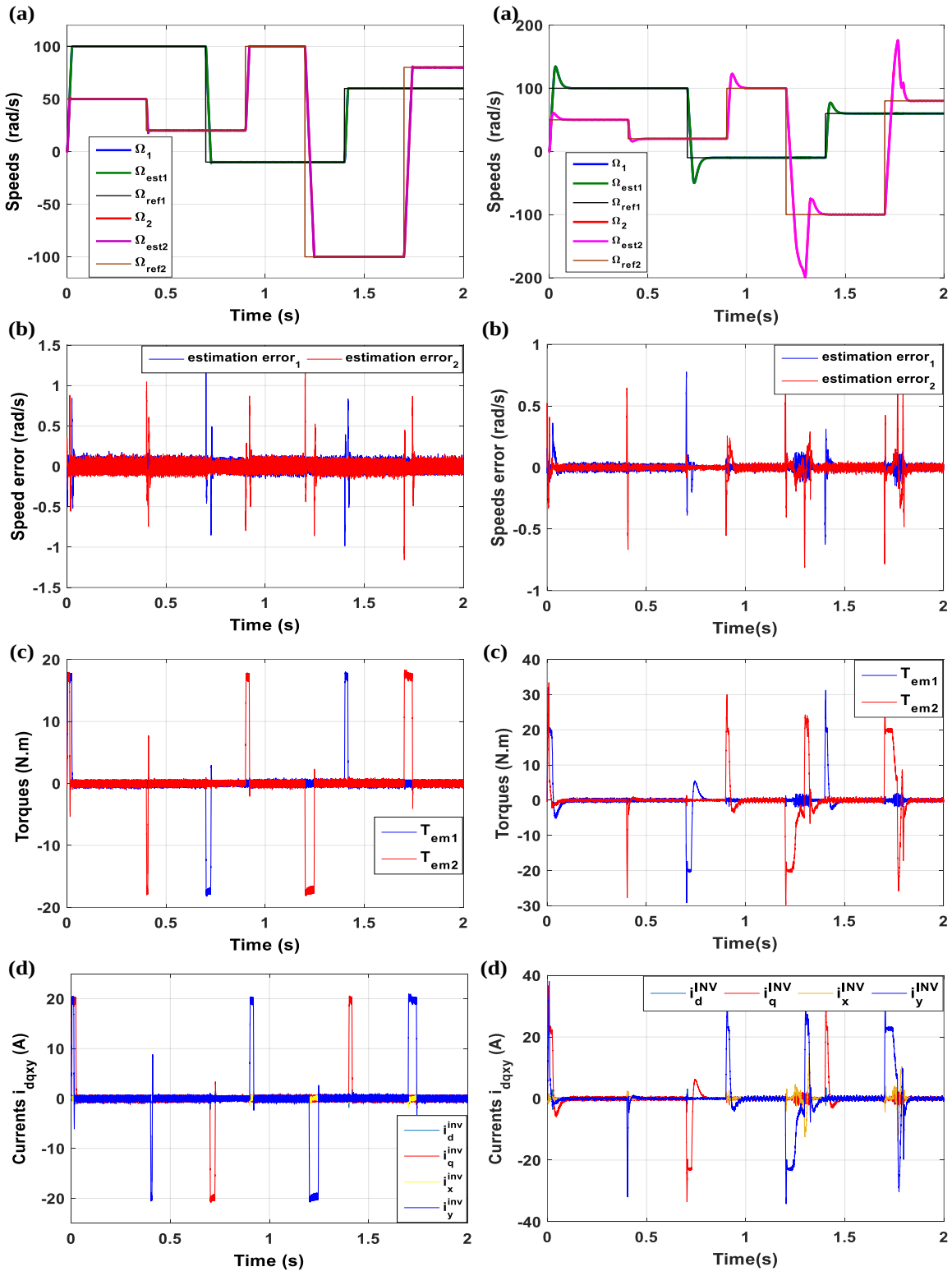

(SMC) (PI)

Fig. (4.4): Dynamic responses of parallel-connected of two sensorless five-phase PMSMs drive controlled by FOC-SMC and PI at different reference speeds values: (a) Reference, actual and estimated speeds, (b) Speed estimation errors, (c) Electromagnetic torques, (d) Inverter currents.

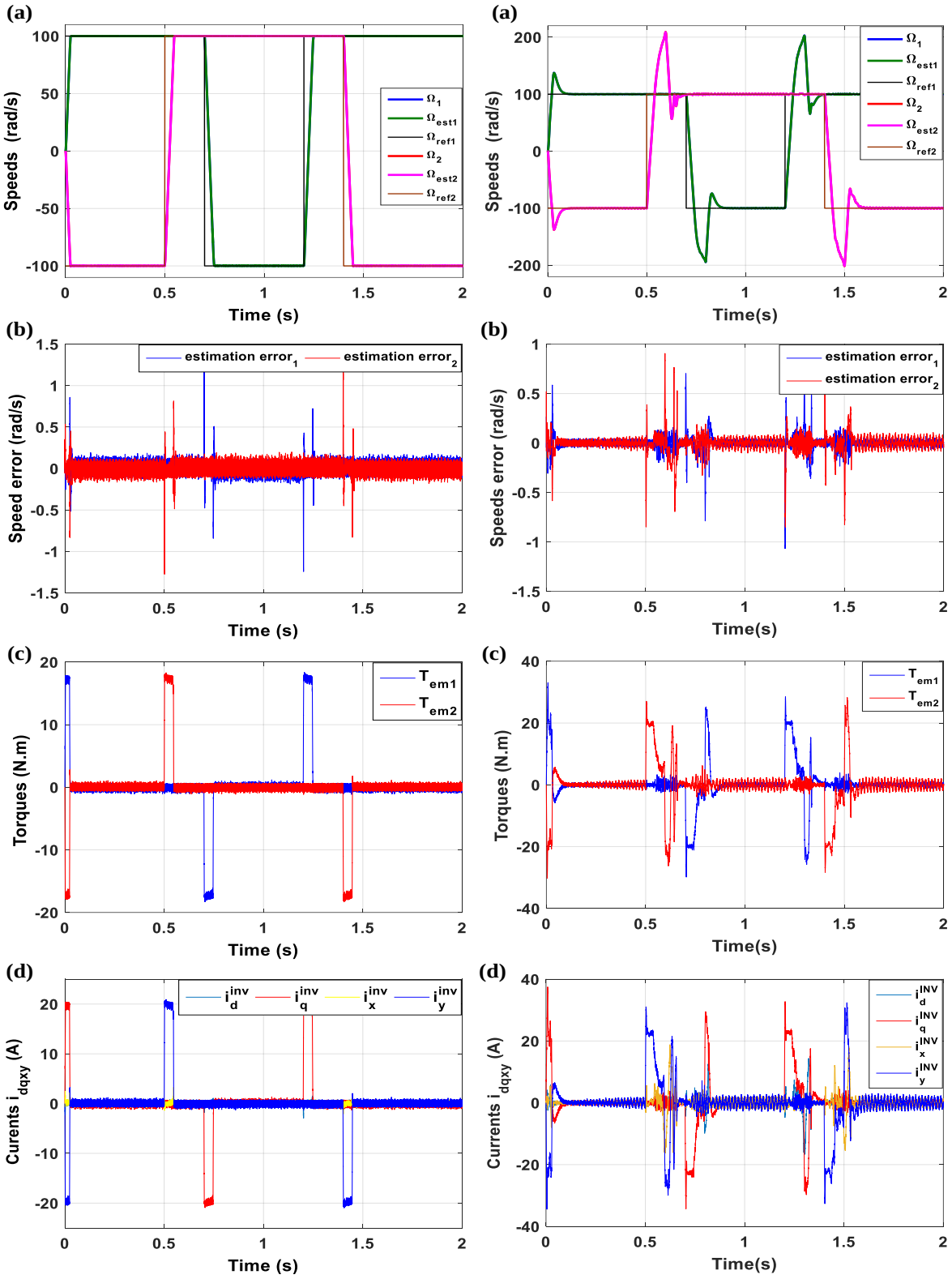

Fig. (4.5): Dynamic responses of parallel-connected of two sensorless five-phase PMSMs drive controlled by FOC-SMC and PI: when the two machines are operating in the opposite directions: (a) Reference, actual and estimated speeds, (b) Speed estimation errors, (c) Electromagnetic torques, (d) Inverter currents.

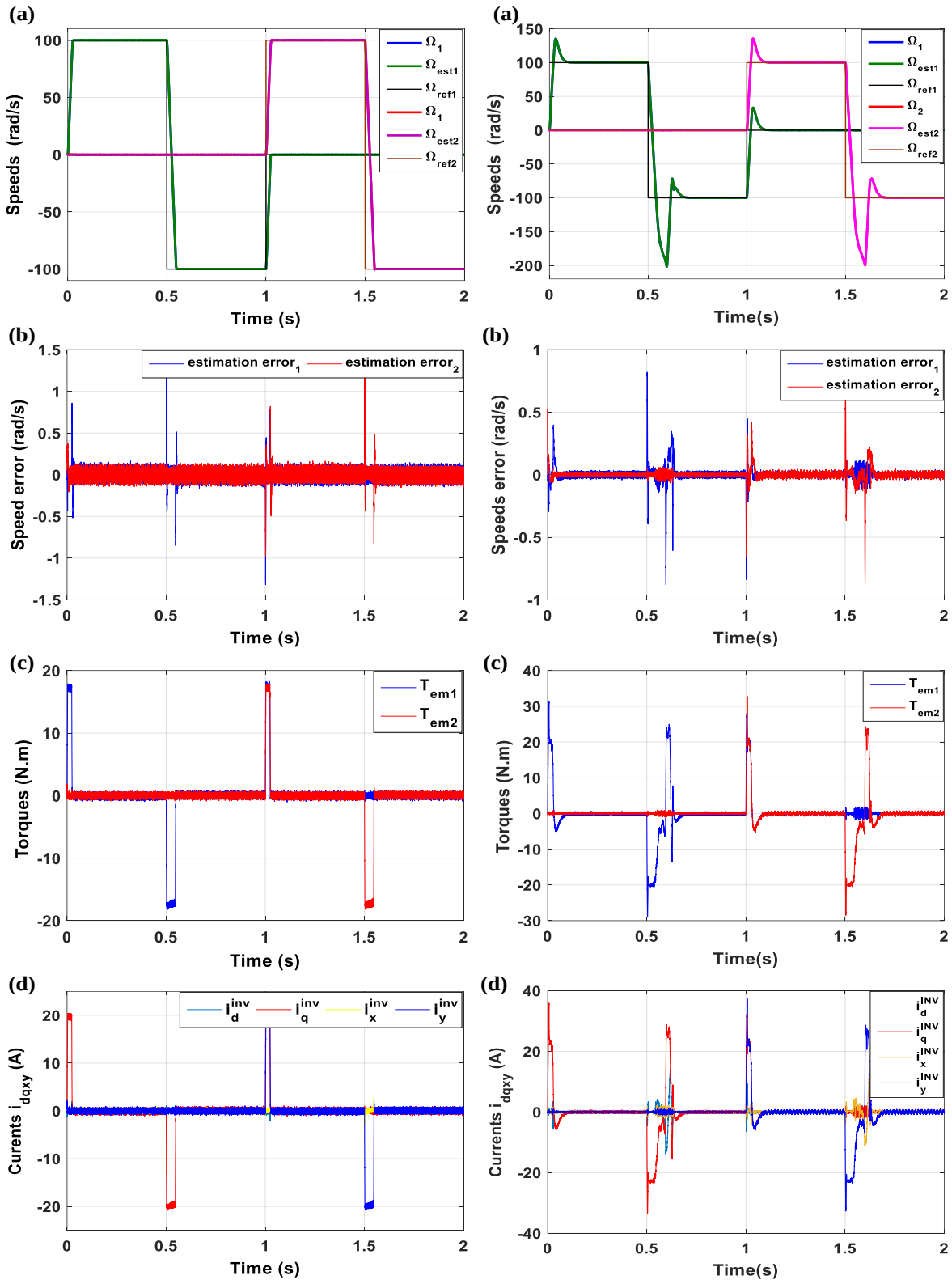

(SMC) (PI)

Fig. (4.6): Dynamic responses of parallel-connected of two sensorless five-phase PMSMs drive controlled by FOC-SMC and PI: when one machine is at standstill and the other is still running: (a) Reference, actual and estimated speeds, (b) Speed estimation errors, (c) Electromagnetic torques, (d) Inverter currents.

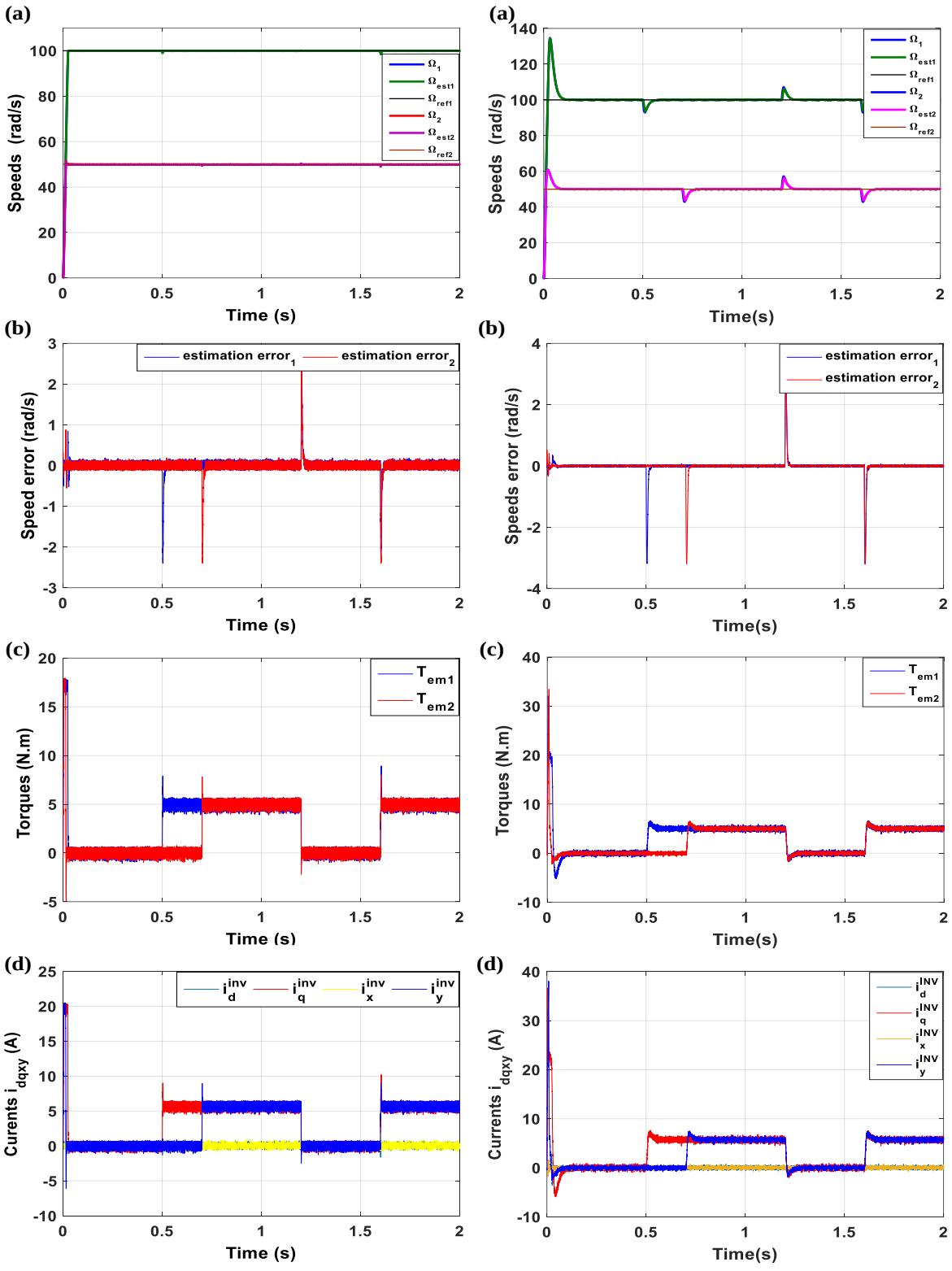

(SMC) (PI)

Fig. (4.7): Dynamic responses of parallel-connected of two sensorless five-phase PMSMs drive controlled by FOC-SMC and PI at different loading conditions: (a) Reference, actual and estimated speeds, (b) Speed estimation errors, (c) Electromagnetic torques, (d) Inverter currents.

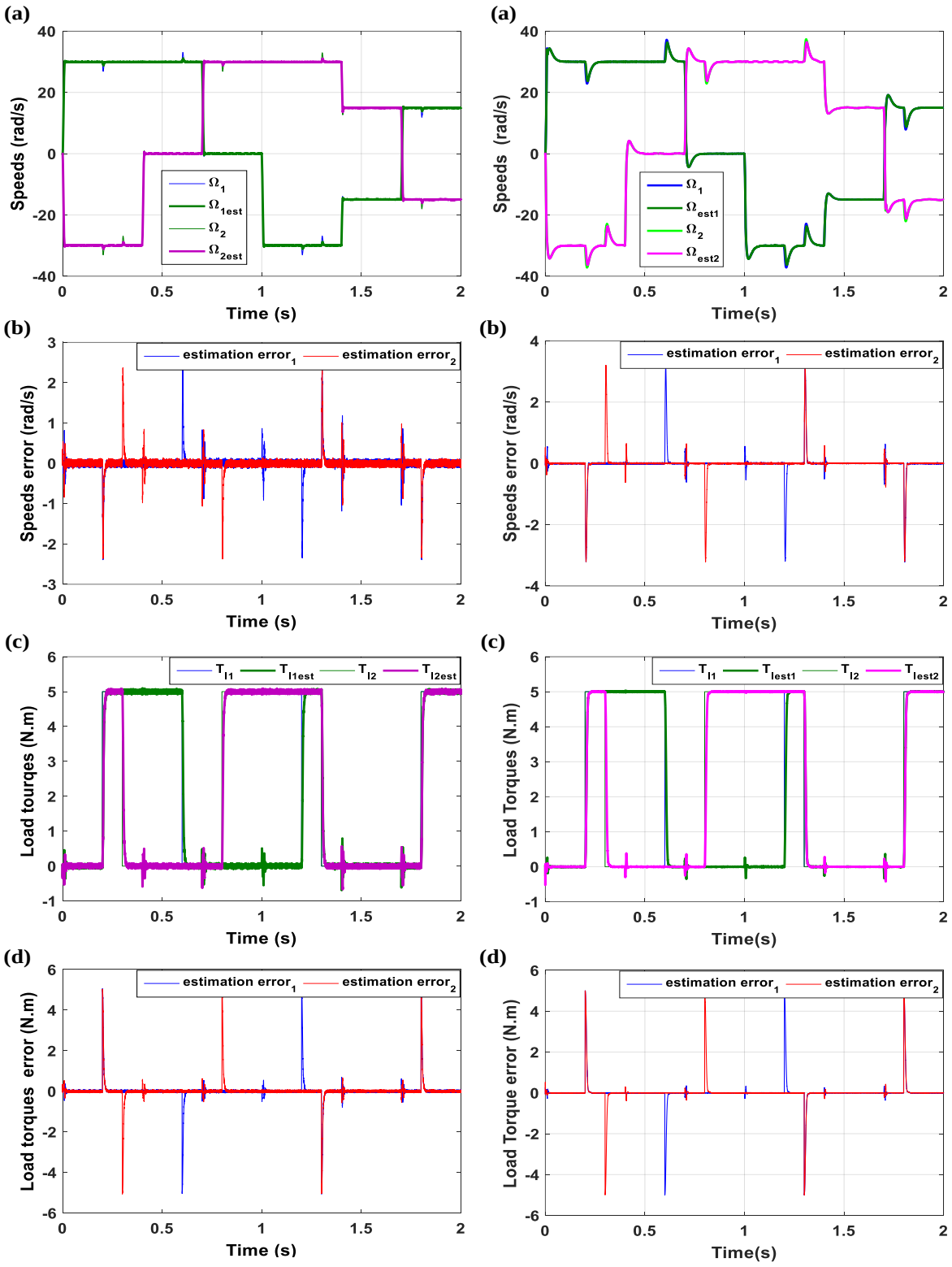

(SMC) (PI)

Fig. (4.8): Dynamic responses of parallel-connected of two sensorless five-phase PMSMs drive controlled by FOC-SMC and PI at low speed operation: (a) Reference, actual and estimated speeds, (b) Speed estimation errors, (c) Load torques and its estimation, (d) Inverter currents.

It is clear from all estimated speeds characteristics that in every test the speed estimators provide accurate speed estimations. These results also prove that both speeds machines are independently controlled even in sensorless mode. Indeed, the speed variations of the first machine in the two-machine drive system do not affect the behavior of the speed of the second machine even in reversal conditions.

The electromagnetic torque generated by each machine during the simulated speed step response is shown in Figs. (4.4-c) to (4.7-c). Note that the generated torques are directly proportional to the *q-y* axes inverter currents and fully decoupled from *d-x* axes inverter currents.

Comparison of results in Fig. (4.4) shows once more that the control of the two machines is completely decoupled. There is hardly any evidence of torque disturbance of one machine during the reversal of the other one. Furthermore, the direct axis currents responses remain completely unaffected during these transients.

As shown from Fig. (4.5), the starting and reversing transients of one machine do not have any tangible consequence on the operation of the second machine. The decoupled control is preserved and the characteristics of both machines are unaffected.

Fig. (4.6) illustrates results for the case when the speed of one machine is kept at zero, while the second is reversed. Speed of one machine and its electromagnetic torque remain completely undisturbed during the reversion of the other machine, indicating a complete decoupling of the control.

Fig. (4.7) shows the inverter currents, machine torques and estimated speed of machines at different loading conditions for parallel-connected two five-phase machines drive system. It is clear from Fig. (4.7) that when one machine is loaded or unloaded, the second machine performance is unaffected; which proves once again that both machines connected in parallel are totally decoupled. In case of sliding mode control, no variation whatsoever can be observed in the speeds responses of the both machines during these transients.

It is worth to notice that there is no impact on the speed and electromagnetic torque of one machine when the speed or the load of the other machine in parallel-connected system changes. Thus, through proper phase transformation rules, the decoupled control of two five-phase PMSMs connected in parallel can be achieved with a single supply from a five-phase voltage source inverter. Furthermore, measured and estimated speeds are in excellent agreement in both steady state and transient operations.

The estimated and actual values of speeds and load torques as well as their estimations errors are reported in Fig. (4.8). The EKF algorithms give accurate and fast speeds estimations over entire speed range including low speed and standstill operations with low speed errors, even in transients. Furthermore, the estimated values of loads torques are very close to their applied ones. Consequently, the load torque estimation errors are almost zeros; this reflects the stability of EKF during load torques variations. These results confirm that the extended Kalman filter is very suitable for two-machine drive system.

4.4.2.1 Comparative study between FOC-SMC and FOC-PI Based EKF

Figs. (4.4) to (4.8) show the behavior of the two-machine drive under different speeds step variations and without load torque. In Figs. (4.4-a (PI) to 4.8-a (PI)), the system comportment using PI-controller exhibits the expected step response characteristics of a second order system. The response has a short rise time, an overshoot of approximately 40% during reverse modes, and settling times close to 0.1s. Figs. (4.4-a (SMC)) to (4.8-a (SMC)) show comparable dynamic behavior using SMC. However, it is clear from these figures that, the system reaches steady state at 0.028s without overshoot.

Figs. (4.4-d) to (4.7-d) illustrate the behavior of the *d*-*q*-axes and *x*-*y*-axes inverter currents for both controllers. In case of the PI-controller, the inverter currents i_q^{inv} and i_y^{inv} peak above 38A, then decay exponentially to the steady state while the currents i_d^{inv} and i_x^{inv} are maintained at zero as illustrated in Figs. (4.4-d (PI), 4.5-d (PI), 4.6-d (PI) and 4.7-d (PI)). Figs. (4.4-d (SMC), 4.5-d (SMC), 4.6-d (SMC) and 4.7-d(SMC)) show inverter currents in case of sliding mode control. In contrast, the i_q^{inv} and i_y^{inv} currents peak slightly above 20A, and continue on this value until the speed reaches its reference value, this leads to a short settling time.

From Fig. (4.7-a (PI)and 4.8-a (PI)) and by analyzing the transient of two-machine drive controlled by PI- controller, it is easy to observe speeds drops taken place at the moments of loads changes. The PI- controller compensates for these speed drops after a necessary recovery time. Fig. (4.7-a (SMC) and 4.8-a (SMC)) shows the drive responses in the same load conditions with sliding mode control. At the moments of load variations, the SMCs keep the speeds close to their references without overshoots and without drops. Therefore, the SMC can be considered as more robust under loads variations.

A general comparison between SMC and PI is given in table (4.1). Compared to PI-controller, SMC shows superiority in terms of settling time and overshoot. However, it needs more energy in starting transient then that needed by the conventional controller.

Table (4.1): Comparison between SMC and PI of sensorless two-machine drive.

Controlled variable	Comparison criterion	FOC-SMC	FOC-PI	Reduction rate (%)
Rotor speed	Settling time (s)	0.028	0.1	72
	Overshoot (rad/s)	0	35	100
	Speeds drops (%)	0.93	7	86.71
	Recovery time (at abrupt load) (s)	0.005	0.08	93.75
	Overshoot in reversal mode (%)	0.77	40	98.07
	The maximum speed estimation error (%)	2.36	1	57.62 (increase)
Electromagnetic torque	Settling time (s)	0.03	0.1	70
	Overshoot (rad/s)	0	5	100
	Ripple (N.m)	1.5	1.7	11
Currents	Settling time (s)	0.018	0.07	74.28
	Overshoot (A)	5	2	60 (increase)
Load Torque estimation	Settling time (s)	0.03	0.04	25
	Overshoot (rad/s)	0	0	0
	The maximum speed estimation error (%)	5	5	0

4.5 Sliding Mode Observer based DTC-SMC for Parallel-Connected Two-machine

In conventional sensorless DTC scheme, one possible solution is to combine a current observer and flux estimator [16][35][78] to perform the sensorless task, which increases the system complexity and reduce the accuracy of the estimation. To solve this problem, a SMO is proposed in this section to improve the sensorless control of each five-phase PMSM by using its flux model in the stationary reference frame. Similar to the SMC, in the SMO algorithm the conventional switching function is replaced also by a smooth function to reduce the chattering phenomenon.

The proposed sensorless DTC-SMC of the parallel-connected two five-phase permanent magnet synchronous machines is presented in Fig. (4.9), where the two main parts SMC and SMO are considered. The SMO has been proved being strong robust and accurate with a fast convergence and having a good estimation performance over full speed rang [83][94]. The SMO is designed to estimate the rotor position, speed, torque and flux of each machine by using voltages and currents measurements. The actual speed, estimated speed and load torques are the inputs of the speeds SMCs to determine the torques references. The estimated flux and torque are processed in DTC-SMCs to obtain as outputs the α-β-x-y axes reference voltages components. These reference voltages become the input signals to the SVM blocks. The SVM transmits the gating signals to the five-leg inverter to drive the two five-phase PMSMs connected in parallel.

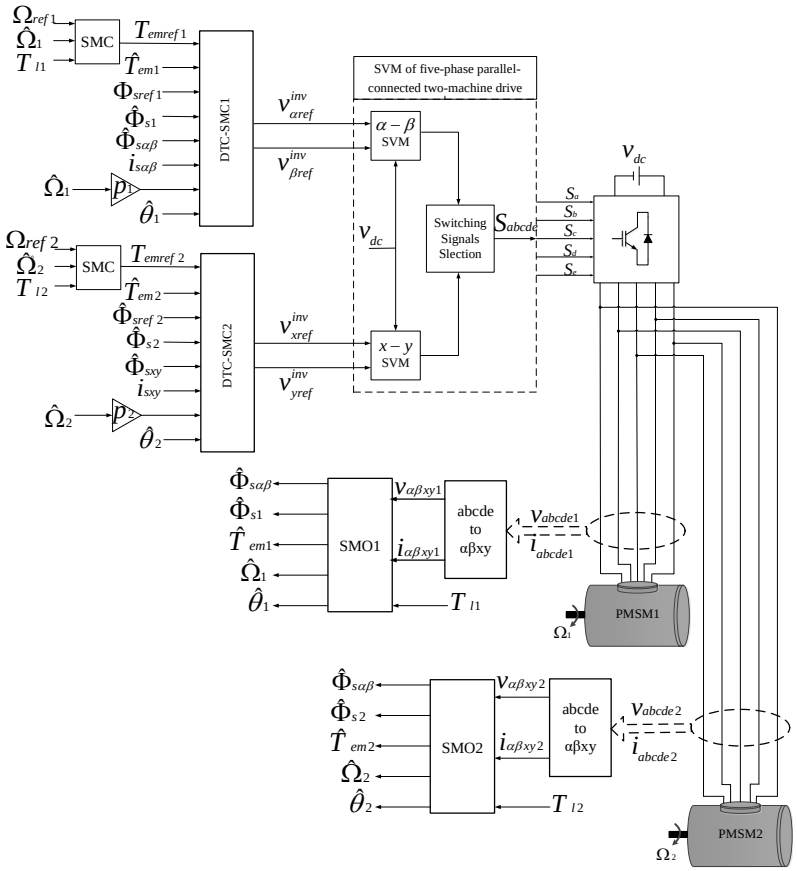

Fig. (4.9): Sensorless DTC-SMC of a parallel-connected two five-phase PMSMs drive system.

4.5.1 Sliding Mode Observer

The sliding mode observer (SMO) is based on the same idea of sliding mode control. This type of observer uses the model of the system, employs high frequency switching to force the trajectory of the estimated variables to remain in the sliding surface [45] [79] [89] [90] [93]. Fig. (4.10) show the general structure of sliding mode observer.

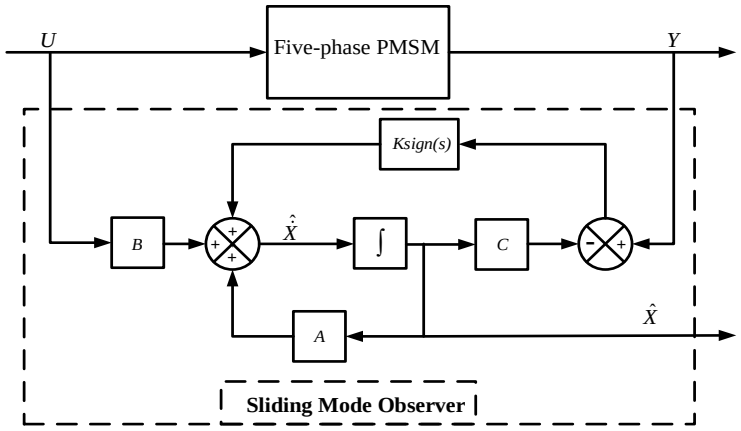

Fig. (4.10): Structure of the sliding mode observer.

The sliding surface is chosen to ensure the observed states converge to the actual states. Once the sliding mode is achieved, the SMO can reject certain external disturbances and internal parameter uncertainties.

The SMO synthesis is based on the comparison between observed and measured variables as follow:

$$\varepsilon = y - \hat{y} \tag{4.21}$$

The design of the SMO consists in converging the error between the measured outputs of the system by using switching function.

The SMO is modeled in the following form:

$$\begin{aligned} \dot{\hat{x}} &= f(\hat{x}, u) + \text{ksign}(y - \hat{y}) \\ \hat{y} &= c(\hat{x}) \end{aligned} \tag{4.22}$$

with:

$\hat{x}$ is the estimated state.

y and $\hat{y}$ are the output and its estimated.

k is observer gain.

From (4.22) its easy, simple and non-complex implementation to estimated the state of the system. This is the reason why the SMO is widely used, and duo to its robustness against parameter variations, disturbances and noise.

4.5.2 Application SMO for Parallel-Connected Two-Machine Drive

Normally, speed observers used for three-phase machines can be easily extended to multi-phase multi-machine drives. For each machine, the speed estimator requires only stator voltages and currents components. In the five-phase PMSM control case, *α-β-x-y* currents and voltages are measured.

In this section, a sliding mode observer based on flux model is presented to estimate directly the flux and speed as well as the electromagnetic torque by using stator voltages and currents as inputs. Using the flux model of the five-phase PMSM and based on the sliding mode structure theory, the proposed sliding mode observer for each five-phase PMSM is designed as:

$$\begin{aligned}
\frac{d\hat{\Phi}_{\alpha sj}}{dt} &= v_{\alpha sj} - (r_{sj} / L_{sj})\hat{\Phi}_{\alpha sj} + r_{sj}\Phi_{fj}\cos(\hat{\theta}_j) + ksmooth(\bar{\Phi}_{\alpha sj}) \\
\frac{d\hat{\Phi}_{\beta sj}}{dt} &= v_{\beta sj} - (r_{sj} / L_{sj})\hat{\Phi}_{\beta sj} - r_{sj}\Phi_{fj}\sin(\hat{\theta}_j) + k\,smooth(\bar{\Phi}_{\beta sj}) \\
\frac{d\hat{\Phi}_{xsj}}{dt} &= v_{xsj} - (r_{sj} / L_{lsj})\hat{\Phi}_{xsj} + k\,smooth(\bar{\Phi}_{xsj}) \\
\frac{d\hat{\Phi}_{ysj}}{dt} &= v_{ysj} - (r_{sj} / L_{lsj})\hat{\Phi}_{ysj} + k\,smooth(\bar{\Phi}_{ysj}) \\
\frac{d\hat{\Omega}_j}{dt} &= \frac{5p_j}{2J_j}(\frac{\Phi_{fj}}{L_{sj}})[\hat{\Phi}_{\beta sj}\cos(\hat{\theta}_j) - \hat{\Phi}_{\alpha sj}\sin(\hat{\theta}_j)] - \frac{f}{J_j}\hat{\Omega} - \frac{1}{J_j}T_{lj} + k_1 smooth(\bar{\Phi}_{\alpha sj}) + k_1 smooth(\bar{\Phi}_{\beta sj}) \\
\frac{d\hat{\theta}_j}{dt} &= \hat{\Omega}_j
\end{aligned} \tag{4.23}$$

with $\bar{\Phi}_{\alpha sj} = \Phi_{\alpha sj} - \hat{\Phi}_{\alpha sj}$, $\bar{\Phi}_{\beta sj} = \Phi_{\beta sj} - \hat{\Phi}_{\beta sj}$, $\bar{\Phi}_{xsj} = \Phi_{xsj} - \hat{\Phi}_{xsj}$ and $\bar{\Phi}_{\beta sj} = \Phi_{ysj} - \hat{\Phi}_{ysj}$ are the sliding surfaces, k, k_1 are the observer gains. $\hat{\Phi}_{\alpha sj}$ $\hat{\Phi}_{\beta sj}$ $\hat{\Phi}_{xsj}$ $\hat{\Phi}_{ysj}$ are the estimated stator flux linkage components. $\hat{\Omega}_j$ and $\hat{\theta}_j$ are the estimated mechanical speed and rotor position, respectively.

The actual flux components can be obtained from:

$$\begin{aligned}
\Phi_{\alpha sj} &= L_{sj} i_{\alpha sj} + \Phi_{fj}\cos(\hat{\theta}_j) \\
\Phi_{\beta sj} &= L_{sj} i_{\beta sj} + \Phi_{fj}\sin(\hat{\theta}_j) \\
\Phi_{xsj} &= L_{lsj} i_{xsj} \\
\Phi_{ysj} &= L_{lsj} i_{xsj}
\end{aligned} \tag{4.24}$$

4.2.2.1 Stability Analysis

The estimation errors dynamics are:

$$\begin{aligned}
\frac{d\bar{\Phi}_{\alpha sj}}{dt} &= -(r_{sj} / L_{sj})\bar{\Phi}_{\alpha sj} + (r_{sj} / L_{sj})\Phi_{fj}(\cos(\theta_j) - \cos(\hat{\theta}_j)) - ksmooth(\bar{\Phi}_{\alpha sj}) \\
\frac{d\bar{\Phi}_{\beta sj}}{dt} &= -(r_{sj} / L_{sj})\bar{\Phi}_{\beta sj} + (r_{sj} / L_{sj})\Phi_{fj}(\sin(\theta_j) - \sin(\hat{\theta}_j)) - ksmooth(\bar{\Phi}_{\beta sj}) \\
\frac{d\bar{\Phi}_{xsj}}{dt} &= -(r_{sj} / L_{lsj})\bar{\Phi}_{xsj} - ksmooth(\bar{\Phi}_{xsj}) \\
\frac{d\bar{\Phi}_{ysj}}{dt} &= -(r_{sj} / L_{lsj})\bar{\Phi}_{ysj} - ksmooth(\bar{\Phi}_{ysj}) \\
\frac{d\bar{\Omega}_j}{dt} &= \frac{5p_j}{2J_j}(\frac{\Phi_{fj}}{L_{sj}})[\Phi_{\beta sj}\cos(\theta_j) - \hat{\Phi}_{\beta sj}\cos(\hat{\theta}_j)) - (\Phi_{\alpha sj}\sin(\theta_j) - \hat{\Phi}_{\alpha sj}\sin(\hat{\theta}_j))] - \frac{f}{J_j}\hat{\Omega} - \frac{1}{J_j}T_{lj} - k_1 smooth(\bar{\Phi}_{\alpha sj}) - k_1 smooth(\bar{\Phi}_{\beta sj}) \\
\frac{d\bar{\theta}_j}{dt} &= \bar{\Omega}_j
\end{aligned} \tag{4.25}$$

with

$\bar{\Omega}_j = \Omega_j - \hat{\Omega}_j$ and $\bar{\theta}_j = \theta_j - \hat{\theta}_j$.

In order to demonstrate the stability of the proposed sliding mode observer, the following Lyapunov function candidate is adopted:

$$V = \frac{1}{2}(\bar{\Phi}_{\alpha sj}^2 + \bar{\Phi}_{\beta sj}^2 + \bar{\Phi}_{xsj}^2 + \bar{\Phi}_{ysj}^2 + \bar{\Omega}_j^2 + \bar{\theta}_j^2) \tag{4.26}$$

Its time derivative is:

$$\dot{V} = \bar{\Phi}_{\alpha sj}\dot{\bar{\Phi}}_{\alpha sj} + \bar{\Phi}_{\beta sj}\dot{\bar{\Phi}}_{\beta sj} + \bar{\Phi}_{xsj}\dot{\bar{\Phi}}_{xsj} + \bar{\Phi}_{ysj}\dot{\bar{\Phi}}_{ysj} + \bar{\Omega}\ \dot{\bar{\Omega}} + \bar{\theta}\,\dot{\bar{\theta}}$$

$$\begin{aligned}\dot{V} = &-(r_{sj}/L_{sj})\bar{\Phi}_{\alpha sj}^2 + \bar{\Phi}_{\alpha sj}(r_{sj}/L_{sj})\Phi_{fj}(\cos(\theta_j) - \cos(\hat{\theta}_j)) - \bar{\Phi}_{\alpha sj}ksmooth(\bar{\Phi}_{\alpha sj}) \\ &-(r_{sj}/L_{sj})\bar{\Phi}_{\beta sj}^2 + \bar{\Phi}_{\beta sj}(r_{sj}/L_{sj})\Phi_{fj}(\sin(\theta_j) - \sin(\hat{\theta}_j)) - \bar{\Phi}_{\beta sj}ksmooth(\bar{\Phi}_{\beta sj}) \\ &-(r_{sj}/L_{lsj})\bar{\Phi}_{xsj}^2 - \bar{\Phi}_{xsj}ksmooth(\bar{\Phi}_{xsj}) - (r_{sj}/L_{lsj})\bar{\Phi}_{ysj}^2 - \bar{\Phi}_{ysj}ksmooth(\bar{\Phi}_{ysj}) \\ &\frac{5p_j}{2J_j}(\frac{\Phi_{fj}}{L_{sj}})[\Phi_{\beta sj}\cos(\theta_j) - \hat{\Phi}_{\beta sj}\cos(\hat{\theta}_j)) - (\Phi_{\alpha sj}\sin(\theta_j) - \hat{\Phi}_{\alpha sj}\sin(\hat{\theta}_j))]\bar{\Omega}_j \\ &-\frac{f}{J}\bar{\Omega}_j - \frac{1}{J}T_{lj}\bar{\Omega}_j - \bar{\Omega}_j k_1 smooth(\bar{\Phi}_{\alpha sj}) - \bar{\Omega}_j k_1 smooth(\bar{\Phi}_{\beta sj}) + \bar{\Omega}_j\bar{\theta}_j\end{aligned} \tag{4.27}$$

To force the observer to converge to its sliding surfaces $\dot{V} < 0$, the observer gains must be chosen to fulfill the following conditions:

$$\begin{aligned}k &> 2p_j\frac{r_s\Phi_{fj}}{L_{sj}}\Omega_{\max} \\ k_1 &> 2p_j\frac{\Phi_{fj}}{J_j L_{sj}}\Phi_{\max}\Omega_{\max}\end{aligned} \tag{4.28}$$

4.5.3 Simulation Results

The DTC-SVM-SMC has been verified through different operation modes. The parameters of each machine are listed in Table A.1 of Appendix A. The tuning parameters for the SMC and SMO are also given in Table B.6 of Appendix B. The switching frequency of the five-phase inverter is set at 10 kHz. The performance of the DTC-SVM-SMC control is compared with that of the DTC-SVM-PI control and conventional DTC.

Simulations results are obtained for both controllers under the same conditions (same DC-link voltage, same switching frequency).

4.5.3.1 Case 1: Two machines operating in the same direction

Fig. (4.11) shows the operation of the two-machine drive system for many different speeds references with no load at starting up phase. At steady state condition, the two machines are loaded simultaneously or not by their nominal loads. At the beginning, the first machine is running at 60 rad/s; at t=0.25 s, it is accelerated to 100 rad/s, after that, its direction of rotation is reversed to -80 rad/s at t=0.5 s and then to -40 at t=0.75 s. For the second machine the speed reference is set at 40 rad/s, 80 rad/s, -100 rad/s, and -60 rad/s at t=0 s, 0.25 s, 0.5 s, 0.75 s, respectively. From Fig. 4.11(a), it can be seen that using DTC-SMC approach the two machines reach their speed references rapidly at starting phase without overshoots compared to the DTC-PI and conventional DTC approach. The load variations have not any tangible effects on the speeds responses contrary to DTC-PI and conventional DTC where drops and rises are observed during the same variations instants. Furthermore, faster dynamic and better reference tracking during the speed reversing operation are observed when the proposed DTC-SMC is used.

The estimations errors are illustrated in Figs. (4.11(b)). From these figures, the speed estimation errors converge toward zero in steady state, which means that the SMO shows good speed estimation, and the load does not have a significant effect on the tracking performance. Indeed, the maximum speeds estimation errors in DTC-SMC scheme are less than 0.08% (Fig. 4.11(b) (DTC-SMC)), but for the DTC-PI and conventional DTC schemes, they are less than 0.11%, Fig. (4.11(b)) (DTC-PI) with noticeable ripples in case of conventional DTC.

The electromagnetic torques, generated by the two machines during the simulated speed step response, are shown in Figs. (4.11(c)). Compared to DTC-PI and conventional DTC controllers, the proposed DTC-SMC controller shows a significant improvement in torque response time as well as in the overshoots and undershoots magnitudes. It can also be seen that DTC-SMC has a better dynamic and faster torque response during the startup and direction reversing states. In addition, it can be seen that the torque ripple in conventional DTC is greater than DTC-PI and SMC

Fig. (4.11(d)) show the stator flux magnitudes using the proposed DTC-SMC, DTC-PI, and conventional DTC, respectively. In case of DTC-SMC controller, it can be observed that the stator flux ripples in steady state are less than those obtained by DTC-PI and conventional DTC.

Figs. (4.11(e)) describe the stator flux trajectories in $\alpha\beta$ and x-y plane. The α-β trajectories are almost circular but the x-y trajectories are closed to zero. In these figures, it can be seen again that DTC-SMC controller offers the better and fast response and less ripple compared to the DTC-PI and conventional DTC.

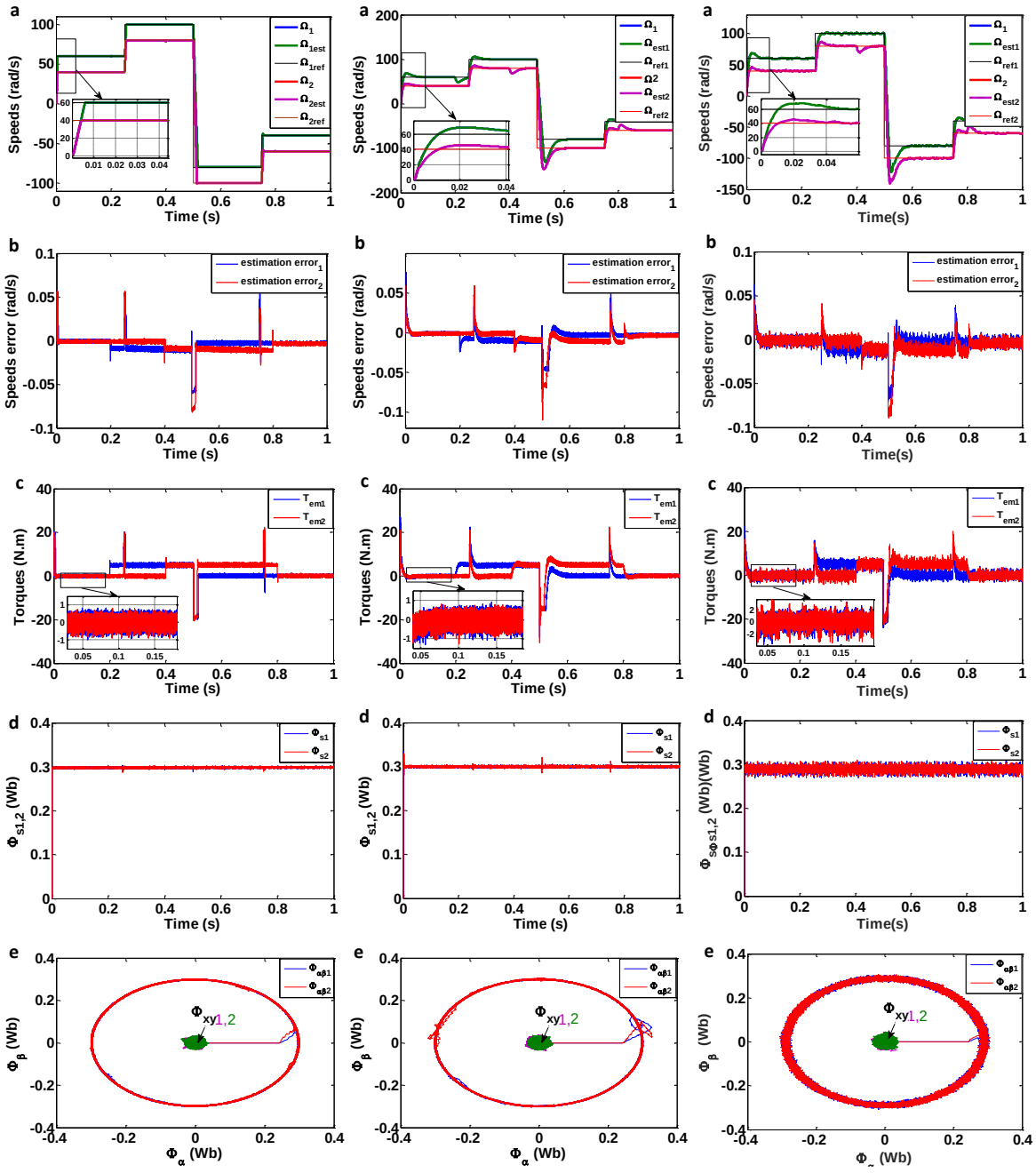

(DTC-SMC) (DTC-PI) (DTC-switching up-table)

Fig. (4.11): Dynamic responses of parallel-connected two five-phase PMSMs drive controlled by SMC based DTC, PI based DTC, and conventional DTC and operating at different reference speeds values: (a) Reference, actual and estimated speeds, (b) Speed estimation errors, (c) Electromagnetic torques, (d) Stator fluxes magnitudes, (e) Stator fluxes trajectories.

4.5.3.2 Case 2: Two machines operating in the opposite directions

The effect of the speed rotation reversion of one machine on the other machine performance is investigated in Fig. (4.12). In the starting phase, the first machine is rotating at +100 rad/s; the other is running at the opposite speed. After that, the speed of the first machine is kept at standstill, while

the speed of the second machine is reversed from -100 to +100 rad/s at t=0.4 s, and it is returned to zero at t=0.6 s. At the subsequent test, the speed of the second machine is held at zero, while the speed of the first machine is set at -100 rad/s at 0.7s.

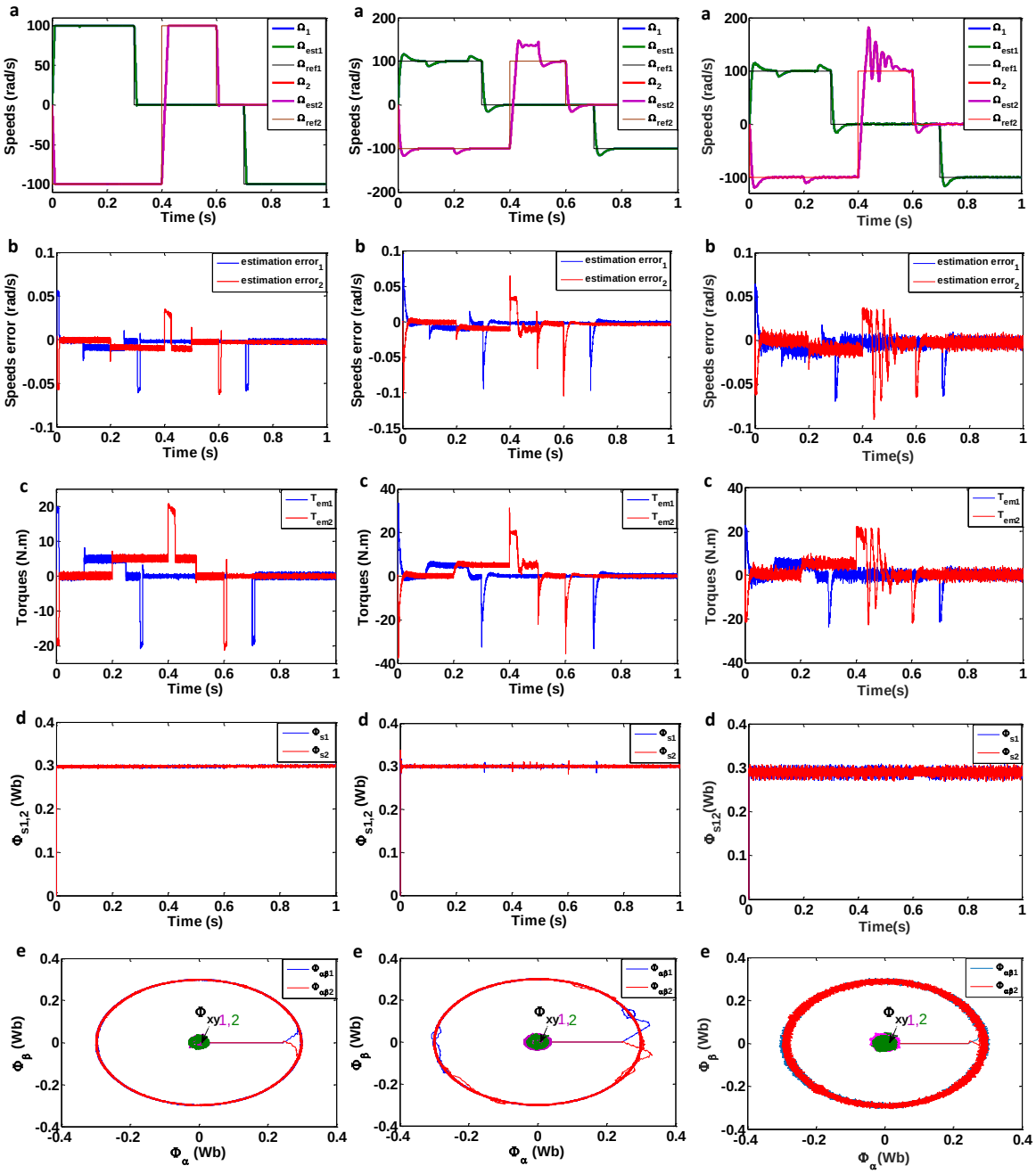

Fig. (4.12): Dynamic responses of parallel-connected two five-phase PMSMs drive controlled by SMC based DTC, PI based DTC, and conventional DTC: when the two machines are operating in the opposite directions: (a) Reference, actual and estimated speeds, (b) Speed estimation errors, (c) Electromagnetic torques, (d) Stator fluxes magnitudes, (e) Stator fluxes trajectories.

Compared with DTC-PI and conventional DTC, the DTC-SMC shows again no overshoots and no significant influence of the load application. Furthermore the results illustrated in Fig. (4.12) show once more that the control of the two machines is completely decoupled. Indeed, the speed of one machine and its electromagnetic torque remain completely undisturbed during the reversion of the other machine, indicating a complete decoupling of the control. Therefore, there is hardly any evidence of torque disturbance of one machine during the reversal of the other one. As shown from Figs. (4.12(a)), the starting and reversing transients of one machine do not have any tangible consequence on the operation of the second machine. The decoupled control is preserved and the characteristics of both machines are unaffected.

4.5.3.3 Case 3: Operation at different loading conditions

Fig. (4.13) shows the performance of the two-machine drive controlled by DTC-SMC, DTC-PI, and conventional DTC controllers under load torques variations condition. The reference of the first speed is set at 100 rad/s, while the speed reference of the second machine is set at 50 rad/s. A set of load torques from 5 Nm to 2.5 Nm are applied on the two machines shafts in different times. It is clear from Fig. (4.13) that, when one machine is either loaded or unloaded, the second machine performance is unaffected, which proves once again that both machines connected in parallel are totally decoupled. In case of sliding mode control, no variation whatsoever can be observed in the speeds responses of the both machines during these transients. It is worth noticing that there is no impact on the speed and electromagnetic torque of one machine when the speed or the load of the other machine in parallel-connected system changes. Thus, through proper phase transformation rules, the decoupled control of two five-phase PMSMs connected in parallel can be achieved with a single supply from a five-phase voltage source inverter. Furthermore, measured and estimated speeds are in excellent agreement in both steady state and transient operations.

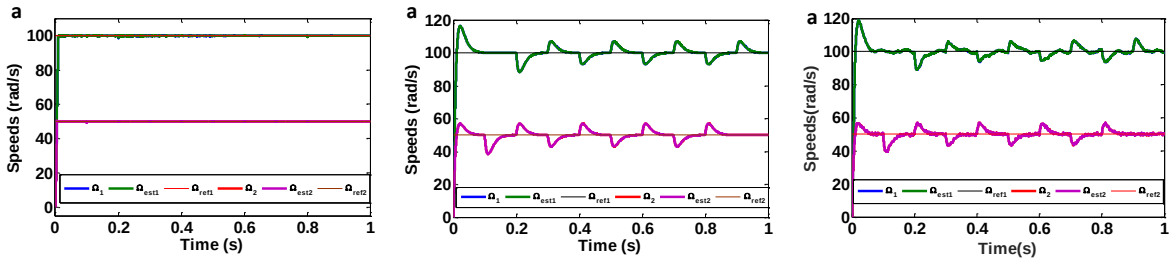

(DTC-SMC) (DTC-PI) (DTC-switching up-table)

Fig. (4.13): Dynamic responses of parallel-connected two five-phase PMSMs drive controlled by SMC based DTC, PI based DTC, and conventional DTC and operating at different loading conditions: (a) Reference, actual and estimated speeds, (b) Speed estimation errors, (c) Electromagnetic torques, (d) Stator fluxes magnitudes, (e) Stator fluxes trajectories.

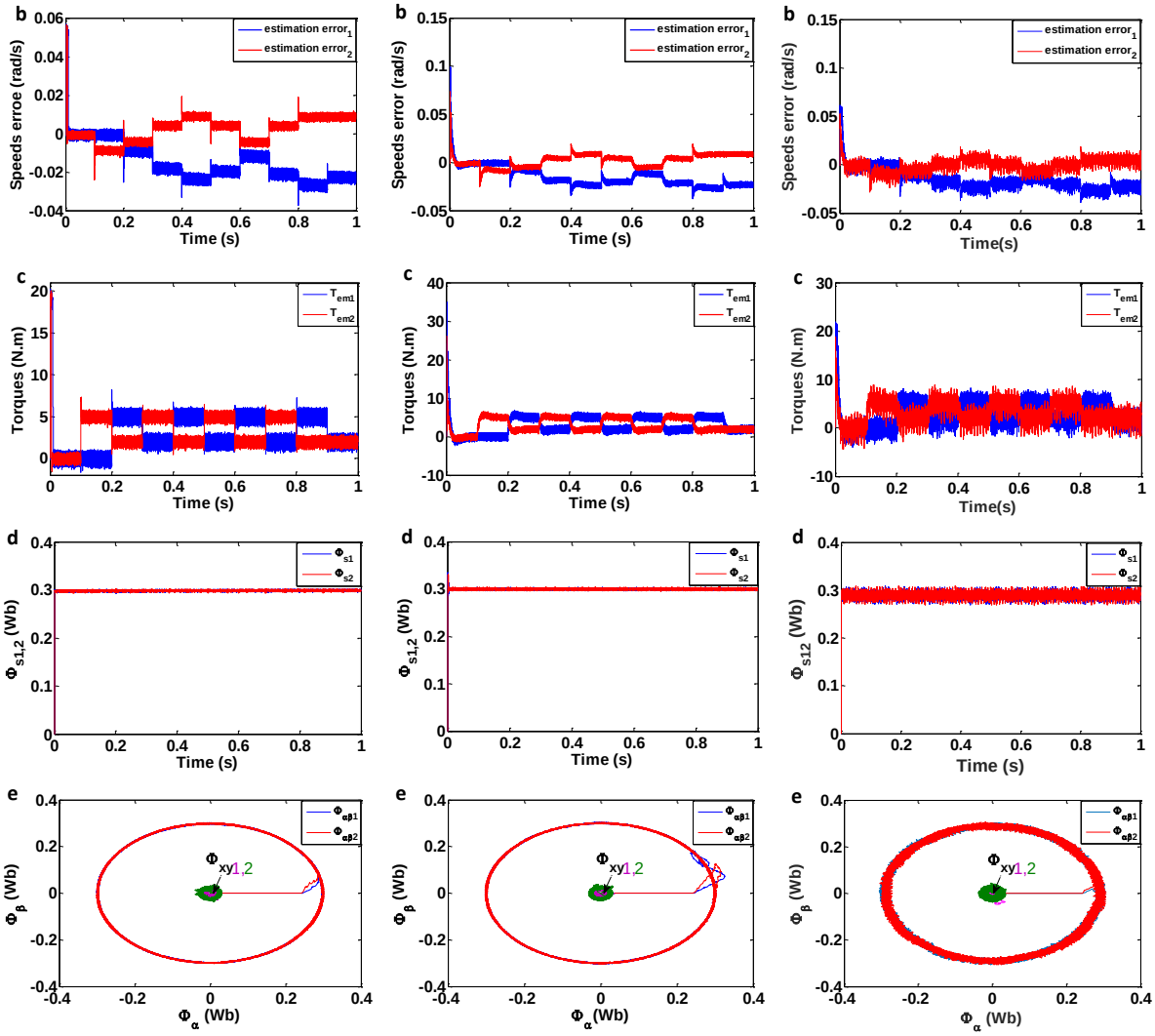

(DTC-SMC) (DTC-PI) (DTC-switching up-table)

Continued Fig. (4.13).

4.5.3.4 Case 4: Low speed operation

Fig. (4.14) shows the performance of the senseorless feedback control under low speed conditions. The speed reference of the first machine is set to 7 rad/s, -3 rad/s, 4 rad/s and -5 rad/s at t=0s, 0.3s, 0.55s, 0.8s, respectively. For the second machine, the speed reference is set to 5 rad/s, -4 rad/s, 5 rad/s, and -7 rad/s at the same times as previous one. A torque of 5 Nm was applied on the shafts of the first and second machines at the instants t = 0.1 s and 0.2 s, respectively. In case of the DTC-PI and conventional DTC controls, the application of the load torque causes a noticeable speed drop up to -5 rad/s. The speed controller compensates for this drop after a necessary recovery time, and it is clear that the conventional DTC suffers during low speed operation. However, with the DTC-SMC control, this influence is reduced and better reference tracking during the speed reversing are observed. Furthermore, it can be seen that in case of DTC-SMC control the estimation using the SMO is more robust during low speed operations.

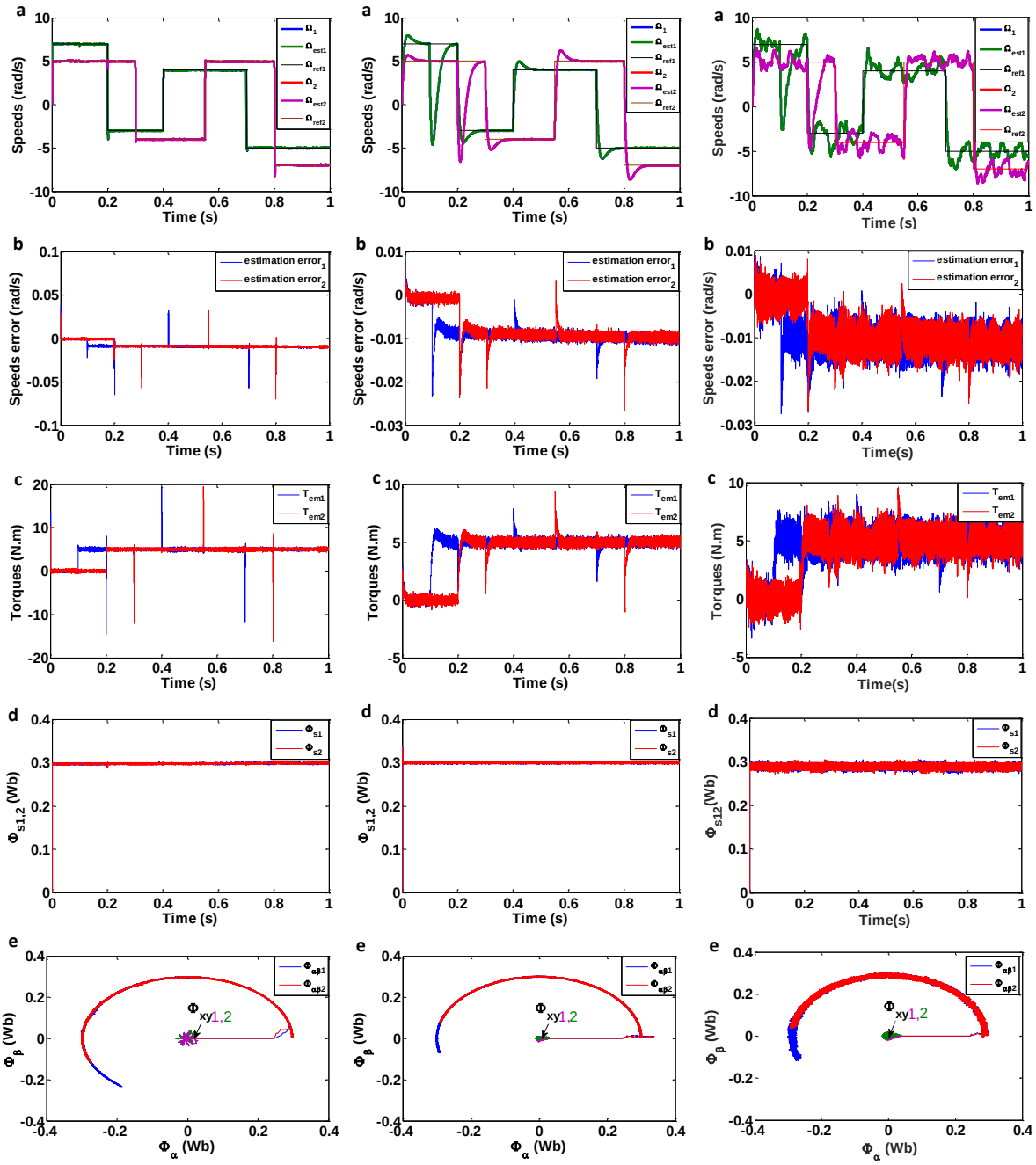

(DTC-SMC) (DTC-PI) (DTC-switching up-table)

Fig. (4.14): Dynamic responses of parallel-connected two five-phase PMSMs drive controlled by SMC based DTC, PI based DTC, and conventional DTC and operating at low speed conditions: (a) Reference, actual and estimated speeds, (b) Speed estimation errors, (c) Electromagnetic torques, (d) Stator fluxes magnitudes, (e) Stator fluxes trajectories.

4.5.3.5 Case 5: Parameters variations

In this test, the influence of the variation of the stator resistance on the decoupling between the flux and the torque and the speed regulation performance is studied. For that end, the resistance of the first machine is increased by +100% at t=0.2 s, whereas the resistance of the second machine

is increased by the same rate at 0.3 s. Fig. 4.15 shows the responses of the five-phase machines under a sudden change in load torque from 0 Nm to 5 Nm at t = 0.2 s and 0.3s, respectively.

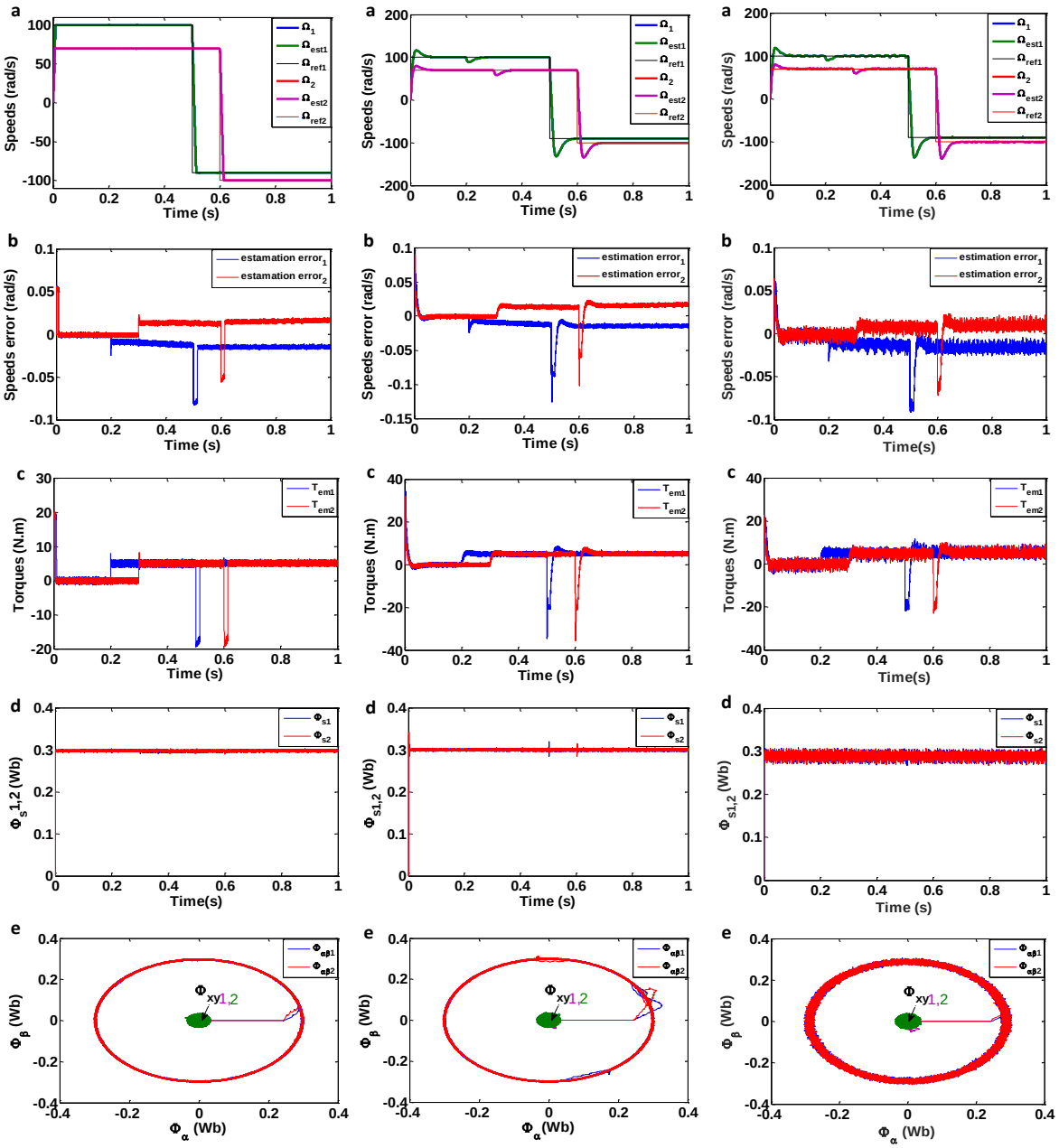

Fig. (4.15): Dynamic responses of parallel-connected two five-phase PMSMs drive controlled by SMC based DTC, PI based DTC, and conventional DTC and operating at stator resistance variations: (a) Reference, actual and estimated speeds, (b) Speed estimation errors, (c) Electromagnetic torques, (d) Stator fluxes magnitudes, (e) Stator fluxes trajectories.

In this test, the reference speed is step changed from 100 rad/s to -90 rad/s at t=0.5 s for the first machine and from 70 rad/s to -100 rad/s at t=0.6 s for the second one. From this figure, this parameter variation has no influence on the decoupling between the flux and the torque.

Furthermore, its influence on the decoupling between the two machines and the estimation errors is not so considerable and has been recovered quickly thanks to of the robustness of the SMO.

A general comparison between DTC-SVM-SMC, DTC-SVM-PI and conventional DTC is given in Table (4.2). Compared to the DTC-SVM-PI and conventional DTC controllers, the DTC-SVM-SMC shows superiority in terms of settling time and overshoot magnitude.

Table (4.2). Comparison between SMC and PI based DTC.

Controlled variable	Comparison criterion	DTC-SVM-SMC	DTC-SVM-PI	Conventional DTC	Reduction rate (%)	
					DTC-SVM-PI	Conventional DTC
Rotor speed	Settling time (s)	0.01	0.09	0.09	88.88	88.88
	Overshoot (rad/s)	0.02	13.63	13.63	99.85	99.85
	Speeds drops (%)	0.9	11.6	11.6	92.24	92.24
	Recovery time (at abrupt load) (s)	0.01	0.08	0.08	87.5	87.5
	Overshoot in reversal mode (%)	0	48	61	100	100
	The maximum speed estimation error (%)	0.04	0.1	0.09	60	55.55
Electromagnetic torque	Settling time (s)	0.009	0.07	0.07	87.71	87.71
	Overshoot (rad/s)	2.5	1.6	10.9	36(increase)	77.06
	Ripple (N.m)	1.16	1.2	3.5	3.33	66.85
Stator flux	Settling time (s)	0.002	0.0046	0.004	56.52	50
	Overshoot (rad/s)	0	0.034	0	100	0
	Overshoot in reversal mode (%)	0	0.016	0	100	0
	Ripple (N.m)	0.007	0.0084	0.28	16.66	97.5

4.6 Conclusion

In this chapter, a sensorless nonlinear sliding mode control based FOC and DTC of the parallel-connected two five-phase PMSMs drive fed by a single inverter has been developed. In the FOC scheme, the Extended Kalman Filter is used for rotor speeds, positions, and load torques estimations. The benefit of EKF based sensorless control is the improvement in system dynamics through the accuracy in speeds, rotor positions, and load torques estimations. While in DTC-SVM scheme, the sliding mode control and sliding mode observer are combined to enhance the direct torque control and to guarantee the system stability. The torques, fluxes and speeds, are estimated by using a sliding mode observer based on a flux model of the five-phase PMSM. The effectiveness of the proposed control approaches has been verified through extensive computer simulations and compared with PI-controller.

Simulation results have demonstrated not only truly decoupled operation between the two machines but also many improvements on the dynamic responses as well as the steady state performances, in terms of time response, accuracy, and ripple reduction.

In addition, the simulation results show that, the stochastic EKF has a great robustness during

the application of the load torque, the reversal mode, and during the measurement noise on the voltages and currents, which is generated by the VSI.

On the other hand, the added value of the SMO based sensorless control is the amelioration in the system dynamics through the accuracy in speeds, fluxes, and torques estimation. Indeed, the obtained simulation results show better speed tracking performance at both dynamic and steady state, acceptable estimations errors, robustness in different tests including speed variation, load application, low speed operation, and stator resistance variation. Therefore, these results affirm the ability of the proposed observer to guarantee good estimations in steady state and transients as well.

General Conclusion

General Conclusion

In this thesis, a various control for a two five-phase PMSMs drive system connected in parallel have been developed, which allows independent control of two five-phase PMSMs supplied from a single voltage source inverter. In this context, the research work has been addressed the principal points of each chapter as follow:

The chapter one has presented the mathematical modeling of the five-phase PMSM, five-phase VSI, and parallel-connected of two five-phase PMSMs. The main outcomes that can be highlighted in this chapter are:

- The reduction in the number of inverter legs, when compared to an equivalent two-machine three-phase drive system. The reduction in the number of inverter leg implies smaller number of electronic components, which can be translate into higher reliability,
- Only two stator currents components (*d*-*q*) are responsible for torque/ flux production, while the other components (*x*-*y*) are not used,
- Through an appropriate phase transposition of the stator windings, the other components (*x*-*y*) can be used to connect in parallel another machine in such a way that the torque/flux producing current components of one machine do not affect the production of torque/flux of the other machine and vice versa.

In chapter two, three controls methods: FOC, conventional DTC and DTC-SVM have been applied to control each machine independently. From simulation results it is easy to see that, FOC, and DTC-SVM reduce the torque/flux ripple. However, the both control methods suffer from their high sensitivity to the parameters variations. In order to make these control approaches less sensitive, the sliding mode control has been adopted.

The main aim of chapter three of this thesis is the improvement of the performance of the two machine connected in parallel controlled by FOC and DTC-SVM using sliding mode control. The main conclusion that can be drawn from theoretical study and simulation results are summarized as follows:

- The nonlinear sliding mode control is a way to improve the robustness of parallel-connected two five-phase PMSMs against parameter variations,
- The reduction in torque/flux ripples,

- The responses of parallel-connected two five-phase PMSMs are without overshoots even in reversal mode and without speed drops as well.

The fourth chapter focus on sensorless mode of parallel-connected two five-phase PMSMs by using two observer structures EKF and SMO have been applied on FOC-SMC and DTC-SVM-SMC, respectively. In the FOC-SMC scheme, the EKF is used for rotor speeds, positions, and load torques estimations. While in DTC-SVM-SMC scheme, the SMO is used to estimate the torques, fluxes and speeds, which is based on the flux model of the five-phase PMSM. From theoretical study and simulation results, the benefits of EKF and SMO can be summarized as follows:

- The system cost is lowered through the reduce of number of sensors,
- The EKF has a good robustness during the application of the load torque, the reversal mode, even with noisy on the voltages and currents measurement,
- The SMO show better speed tracking performance at both dynamic and steady state, acceptable estimations errors, and robustness in different tests.

Future Works

For the continuity of research, the future work could be oriented to a vast area in this field. Therefore, some possible suggestions and perspectives are as follows:

- Application of high order sliding mode approach for control and observers design;
- Fault tolerant control of the parallel-connected two five-phase PMSMs system;
- Development an appropriate SVM for multi-level VSI feeding two five-phase PMSMs connected in parallel:
- Application of other nonlinear and intelligent control methods based FOC and DTC.

Appendices

APPENDIX A

TABLE A.1. Five-phase PMSM parameters [95].

Rated power	2 kW
Rated speed	400 rad/s
Pole pairs (p)	4
Winding resistance (r_s)	$1\,\Omega$
d-axis inductance L_d	8.5 mH
q-axis inductance L_q	8 mH
Leakage inductance L_{ls}	0.2 mH
Rotor inertia	0.004 kg.m^2
Frictional torque constant	0
Permeant magnet flex Φ_{fj}	0.175 Wb

APPENDIX B

Controllers Parameters

1-FOC-PI

TABLE (B.1): PI parameters.

	Speed controller	i_{sd} controller	i_{sq} controller	i_{sx} controller	i_{sy} controller
PI Controllers	$k_p=0.8$ $k_i=40$	$k_p=33$ $k_i=32000$	$k_p=33$ $k_i=32000$	$k_p=33$ $k_i=32000$	$k_p=33$ $k_i=32000$

2-Conventional DTC

TABLE (B.2): PI parameters.

	Speed controller
PI	$k_p=0.8$ $k_i=40$

3-DTC-SVM

TABLE (B.3): PI parameters.

	Speed controller	*Flux* controller (PMSM1)	*Flux* controller (PMSM2)	*Torque* controller (PMSM 1)	*Torque* controller (PMSM 2)
PI Controllers	$k_p=0.8$ $k_i=40$	$k_{p\Phi s1}=95$ $k_{i\Phi s1}=48$	$k_{p\Phi s2}=95$ $k_{i\Phi s2}=48$	$k_{pT_{em1}}=163.86$ $k_{iT_{em1}}=81$	$k_{pT_{em2}}=163.86$ $k_{iT_{em2}}=81$

4-FOC-SMC

TABLE (B.4): PI and SMC parameters.

	Speed controller	i_{sd} controller	i_{sq} controller	i_{sx} controller	i_{sy} controller
SMC Controllers	$k_{\Omega j}=5$	$k_{idj}=4000$	$k_{iqj}=7000$	$k_{ixj}=4000$	$k_{iyj}=7000$

4.1-Parameter of EKF

$$Q=10^{-3}\begin{bmatrix}10^{-6}&0&0&0&0&0&0\\0&10^{-6}&0&0&0&0&0\\0&0&10^{-6}&0&0&0&0\\0&0&0&10^{-6}&0&0&0\\0&0&0&0&10^{-2}&0&0\\0&0&0&0&0&10^{-4}&0\\0&0&0&0&0&0&10^{-2}\end{bmatrix}$$

$$R=10^{-2}\begin{bmatrix}1&0&0&0\\0&1&0&0\\0&0&1&0\\0&0&0&1\end{bmatrix}$$

5-DTC-SMC

TABLE (B.5): SMC parameters.

SMC Controllers	Speed controller	Flux controller (PMSM 1)	Flux controller (PMSM 2)	Torque controller (PMSM 1)	Torque controller (PMSM 2)
	$k_{\Omega j}=4$	$k_{\Phi 1}=4000$	$k_{\Phi 2}=4000$	$k_{Tem1}=9000$	$k_{Tem2}=9000$

6-DTC-SMC based SMO

TABLE (B.6): SMC and SMO parameters.

SMC	Speed controller	Torque controller	flux controller
	$k_{\Omega j}=4$	$k_{Temj}=9000$	$k_{\Phi j}=9000$
SMO	*k=99000, k1=300*		

References

References

[1] M. Bermudez, I. Gonzalez-Prieto, F. Barrero, H.Guzman, M. J. Duran, and X. Kestelyn, "Open-Phase Fault-Tolerant Direct Torque Control Technique for Five-Phase Induction Motor Drives", IEEE Transactions on Industrial Electronics, vol. 64, no. 2, pp. 902-911, 2017.

[2] S. Payami, R. K. Behera, X. Yu, and M. Gao, "An Improved DTC Technique for Low Speed Operation of a Five-Phase Induction Motor", IEEE Transactions on Industrial Electronics, vol. 64, no. 5, pp. 3513-3523, 2017.

[3] B. Tian, Q.-T. An, J.-D. Duan, D.-Y. Sun, L. Sun, and D. Semenov, "Decoupled Modeling and Nonlinear Speed Control for Five-Phase PM Motor Under Single Phase Open Fault", IEEE Transactions on Industrial Electronics, vol. 32, no. 7, pp. 5473-5486, 2017.

[4] C. Sneessens, T. Labbe, F. Baudart, and E. Matagne, "Position Sensorless Control For Five-Phase Permanent-Magnet Synchronous Motors", International Conference on Advanced Intelligent Mechatronics, Besançon, France, pp.794-799, July 8-11, 2014.

[5] H. H.Chen and Chong-Xian Su, " Current Control For Single-Inverter-Fed Series-Connected Five-Phase PMSMS", IEEE International Symposium on Industrial Electronics, Taipei, Taiwan, pp.1-6, May 28-31, 2013.

[6] Z. Wang, X. Wang, J. Cao and M. Cheng; Y. Hu, "Direct Torque Control of T-NPC Inverters Fed Double-Stator-Winding PMSM Drives With SVM", IEEE Transactions on Power Electronics , vol. 33, no. 2, pp. 1541-1553, Feb. 2018.

[7] X. Wang, Z. Wang, M. Cheng and Y. Hu, "Remedial Strategies of T-NPC Three-Level Asymmetric Six-Phase PMSM Drives Based on SVM-DTC", IEEE Transactions on Industrial Electronics , vol. 64, no. 9, pp. 6841-6853, Sept. 2017.

[8] M. Jones, S. N. Vukosavic, and E. Levi, "Parallel-Connected Multiphase Multidrive Systems With Single Inverter Supply", IEEE Transactions on Industrial Electronics, vol. 56, no. 6, pp. 2047-2057, June 2009.

[9] H. Zhang, S. Luo, Y. Yu, and L. Liu, "Study on Series Control Method for Dual Three-Phase PMSM Based on Space Vector Pulse Width Modulation", International Journal of Control and Automation, vol. 8, no. 1, pp. 197-210, 2015.

[10] M. Jones, E. Levi, and S. N. Vukosavic, "Independent Control of Two Five-Phase Induction Machines Connected in Parallel to a Single Inverter Supply", IEEE Industrial Electronics Conference, Paris, France, pp. 1257-1262, 6-10 November 2006.

[11] D. Dujic, G. Grandi, M. Jones, and E. Levi, "A Space Vector PWM Scheme for Multi Frequency Output Voltage Generation With Multiphase Voltage-Source Inverters", IEEE Transactions on Industrial Electronics, vol. 55, no. 5, pp. 1943-1955, May 2008.

[12] K. Suman, K. Suneeta, and M. Sasikala," Direct Torque Controlled Induction Motor Drive with Space Vector Modulation Fed with Three-level Inverter", The IEEE International Conference on Power Electronics, Drives and Energy Systems, Bengaluru, India, pp.1-6, Dec16-19, 2012.

[13] Emre Ozkop and Halil I. Okumus," Direct Torque Control of Induction Motor Using Space Vector Modulation (SVM-DTC)", 12th International Middle-East Power System Conference, Aswan, pp. 368 - 372, 12-15 March 2008.

[14] Farouk M. Abdel-kader, A. EL-Saadawi, A. E. KALAS, and Osama M.EL-baksawi," Study In Direct Torque Control of Induction Motor By Using Space Vector Modulation", 12th International Middle-East Power System Conference, Aswan, pp. 224-229, 12-15 March 2008.

[15] Chebaani Mohamed, A. Golea, and M.T. Benchouia," Implementation of a Predictive DTC-SVM of an Induction Motor", The 4th International Conference on Electrical Engineering (ICEE2015), Boumerdes, pp. 1-4, 13-15 Dec 2014.

[16] B. S. Khaldi, H. Abu-Rub, A. Iqba, R. Kennel, O. Mahmoudi, and D. Boukhetala," Sensorless Direct Torque Control of Five-Phase Induction Motors Drives", IECON 2011 - 37th Annual Conference on IEEE Industrial Electronics Society, Melbourne, VIC, pp. 3501 - 3506, 7-10 Nov. 2011.

[17] B. S. Khaldi, H. Abu-Rub, A. Iqba, R. Kennel, O. Mahmoudi2, D. Boukhetala," Comparison Study between a Simple Sensorless Method and Adaptive Observer for DTC-SVM Five-Phase Induction Motor Drive", IEEE International Conference on Industrial Technology (ICIT), Athens, pp. 743-748, 19-21 March 2012.

[18] Mohammad Hossein Vafaie, Behzad Mirzaeian Dehkordi, Payman Moallem, and Arash Kiyoumarsi, "A New Predictive Direct Torque Control Method for Improving Both Steady-State and Transient-State Operations of the PMSM", IEEE Transactions On Power Electronics, vol. 31, no.5, pp.3738-3753, may 2016.

[19] Xiaoguang Zhang, Lizhi Sun, Ke Zhao, and Li Sun, "Nonlinear Speed Control for PMSM System Using Sliding-Mode Control and Disturbance Compensation Techniques", IEEE Transactions on Power Electronics, vol. 28, no.3, pp. 1358-1365, March 2013.

[20] B. Ning, S. Cheng, and Y. Qin, "Direct Torque Control of PMSM Using Sliding Mode Backstepping Control with Extended State Observer", Journal of Vibration and Control, pp. 1-14, 2016.

[21] Zaafouri, C. Regaya, H. Azza and A. Châari, "DSP-Based Adaptive Backstepping Using the Tracking Errors for High-Performance Sensorless Speed Control of Induction Motor Drive", ISA Transactions, vol. 60, pp. 333-347, 2016.

[22] F. Ben Salem and N. Derbel, "Second-Order Sliding-mode Control Approaches to Improve Low-speed Operation of Induction Machine Under Direct Torque Control", Electric Power

Components and Systems, vol. 44, no. 17, pp. 1969-1980, June 2016.

[23] A. Ammar, A. Bourek, and A. Benakcha, "Nonlinear SVM-DTC for Induction Motor Drive Using Input-Output Feedback Linearization and High Order Sliding Mode Control", ISA Transactions, vol. 67, pp. 428-442, 2017.

[24] Faa Seyed Mohammad Jalal Rastegar Fatemi, Navid Reza Abjadi, Jafar Soltani, and Saeed Abazari, "Speed Sensorless Control of a Six-Phase Induction Motor Drive Using Backstepping Control", IET Power Electron, vol. 7, no. 1, pp. 114-123, January 2014.

[25] Anissa Hosseyni, Ramzi Trabelsi, Atif Iqbal, and Med Faouzi Mimouni, "Backstepping Control for a Five-Phase Permanent Magnet Synchronous Motor Drive", International Journal of Power Electronics and Drive System (IJPEDS), vol. 6, no. 4, pp. 842-852, December 2015.

[26] M. Ahmed, F. M. Karim, M. Abdelkader, and B. Abdelber, "Input Output Linearization and Sliding Mode Control of a Permanent Magnet Synchronous Machine Fed by a Three Levels Inverter", Journal of Electrical Engineering, vol. 57, no. 4, 205-210, 2006.

[27] Le-Bao Li, Ling-Ling Sun, Sheng-Zhou Zhang, and Qing-Quan Yang, "PMSM Speed Tracking and Synchronization of Multiple Motors Using Ring Coupling Control and Adaptive Sliding Mode Control", ISA Transactions, vol.58, pp. 635-649, September 2015.

[28] A. Ammar, A. Bourek, and A. Benakcha, "Robust SVM-Direct Torque Control of Induction Motor Based on Sliding Mode Controller and Sliding Mode Observer", Frontiers in Energy, pp. 1-14, 2017.

[29] V.I. Utkin, "Sliding Mode Control Design Principles and Applications to Electric Drives", IEEE Transactions on Industrial Electronics, vol. 40, no. 1, pp. 23- 36, 1993.

[30] Mohamed S. Diab, Ahmed A. Elserougi, Ayman S. Abdel-Khalik, Ahmed M. Massoud and Shehab Ahmed, "A Nine-Switch-Converter-Based Integrated Motor Drive and Battery Charger System for EVs Using Symmetrical Six-Phase Machines", IEEE Transactions on Industrial Electronics, vol. 63, no. 9, pp. 5326-5335, April 2016.

[31] Antoine Bruyere "Modelisation et Commande d'un Alterno-Demarreur Heptaphase Pour Application Automobile Micro-Hybride", Ph.D. Thesis, Lille University, France, 2009.

[32] Djafar HADIOUCHE "Contribution À L'étude de la Machine Asynchrone Double Étoile: Modélisation, Alimentation et Structure", Ph.D. Thesis, Nancy University, France, 2001.

[33] Navid R. Abjadi, "Sliding-Mode Control of a Six-Phase Series/Parallel Connected Two Induction Motors Drive", ISA Transactions, vol.53, no.6, pp. 1847-1856, 2014.

[34] Lei Yuan, Ming-liang Chen, Jian-qingShen, and Fei Xiao, "Current Harmonics Elimination Control Method for Six-Phase PM Synchronous Motor Drives", ISA Transactions, vol. 59, pp. 443-449, Nov. 2015.

[35] Leila Parsa and Hamid A. Toliyat, "Sensorless Direct Torque Control of Five-Phase Interior Permanent-Magnet Motor Drives", IEEE Transactions on Industry Applications, vol. 43, no. 4, pp. 952-959, July/August 2007.

[36] Siavash Sadeghi, Lusu Guo, Hamid A. Toliyat, and Leila Parsa, "Wide Operational Speed Range Of Five-Phase Permanent Magnet Machines by Using Different Stator Winding Configurations", IEEE Transactions on Industrial Electronics, vol. 59, no. 6, pp. 2621-2631, June 2012.

[37] E. Levi, M. Jones, S.N. Vukosavic, A. Iqbal, and H. A. Toliyat, "Modeling, Control, and Experimental Investigation of A Five-Phase Series-Connected Two-Motor Drive With Single Inverter Supply", IEEE Transactions on Industrial Electronics, vol. 54, no. 3, pp. 1504-1516, June 2007.

[38] Emil Levi, Martin Jones, Slobodan N. Vukosavic, and Hamid A. Toliyat, "Steady-State Modeling Of Series-Connected Five-Phase and Six-Phase Two-Motor Drives", IEEE Transactions on Industry Applications, vol. 44, no. 5, pp. 1559-1568, 2008.

[39] F. Mekri, J. F.Charpentier, and E. Semail, "An Efficient Control of a Series Connected Two-Synchronous Motor 5-Phase With Non-Sinusoidal EMF Supplied by a Single 5-Leg VSI: Experimental and theoretical investigations", Electric Power Systems Research, vol. 92, pp.11-19, 2012.

[40] Fabrice Locment, "Conception et Modélisation d'une Machine Synchrone À 7 Phases À Aimants Permanents et Flux Axial : Commande Vectorielle En Modes Normal et Dégradé", Ph.D. Thesis, lille University, France, 2006.

[41] Martin Jones, "A Novel Concept of Series Connected Multi-Phase, Multi-Motor Drive Systems", Ph.D. Thesis, Liverpool John Moores University, UK, 2005.

[42] Samuli Kallio, "Modeling and Parameter Estimation of Double-Star Permanent Magnet Synchronous Machines ", Ph.D. Thesis, Lappeenranta University, Finland, 2014.

[43] Alberto Tessarolo, "Modeling and Analysis of Multiphase Electric Machines For High-Power Application", Ph.D. Thesis, Trieste University, Italy 2011.

[44] Atif Iqbal, "Modelling and Control of Series connected Five-Phase and Six-phase Two-Motor Drives" Ph.D. Thesis, Liverpool John Moores University, UK, 2005.

[45] Marwa Ezzat, "Commande Non Lineaire Sans Capteur de la Machine Synchrone a Aimants Permanents", Ph.D. Thesis, Nantes University, France, 2011.

[46] Leila Parsa, "Performance Improvement of Permanent Magnet AC Motors", Ph.D. Thesis, Khaje Nasir Toosi University, Iran, 2005.

[47] Bassel Aslan, "Conception de Machines Polyphasées à Aimants et Bobinage Concentré à Pas Fractionnaire Avec Large Plage de Vitesse", Ph.D. Thesis, lille University, France, 2013.

[48] Enrique L. Carrillo Arroyo, "Modeling And Simulation of Permanent Magnet Synchronous Motor Drive System", Ph.D. Thesis, Puerto Rico University, Mayagüez, Puerto Rico, 2013.

[49] M. Paul Akiki, "Conception Multi-Physique De Machines Electriques à Flux Radial et Axial Pour des Applications A Entraînement Direct", Ph.D. Thesis, Paris-Saclay University, France, 2017.

[50] Boukais Boussad, "Contribution a La Modelisation des Systemes Couples Machines Convertisseurs : Application aux Machines a Aimants Permanents (Bdcm-Pmsm)", Ph.D. Thesis, Tizi-Ouzou University, Algeria, 2012.

[51] Abdelkader DJAHBAR, "Contribution a La Commande Multimachines Connectees en Serie", Ph.D. Thesis, Oran University, Algeria, 2008.

[52] Bogdan M. Wilamowski and J. david Irwin, "The Industrial Electronics Handbook Second Edition **(**Power Electronics And Motor Drives**)**", 2011 by Taylor and Francis Group, LLC.

[53] DRAZEN DUJIC, "Development of Pulse-Width-Modulation Techniques for Multi-Phase and Multi-Leg Voltage Source Inverters", Ph.D. Thesis, Liverpool John Moores University, UK, 2008.

[54] Y. N. Tatte and M. V. Aware, "Torque Ripple and Harmonic Current Reduction in Three-Level Inverter Fed Direct Torque Controlled Five-Phase Induction Motor", IEEE Transactions on Industrial Electronics, vol. 64, no. 7, pp. 5265-5275, 2017.

[55] A. Taheri, " Harmonic Reduction of Direct Torque Control of Six-Phase Induction Motor", ISA Transactions, vol. 66, pp. 299-314, 2016.

[56] J. K. Kang and S. K. Sul, "New Direct Torque Control of Induction Motor for Minimum Torque Ripple and Constant Switching Frequency", IEEE Trans. Ind. Appl, vol. 35, no. 5, pp. 1076–1082, Sep. Oct. 1999.

[57] Khoa Dang Hoang, Yuan Ren, Zi-Qiang Zhu, and Martin Foster," Modified Switching-Table Strategy for Reduction of Current Harmonics In Direct Torque Controlled Dual Three-Phase Permanent Magnet Synchronous Machine Drives", IET Electric Power Applications, vol.9, no.1, pp.10-19, May 2015.

[58] Libo Zheng, John E. Fletcher, Barry W. Williams, and Xiangning He,"A Novel Direct Torque Control Scheme for a Sensorless Five-Phase Induction Motor Drive", IEEE Transactions On Industrial Electronics, vol. 58, no. 2, Feb 2011.

[59] Libo Zheng, John E. Fletcher, Barry W. Williams, and Xiangning He, "Low-Speed Control Improvements for a Two-Level Five-Phase Inverter-Fed Induction Machine Using Classic Direct Torque Control", IEEE Transactions On Industrial Electronics, vol. 58, no. 7, July 2011.

[60] Dariusz Świerczyński, M. Sc. "Direct Torque Control with Space Vector Modulation (DTC-SVM) of Inverter-Fed Permanent Magnet Synchronous Motor Drive", Ph.D. Thesis, WARSAW University, Polonais, 2005.

[61] Djamel BOUDANA, "Sur La Commande DTC Basée sur les Techniques de Contrôle Robuste de la Machine Synchrone a Double Etoile Alimentée par Convertisseurs Multiniveaux", Ph.D. Thesis, Polytechnique University, Polonais, 2005.

[62] M. Rizwan Khan, and Atif Iqbal, "Speeds Estimation of Series-Connected Five-Phase Two-Motor Drive System Using Adaptive Flux Observers", Asian Power Electronics Journal, vol. 2, no. 1, Apr. 2008.

[63] L. Parsa and H. A. Toliyat, "Sensorless Direct Torque Control of Five-phase Interior Permanent Magnet Motor Drives", Industry Applications Conference, 2004. 39th IAS Annual Meeting, vol. 2, pp. 992-999, 3-7 Oct. 2004.

[64] I. M. Alsofyani and N. R. N. Idris, "Simple Flux Regulation for Improving State Estimation at Very Low and Zero Speed of a Speed Sensorless Direct Torque Control of an Induction Motor", IEEE Trans. Power Electron., vol. 31, no. 4, pp. 3027-3035, Apr. 2016.

[65] Abdelkarim AMMAR, Amor BOUREK, Abdelhamid BENAKCHA, "Modified Load Angle Direct Torque Control for Sensorless Induction Motor Using Sliding Mode Flux Observer", The 4th International Conference on Electrical Engineering (ICEE2015), Boumerdes, pp. 1-6, 13-15 Dec 2014.

[66] C. Lascu, and A. M. Trzynadlowski, "Combining the Principles of Sliding Mode, Direct Torque Control and Space-Vector Modulation in a High-Performance Sensorless AC Drive", IEEE Transactions on Industry Applications, vol. 40, no. 1, January/February 2004.

[67] S F.-J. Lin, Y.-C. Hung, and M.-T. Tsai, "Fault-Tolerant Control for Six-Phase PMSM Drive System Via Intelligent Complementary Sliding Mode Control Using TSKFNN-AMF", IEEE Transactions on Industrial Electronics, vol. 60, no. 12, pp. 5747-5762, 2013.

[68] S. Chen, Y. Luo, and Y. Pi, "PMSM Sensorless Control with Separate Control Strategies and Smooth Switch From Low Speed to High Speed", ISA Transactions, vol. 58, pp. 650-658, September 2015.

[69] Huangfu Yi-geng, "Research of Nonlinear System High Order Sliding Mode Control and its Applications for PMSM", Ph.D. Thesis, Belfort-Montbéliard University, France, 2005.

[70] Claudio Vecchio, "Theoretical Developments and Applications to Uncertain Mechanical Systems", Ph.D. Thesis, Degli Studi Di Pavia University, Italy.

[71] Thierry Floquet, "Contributions a La Commande Par Modes Glissants D'ordre Superieur", Ph.D. Thesis, Lille University, France, 2005.

[72] Jinkun Liu, and Xinhua Wang, "Advanced Sliding Mode Control for Mechanical Systems **(**Design, Analysis and MATLAB Simulation**)**", 2011 by springer.

[73] DAIKH Fatima Zohra, "Contribution des Approches de L'intelligence Artificielle Pour la Stabilisation Robuste des Systèmes Non Linéaires", Ph.D. Thesis, Oran University, Algeria, 2015.

[74] Arnaud VIDET, "Variateur de Vitesse a Impact Electromagnétique Réduit : Onduleur Multiniveaux et Nouvelles Stratégies De Modulation", Ph.D. Thesis, Lille University, France, 2008.

[75] Fezzani Amor, "Commande Robuste de la Machine Synchrone à Aimants Permanents", Ph.D. Thesis, Patna University, Algeria, 2015.

[76] J. J. Slotine, "Applied nonlinear control", Englewood Cliffs NJ. Tice Hall, 1991.

[77] Ahmad Asri Abd Samat, Dahaman Ishak, Pais Saedin, and Shahid Iqbal, "Speed-Sensorless Control of Parallel-Connected PMSM Fed by a Single Inverter Using MRAS", IEEE International Power Engineering and Optimization Conference, Melaka, Malaysia, pp.35-39, 6-7 June 2012.

[78] Nguyen Khanh Quang, Nguyen Trung Hieu, and Q. P. Ha, "FPGA-Based Sensorless PMSM Speed Control Using Reduced-Order Extended Kalman Filters", IEEE Transactions on Industrial Electronics, vol. 61, no.12, pp. 6574-6582, December 2014.

[79] Z. Xu and M. F. Rahman, "Comparison of a Sliding Observer and a Kalman Filter for Direct-Torque-Controlled IPM Synchronous Motor Drives", IEEE Transactions on Industrial Electronics, vol. 59, no. 11, pp. 4179-4188, November 2012.

[80] D. Xu, S. Zhang, and J. Liu, "Very-Low Speed Control of PMSM Based on EKF Estimation with Closed Loop Optimized Parameters," ISA Transactions, vol. 52, no. 6, pp. 835-843, November 2013.

[81] A. Najjar-Khodabakhsh and J. Soltani, "MTPA Control of Mechanical Sensorless IPMSM Based on Adaptive Nonlinear Control", ISA Transactions, vol. 61, pp. 348-356, 2016.

[82] M. Rizwan Khan, and Atif Iqbal, "MRAS Based Sensorless Control of a Series-Connected Five-Phase Two-Motor Drive System", Journal of Electrical Engineering & Technology, vol. 3, no. 2, pp. 224-234, 2008.

[83] M. Rizwan Khan, and Atif Iqbal, "Extended Kalman Filter Based Speeds Estimation of Series-Connected Five-Phase Two-Motor Drive System", Simulation Modelling Practice and Theory, vol. 17, no. 7, pp. 1346-1360, August 2009.

[84] A. Hosseyni, Ramzi Trabelsi, Med Faouzi Mimouni, Atif Iqbal, and Rashid Alammari, "Sensorless Sliding Mode Observer for a Five-Phase Permanent Magnet Synchronous Motor Drive", ISA Transactions, vol.58, pp.462-473, September 2015.

[85] A. Hosseyni, R. Trabelsi, S. Kumar, M. F. Mimouni, and A. Iqbal, "New Sensorless Sliding Mode Control of a Five-Phase Permanent Magnet Synchronous Motor Drive Based on Sliding Mode Observer", International Journal of Power Electronics and Drive System (IJPEDS), vol. 8, no. 1, pp. 184-203, March 2017.

[86] W. H. Ali, M. Gowda, P. Cofie, and J. Fuller, "Design of a Speed Controller Using Extended Kalman Filter for PMSM", IEEE 57th International Midwest Symposium on Circuits and Systems, College Station, TX, pp. 1101-1104, July 8-11, 2014.

[87] W. K. Wibowo1and S.-K. Jeong, "Improved Estimation of Rotor Position for Sensorless Control of a PMSM Based on a Sliding Mode Observer", Journal of Central South University, vol. 23, no. 07, pp. 1643-1656, July 2016.

[88] Ming Qiu, "Extended Kalman Filter Application in Permanent Magnet Synchronous Motor Sensorless Control", Ph.D. Thesis, Ryerson University, Canada, 2003.

[89] MOKHTARI BACHIR, "DTC Intelligente Appliquée À La Commande De La Machine Asynchrone", Ph.D. Thesis, Batna University, Algeria, 2014.

[90] BIRAME M'hamed, "Commande Sans Capteur de Vitesse d'un Moteur a Reluctance Variable Par L'utilisation Des Techniques De L'intelligence Artificielle" Ph.D. Thesis, Batna University, Algeria, 2015.

[91] KENDOUCI Khedidja, "Contribution a la Commande Sans Capteur Mécanique d'une Machine Synchrone a Aimants Permanents", Ph.D. Thesis, Oran University, Algeria, 2012.

[92] Ramin Salehi Arashloo, "Fault Tolerant Vector Control of Five-Phase Permanent Magnet Motors", Ph.D. Thesis, Politècnica De Catalunya Barcelonatech University, Spain, 2014.

[93] Amor KHLAIEF, "Contribution à la Commande Vectorielle sans Capteur Mécanique des Machines Synchrones à Aimants Permanents (MSAP)", Ph.D. Thesis, Ecole Centrale Marseille University, France, 2012.

[94] Z. Qiao, T. Shi, Y. Wang, Y. Yan, C. Xia, and X. He, "New Sliding-Mode Observer for Position Sensorless Control of Permanent-Magnet Synchronous Motor", IEEE Transactions on Industrial Electronics, vol. 60, no. 2, February 2013.

[95] P. Sala-Perez, S. Galceran-Arellano, and D. Montesinos-Miracle, "A sensorless stable V/f control method for a five-phase PMSM", 2013 15th European Conference on Power Electronics and Applications (EPE), Lille, France, pp. 1-10, 2-6 Sept. 2013.